Die approbierte Originalversion dieser Dissertation ist in der Hauptbibliothek der Technischen Universität Wien aufgestellt und zugänglich.
http://www.ub.tuwien.ac.at

The approved original version of this thesis is available at the main library of the Vienna University of Technology.
http://www.ub.tuwien.ac.at/eng

Diese Dissertation haben begutachtet:

Prof. Vasiliki-Maria Archodoulaki
Vienna University of Technology

Assoc. Prof. Martina Marchetti-Deschmann
Vienna University of Technology

TECHNISCHE UNIVERSITÄT WIEN
Vienna University of Technology

DISSERTATION

The impact of bio-compartments on polymers used for artificial bio-replacement by mass spectrometry imaging and conventional bio-analytics.

ausgeführt zum Zwecke der Erlangung des akademischen Grades einer Doktorin der technischen Wissenschaften unter der Leitung von

Assoc. Prof. Dr. Martina Marchetti-Deschmann

IAC-164
Insititute of Chemical Technologies and Analytics
eingereicht an der Technischen Universität Wien
Fakultät für Technische Chemie

von

Sophie Fröhlich, MSc.

0300019
Mühlgasse 30, 2380 Perchtoldsdorf

Wien, April 2014

Name der Kandidatin: Sophie Fröhlich, MSc.
Namen der Prüferinnen: Associate Prof. Mag.rer.nat. Dr.rer.nat. Martina Marchetti-Deschmann, Ao.Univ.Prof. Dipl.-Ing. Dr.mont. Vasiliki Maria Archodoulaki
Titel der Dissertation: The impact of bio-compartments on polymers used for artificial bio-replacement by mass spectrometry imaging and conventional bio-analytics.

Zusammenfassung

Der Schwerpunkt der vorgelegten Dissertation liegt in der Kombination bildgebender massenspektrometrischer (MSI) Analyse mit konventioneller Bioanalytik zur Charakterisierung verschiedener Biomaterialien und Gewebearten in ihrer biologischen Umgebung. Im Rahmen der Methodenentwicklung wurden die physikalischen Aspekte verschiedener Proben und ihre Auswirkungen auf Reproduzierbarkeit und Genauigkeit in MSI Experimenten untersucht. Die Einflussfaktoren stabilisierender Additive und Fixative aus dem Bereich etablierter histologischer Techniken auf MSI Analysen wurden anhand von Nierengewebe näher charakterisiert. Der analytische Schwerpunkt dieser Dissertation liegt im Besonderen auf der Analyse ultrahochmolekularen Polyethylens, welches in Hüftgelenksprothesen zum Ersatz der Hüftpfanne eingesetzt wird. Ergebnisse aus dem Bereich der Materialwissenschaften lieferten Einblick in den Prozess der Materialalterung, welche mehrheitlich durch Oxidation hervorgerufen wird. Die Annahme, dass das biologische Umfeld dabei eine wesentliche Rolle spielt konnte in den durchgeführten MSI Analysen klar dargelegt werden. Modellversuche wurden etabliert, um die zeitliche Einwirkung von Synovialflüssigkeit auf adsorbierte Komponenten am Polymer zu lokalisieren und identifizieren. Es wurde gezeigt, dass für den Schmierungsprozess relevante Lipide am Polymer adsorbieren und auch in das Polymer diffundieren. Zur näheren Identifikation wurden die Lipide mit speziellem Fokus auf Phospholipide und Cholesterol nach Extraktion mittels Dünnschichtchromatographie und MALDI-TOF/RTOF in Kombination mit kollisionsinduzierter Dissoziation näher charakterisiert. Hinsichtlich der Proteinanalyse konnten vor allem quantitativ dominante Proteine sowie mit Lipidtransport und -synthese assoziierte Proteine am Polymer identifiziert werden. Hierbei wurde die nähere Charakterisierung durch 1-dimensionale Gelelektrophorese gefolgt von enzymatischen Verdau und massenspektrometrischer Analyse (MS und MS/MS) durchgeführt. In weiterer Folge konnten die Ergebnisse an explantierten Proben bestätigt werden. Die entwickelte Methodik wurde ebenso zur Analyse biologisch abbaubarer Gefäßprothesen in Mausmodellen herangezogen, um den Verlauf der gewünschten Biodegradation und dabei relevanter Lipid- und Proteinspezies zu verfolgen.

Abstract

The focus of the present thesis lies on the combination of mass spectrometry imaging (MSI) and state-of-the-art instrumental bioanalytical techniques for the detailed characterization of biomaterials and tissue samples in their biological environment. Method development for MSI applications lead to new findings concerning the impact of physical sample characteristics on reproducibility and accuracy in MSI experiments. Stabilizing additives and fixatives, conventionally used in histology, were investigated regarding their influence on MSI analysis based on results obtained for rat kidney tissue samples. The present thesis focuses on the analysis of ultrahigh molecular weight polyethylene (UHWMPE), a polymer commonly used in acetabular hip joint replacement systems. Material science revealed that material aging, relevant for implant failure, is often correlated to oxidative degradation. The high relevance of the biological environment and its interaction with the polymer could be demonstrated by MSI analysis. *In vitro* experiments showed the time dependent adsorption of components related to synovial fluid on the polymer. Lipids, identified directly from the surface and associated to joint lubrication, were adsorbed onto and diffused into the polymer samples. Focusing on phospholipids and cholesterol, lipids were extracted and further identified by thin layer chromatography separation followed by MALDI-TOF/RTOF analysis in combination with collision-induced dissociation. Protein analysis revealed high contents of proteins adsorbed on UHMWPE samples, which are either high abundance proteins or associated with lipid transportation and synthesis,. Protein identification was performed by 1-dimensional gel electrophoresis followed by enzymatic digestion and peptide mass fingerprinting and peptide sequencing. The obtained results were confirmed by explanted polymer samples after revision surgery. The established method was further transferred to the analysis of biodegradable graft materials used in artificial vascular prosthetics in mouse models, where biodegradation and associated lipid and protein species were investigated.

Acknowledgements

Thank you Martina Marchetti-Deschmann for being a supporting supervisor, mentor and companion. Thank you for your passion for science and undaunted patience and for providing me multifaceted possibilities to grow. Most of all thank you for your loyalty.

Thank you Günter Allmaier for being part of your group and institute. Thank you both for giving me the high amount of chances and opportunities during my PhD time and for providing so much support and encouragement.

Thank you Vasiliki-Maria Wilma Archodoulaki for your lighthearted discussions and sharing your profound knowledge anytime I knocked at your door.

Thank you Dontscho Kerjaschki and Helga Schachner for your support with biological questions and techniques and the fruitful discussions we had.

Thank you Thomas Koch, Sonia Walzer, Magdalena Strobl, Helga Bergmeister, Barbara Cvack, Theo Luider, Lennard Dekker, Dominik Rünzler, Janek von Byern, Emanuelle Claude, Michael Kawall for your support and curiosity.

Thank you Max, Theresa, Benedikt, Charlotte, Victoria, Jasmin, Max and Sabrina for being wonderful, challenging and cheerful students I'm proud to have supervised.

Thank you Victor, Wolfgang, Stefan, Albert, Ela, Marlene, Angie, Paul, Bianca, Vicky, Max, Mätti, Petra, Lukas, Ben, Edita and Anna for forming a very diverse and lovable group with a pleasant atmosphere.
Thank you Ernst for your kind advises and for sharing your knowledge and helping hands any time.
Thank you Max, Michi, Manuel and Nicky for your synovial assistance, discussions, reliability and most of all for all the joy, fun and good times we had.

Thank you Birgit, Hong, Michaela and Martina for your inspirations and views.

Thank you mom and dad for your unswerving believe in me and giving me trust, humor and easiness to take with me. You've been a really good choice.

We made it

Whether you think you can, or you think you can't – you're right.

Henry Ford

Table of Contents

1. MALDI Mass Spectrometry 1
a. Desorption/Ionization – the MALDI process 1
b. Analysis 4
i. Time of Flight - TOF 4
ii. Reflector TOF – RTOF 5
iii. Orthogonal TOF – oTOF 6
c. Analyte fragmentation 7
d. Detection 7

2. Mass spectrometry imaging 13
a. Sample preparation 13
i. Sample acquisition and pre-handling 13
ii. Matrix deposition 16
1. Piezo printing (ChIP-1000) 19
2. Sublimation 20
b. MALDI-TOF 21
c. Data analysis 24
d. Statistical data analysis 26

Aspects of mass spectrometry based surface analysis: tissues and biomaterials ... 33
a. Biological tissue 33
i. Kidney 33
ii. Mamma carcinoma – metastatic tumor tissue 34
b. Biomaterials 35
i. Non-degradable polymers used in artificial joint replacement surgery – UHMWPE 35
ii. Biodegradable polymer materials used for vacular prosthesis 37

4. Analyte identification 40
a. Protein analysis by gel electrophoretic separation and MALDI-TOF analysis 40
b. Lipid analysis by thin layer chromatography separation and MS/MS analysis 42
c. Histology 46

5. Renopathological Microstructure Visualization from Formalin Fixed Kidney Tissue by Matrix-Assisted Laser Desorption/Ionization-Time-of-Flight Mass Spectrometry Imaging 52

6. The influence of sample type and preparation on MALDI-TOF mass spectrometry imaging 57

7. Synovial Fluid Protein Adsorption on Artificial, Polymer-based Hip Joint Material Investigated by MALDI-TOF Mass Spectrometry Imaging 99

8. MALDI-TOF mass spectrometry imaging reveals changes on molecular level for ultra-high molecular weight polyethylene joint implants in correlation with lipid adsorption 126

9. Additional Findings 162
a. Feasibility study to investigate biodegradable graft material used for artificial blood vessel replacement by mass spectrometry imaging 162
b. Analytical investigations for biodegradable graft material used for artificial blood vessel replacement 163
c. Feasibility study to use MSI for salamander secrete 176

d. Sample preparation strategies and differentiation of mamma carcinoma and associated lung metastasis by MSI and intact cell mass spectrometry 180

10. CV 193

1. MALDI Mass Spectrometry

Mass spectrometry as an instrumental analytical technique provides the possibility to determine the molecular weight of proteins with high precision. Conventionally in mass spectrometry ions are generated in an ion source and transferred to the analyzer for separation based on their mass-to-charge ratio before detection and further data processing. Ionization initially was conducted by "hard" ionization techniques, such as electron or chemical ionization, inducing partial analyte fragmentation. Later "soft" ionization techniques, matrix assisted laser desorption/ionization (MALDI) and electrospray ionization (ESI) were developed, enabling the transfer of intact ions of higher molecular weights into the gas phase. Both methods, appropriate for polar and non-polar compounds appeal a broad range of applications and had a tremendous impact on science in general since their invention.

The introduction of MALDI in 1985 to the European and American mass spectrometry community by Karas and Hillenkamp [1] was the consequence after a long history of observing ion formation and desorption. The development of field desorption [2] in the late 1960s and the presentation of secondary ion mass spectrometry (SIMS) in 1978 [3] lead to fast atom bombardment being the first technique to observe "matrix" as an assistive substance for ionization and desorption in 1981 [4]. In combination with time of flight (TOF) analysis the technical development for analyzing biological samples increased [5-7] opening up the huge field of "omics" applications [8, 9]. Soon new frontiers were crossed for sensitivity, reaching the attomol range [10, 11] and mass ranges from 0 to 2 MDa. Throughout the history of MALDI MS applications MALDI has been coupled with almost all analyzer systems, however the majority of scientific articles describe combinations with TOF in axial or orthogonal set up or coupled to fourier transformation ion cyclotron resonance (FT-ICR). The focus of the present thesis lies on MALDI-TOF applications in both geometrical configurations. Though MALDI provides a very large instrument and application field, the basic principle of incorporating an analyte in matrix, transferring energy after laser irradiation for desorption remains the same.

a. Desorption/Ionization – the MALDI process

The MALDI process has been under discussion for a very long time and still is not completely understood. Simplified, analytes are incorporated in a matrix system suitable for laser energy transfer, which causes desorption and ionization. Ions are accelerated by the applied electrical field and transferred to the mass analyzer.

Lasers are usually focused to a diameter between 10 and 200 µm delivering average laser pulse energy levels of 5-7 J/cm^2 [12]. The ion intensity yield is determined by the laser pulse fluency, resulting in a reciprocal proportion between laser area and pulse energy. The minimal laser energy needed for ionization, which is comparable for almost all available UV lasers, amounts approximately 10^6 W/cm² [13]. Above this limit, ion signal intensities increase considerably, revealing the exponential rise of ion signals as a function of pulse energy [14, 15]. The signal decreases again with energy levels between 3 to 10 MJ/m^2 as a consequence of analyte fragmentation or heat destruction.

Early developments of MALDI applications included IR lasers, however, today mostly UV-lasers are used for conventional instrument design. Pulsed N_2 lasers (λ = 377 nm) were one of the first UV lasers implemented and used in MALDI, providing high laser fluency and a rectangular laser energy profile. N_2 lasers are however, limited in the laser repetition rate, which usually does not exceed 100 Hz.

As a consequence new lasers were applied to MALDI including the frequency tripled neodymium-doped yttrium aluminum garnet (Nd:YAG, λ = 355 nm) laser, being one of the first solid lasers in MALDI. Compared to the N_2 laser, Nd:YAG lasers can easily be focused to diameters below 5 µm (full width half maximum, FWHW) with a Gaussian emission profile, resulting in high energy fluency and eventual analyte destruction. Depending on the application the laser profile is of high interest. Mass spectrometric imaging (MSI) experiments (see Chapter 2.c) favor rectangular laser profiles, which have an almost even emission profile and are focused to a preferably small laser diameter to increase lateral resolution. Bruker accomplished the favored qualities in developing the SmartBeam™ laser, providing a modulated Nd:YAG profile with a theoretical diameter as small as 10 µm [16].

Applying laser energy to crystalline samples, or analytes embedded in matrix crystals, transfers the laser energy to the abounding matrix crystals. The adsorbed energy is converted to thermal energy. This concept is the initial step of the MALDI process. The proper co-crystallization of analyte and matrix is essential. Matrix crystals, incorporating the analyte, are different in size and shape and strongly depend on the application and solvent system. 1,5-dihydroxybenzoic acid (DHB) was one of the first matrices used for protein analysis by MALDI-TOF [17]. Nowadays DHB is one of the most commonly used matrices with a very broad analytical spectrum ranging from lipid applications [18, 19] to glycoprotein analysis [20]. DHB crystallizes in a ring with sharp and long centroid growing needles. Highest signal intensities can be found exactly on the rim region, whereas recrystallization or certain preparation techniques reduce crystal size and increase homogeneity [21]. Sinapinic acid (SA) was found to show good ionization properties for protein and peptide analysis [22, 23]. It is described as a “soft” matrix, with comparably low energy transition rates, making analyte fragmentation less likely. α-cyano-4-hydroxy-cinnamic (CHCA) acid is one of the most popular matrices for peptide analysis [24] producing very fine, roundly shaped and homogeneous crystals. CHCA is known as a “hot” matrix, transmitting high amounts of energy to analyte molecules, causing eventual fragmentation, which is favored for post source decay (PSD) analysis.

In general commonly used matrices are structurally similar including aromatic acids or carbonyl components. Quickest and highest energy transfer was found for matrix molecules, having an adsorption coefficient similar to the laser light. However, it was found that all matrix molecules ionizing small analyte molecules have a high wavelength tolerance for efficient energy transfer at nano-second pulse length [25]. The typical ionization energy for matrix molecules, which leads to the release of an electron, is 8 keV [26].

Three different methods have been described for MALDI sample preparation, the initial step for co-crystallization: dried droplet, thin layer and double layer preparation [27] besides new developments [28]. For dried droplet preparation matrix and analyte solution are mixed at equal volumes and applied to the MALDI target. Homogeneous crystal surfaces are formed, which can further be recrystallized or washed with trifluoracetic acid (TFA) to remove salt residues. Thin and double layer preparations use a pre-spotted matrix layer on the target on which the analyte is applied followed by another matrix layer for the double layer technique. Washing usually improves analyte incorporation, however, washing thin layer preparations comprises the risk of washing off surface analytes as well. Pre-spotted matrix layer provide seed crystals, which enhance quick crystallization and homogeneous distribution if the initial layer was perfectly applied. Other techniques provide further possibilities such as water vapor or saturated atmosphere for matrix recrystallization. Adding small amounts of salts to the matrix solvent can help to cationize analytes, which have a critical ionization

potential. MALDI shows low sensitivity towards salt contaminations or residues from buffers or detergents compared to other ionization techniques [29, 30].

Knochenmuss described multiple parameters of high influence for the MALDI process in 2003 [31]. During the MALDI process, matrix analytes receive a very high amount of energy by the irradiating laser, causing vibrational excitation. Matrix and analyte molecules undergo phase transition from solid to gas phase resulting in a matrix plume containing charged and neutral elements. The initial velocity ions receive during this desorption process depends on the analyte, the matrix molecules and the laser fluence [32]. Ionization models divide the MALDI process into primary and secondary ionization mechanisms. Karas et al described the characteristic phenomenon of majorly formed single charged ions for MALDI [33]. The so-called "lucky survivor theory" correlates ionization with the applied laser fluence. If the transmitted energy exceeds the minimum requirement for successful ionization, large clusters containing charged molecules are ablated from the sample. If the energy is too low, only neutral molecules are ablated. Both, matrix and analyte molecules are ionized and can be detected. The main assumption of the lucky survivor concept is the presence of already existing ions in the MALDI sample. In contrary the pooling theory, developed by Ehring [34] and further developed by Knochenmuss [35, 36] assumes uncharged molecules. Ions are formed after ablation in the plume by primary and secondary ionization [31]. The plume is described to contain a high amount of matrix molecules and analytes, with different velocity vectors, which consequently leads to collision in the gaseous cloud. The described collisions form the basis for secondary ionization phenomena, claiming the ionization of analyte molecules as a consequence of proton transfer.

After the ablation process and the resulting collision in the plume, fragmentation of molecules, mainly matrix molecules might occur. If the initial energy is too high, fragmentation is also likely for analyte molecules, described as post source decay (PSD). Fragmentations occurring directly after or along with the ablation process are referred to as in source decay (ISD) [37, 38].

The last step of the MALDI process transfers the ions to the analyzer by applying an electrical acceleration field. MALDI is described as an ionization technique with highest ion transmission rates [39, 40].

The total acceleration potential usually does not exceed 20 kV, avoiding fragmentation due to energy overload. In many instruments the ion source geometry contains partitioned acceleration fields, applying at first only 40 % of the total acceleration voltage to the sample [41, 42]. Ions are further accelerated after they have passed an intermediate field free drift region. The main advantage is the decreased velocity resulting in more stable ions and the possibility to efficiently apply a delayed extraction time, which will be explained in detail in the TOF section (see Chapter 1.b).

Applying elevated pressures during analyte desorption/ionization can reduce the vibrational heating of ions, decreasing therefore fragmentation events during the MALDI process. Inert gas is used to cool ions and increase their stability [43]. Further developments used atmospheric pressure for vibrational cooling. However, atmospheric pressure ionization requires efficient transfer of ions to the vacuum analyzer. A molecular beam skimmer similar to ESI constructions usually conducts this. Losses on the skimmer and capillary walls are likely to occur, decreasing detection sensitivity compared to vacuum MALDI systems [44-46].

The main disadvantage in MALDI applications is the poor shot to shot reproducibility [47, 48]. Crystallization and analyte incorporation differs highly depending on the sample preparation

technique, the analyte/matrix proportion, the solvent system and the target surface. If crystals are not formed perfectly homogeneous the shot-to-shot variability is too high for unsupervised data acquisition.

b. **Analysis**

MALDI has been coupled to a large variety of mass analyzers. However MALDI is based on the application of pulsed lasers sending ion packages to the analyzer, which made time of flight (TOF) analysis the most frequently used instrument configuration. TOF analyzers were already developed in 1946 by Stephens [49] and 1955 by Wiley and McLaren [50], before the commercial interest rose due to the introduction of MALDI in the 1980s.

The mass analyzer performance is determined by its mass resolution, signal to noise ratio (S/N), abundance sensitivity and mass accuracy.

i. Time of Flight - TOF

TOF analysis separates ions based on their time of flight. The short ion packages generated by the laser pulse are accelerated towards a field free drift region in the flight tube until they hit the detector. Ion signals are detected and recalculated for their flight time. Technically often digital storing oscilloscopes are used for detecting the ions start and arrival time. Scans start usually after a photodiode has detected laser light and end when ions hit the detector, inducing current flow. The time jitter is usually a tiny proportion of the laser pulse time.

During the MALDI process the ions receive a potential energy E_p, which is immediately transferred into kinetic energy E_{kin}. An electrical field U accelerates ions with a particular charge q, composed of the charge state z and the elemental charge e. According to equation 1 E_{kin} can also be described by the ion's mass m and velocity v.

$$E_p = E_{kin} = qU = zeU = \frac{1}{2}mv^2 \qquad (1)$$

The velocity can be explained as follows in equation 2 based on E_{kin}.

$$v = \sqrt{\frac{2E_{kin}}{m}} = \sqrt{\frac{2zeU}{m}} \qquad (2)$$

Considering the velocity as a function of time t and the path s the time of flight can be described as in equation 3.

$$t = s\sqrt{\frac{m}{2E_{kin}}} = s\sqrt{\frac{m}{2zeU}} \qquad (3)$$

Based on the time of flight, the relation between mass m and charge state z, can be concluded as the main output value for analyte separation (Equ. 4).

$$\frac{m}{z} = 2eU(\frac{t}{s})^2 \qquad (4)$$

The separation of different ions, referred to as mass resolving power R_m is determined by the mass m divided by the mass resolution δ_m (Equ. 5).

$$R_m = \frac{m}{\delta_m} \quad (5)$$

TOF instruments are usually built with an axial geometry (Fig. 1). The simple set up is referred to as linear TOF (LTOF). LTOF applications have a wide dynamic mass range providing a very broad application field for analysis ranging from small but fragile analytes, e.g. glycosylated peptides in the kDa range, to large molecules, e.g. proteins in the MDa range. High molecular weight analysis does not intend to obtain monoisotopic resolution, however, this is an essential part to obtain information about peptides, lipids or other organic compounds in the low molecular mass range. The energy distribution, as a consequence of the direct relation between time of flight and mass, leads to a statistical TOF distribution resulting in peak broadening. Very broad, consequently badly resolved peaks in LTOF mass spectra result from the lack of mass resolution to detect separated isotopic pattern, especially in the protein mass range. Furthermore the internal energy distribution during the acceleration process leads to signal degradation besides biological variation, e.g. glycosylation, contributing isoform variability. To increase resolution and mass accuracy two technical set ups were constructed: the implementation of a delayed extraction time and the integration of an ion mirror to elongate the flight path and reduce energy distributions – the reflector TOF (RTOF).

DE also referred to as pulsed extraction (PE) or time-lag-focusing, is the delayed application of the extractive acceleration field [50, 51]. Ions in the plume receive a statistically distributed internal energy, depending on their position relative to the neighbor matrix molecule and the sample surface. Those energy distributions lead to variations in the first acceleration distance and transformed velocity. Applying the acceleration field a few ns after the laser pulse, leads to equilibrating ion momentums and the compensation of internal energy variations [52]. Ions remaining at the initial position because less energy was transferred receive a higher acceleration and obtain higher velocities compared to ions at the surface. The compensation mechanisms result in an evened velocity distribution for ions entering the field free drift region, leading to enhanced mass resolution and mass accuracy.

Compensating the internal energy distribution and additionally increasing the TOF path is conducted by the RTOF geometry [53, 54].

ii. Reflector TOF – RTOF

Mamyrin in St. Petersburg [53] developed the idea of RTOF instrument design. The main aim was to further adjust the ions energy distribution by deceleration and acceleration using an ion mirror. Additionally, ion packages entering the ion mirror are refocused during the acceleration towards the detector as ions with a high velocity, respectively higher internal energy, travel a longer distance through the reflector compared to ions with a lower velocity. Consequently the acceleration path is longer and the time of flight increased, compensating the former velocity distribution.

Technically the reflectron is located directly after the field free drift region (Fig. 1). The implementation can be manifold. The simplest configuration is a single stage reflector, containing several equally spaced grid or ring electrodes generating a homogeneous electrical field [55]. Two stage reflectron instruments provide two homogeneous electrical fields with different potential gradient. The first stage induces an electrical field of high intensity and efficiently decelerates entering ions, whereas the second stage provides a weaker field. Geometrically, those constructions are smaller, however suffer from decreased ion transmission [56]. In both configurations, the electrical field is adapted to a very specific mass range, if not to one particular m/z value for optimal

energy spread compensation. In further development, the quadratic reflectron, the dynamic mass range is increased. Voltages are applied as a quadratic function in a voltage versus penetration depth profile.

The major critical point for the implementation is the electrical field shape, which is not ideally and contains high-density field lines in the centroid area compared to low densities at the periphery. As a consequence the ion beam diverges and ion transmission is reduced [57].

A very efficient method for constructing an ion mirror is the curved field reflectron (CFR) [58]. The CFR is a technical compromise between the so far described reflector designs, aiming to compensate for ion transmission. The discontinuous entrance grid is similar to the single and dual stage potentials whereas the field shape is comparable to the linear potential [59].

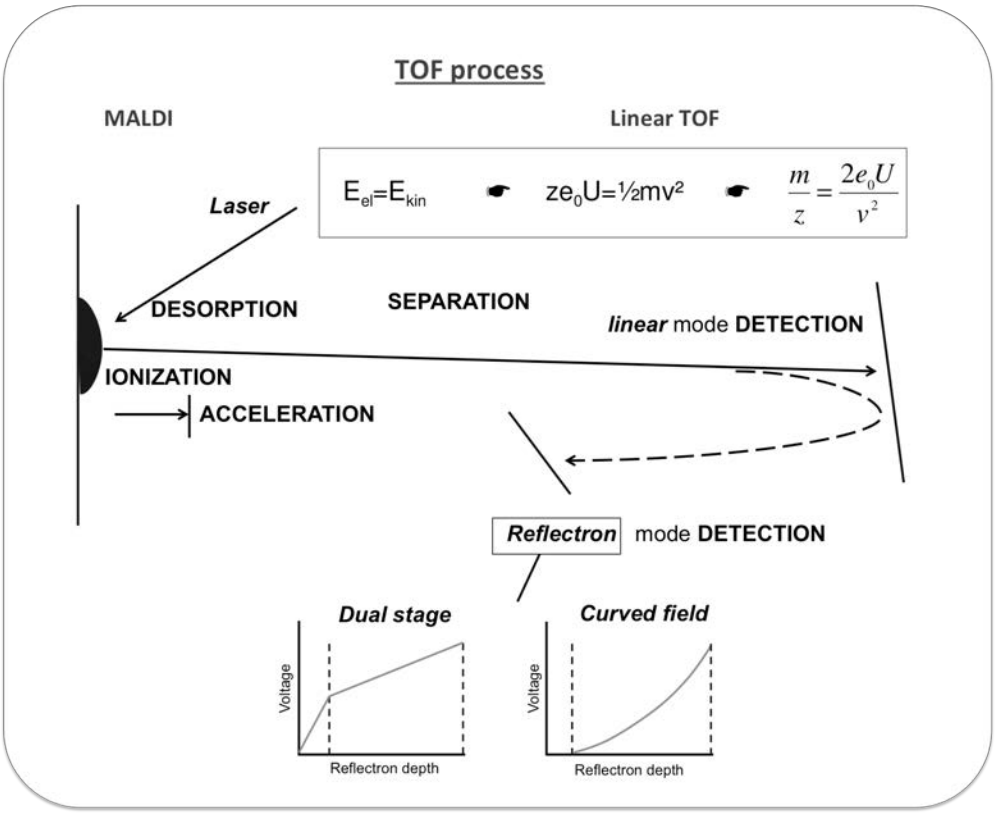

Figure 1: Schematic outline of the MALDI-TOF process: the desorption/ionization process is followed by acceleration of the ions, which are detected either in linear or reflectron mode. For the reflection process ions are decelerated and accelerated again by voltages applied to a dual stage or curved electrical field. During TOF analysis ions are separated according to their mass to charge ratio, which is determined by the ion's velocity.

The newest technical improvements to increase mass resolution combine up to 4 ion mirrors obtaining an ion flight path of approximately 20 m in a spiral trajectory [60, 61]. Mass resolving power up to 80.000 FHWM at m/z 2564 can be obtained, which is sufficient for accurate mass determination. Mass accuracy for the low mass range was described to exceed 2 ppm.

iii. Orthogonal TOF – oTOF

The principal of MALDI-TOF is identical in orthogonal TOF (oTOF) instrumental configurations, however, with significantly increased resolving power and mass accuracy. The high initial axial velocity distribution is electrically eliminated and ions are collimated by the initial ion-transfer optics,

e.g. quadrupole, hexapole or octapole. By the implementation of ion-transfer optics, which also stabilizes ions by thermalization, the ion source is completely decoupled from the TOF analyzer. High laser pulse rates theoretically transform the pulsed principal into continuous transfer to the TOF pulser region. Ions are collected at the entrance system of the flight tube after injection and accelerated, "pushed", towards the drift region. From here on the process is similar to the axial built TOF instruments [62]. Despite the increased mass accuracy, oTOF instruments deal with increased processing times in the millisecond range and their mass range is limited to the capacities of the ion-transfer system.

oTOF systems are based on their construction hybrid systems equipped with additional functions [63], which embed further dimensions of analyte separation, e.g. Ion mobility separation was implemented by Waters [64, 65] and Agilent. Both instruments are designed as QTOF instruments with a drift cell located before TOF separation. Ion mobility separation is based on the ions collision cross section. Ions travel by the accelerative electrical field through the drift cell, whereas inert gas is used as a counteracting force working against the electrical field. As a consequence ions are separated based on their collision cross section additionally to the electrical charge and mass related analysis.

c. **Analyte fragmentation**

As described the initial energy of ions after laser irradiation is very high. If it exceeds the bond energies of the molecule, fragmentation can occur, which is referred to as metastable decay. Using MALDI ion sources those fragmentations are further classified as the described PSD and ISD fragmentations. PSD fragments, which are often used for analyte characterization in terms of peptide sequencing or lipid identification, travel with the same velocity as their parent ion and cannot be detected in linear TOF acquisition mode. Yet, the ion mirror separates fragment from parent ions due to their reduced internal energy [66].

Collision induced dissociation (CID) is based on the collision of ions with gas molecules. Instruments are equipped with a gas chamber located in the flight path, which is filled with gas. Ions collide while crossing the chamber and fragments are detected. Usually CID ions have a higher abundance resulting in enhanced signal quality due to a higher total ion current. After the collision with gas molecules analyte ions receive a very high amount of energy, which is distributed equally in the molecule and results in vibration among the axes [67, 68]. The efficiency of energy conversion after collision, strongly depends on the analyte mass and structure, the collision gas and their initial energy. The mechanism of CID is often applied for structural analysis because of the increased number of fragments compared to PSD or ISD. The fragmentation pathway is directly linked to the amount of energy the analyte ion receives. CID is possible for high (20 eV) and low (8 eV) energy collision [69, 70]. To compensate the abundance differences between fragments and associated parent ions, some instruments provide the possibility to eliminate parent ions before detection to improve spectral quality. This artificially increases sensitivity for fragment ions by avoiding detector saturation [71]. Further details of fragmentation and fragment ion formation will be discussed later in the analyte verification sections (see Chapter 4.a and 4.b).

d. **Detection**

While ion detection was formerly conducted using spectroscopic instrument configurations, such as photo plates, detection developed towards digital signal conversion.

MS applications usually deal with the total ion current. Ions hitting the detector trigger current signals, which are amplified and translated to information. The most important quality of detectors is, to deliver quantitative information, which means that the signal is proportional to the ion abundance, while hitting the detector surface. Amplification is mandatory for detection, especially for low abundant analytes.

The most frequently used commercially available detectors to date are electron multiplier tube (EMT) and multichannel plate detectors (MCP). Both work at the same principle of amplifying ion signals by a cascade of secondary electrons [72].

EMT detectors contain several conversion dynodes of inverse potential to the analyte ion to amplify signals. Ions hitting the first conversion dynode induce the immersion of inversely charged secondary particles, e.g. electrons. After emitting electrons from the first dynode, the conversion dynode, those electrons are amplified in the dynode cascade and translated into current. The dynodes in these detectors are discrete. Another detector form is the use of continuous dynodes, which are usually made of lead doped glass, often referred to as channeltron detectors. Channeltron detectors are usually arranged as small circular plates, containing a large number of channeltrons, referred to as multichanneltron plate (MCP). MCPs are characterized by their high amplification power and quick scanning time. However, their short life span of approximately 2 years is often reduced by ion contamination or poor vacuum stability.

Signals are further amplified by conventional signal amplifiers and converted into data. According to the systems calibration for masses and flight times, information is processed and transferred into mass spectra plotting m/z values against intensities.

References

1. Karas M, B.D., Hillenkamp F *Influence of the wavelength in high-irradiance ultraviolet laser desorption mass spectrometry of organic molecules.* Analytical chemistry, 1985. **57**: p. 2935-2939.
2. Beckey, H.D., *Field desorption mass spectrometry: a technique for the study of thermally unstable substances of low volatality.* Int. J. Mass Spec. Ion Phys., 1969. **2**: p. 500-503.
3. Benninghoven, A., Sichtermann, W., *Detection, identification and structural investigation of biologically important compounds by secondary ion mass spectrometry.* Analytical chemistry, 1978. **50**: p. 1180-1184.
4. Zakett, D., Schoen, A.E., Cooks, R.G., Hemberger, P.H., *Laser-desorption mass spectrometry/mass spectrometry and the mechanism of desorption ionization.* J. Am. Chem. Soc., 1981. **103**: p. 1295-1297.
5. Karas M, H.F., *Laser desorption ionization of proteins with molecular masses exceeding 10000 daltons.* Analytical chemistry, 1988. **60**: p. 2299-2301.
6. Tanaka K, W.H., Ido Y, Akita S, Yoshida Y, Yoshida T, *Protein and polymer analyses up to m/z 100000 by laser ionization time-of-flight mass spectrometry.* Rapid communications in mass spectrometry : RCM, 1988. **2**: p. 151-153.
7. Karas M, B.U., *Laser Desorption Ionization Mass Spectrometry of Large Biomolecules.* Trends Analyt Chem, 1990. **9**: p. 321-325.
8. Ferguson, P.L.S., R. D., *Proteome analysis by mass spectrometry.* Annu. Rev. Biophys. Biomol. Struct., 2003. **32**: p. 399-424.
9. Schiller J, S.R., Fuchs B, Muller M, Zschornig O, Arnold K., *MALDI-TOF MS in lipidomics.* Front. Biosci., 2007. **12**: p. 2568-2579.
10. Jespersen S, N.W.M.A., Tjaden U R, van der Greef J, Litborn E, Lindberg U, Roeraade J, Hillenkamp F *Attomole detection of proteins by matrix-assisted laser desorption/ionization mass spectrometry with the use of picolitre vials.* Rapid communications in mass spectrometry : RCM, 2005. **8**(8): p. 581-584.
11. Nordhoff E, L.H., Gobom J, *Exploring the limits and losses in MALDI sample preparation of attomole amounts of peptide mixtures.* Int. J. Mass Spec. , 2007. **268**(2-3): p. 139-146.
12. Guenther, S., et al., *Laser spot size and laser power dependence of ion formation in high resolution MALDI imaging.* International Journal of Mass Spectrometry, 2010. **294**(1): p. 7-15.
13. Dreisewerd K, S.M., Karas M, Hillenkamp F, *Influence of the laser intensity and spot size on the desorption of molecules and ions in matrix-assisted laser desorption/ionization with uniform beam profile.* Int. J. of Mass Spectrom. and Ion Proc, 1995. **141**: p. 127-148.
14. Westmacott G, E.W., Hillenkamp F, Dreisewerd K, Schurenberg M, *Influence of the laser intensity and spot size on the desorption of molecules and ions in matrix-assisted laser desorption/ionization with uniform beam profile.* Int. J. of Mass Spectrom., 2002. **221**: p. 67-81.
15. Qiao, H., V. Spicer, and W. Ens, *The effect of laser profile, fluence, and spot size on sensitivity in orthogonal-injection matrix-assisted laser desorption/ionization time-of-flight mass spectrometry.* Rapid Commun Mass Spectrom, 2008. **22**(18): p. 2779-2790.
16. Holle, A., et al., *Optimizing UV laser focus profiles for improved MALDI performance.* J Mass Spectrom, 2006. **41**(6): p. 705-716.
17. Strupat K, K.M., Hillenkamp F, *2,5-dihydroxybenzoic acid:a new matrix for laser desorption-ionization mass spectrometry.* Int. J.of Mass Spectrom., 1991. **111**: p. 89 – 102.
18. Han, X., K. Yang, and R.W. Gross, *Multi-dimensional mass spectrometry-based shotgun lipidomics and novel strategies for lipidomic analyses.* Mass Spectrom Rev, 2012. **31**(1): p. 134-178.
19. Sparvero, L.J., et al., *Mapping of phospholipids by MALDI imaging (MALDI-MSI): realities and expectations.* Chem Phys Lipids, 2012. **165**(5): p. 545-562.

20. Wa, C., et al., *Characterization of glycation adducts on human serum albumin by matrix-assisted laser desorption/ionization time-of-flight mass spectrometry.* Clin Chim Acta, 2007. **385**(1-2): p. 48-60.
21. Yang, J.H. and R.M. Caprioli, *Matrix Sublimation/Recrystallization for Imaging Proteins by Mass Spectrometry at High Spatial Resolution.* Analytical Chemistry, 2011. **83**(14): p. 5728-5734.
22. Beavis R C, C.B.T., Fales H M, *Cinnamic acid derivates as matrices for ultraviolet laser desorption mass spectreomtry of proteins* Rapid communications in mass spectrometry : RCM, 1989. **3**(2): p. 432-435.
23. Beavis R C, C.B.T., Fales H M, *Matrix-assisted laser-desorption mass spectrometry using 355 nm radiation.* Rapid communications in mass spectrometry : RCM, 1989. **3**(12): p. 436-439.
24. Gobom, J., et al., *Alpha-cyano-4-hydroxycinnamic acid affinity sample preparation. A protocol for MALDI-MS peptide analysis in proteomics.* Anal Chem, 2001. **73**(3): p. 434-438.
25. Papantonakis M R, K.J., Hess W P, Haglund Jr R F, *What do matrix-assisted laser desorption/ionization mass spectra reveal about ionization mechanisms?* JOURNAL OF MASS SPECTROMETRY, 2002. **37**: p. 639–647.
26. Karbach V, K.R., *Do single matrix molecules generate primary ions in ultraviolet matrix-assisted laser desorption/ionization.* Rapid communications in mass spectrometry : RCM, 1998. **12**: p. 968–974.
27. Kussmann M, N.E., Rahbek-Nielsen H, Haebel S, Rossel-Larsen M, Jakobsen L, Gobom J, Mirgorodskaya E, Kroll-Kristensen A, Palm L, Roepstorff P, *Matrix-assisted Laser Desorption/Ionization Mass Spectrometry Sample Preparation Techniques Designed for Various Peptide and Protein Analytes.* JOURNAL OF MASS SPECTROMETRY, 1997. **32**(6): p. 593-601.
28. Fenyo, D., et al., *MALDI sample preparation: the ultra thin layer method.* J Vis Exp, 2007(3): p. 192.
29. Pan, C., et al., *Recent developments in methods and technology for analysis of biological samples by MALDI-TOF-MS.* Anal Bioanal Chem, 2007. **387**(1): p. 193-204.
30. Kussmann, M. and P. Roepstorff, *Sample preparation techniques for peptides and proteins analyzed by MALDI-MS.* Methods Mol Biol, 2000. **146**: p. 405-424.
31. Knochenmuss, R. and R. Zenobi, *MALDI ionization: The role of in-plume processes.* Chemical Reviews, 2003. **103**(2): p. 441-452.
32. Karas, M., et al., *The initial-ion velocity as a marker for different desorption-ionization mechanisms in MALDI.* International Journal of Mass Spectrometry, 2003. **226**(1): p. 239-248.
33. Karas, M., M. Gluckmann, and J. Schafer, *Ionization in matrix-assisted laser desorption/ionization: singly charged molecular ions are the lucky survivors.* Journal of Mass Spectrometry, 2000. **35**(1): p. 1-12.
34. Ehring H, K.M., Hillenkamp F, *Role of photoionization and photochemistry in ionization process of organic molecules and relevance for matrix-assisted laser desorption ionization mass spectrometry.* Org. Mass Spectrom., 1992. **27**: p. 473-480.
35. Knochenmuss, R., *A quantitative model of ultraviolet matrix-assisted laser desorption/ionization.* J Mass Spectrom, 2002. **37**(8): p. 867-877.
36. Knochenmuss, R., *A quantitative model of ultraviolet matrix-assisted laser desorption/ionization including analyte ion generation.* Anal Chem, 2003. **75**(10): p. 2199-2207.
37. Suckau, D. and D.S. Cornett, *Protein sequencing by ISD and PSD MALDI-TOF MS.* Analusis, 1998. **26**(10): p. M18-M21.
38. Kocher, T., A. Engstrom, and R.A. Zubarev, *Fragmentation of peptides in MALDI in-source decay mediated by hydrogen radicals.* Analytical Chemistry, 2005. **77**(1): p. 172-177.
39. Shen Z, T.J., Averbuj C, Broo K M, Engelhard M, Crowell J E, Finn M G, Suizdak G, *Porous Slicon as a Versatile Platform for Laser Desorption/Ionization Mass Spectrometry.* Analytical chemistry, 2001. **73**(3): p. 612-619.

40. Laiko, V.V., M.A. Baldwin, and A.L. Burlingame, *Atmospheric pressure matrix-assisted laser desorption/ionization mass spectrometry.* Anal Chem, 2000. **72**(4): p. 652-657.
41. Yamagaki, T. and H. Nakanishi, *Influence of acceleration voltages on relative ion intensities in the post-source decay fragmentation of isomeric cyclic oligosaccharides by matrix-assisted laser desorption/ionization time-of-flight mass spectrometry.* Rapid Commun Mass Spectrom, 1999. **13**(21): p. 2199-2203.
42. Kovtoun, S.V., R.D. English, and R.J. Cotter, *Mass correlated acceleration in a reflectron MALDI TOF mass spectrometer: an approach for enhanced resolution over a broad mass range.* J Am Soc Mass Spectrom, 2002. **13**(2): p. 135-143.
43. Soltwisch, J., et al., *Effect of Gas Pressure and Gas Type on the Fragmentation of Peptide and Oligosaccharide Ions Generated in an Elevated Pressure UV/IR-MALDI Ion Source Coupled to an Orthogonal Time-of-Flight Mass Spectrometer.* Analytical Chemistry, 2009. **81**(8): p. 2921-2934.
44. Konn, D.O., et al., *Comparison of the effects of ionization mechanism, analyte concentration, and ion "cool-times" on the internal energies of peptide ions produced by electrospray and atmospheric pressure matrix-assisted laser desorption ionization.* Journal of the American Society for Mass Spectrometry, 2005. **16**(5): p. 743-751.
45. Miller, C.A., D.H. Yi, and P.D. Perkins, *An atmospheric pressure matrix-assisted laser desorption/ionization ion trap with enhanced sensitivity.* Rapid Communications in Mass Spectrometry, 2003. **17**(8): p. 860-868.
46. Moyer, S.G. and R.J. Cotter, *Atmospheric pressure MALDI.* Analytical Chemistry, 2002. **74**(17): p. 468a-476a.
47. Albrethsen, J., *Reproducibility in protein profiling by MALDI-TOF mass spectrometry.* Clinical Chemistry, 2007. **53**(5): p. 852-858.
48. Callesen, A.K., et al., *Reproducibility of serum protein profiling by systematic assessment using solid-phase extraction and matrix-assisted laser desorption/ionization mass spectrometry.* Rapid Communications in Mass Spectrometry, 2008. **22**(3): p. 291-300.
49. E, S.W., *A pulsed mass spectrometer with time dispersion.* Bull Am Phys Soc, 1946. **21**(2): p. 22.
50. Wiley W C, M.I.H., *Time-Of-Flight Mass Spectrometer with Improved Resolution.* The Rev. of Sci. Instrum., 1955. **26**(12): p. 1150.
51. Whittal, R.M. and L. Li, *High-resolution matrix-assisted laser desorption/ionization in a linear time-of-flight mass spectrometer.* Anal Chem, 1995. **67**(13): p. 1950-1954.
52. Juhasz, P., et al., *Applications of delayed extraction matrix-assisted laser desorption ionization time-of-flight mass spectrometry to oligonucleotide analysis.* Anal Chem, 1996. **68**(6): p. 941-946.
53. Mamyrin B A, K.V.I., Shmikk D V, Zagulin V A, *The mass-reflectron, a new nonmagnetic time-of-flight mass spectrometer with high resolution.* Sov. Phys JETP, 1973. **37**: p. 45.
54. A, M.B., *Time-of-flight mass spectrometry (concepts, achievements and prospects).* Int. J. Mass Spec., 2001. **206**(3): p. 251-266.
55. Doroshenko, V.M. and R.J. Cotter, *Ideal velocity focusing in a reflectron time-of-flight mass spectrometer.* J Am Soc Mass Spectrom, 1999. **10**(10): p. 992-999.
56. Cornish, T.J., Cotter R J, *A Dual-Reflectron Tandem Time-of-Flight Mass Spectrometer.* ACS Symposium Series, 1993. **6**: p. 95-107.
57. Scheinfein M R, S.D.N., *Time aberrations of uniform fields: An improved reflectron mass spectrometer for an atom-probe field-ion microscope.* Rev. Sci. Instrum, 1993. **64**(11): p. 3126-3131.
58. Cornish, T.J. and R.J. Cotter, *A curved-field reflectron for improved energy focusing of product ions in time-of-flight mass spectrometry.* Rapid Commun Mass Spectrom, 1993. **7**(11): p. 1037-1040.
59. Cotter, R.J., W. Griffith, and C. Jelinek, *Tandem time-of-flight (TOF/TOF) mass spectrometry and the curved-field reflectron.* J Chromatogr B Analyt Technol Biomed Life Sci, 2007. **855**(1): p. 2-13.

60. Satoh, T., et al., *The design and characteristic features of a new time-of-flight mass spectrometer with a spiral ion trajectory.* J Am Soc Mass Spectrom, 2005. **16**(12): p. 1969-1975.
61. Satoh, T., T. Sato, and J. Tamura, *Development of a high-performance MALDI-TOF mass spectrometer utilizing a spiral ion trajectory.* J Am Soc Mass Spectrom, 2007. **18**(7): p. 1318-1323.
62. Guilhaus, M., D. Selby, and V. Mlynski, *Orthogonal acceleration time-of-flight mass spectrometry.* Mass Spectrom Rev, 2000. **19**(2): p. 65-107.
63. Stone, E., et al., *Surface-induced dissociation on a MALDI-ion mobility-orthogonal time-of-flight mass spectrometer: sequencing peptides from an "in-solution" protein digest.* Anal Chem, 2001. **73**(10): p. 2233-2238.
64. Salbo, R., et al., *Traveling-wave ion mobility mass spectrometry of protein complexes: accurate calibrated collision cross-sections of human insulin oligomers.* Rapid Commun Mass Spectrom, 2012. **26**(10): p. 1181-1193.
65. Bohrer, B.C., et al., *Biomolecule analysis by ion mobility spectrometry.* Annu Rev Anal Chem (Palo Alto Calif), 2008. **1**: p. 293-327.
66. Hoteling, A.J. and K.G. Owens, *Improved PSD and CID on a MALDI TOFMS.* Journal of the American Society for Mass Spectrometry, 2004. **15**(4): p. 523-535.
67. Wells, J.M. and S.A. McLuckey, *Collision-induced dissociation (CID) of peptides and proteins.* Methods Enzymol, 2005. **402**: p. 148-185.
68. Sleno, L. and D.A. Volmer, *Ion activation methods for tandem mass spectrometry.* J Mass Spectrom, 2004. **39**(10): p. 1091-1112.
69. Nizigiyimana L, V.d.H.H., Claey M, *Comparison of Low- and High-energy Collision-induced Dissociation Tandem Mass Spectrometry in the Analysis of Ricinoleic and Ricinelaidic Acid.* JOURNAL OF MASS SPECTROMETRY, 1997. **32**(3): p. 277-286.
70. Pittenauer, E. and G. Allmaier, *High-energy collision induced dissociation of biomolecules: MALDI-TOF/RTOF mass spectrometry in comparison to tandem sector mass spectrometry.* Comb Chem High Throughput Screen, 2009. **12**(2): p. 137-155.
71. Neubert, H., et al., *MALDI post-source decay and LIFT-TOF/TOF investigation of alpha-cyano-4-hydroxycinnamic acid cluster interferences.* J Am Soc Mass Spectrom, 2004. **15**(3): p. 336-343.
72. Dubois F, K.R., Zenobi R, Brunelle A, Deprun C, Le Beyec Y, *A comparison between ion-to-photon and microchannel plate detectors.* Rapid communications in mass spectrometry : RCM, 1999. **13**(9): p. 786-791.

2. Mass spectrometry imaging

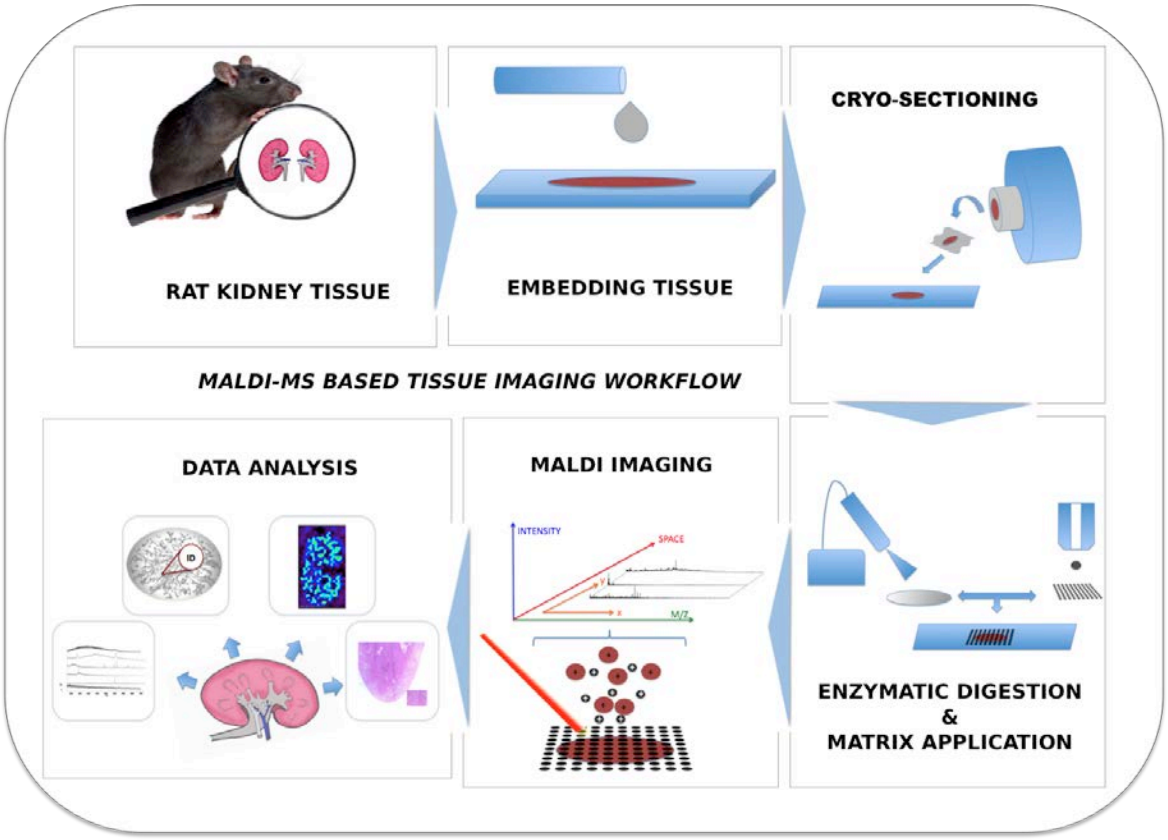

Figure 2: Scheme of a MSI workflow exemplary visualized for tissue samples; Samples are dissected followed by immediate fixation and embedding to avoid analyte degradation; Thin sections are obtained by microtome sectioning e.g. cryo-sectioning; For MSI, samples are either treated enzymatically or MALDI matrix is applied; MSI analysis is followed by data analysis and interpretation.

a. Sample preparation

MSI experiments are despite exceptions, usually conducted by conventionally built MALDI ion sources, very often combined with a TOF analyzer. As a consequence high similarity with conventionally MALDI sample preparations is demanded. Flat surfaces with very homogeneous matrix crystallization and negligible, insulating properties are preferred. To achieve this conditions careful sample preparation is needed.

i. Sample acquisition and pre-handling

MSI analysis often requires very long and invasive procedures of sample preparation. Furthermore long data acquisition times require good analyte sustainment to stabilize analytical information. Starting from the dissection of material, quick analyte preservation is necessary [1]. For biomedical materials the most common established method is to immediately snap freeze samples [2]. Proteins and lipids can be preserved for a long time when stored below - 70 °C [3]. Depending on the sample and the analytical question storing conditions can be reduced to -20 °C. Plasma has been shown to be sufficiently stable at -20 °C [4], lipids however, rapidly degrade or oxidize [5]. For polymers no

comparable analysis has ever been conducted, however it is assumed that polymers are stable over a wide temperature range, despite thermal expansion [6].

For tissues fixation, methods are required keeping the morphology and analytes preserved. So, the main goal is to prevent protein autolysis and enzymatic degradation. The most commonly used fixing technique for tissue samples in histological databases is formalin fixation. Formaldehyde is inducing protein cross-linking by methylene bridges. The process stabilizes proteins and prevents enzymatic degradation. Lipids are washed out during the formalin infusion procedure, where the tissue is dehydrated in baths with decreasing alcohol content. For MSI experiments, proteins fixed in tissue have to be denatured to be accessible for desorption/ionization, similar to antigen retrieval established for histological analysis [7]. Physical and chemical treatments help to break cross-linking, besides the use of MS compatible detergents (e.g. Rapigest SF) [8]. Antigen-retrieval is also conducted by washing procedures or even microwave treatment [9]. Especially citric acid buffers and extreme pH values showed good success for reversing the effect of formalin fixation. Harsh washing procedures can be avoided by snap freezing of tissue using liquid nitrogen or isopentane [10]. However, the freezing process affects the tissues morphology. Additionally it has to be considered that frozen samples are less stable for long-term storage and not suited for bio bank sampling due to their poor morphological preservation.

As for microscopic or histological analysis, also for MSI tissue samples have to be mechanically stabilized and sectioned using microtomy. Histology has developed a huge variety of embedding media for tissue stabilization, which are now frequently used for MSI analysis as well. Paraffin, Optimal Cutting Temperature (O.C.T. TissueTek) and sucrose are the most frequently used, besides resins or gelatin. Paraffin provides very good morphological stability and analyte preservation and is the most commonly used medium for bio banks. Yet for MSI analysis paraffin residues induce high signal background. The described side effects can be reduced by extensive washing procedures to remove paraffin and also buffer residues. Low pH solvents combined with microwave treatment also reverse the extensive cross-linking. O.C.T. has been reported to show significant polymer background signals when used in MS applications. However, the embedding medium is water-soluble and can easily be removed by simple washing procedures. Analytes with good ionization properties, either highly concentrated or easier ionized than others (e.g. phosphatidylcholine), are less affected by the described interferences. Furthermore O.C.T. provides due to its water solubility very good compatibility with hydrophobic analytes, which are not affected by the washing procedures. The high viscosity and temperature dependent strength, features O.C.T. for biomaterial applications that need microtome sectioning. Mounting and sample fixation can easily be conducted without material interference or harming. A very ancient embedding medium is sucrose, which is used especially for ultra-cryo-microtomy. Sucrose is comparable easy to handle and removed due to its water solubility without interfering signals. Sucrose embedded tissue is rarely used, despite its convincingly fixation supporting properties [11] and high compatibility with MS [12].

The technology of microtome slicing is primarily used in histology and microscopy science for cutting tissue sections into thin slices for histological staining and morphological analysis. Microtome instruments are characterized by their rotary configuration, operating temperature and the least possible cutting thickness. For MSI analytical sample preparation the most important factors are reproducibility of the cutting process and the homogeneous surface, which is determined by the knife and the operator. Ceramic, diamond and stainless steel knives are favored, due to reduced sample smearing and stability. The main aim is to obtain representative cuts through cells in tissue

samples, respectively polymer structures in biomedical materials. Vertical resolutions through any sample can be obtained between 125 nm for cryo-sectioning and up to 40 µm, depending on sample stability. Obtaining ultra-thin sections, allows insight far below the cellular level by three-dimensional reconstruction of consecutive slices [13].

For MSI cut samples are mounted on indium tin coated (ITO) target surfaces or stainless steel MALDI targets. ITO targets are amongst the most commonly used surfaces in MALDI imaging due to their usability as transparent slides for microscopic analysis without a lack of conductivity obligatory for MALDI. The targets are coated with a very thin and robust conductive metal layer, which is sputtered in nm thickness on the glass. The surface resistivity lies between 20 and 200 Ω/sp and is sufficient for transmitting homogeneous electrical fields. Other target possibilities are the conventional stainless steel MALDI targets. Conventional microscopic glass slides used in histology, e.g. with lysine coating for improved sample attachment, are rarely used because of inefficient acceleration field application leading to reduced sensitivity. In many cases, samples have no adhesive properties, which is why conductive tape has to be used for surface attachment. Steel filaments are incorporated in a double-sided adhesive tape allowing proper sample mounting and efficient electrical field transfer.

For whole body samples or very fragile tissues, tape transfer is often used. The sample is covered with an adhesive tape before slicing to enhance sample stability [14]. To increase sample dimensions in space, stretching methods have been established and proved successfully for MSI analysis [15, 16]. Stretching the samples artificially increases the lateral resolution and adapts it to the determining laser diameter.

A critical point for sample and analyte stability is storage and thawing. As explained, most samples need storage temperatures below -20 °C. During thawing thin water films are induced by condensation very likely dislocating the analyte. Thawing under vacuum or air-drying under N_2 stream is therefore recommended [17].

Biological samples usually contain high amounts of salts [18]. Even though MALDI is a technique moderately sensitive to salt residues, removing salts clearly improves signals quality [19, 20]. A lot of established washing procedures exist for diverse analytical approaches. Many of them demand the removal of lipids to reduce ion suppression effects [21] towards proteins or peptides. Especially those lipids carrying natively charged head group, especially phospholipids are favored in ionization. Tissue washing procedures described for peptide and protein analysis therefore use alcohol baths to extract and remove lipids. The big advantage is, that also residues of embedding media are removed by the use of organic solvents. Ultra thin samples, however, might loose their adhesive properties and can be washed off.

The most critical point in sample washing procedures is again analyte dislocation. Formalin fixed samples have been reported to be very robust, whereas unfixed samples need cautious washing strategies, which do not harm morphology (e.g. strong acids or bases). Nevertheless, especially for peptide and protein analysis, sample washing can lead to a tremendous increase in ion signal yield [1]. Washing with 70-100 % ethanol leads to significant increases in intensity and signal to noise ratio for the higher mass range above 20 kDa [22]. Also lipid signals have been reported to benefit from washing cycles using ammonium formiate or ammonium acetate at specific pH [23, 24]. Removal of salts or interfering analytes is not the only goal for applying washing procedures. Acidic solvents easily remove histological stains, e.g. toluidine blue and hematoxylin/eosin stains, which will be discussed in the analyte identification section (see Chapter 4.a and 4.b).

Protein and peptide analysis conducted by MSI is inhibited by the sample's poor conductivity, the strong cross-linking of the fixation and the difficult accessibility of analytes due to their integration in tissue. Several strategies have been established to improve the accessibility of analytes for MS analysis, including enzymatic cleavage. In that approach proteins are reduced to a size, accessible for efficient desorption, ionization and detection. Additionally smaller peptides can be analyzed more easily regarding the amino acid composition by MS/MS sequencing compared to intact proteins. Trypsin has so far remained the most frequently used protease for enzymatic cleavage in MSI experiments. The cleaving sites for trypsin, arginine and lysine, are very frequent in every protein. As a consequence, accessibility of potential cleavage sites is improved and digestion is more efficient. Also combinations with other proteases, e.g. chymotrypsin or Lys C, lead to promising results, due to different cleaving sites, increasing overall information. However, pH values often do not fit the tissue properties and combined automatic data base search is not possible to date.

The most critical issue for "*on tissue*" digestion is finding the ideal conditions. Tissues are frequently stored in various buffer systems, throughout the fixation and embedding process. Washing procedures before enzymatic treatment, also have to adjust the pH according to the enzyme's preferences. Typically digestions applied in proteomics for in gel or in solution digestion include protein reduction and alkylation. This is often abandoned for MSI experiments because of poor disulfide bond accessibility and possible analyte dislocation during the treatment. Furthermore reducing agents and alkylation agents are not MS compatible and have to be removed before measurement, which introduces even more unsuitable sample handling steps. Yet analyte dislocation is still critical for the digestion process. The applied enzyme layer has to be kept moist to keep proteolytic activities. Enzymes are usually applied similar to the MALDI matrix, which will be discussed later (see Chapter 2.b). In general discrete spotting or homogeneous spray coating is used. The major problem with enzymatic treatment of tissue sections is the homogeneous accessibility of present proteins. Obtained peptide fragments are not supposed to have equally distributed accessible cleavage sites, which makes reliable localization difficult [25, 26]. The choice of inevitable washing procedures is also crucial for the information delivered. If no washing is applied, enzymatic autolytic products can be observed enhancing complexity of spectra. Furthermore dislocation or complete loss of generated peptides is possible. Remaining peptides however, are very likely retained in a preserved position, allowing insight to accessible cleavage sites of the respective protein. However, the loss of analytes is a critical issue in this case.

So far no qualification criterion has been developed for on tissue digestion protocols. The number of identified peptides necessary for valid identification is still under discussion and databases are being developed for identified peptides and proteins in MSI experiments on various tissue samples [27].

If samples have gone through the procedure of sample preparation with the final step of drying by vacuum desiccation or N_2 stream, matrix can be applied.

ii. Matrix deposition

Matrix application for MSI experiments favors small droplets applied in a reproducible manner ensuring perfect analyte incorporation and localization. The requirements for matrices used in MSI experiments are rather similar to general MALDI applications [1]. Analyte compatibility is the major determining factor of choice as well as homogeneous crystallization properties. For MSI, maybe the solvent system is of even higher influence. Solvent systems are ideally very quickly evaporating to

accelerate matrix crystallization, however, they have to induce efficient analyte solvation. The balance between dissolving and delocalizing the analyte of interest is of high importance.

For positive ion analysis, especially peptides and proteins, trifluoroacetic acid addition in proportions between 0.1 and 1 % has been reported to efficiently increase ionization yield for MSI [28] as already experienced for conventional MALDI measurements of peptides or proteins. Matrices commonly used for MALDI applications such as CHCA, SA or DHB are used for MSI experiments, too. However, the applied concentrations are much higher. For MSI analysis the described matrices are often used at saturated levels, which are 10-15 mg/mL for CHCA, 10-30 mg/mL for SA and more than 50 mg/mL for DHB dissolved in acetone or acetonitrile, all commonly used for proteomic MSI approaches [29-31]. Many matrices have been evaluated for their qualities in MSI applications, especially 1,5-diaminonaphtalene, aminoacridine, azathiothymin and coumaric acid are often mentioned matrices [32, 33]. The use of ionic liquid matrices is often reported for analytes with critical ion yield. CHCA in combination with N,N-dimethylaniline is most likely reported besides 2-amino-4-methyl-5-nitropyridine. Those matrices were reported to show improved ionization properties combined with increased signal to noise ratios and quantitatively increased signals [34]. However, most ionic liquid matrices are not stable under high vacuum conditions [35]. MSI experiments with large sample areas measured at high resolution are therefore critical due to progressive but unpredictable loss of signal intensities. The possibility of application to atmospheric pressure MALDI however proved successfully, even for repeatedly MSI analysis [36]. In general the matrix and the analyte itself are limiting factors, often of unknown stability [37].

To improve ionization qualities for lipids, besides the use of metal additives, the use of graphite nanoparticle and carbon tube coatings has been under recent investigation [38, 39]. The idea of sputtering metal on tissue surfaces to enhance conductivity and provide a homogeneous layer of potential adducts for better ion formation reveals furthermore good properties to reduce charge effects for large tissue areas. Gold molecules directly on the surface layer of matrix are reported to neutralize tissue electrostatic effects and therefore improve signal quality. Certainly, those techniques are still rarely used [40]. Furthermore it has been demonstrated that adding potential adduct forming salts to the matrix solution, e.g. lithium or silver, increased the fragmentation efficiency for lipids, which is often beneficial for identification within an MSI experiment with low abundant analytes [41]. Lithium cluster formation proved even more efficient to aid lipid analysis, when tissue is already incorporated in embedding medium [42].

For matrix application a large variety of commercially available or in-house built sample preparation techniques have been developed and discussed [43]. Matrix is the crucial step during MALDI-MSI sample preparation. The applied matrix layer is determining the validity of abundance distribution for detected analytes. Matrix crystals, as a consequence of their size, position and shape limit the lateral resolution of a MSI experiment. During the crystallization process the efficiency of analyte incorporation is highly influenced by analyte solubility in the solvent system. The variety of parameters impacting good analyte incorporation (e.g. temperature, humidity etc.) are therefore defining the experimental quality and have to be individually optimized for each analyte and experiment [44-46].

For MSI experiments matrix can be applied discretely or continuously by manual, automatic or physicochemical methods. Manual matrix application is due to the high minimal volume of 0.1 µL not favorable. Crystallization is very inhomogeneous and similar to conventional MALDI experiments ring

effects with intense matrix clusters at the rim of the deposited droplet are observed [47-49]. Furthermore the large solvent volumes are very likely to induce analyte dislocation during crystallization and solvent evaporation as a consequence of the large droplet diameter (above 200 µm), which also increases lateral resolution far beyond the laser diameter.

For liquid matrix application spraying is an obvious possibility. Airbrush devices usually form very small droplets terminated by the nozzle orifice. The critical issues for all airbrush applications are comparability and reproducibility. Angle adjustment, spraying distance, spraying pressure and air supply are parameters, which can be adjusted by the user but not in a highly regulated manner. The method in general is very easy to learn, however, differences between the users' experiences are significantly influencing comparability. Besides, for airbrush applications a much higher solvent, respective matrix volume is necessary (liquid loss during spraying and at vessel surfaces). For matrix application gentle movement is necessary to cover the whole sample homogeneously and to provide enough time for solvent evaporation. Technically this is either realized by moving the sprayer over a static sample plate or by moving the sample plate at static sprayer position, both in horizontal or vertical position. Despite all critical issues, a lot of interesting MSI investigations were successfully published revealing the power of matrix application using an airbrush.

Besides those very simple application methods further strategies for liquid or dry matrix deposition have been developed. In particular chemical inkjet printing and sublimation will be presented. Fig. 3 gives an overview of the hardware and operating principal of the matrix applications used in the present thesis. Furthermore SEM images are presented to demonstrate crystal size and homogeneity of applied matrix layers.

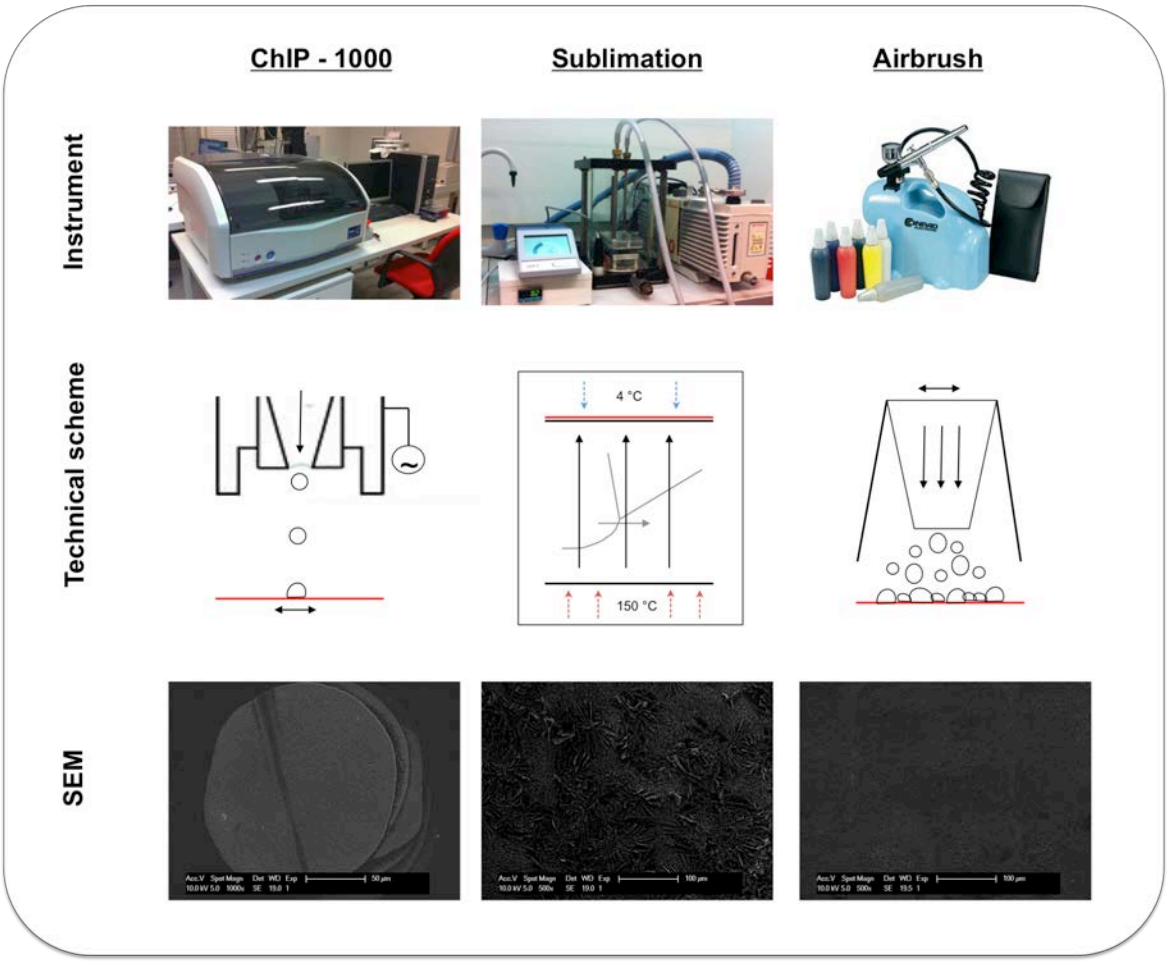

Figure 3: The 3 most common MALDI matrix application techniques: chemical inkjet printing (ChIP-1000), sublimation and airbrushing. Instrumentation, basic principals of matrix application and SEM analysis of matrix droplets are outlined.

1. Piezo printing (ChIP-1000)

The Chemical Inkjet Printer (ChIP-1000) was developed based on findings that precise matrix application of preferably low volumes leads to favorable analyte incorporation in MSI experiments. Several in house built devices designed similar to the ChIP-1000 proved the quality of MSI results and thus showed good desorption for peptides and lipids [50, 51].

The ChIP-1000 is working with piezo crystal print heads [52]. The design of the modified inkjet printer consists of a sample holder carrier, placed on a mechanical unit moving the sample to either the camera unit for sample acquisition or the printing unit for matrix droplet deposition (Fig. 3). For solvent deposition, MALDI matrix or enzyme application, small droplets are favorable to ensure solvent vaporization before diffusion, yet efficient analyte mobilization from deeper parts of the tissue to sufficiently desorb and ionize molecules. The precise application was realized by embedding a piezoelectric element in the print head. The piezoelectric effect causes mechanical pressure to induce an electric field in crystals, or any piezoelectric material, as a result of reconfiguration of dipole moments or rearrangement of dipole molecules within the material. Piezoelectricity combines the materials electrical behavior and the electrical charge density displacement and strain. In principal any crystal, with no magnetic point group that has a symmetric center can be piezoelectric. Polarization by mechanical stress leads to an electrical field and backwards (converse piezoelectric

effect). The induced change in length is proportional to the applied electrical field according to the Hooke's law [53, 54]. In the ChIP-1000 the print head unit, made of stainless steel and containing the piezo element, is connected to a power source and a vacuum pump. A high backpressure is necessary to ensure no liquid loss and enable droplet formation. Using the converse piezoelectric effect, voltage is transformed to mechanical movement, which is proportional to the distance between the applied electrodes. Initially a low amplitude and high frequency is necessary to induce ideally conducted movement. To fulfill the described technical requirements, a glass capillary micro jet device with a 55 µm orifice was implemented. Droplets can be deposited with a minimal volume of 87 pL, resulting in droplets with 55 µm cross section dimension according to the manufacturer. Depending on the application the user can choose the pitch size (distance between two deposited spots) and the print mode (routine, area mode, iterative, random), both determined by the volatility of the solvent system chosen.

Not only has the ChiP-1000 been demonstrated to lead to enhanced ionization and desorption quality, it has also been used in enzyme application [55]. Enzymes and proteins of choice can be applied in defined areas before MALDI matrix is deposited on exactly the same position. For peptide analysis after enzymatic treatment of tissue using the ChIP-1000, the number of peaks detected was increased significantly as well as the average peak amplitude [25].

2. Sublimation

Sublimation is also referred to as endothermic phase transition, the process were solid substances transit directly to the gas phase without any liquid intermediate phase. The transition between solid and vapor phase can be calculated by the Clapeyron equation, correlating temperature and pressure [56, 57]. For MALDI matrix application, sublimation is relevant as phase transition of matrix molecules from solid to gas and back again to solid phase, latter including the deposition process.

Sublimation is a sufficient solvent free matrix application technique for analytes, which are easily accessed. If analytes are strongly cross-linked and embedded in tissue, solvents are often necessary to mobilize them and enhance matrix incorporation. This might also be necessary for analytes, which are difficult to analyze due to their ionization properties, e.g. glycosylated peptides, glycans or proteins. The addition of TFA, often added as a supportive additive for protonation, is however not possible in solvent free matrix application. Yet the dry deposition is very sufficient for surface located analytes with good ionization characteristics (e.g. phosphatidylcholine).

For MSI experiments, due to the large variety of sample surface parameters and qualities, analyte incorporation is often difficult and matrix crystallization itself is influenced by the samples and the choice of matrix. Therefore sublimation provides especially for very hydrophobic surfaces, e.g. polymers, the possibility to homogeneously cover larger areas in a short time in a solvent free approach. The method is also of high interest for very instable analytes that would otherwise suffer from long processing times during MALDI matrix application. Crystallization after sublimation provides very small crystals, which usually also directly affects the lateral resolution in MSI experiments. For sublimation the lateral resolution is assumed to be limited only by the laser properties but not crystal size. For DHB very small crystal diameters below a few µm are observed, compared to the long needle shaped crystals induced by liquid DHB application. The most essential benefit is of course the solvent free application over larger areas as even very little amounts of solvent can lead to analyte diffusion [33, 58, 59].

However, sublimation also suffers from several drawbacks and limitations. The process of sublimation depends on matrix properties. Most commonly used matrices are not adaptable to the sublimation process, since phase transition is beyond the operation range regarding temperature and pressure. Studies, screening for potential matrix candidates for lipid analysis evaluated 12 different matrices, revealing only two of them as sufficient regarding vacuum stability, cluster formation and ionization efficiency. 1,5-diaminonaphtalene and DHB were found to be effective candidates for lipid detection in positive and negative mode, providing sufficient vacuum stability and sublimation properties [60]. Most other candidates were excluded due to difficulties in the sublimation process or poor ionization/desorption efficiency. For proteins and peptides sinapic acid was investigated to be sufficient for reproducible analysis at high resolution [61].

To date sublimation devices used for MSI experiments are in house built. Figure 3 shows an in house built device at the Erasmus Centre Rotterdam [62] consisting of a sublimation chamber, a vacuum control system and a vacuum pump. Samples are placed in the sublimation chamber on the upper target holder. Matrix dissolved in organic solvent systems is deposited on the heating plate. Applying heat and vacuum allows the matrix to sublimate and recrystallize on a cooled sample surface.

b. MALDI-TOF

MALDI-TOF is the most frequently used instrumental configurations for MSI approaches, despite the use of less common set ups, e.g. MALDI combined with fourier transformation ion cyclotron resonance (FT-ICR) MS, quadropole/ion trap TOF MS or Orbitrap MS. The broad dynamic range, good sensitivity and high flexibility make TOF a suitable approach for a large variety of MSI questions. For MSI experiments, the quick accessibility of analytes combined with a short analysis time is essential, as large tissue areas should be analyzed under the same conditions.

For most commercially available MALDI-TOF instruments a software user interface is provided for proper MSI experiment setup. In a MSI experiment, samples are scanned step-by-step, accumulating mass spectra for each position. The complete signal information is processed to obtain abundance distribution information for each detected m/z signal. The analyzed grid, defined for the whole area, is constant in spatial resolution. Ion signals are extracted from the data set and their intensities are plotted as a function of positions for the whole defined area. The technically untaught approach provides specific molecular images for every signal detected in the defined area. Defining spots, which can be localized by light microscopy and MS analysis, enhances accuracy of histological data correlation especially at high lateral resolution and homogeneous sample structure.

Two definitions are important for MSI analysis: MS profiling and MS imaging [63]. Profiling experiments aim at obtaining general information at very low spatial resolution. The analyte's localization is not the primary intention but obtaining meaningful spectral pattern is intended. Data acquisition may be stochastically only to compare large data sets of lipid or protein MS profiles in tissue e.g. regarding their species or pathology. Imaging on the contrary, obtains information for each defined spot within an x/y array at preferably high spatial resolution. Large amounts of data points are gathered to localize all detected analytes and compare regional variation.

Within the MALDI process, as described the laser interacts with matrix molecules to transmit energy to the analyte. However, in MSI experiments the laser interacts not only with the analyte, but also with its environment, i.e. biological tissue or polymer material. Matrices have been reported to absorb and transform energy to different extent and similar observations have been made for tissue

structures. Form laser surgery it is known that different tissue structures react diversely to laser energy [64, 65]. So, depending on the molecular composition, the laser energy is absorbed with varying effectiveness by the biological material. The laser fluence is therefore a critical parameter for MSI experiments. Tissue can easily be burned by high laser energy absorption, resulting in different abundance profiles for particular sensitive regions, e.g. adipose regions are more affected by ablation due to the laser irradiance than septum. Fig. 4 visualizes the influence of thermal sample properties on the ablated area in correlation to different laser diameters. Comparing thermal paper to formalin-fixed paraffin embedded (FFPE) cancerous tissue, cut at 5 µm and covered with MALDI matrix (CHCA 6 mg/mL in ACN/0.1 % TFA, 50/50, v/v), reveals significant differences of laser spot diameters and profiles under identical parameters. In our experience but also taken from surgical reports, FFPE tissue is much more stable towards laser irradiation, meaning that less material is ablated. Even though it is not determined exactly to what extent the desorption/ionization process is affected, it can be assumed that heterogeneous tissue structures also respond slightly different to the laser.

The laser diameter itself is a critical parameter, determining lateral resolutions of MSI experiments. For MSI more often Nd:YAG lasers or Nd:YAG laser with modified profiles are used. The smallest laser profile available for efficient but non-destructive analyte ablation is reported between 5 and 10 µm [66]. If however, the material is negatively affected by the laser energy or the applicable laser diameter is higher than intended, oversampling is a possible method to technically increase the spatial resolution [67, 68]. Oversampling means that the raster increment of the sample stage movement is smaller than the actual laser diameter with complete ablation of matrix at every pixel. Therefore for each spot a defined percentage of the area is completely matrix free leading consequently to no ion current, respectively no signal from this area. This effectively increases the lateral resolution of an MSI experiment without altering the laser spot size. However, the technique is very good applicable for analytes with good ionization/desorption qualities or if the mass window is limited to one particular analyte of interest.

Laser/sample interaction is a critical topic for biological as well as biomaterial samples. The high energy may not cause only disruption in tissue samples, but may also induce hydrolysis, radical formation or carbon cluster formation in polymer material [69]. Yet it is not possible to differentiated between analytes and unwanted by-products induced by the laser energy *per se* in a mass spectrum, false conclusion can be drawn.

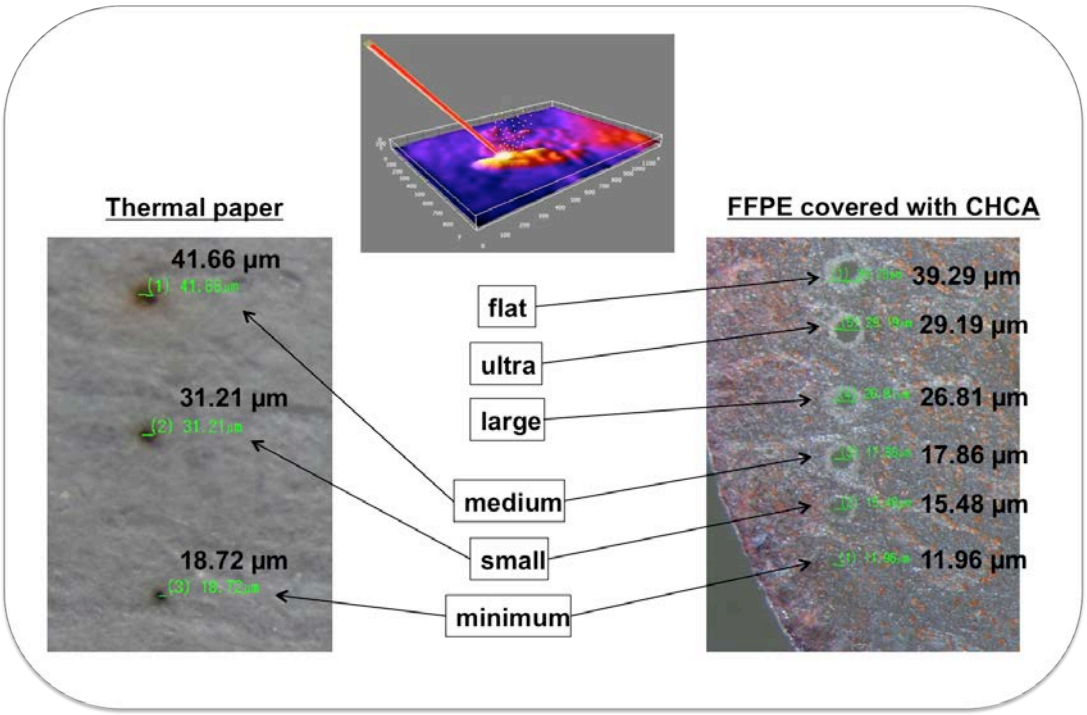

Figure 4: Evaluation of the SmartBeam [70] laser diameter on thermal paper and FFPE tissue (thickness 5 µm covered with CHCA.

MSI using TOF mass analyzers implies difficulties for mass accuracy. As described, TOF mass analysis is highly affected in accuracy by the internal energy distribution of desorbed ions. The energy spread is even more tremendous, if ions start at different initial points of localization. Methods for internal calibration or recalibration based on internal standard have been reported but also m/z adjustment after correlating results with classical proteomics approaches (i.e. bulk analysis of tissue samples after digestion and chromatographic separation). Introducing internal standards bears the problem of probably higher ionization efficiencies for the standards or ion suppression effects, both leading to information loss. m/z adjustment after comparison with results from orthogonal, proteomics methods is especially suitable for peptides but difficult for other species. This approach has the further advantage that the use of peptides generated by enzymatic digestion as internal standard does not lead to unpredictable ion suppression effects [71]. Both mentioned approaches are however, limited to samples with sufficiently available quantities.

Mass accuracy can be increased by decoupling the ion source from the TOF analyzer, e.g. oTOF instruments as described earlier (see Chapter 1.b.iii). Other possibilities include instruments providing higher accuracy, e.g. Orbitrap or FT-ICR MS [40]. Approaches to estimate mass deviation theoretically and for MSI applications are presented in the present thesis (see Chapter 2.).

Accurate analyte identification is often linked to the interest in quantitation. The use of MALDI-TOF MS for quantification or at least relative quantification has controversially been discussed. Quantification is difficult because of described effects (e.g. ion suppression, tissue ablation, ionization efficiencies in tissue) or eventual matrix hot spots. Studies evaluating the quantification properties of ion intensities, compared standard peptides with defined analyte concentration in complex mixtures and came to the conclusion that isotopic labeling represents the most accurate and reliable possibility to try relative quantifying peptides [72]. Other approaches include algorithms for the calculation of peptide ionization efficiency and signal response to quantify urinary biomarkers

[73]. MSI approaches also included the correlation with quantitative LC-MS data to obtain reliable methods based on ion response determination for small molecules [74, 75].

c. Data analysis

The basic principal of MSI analysis is, to qualitatively and ultimately also quantitatively visualize distributions of selected ion signal abundances. Data visualization is simple and easy to conduct, if no particular processing is intended, using e.g. MATLAB, R or any other software capable of reading out DICOM source code. Each instrument supplier provides additional software for MSI workflow and data analysis. Visualization based on signal or region selection are state of the art, however, further data processing for individual applications is often required to improve signal and image quality. Comparisons of different MSI instruments or even different technical approaches, e.g. computer tomography or positron emission tomography are further required to comprehensively analyze data.

One of the first open source approaches combining all kinds of data formats with the possibility to analyze, process and correlate differently sources images was Biomap [76]. Biomap is capable of reading DICOM as well as MSI files after conversion and therefore covers almost all applications of interest regarding imaging. Biomap enables spectrum and position based visualization as well as 3-dimensional (3D) reconstruction of multi-dimensional data sets [77] and the definition of regions of interest (ROI). However, the large data packages and data sets lead to new requirements, including also data processing tools tailored for MSI instrumentation and application. Nevertheless Biomap was never intended to be of public use and never programmed in a user friendly way. Therefore it was never fully accepted in the MSI community for 3D reconstruction and multidimensional data sets.

Bruker provided one of the first commercially available, however instrument based, software tools for data processing combined with statistical analysis (FlexImaging, ClinProt, Bruker, Germany). Even though the basic processing tools of data normalization, which will be discussed later on, are implemented, the software is limited in spatial pixel resolution to 10 µm and large data sets beyond a few GB cannot be processed sufficiently (despite user defined data reduction sets). ClinProt, the associated statistical tool for performing cluster analysis or principal component analysis, also shows limitation for data size (only a few GB of data can be processed). Waters, providing an MSI solution including ion mobility data solved the problem of large data sets also by user defined data reduction mechanisms, however, so far does not provide any statistical analysis tools.

Consequently for instrumental comparison, individual data processing or normalization and statistical analysis open source software solutions were developed addressing different analytical requirements.

The main approach for instrumental comparison is to find a compatible data format, which can be read by the software of choice, contains the raw and unprocessed data and provides small data size. imzML was introduced as data format at the Justus Liebig University in Germany by Andreas Römpp [78] in parallel to the Datacube Explorer (DCE) developed at the FOM-AMOLF institute by Ivo Klinkertin the Netherlands [79]. The combination of both allowed a very efficient way of data reduction, enabling data storage, visualization, handling and transfer with high compatibility. To date data conversion executives are available for all commercially available instruments.

Data processing, independent from the software used, intends to enhance image quality and reduce eventual blurred areas affected by unwanted background signals. The basic features are similar to conventional MS spectra processing: smoothing and baseline subtraction. The most commonly used smoothing algorithms are Gaussian and Savitzky-Golay. Whereas Gauss attempts median based correction, which favors the higher mass range above a few kDa, Savitzky-Golay algorithms performs least square regression, enhancing monoisotopic resolved data sets. Baseline correction is applied to redefine the eventually "drifted" baseline due to high interfering signal background, e.g. paraffin.

For MSI data normalization applied to the whole data set is relevant to reduce pixel-to-pixel variation. Those variations occur due to inhomogeneities on the sample surface, e.g. caused by matrix cluster formation leading to increased or decreased signal intensities, or ion suppression effects. To obtain a normalized data set, each spectrum is divided by the calculated normalization factor *f*. Route-mean-square (RMS), total ion current (TIC) and median normalization are the most commonly used algorithms. RMS normalization (Equ. 6) is one of the first algorithms implemented for MSI approaches, providing good spectral denoising for homogeneous samples by summing up the RMS for all data points *y*, divided by the number of spectra. Its pitfall is the sensitivity to strong outliers, which are not detected and the general favoring to display intense signals.

$$f = \sqrt{\frac{y_1^2+y_2^2+\cdots+y_n^2}{n}} \qquad (6)$$

For calculating the TIC normalization factor (Equ. 7) the mean of all data points is calculated. Considering the spectral area is sufficient for reducing noise, however this approach is rather insensitive to peak intensity variations.

$$f = \frac{y_1+y_2+\cdots+y_n}{n} \qquad (7)$$

For median normalization, simply the median of all data points is calculated (Equ. 8). For this algorithm it is necessary that all data points are included and not cut off or excluded during baseline subtraction. Therefore it is very efficient for noise reduction and very robust towards artifacts, except if no signal and consequently no noise is generated.

$$f = median(y_1, y_2, \ldots, y_n) \qquad (8)$$

Other normalization algorithms, e.g. peak picking, exclude one major peak from proportional abundance calculations. Frequently matrix cluster signals are chosen, due to their intensive signals [80]. Comparison of normalization algorithms implemented in commercially available software revealed that processing methods, which not only include intensity values, but also peak shapes, performed best for obtaining reliable results [81, 82]. Besides sufficient data normalization the large size of average data sets for one singular run is problematic for soft- and hardware processing [83]. As a consequence, statistical data analysis is, despite a few exceptions, e.g. SCiLS Lab (SCiLS GmbH, GER), outsourced to other programs or implemented in the context of Matlab or R analysis.

d. Statistical data analysis

Within MSI experiments, a large amount of signals are detected originating either from actual analytes but also from unwanted background (i.e. polymer clusters, salts or like wise). It is therefore necessary to correctly determine the analyte of interest or even areas of interest.

For large data sets automated analysis is in many cases essential. For MSI data this means that analyte differentiation from less interesting signals for large sample numbers is necessary but also the analytes' spatial differentiation within only one sample are obligatory. Statistical analysis is already automated and can also be applied to MSI data.

Statistical analysis methods can be divided into supervised and unsupervised approaches. Unsupervised analysis does not require any previous knowledge about the data set and is often used for obtaining general information about structures in data sets. Supervised methods are most often used for classification and require previous assignment of certain features for each data set.

The currently most frequently used statistical classification method is known as principal component analysis (PCA). PCA aims at transferring the huge complexity of influencing parameter, e.g. m/z values, into a different and simpler coordinate system. For this each value is averaged and its aberration calculated (Equ. 9 and 10) before the transformation value is calculated (Equ. 11).

$$\bar{x} = \frac{1}{n} \sum_{i=1}^{n} x_i \qquad (9)$$

$$S = \frac{1}{n} \sum_{i=1}^{n} (x_i - \bar{x})(x_i - \bar{x})^T \qquad (10)$$

$$s_{ij} = \gamma_j^T \, (x_i - \bar{x}) \qquad (11)$$

Based on those calculations principal components are identified, which can be single or groups of m/z values or particular regions. However, PCA scores are still part of a mathematical model, which can also providing negative scores theoretically. Detailed examination of statistical results is consequently mandatory.

Statistical analysis can also be used to find similarities. Grouping spectra, or data in general, according to their similar profiles is referred to as cluster analysis. Similarity factors (Formula 12) or distances are introduced based on the squared difference between obtained comparable data points.

$$\boldsymbol{d_{ij}} = \sqrt{(\boldsymbol{x_{i1}} - \boldsymbol{x_{j1}})^2 + (\boldsymbol{x_{i2}} - \boldsymbol{x_{j2}})^2 + \cdots + (\boldsymbol{x_{ip}} - \boldsymbol{x_{jp}})^2} \qquad (12)$$

Based on those calculations mass spectra from different positions are grouped together to obtain regional information. For results visualized in dendrogramms, which can be rearranged, those classification systems are defined as hierarchical cluster analysis. Those algorithms are also frequently used for image segmentation.

Despite the described statistical methods, several other approaches, e.g. factorizing methods or fuzzy clustering, have been discussed for their effect on data analysis in MSI experiments. The discussion of tactical classification algorithms is valuable for the identification of biomarkers and

disease classification based on large data cohorts, due to the data extraction, not possible applying manual data interpretation. However, the valuable effect can further be applied to reduce noise and bias and improve image quality for further analysis [84].

For all described data processing steps, the crucial problem is the data set size, which will definitely lead to new challenges, developments and requirements for MSI experiments [84-86]. Multivariate data analysis to classify healthy and cancerous tissue was successfully established based on data reduction and consideration of signal groups allowing even further intra-tumor specific differentiation for kidney tissue [87]. Comparable validated prediction models further allow the application large sets of completely unknown samples.

References

1. Nimesh, S., et al., *Current status and future perspectives of mass spectrometry imaging.* Int J Mol Sci, 2013. **14**(6): p. 11277-301.
2. Kaletas, B.K., et al., *Sample preparation issues for tissue imaging by imaging MS.* Proteomics, 2009. **9**(10): p. 2622-33.
3. Qing, Z., et al., *Relationship of advanced oxidative protein products in human saliva and plasma: age- and gender-related changes and stability during storage.* Free Radic Res, 2012. **46**(10): p. 1201-6.
4. Pasella, S., et al., *Pre-analytical stability of the plasma proteomes based on the storage temperature.* Proteome Sci, 2013. **11**(1): p. 10.
5. Passi S, C.S., Tiano L, Littarry G P, *Dynamics of lipid oxidation and antioxidant depletion in Mediterranean fish stored at different temperatures.* Biofactors, 2005. **25**(1-4): p. 241-244.
6. Oral, E., et al., *Diffusion of vitamin E in ultra-high molecular weight polyethylene.* Biomaterials, 2007. **28**(35): p. 5225-37.
7. Otali D, S.C.R., Oelschlager D K, Wan W, Manne U, Watts S A, Grizzle W E, *The Combined Effects of Formalin Fixation and Individual Steps in Tissue Processing on Immuno-Recognition.* Biotech Histochem., 2010. **84**(5): p. 223-247.
8. Chaurand, P., et al., *Imaging mass spectrometry of intact proteins from alcohol-preserved tissue specimens: bypassing formalin fixation.* J Proteome Res, 2008. **7**(8): p. 3543-55.
9. Shi, S.R., M.E. Key, and K.L. Kalra, *Antigen retrieval in formalin-fixed, paraffin-embedded tissues: an enhancement method for immunohistochemical staining based on microwave oven heating of tissue sections.* J Histochem Cytochem, 1991. **39**(6): p. 741-8.
10. Zaima, N., et al., *Matrix-assisted laser desorption/ionization imaging mass spectrometry.* Int J Mol Sci, 2010. **11**(12): p. 5040-55.
11. Jovanovic N, B.A., Hofland G W, Witkamp G J, Crommelin D J A, Jiskoot W, *Distinct effects of sucrose and trehalose on protein stability during supercritical fluid drying and freeze-drying.* European Journal of Pharmaceutical Sciences, 2006. **27**(4): p. 336-345.
12. Palmer, A.D., et al., *Sucrose cryo-protection facilitates imaging of whole eye sections by MALDI mass spectrometry.* J Mass Spectrom, 2012. **47**(2): p. 237-41.
13. Trese D, S.S., Becker M, Wirtz S, Steinhorst K, Strehlow J, Aichler M, Kobarg J H, Oetjen J, Dyatlov A, Heldmann S, Walch A, Thiele H, Maass P, Alexandrov T, *Exploring Three-Dimensional Matrix-Assisted Laser Desorption/ Ionization Imaging Mass Spectrometry Data: Three-Dimensional Spatial Segmentation of Mouse Kidney.* Analytical chemistry, 2012. **84**: p. 6079-6087.
14. Goodwin R J, N.A., Borg D, Langridge-Smith P R, Harrison D J, Mackay C L, Iverson S L, Andren P E, *Conductive carbon tape used for support and mounting of both whole animal and fragile heat-treated tissue sections for MALDI MS imaging and quantitation.* Journal of Proteomics, 2012. **75**(16): p. 4912-4920.
15. Zimmerman T A, R.S.S., Sweedler J V, *Mass spectrometry imaging using the stretched sample approach.* Methods Mol Biol, 2010. **656**: p. 465-479.
16. Tucker, K.R., et al., *Stretched tissue mounting for MALDI mass spectrometry imaging.* Anal Chem, 2011. **83**(23): p. 9181-5.
17. J, G.R., *Sample preparation for mass spectrometry imaging: small mistakes can lead to big consequences.* J Proteomics, 2012. **75**(16): p. 4893-4911.
18. Mahboob, T., M. Mumtaz, and M.A. Haleem, *Electrolyte content of serum, erythrocyte, kidney and heart tissue in salt induced hypertensive rats.* Life Sci, 1996. **59**(9): p. 731-7.
19. Berman, E.S., et al., *Preparation of single cells for imaging/profiling mass spectrometry.* J Am Soc Mass Spectrom, 2008. **19**(8): p. 1230-6.

20. Wang, H.Y., C.B. Liu, and H.W. Wu, *A simple desalting method for direct MALDI mass spectrometry profiling of tissue lipids.* J Lipid Res, 2011. **52**(4): p. 840-9.
21. van Hove, E.R., et al., *An alternative paper based tissue washing method for mass spectrometry imaging: localized washing and fragile tissue analysis.* J Am Soc Mass Spectrom, 2011. **22**(10): p. 1885-90.
22. Mainini, V., et al., *Detection of high molecular weight proteins by MALDI imaging mass spectrometry.* Mol Biosyst, 2013. **9**(6): p. 1101-7.
23. Angel, P.M., et al., *Enhanced sensitivity for high spatial resolution lipid analysis by negative ion mode matrix assisted laser desorption ionization imaging mass spectrometry.* Anal Chem, 2012. **84**(3): p. 1557-64.
24. Elis S R, B.S.H., In Het Panhuis M, Blanksby S J, Mitchell T W, *Surface analysis of lipids by mass spectrometry: more than just imaging.* Prog Lipid Res., 2013. **52**(4): p. 329-353.
25. Stauber, J., et al., *On-tissue protein identification and imaging by MALDI-ion mobility mass spectrometry.* J Am Soc Mass Spectrom, 2010. **21**(3): p. 338-47.
26. MacAleese, L., J. Stauber, and R.M. Heeren, *Perspectives for imaging mass spectrometry in the proteomics landscape.* Proteomics, 2009. **9**(4): p. 819-34.
27. McDonnell, L.A., et al., *MSiMass List: A Public Database of Identifications for Protein MALDI MS Imaging.* J Proteome Res, 2013.
28. Schwamborn, K. and R.M. Caprioli, *Molecular imaging by mass spectrometry--looking beyond classical histology.* Nat Rev Cancer, 2010. **10**(9): p. 639-46.
29. Sugiura, Y., S. Shimma, and M. Setou, *Two-step matrix application technique to improve ionization efficiency for matrix-assisted laser desorption/ionization in imaging mass spectrometry.* Anal Chem, 2006. **78**(24): p. 8227-35.
30. Taverna, D., et al., *Spatial mapping by imaging mass spectrometry offers advancements for rapid definition of human skin proteomic signatures.* Exp Dermatol, 2011. **20**(8): p. 642-7.
31. Gode, D. and D.A. Volmer, *Lipid imaging by mass spectrometry - a review.* Analyst, 2013. **138**(5): p. 1289-315.
32. Zimmerman, T.A., et al., *An analytical pipeline for MALDI in-source decay mass spectrometry imaging.* Anal Chem, 2011. **83**(15): p. 6090-7.
33. Thomas A, C.J.L., Fournaise E, Chaurand P, *Sublimation of new matrix candidates for high spatial resolution imaging mass spectrometry of lipids: enhanced information in both positive and negative polarities after 1,5-diaminonapthalene deposition.* Anal Chem, 2012. **84**(4): p. 2046-54.
34. Meriaux, C., et al., *Liquid ionic matrixes for MALDI mass spectrometry imaging of lipids.* J Proteomics, 2010. **73**(6): p. 1204-18.
35. Steven R T, R.A.M., Bunch J, *para-Nitroaniline is a Promising Matrix for MALDI-MS Imaging on Intermediate Pressure MS Systems.* J Am Soc Mass Spectrom, 2013. **24**: p. 801-804.
36. Steven R T, B.J., *Repeat MALDI MS imaging of a single tissue section using multiple matrices and tissue washes.* Analytical and Bioanalytical Chemistry, 2013. **405**(14): p. 4719-4728.
37. Tarzi O I, S.L., Arguello J E, Oksdath-Mansilla G, Erra-Balsells R, *Photochemical and Thermal Stability of Some Dihydroxyacetophenones Used as UV-MALDI-MS Matrices.* Photochemistry and Photobiology, 2013. **89**(6): p. 1368-1374.
38. Cha, S. and E.S. Yeung, *Colloidal graphite-assisted laser desorption/ionization mass spectrometry and MSn of small molecules. 1. Imaging of cerebrosides directly from rat brain tissue.* Anal Chem, 2007. **79**(6): p. 2373-85.
39. Liu Q, X.Y., Pagan-Miranda C, Chiu Y M, He L, *Metabolite Imaging Using Matrix-Enhanced Surface-Assisted Laser Desorption/Ionization Mass Spectrometry (ME-SALDI-MS).* Journal of the American Society for Mass Spectrometry, 2009. **20**(1): p. 80-88.
40. Taban I M, M.A.A.F., van der Burgt Y E M, McDonnel L A, Heeren R M A, Fuchser J, Baykut G, *Imaging of Peptides in the Rat Brain Using MALDI-FTICR Mass Spectrometry.* J Am Soc Mass Spectrom, 2007. **18**(1): p. 145-151.
41. Cerruti, C.D., et al., *MALDI imaging mass spectrometry of lipids by adding lithium salts to the matrix solution.* Anal Bioanal Chem, 2011. **401**(1): p. 75-87.

42. Griffiths, R.L., et al., *Formal lithium fixation improves direct analysis of lipids in tissue by mass spectrometry.* Anal Chem, 2013. **85**(15): p. 7146-53.
43. Tu, T. and M.L. Gross, *Miniaturizing sample spots for matrix-assisted laser desorption/ionization mass spectrometry.* Trends Analyt Chem, 2009. **28**(7): p. 833-841.
44. Vegvari, A., et al., *Essential tactics of tissue preparation and matrix nano-spotting for successful compound imaging mass spectrometry.* J Proteomics, 2010. **73**(6): p. 1270-8.
45. Shimma, S., et al., *Alternative two-step matrix application method for imaging mass spectrometry to avoid tissue shrinkage and improve ionization efficiency.* J Mass Spectrom, 2013. **48**(12): p. 1285-90.
46. Franck, J., et al., *Improving tissue preparation for matrix-assisted laser desorption ionization mass spectrometry imaging. Part 1: using microspotting.* Anal Chem, 2009. **81**(19): p. 8193-202.
47. Wang, J., et al., *Advancing matrix-assisted laser desorption/ionization-mass spectrometric imaging for capillary electrophoresis analysis of peptides.* Anal Chem, 2011. **83**(9): p. 3462-9.
48. Puolitaival, S.M., et al., *Solvent-free matrix dry-coating for MALDI imaging of phospholipids.* J Am Soc Mass Spectrom, 2008. **19**(6): p. 882-6.
49. Chen Y, A.J., Liu Y, Wang E, Cachon-Gonzalez B, Cox T M, Merrill A H Jun, Sullards M C, *Imaging MALDI Mass Spectrometry Using an Oscillating Capillary Nebulizer Matrix Coating System and Its Application to Analysis of Lipids in Brain from a Mouse Model of Tay-Sachs/Sandhoff Disease.* Anal Chem, 2008. **80**(2780-2788).
50. Sloane A, D.J.L., Wilson N L, Gandhi P S, Hill C J, Hopwood F G, Smith P E, Thomas M L, Cole R A, Packer N H, Breen E J, Cooley P W, Wallace D B, Williams K L, Gooley A A, *High Throughput Peptide Mass Fingerprinting and Protein Macroarray Analysis Using Chemical Printing Strategies.* Molecular & Cellular Proteomics, 2002. **1**(7): p. 490-499.
51. Ryu J, B.G., Lee J H, Choi S H, Jung YS, Kim K P, Kim Y H, Kim H K, *Lipid MALDI MS Profiling Accurately Distinguishes Papillary Thyroid Carcinoma from Normal Tissue.* Proteomics & Bioinformatics, 2013. **6**(4): p. 65-71.
52. Percin G, K.-Y.B.T., *Piezoelectric droplet ejector for ink-jet printing of fluids and solid particles.* Review of Scientific Instruments, 2004. **74**(2): p. 1120-1127.
53. Abe, K., K. Suzuki, and D. Citterio, *Inkjet-printed microfluidic multianalyte chemical sensing paper.* Anal Chem, 2008. **80**(18): p. 6928-34.
54. Calvert, P., *Inkjet Printing for Materials and Devices.* Chemistry of Materials, 2001. **13**(10): p. 3299-3305.
55. Tucker, K.R., et al., *The modified-bead stretched sample method: development and application to MALDI-MS imaging of protein localization in the spinal cord.* Chem Sci, 2011. **2**(4): p. 785-795.
56. Clausius, R., *Ueber die bewegende Kraft der Waerme und die Gesetze, welche sich daraus fuer die Waermelehre selbst ableiten lassen.* Annalen der Physik, 1850. **155**: p. 500-524.
57. Claperyon, M.C., *Mémoire sur la puissance motrice de la chaleur.* Journal de l'École polytechnique, 1834. **23**: p. 153-190.
58. Hankin J A, B.R.M., Murphy R C, *Sublimation as a method of matrix application for mass spectrometric imaging.* J Am Soc Mass Spectrom, 2007. **18**(9): p. 1646-1652.
59. Yang J, C.R.M., *Matrix Sublimation/Recrystallization for Imaging Proteins by Mass Spectrometry at High Spatial Resolution.* Analytical chemistry, 2011. **83**(14): p. 5728-5734.
60. Thomas, A., et al., *Sublimation of new matrix candidates for high spatial resolution imaging mass spectrometry of lipids: enhanced information in both positive and negative polarities after 1,5-diaminonapthalene deposition.* Analytical chemistry, 2012. **84**(4): p. 2048-54.
61. Yang, J. and R.M. Caprioli, *Matrix sublimation/recrystallization for imaging proteins by mass spectrometry at high spatial resolution.* Analytical chemistry, 2011. **83**(14): p. 5728-34.

62. Dekker, L.J., et al., *A mass spectrometry based imaging method developed for the intracellular detection of HIV protease inhibitors.* Rapid communications in mass spectrometry : RCM, 2009. **23**(8): p. 1183-8.
63. Chaurand, P., S.A. Schwartz, and R.M. Capriolo, *Profiling and imaging proteins in tissue sections by MS.* Anal Chem, 2004. **76**(5): p. 87A-93A.
64. Mehl, A., et al., *3D volume-ablation rate and thermal side effects with the Er:YAG and Nd:YAG laser.* Dent Mater, 1997. **13**(4): p. 246-51.
65. Stelzle, F., et al., *The impact of laser ablation on optical soft tissue differentiation for tissue specific laser surgery-an experimental ex vivo study.* J Transl Med, 2012. **10**: p. 123.
66. Yang, J.H. and R.M. Caprioli, *Matrix Sublimation/Recrystallization for Imaging Proteins by Mass Spectrometry at High Spatial Resolution.* Analytical Chemistry, 2011. **83**(14): p. 5728-5734.
67. Jurchen J C, R.S.S., Sweedler J V, *MALDI-MS Imaging of Features Smaller than the Size of the Laser Beam.* J Am Soc Mass Spectrom, 2005. **16**(10): p. 1654-1659.
68. Snel, M.F. and M. Fuller, *High-spatial resolution matrix-assisted laser desorption ionization imaging analysis of glucosylceramide in spleen sections from a mouse model of Gaucher disease.* Anal Chem, 2010. **82**(9): p. 3664-70.
69. Krueger, K., et al., *Characterization of polymer membranes by MALDI mass-spectrometric imaging techniques.* Anal Chem, 2013. **85**(10): p. 4998-5004.
70. Holle, A., et al., *Optimizing UV laser focus profiles for improved MALDI performance.* J Mass Spectrom, 2006. **41**(6): p. 705-16.
71. Gustafsson, J.O.R., Eddes J S, Meding S, Koudelka T, Oehler M K, McColl S R, Hoffmann P, *Internal calibrants allow high accuracy peptide matching between MALDI imaging MS and LC-MS/MS* Journal of Proteomics. **75**(16): p. 5093-5105.
72. Szajli, E., T. Feher, and K.F. Medzihradszky, *Investigating the quantitative nature of MALDI-TOF MS.* Mol Cell Proteomics, 2008. **7**(12): p. 2410-8.
73. Albalat, A., et al., *Improving peptide relative quantification in MALDI-TOF MS for biomarker assessment.* Proteomics, 2013. **13**(20): p. 2967-75.
74. Koeniger, S.L., et al., *A quantitation method for mass spectrometry imaging.* Rapid Commun Mass Spectrom, 2011. **25**(4): p. 503-10.
75. Takai, N., et al., *Quantitative analysis of pharmaceutical drug distribution in multiple organs by imaging mass spectrometry.* Rapid Commun Mass Spectrom, 2012. **26**(13): p. 1549-56.
76. Stoeckli, M., et al., *Molecular imaging of amyloid beta peptides in mouse brain sections using mass spectrometry.* Anal Biochem, 2002. **311**(1): p. 33-9.
77. Andersson, M., et al., *Imaging mass spectrometry of proteins and peptides: 3D volume reconstruction.* Nat Methods, 2008. **5**(1): p. 101-8.
78. Rompp, A., et al., *imzML: Imaging Mass Spectrometry Markup Language: A common data format for mass spectrometry imaging.* Methods Mol Biol, 2011. **696**: p. 205-24.
79. Chughtai, K. and R.M. Heeren, *Mass spectrometric imaging for biomedical tissue analysis.* Chem Rev, 2010. **110**(5): p. 3237-77.
80. Fonville, J.M., et al., *Robust data processing and normalization strategy for MALDI mass spectrometric imaging.* Anal Chem, 2012. **84**(3): p. 1310-9.
81. Chaurand, P., et al., *Integrating histology and imaging mass spectrometry.* Anal Chem, 2004. **76**(4): p. 1145-55.
82. Norris, J.L., et al., *Processing MALDI Mass Spectra to Improve Mass Spectral Direct Tissue Analysis.* Int J Mass Spectrom, 2007. **260**(2-3): p. 212-221.
83. McDonnell, L.A., et al., *Imaging mass spectrometry data reduction: automated feature identification and extraction.* J Am Soc Mass Spectrom, 2010. **21**(12): p. 1969-78.
84. Jones, E.A., et al., *Imaging mass spectrometry statistical analysis.* J Proteomics, 2012. **75**(16): p. 4962-89.
85. Alexandrov, T., *MALDI imaging mass spectrometry: statistical data analysis and current computational challenges.* BMC Bioinformatics, 2012. **13 Suppl 16**: p. S11.

86. Race, A.M., et al., *Memory efficient principal component analysis for the dimensionality reduction of large mass spectrometry imaging data sets.* Anal Chem, 2013. **85**(6): p. 3071-8.
87. Dill, A.L., et al., *Multivariate statistical differentiation of renal cell carcinomas based on lipidomic analysis by ambient ionization imaging mass spectrometry.* Anal Bioanal Chem, 2010. **398**(7-8): p. 2969-78.

3. Aspects of mass spectrometry based surface analysis: tissues and biomaterials

A lot of scientific questions, either in biology or material science benefit from spatial knowledge. For biological samples, tissue heterogeneity and biomarker identification are essential issues, often investigated by MSI. Biomaterials on the contrary are in constant interaction with biological compartments. Here the understanding of biodegradation and interaction is of high interest.

a. Biological tissue

Tissues, either animal or plant, are functionally and structurally combined clusters of cells. The organization pyramid can be defined as cells forming tissue, which is the basis for organs. The focus for tissue samples within this thesis lies on soft tissue from rats and humans. From the analytical point of view, and especially for MSI, the physical properties of different tissues are of high importance, besides their molecular constitution. Different concentrations of salt or compositions of saccharides, lipid or proteins highly influence the tissue morphology and consistency. Electrophysical properties impact artifact formations and sensitivity of MSI experiments. The electrical conductivity and relative permittivity varies not only for different tissues, but also between singular cell compartments within the tissue, depending on the laser frequency irradiating the tissue sample [1]. The fact that freezing points or thermal expansion coefficient of various tissues are influencing the choice of fixation technique, the embedding medium and microtome procedure have also to be considered for subsequent MS analysis. Compared to brain, which can only be cut above -5 °C, kidney and other tissue with a higher connective tissue proportion, have to be cut at -20 °C or even below. Embedding procedures disadvantageous for MS, like formalin fixation and paraffin embedding procedures, can however expanding thermal operation limits. Tissue cutting thickness is determined by the percentage of connective cells and the thinner the sample, the more affected is the sample's morphology. Again fixing and embedding improves sample preparation but is negatively affecting MS analysis.

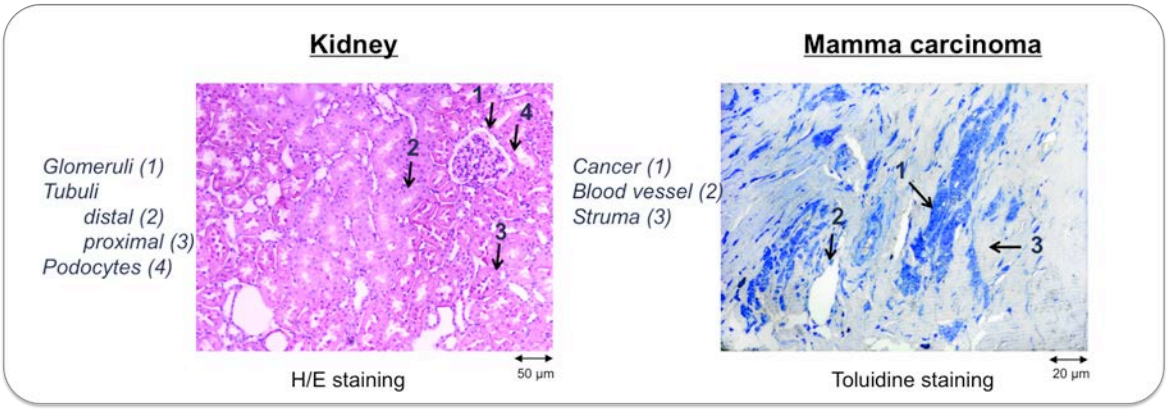

Figure 5: Tissue samples from healthy kidney and carcinogen breast tissue. The H/E stained kidney shows the functional subunits of glomeruli and tubuli after formalin fixation and paraffin embedding. The toluidine stained mamma carcinoma tissue shows highly adipose proportions (stroma) besides several blood vessels cancerous cells. In both cases the tissue was formalin fixed and either paraffin (kidney) or sucrose (mamma carcinoma) embedded.

i. Kidney

Kidneys are the central organ of the urinary system, responsible for detoxification, excretion, resorption and homeostasis. Based on macroscopic levels, kidney tissue can be differentiated into renal pelvis, the medullary renal pyramids and the cortex. Within those regions are very

homogeneous blood vessels, tubuli and glomeruli. One of the major functions, blood filtration and nutrient resorption, is taking place in the glomeruli, ball formed loop structures. The capillaries of the glomeruli, located in the Bowman's capsula (in the medulla), are surrounded by podocytes, cells majorly impacting nephropathology. Podocytes play an essential role in the filtration process.

Kidney tissue is very favorable for MSI analysis, due to its homogeneous structure and high conductivity. MALDI lasers in the normal application range between 20 Hz and 2 GHz diminish dielectrically properties, resulting in conductive samples comparable to stainless steel.

MSI has already been applied to kidney tissues earlier, for investigations of glomerulosclerosis for differentiating healthy and pathological glomeruli on protein profiling level [2]. The average size of one glomeruli is between 60 and 150 µm allowing MSI already at early times of this technique with rather high lateral resolutions. Besides enzymatic metabolism studies of angiotensin and its subforms [3], also in situ experiments for nephrological toxicity and crystal deposits were successful [4]. However, rhenopathology did not only focus on proteins and metabolites, also lipids revealed profound insight into pathological pathways, e.g. for hyper Immunoglobulin A nephropathy or glomerulonephritis [5]. MSI demonstrated that certain long chained phosphatidylcholine species, specific for this disease, are found primarily in tubuli but have no yet determined function [6].

Due to its characteristics of high morphological stability and homogeneity, kidney tissue is compatible with a large variety of embedding media, ranging from resins, to sugar based solutions over FFPE and O.C.T embedding. Kidney tissue is even stable enough to be analyzed in a snap frozen state. This is the reason why kidney material was chosen in the beginning of the presented thesis, for proper MSI adjustment and to study the loss of analyte signal due to fixation an embedding processes. Furthermore fixation methods and embedding media were tested for their suitability for on tissue digestion. Cell and microstructure differentiation based on MSI experiments were compared to histological staining with respect to advantages and limits.

Within the present thesis, the biological question was focused on the identification and differentiation of podocytes based on peptide and protein profiles. The large biobank available at the Medical University of Vienna made the comparison of different pathological stages, fixation techniques and embedding media feasible. The obtained results formed the basis for identifying the limits of MSI experiments with available equipment. (see Chapter 5)

ii. Mamma carcinoma – metastatic tumor tissue

Breast cancer is known as the type of cancer with the highest prevalence and mortality in Western civilization. Tumor biopsies are very contrary to kidney tissue samples. Tissue structures contain high amounts of stroma and lipoid tissue. The consequences are the need for even enhanced tissue fixation and embedding strategies to preserve original morphology. Moreover, laser/tissue interaction and ion suppression effects have to be reconsidered for tissues with high amounts of septum as septum consists mainly of adipose tissue, which is easily ablated completely.

Mamma carcinoma metastases are frequently found in the lymph nodes of surrounding organs such as lung or bone marrow and liver. However often also brain and colon regions are affected. So far the underlying mechanism of cancer spreading has not been characterized completely and tissue congruities have not been matched completely. Furthermore the heterogeneity of tumor tissue in

primary tumors and metastatic tissue is of high interest, since it provides information about tumor proliferation.

Even though the breast cancer associated proteome is well characterized [7] and several MSI approaches have been published [8-11], little is known about proteins associated with tumor heterogeneity. The difficulties to access low abundance proteins and/or peptides relevant for the differentiation between healthy tissue, mamma carcinoma and metastasis will be outlined in the additional section of the thesis (see Chapter 9.c).

b. Biomaterials

Biomaterials have already been used in ancient times when Romans used gold as a replacement system for teeth. External aids were also found in supporting broken extremities by wood. Continuous developments in biomaterial lead to the possibility of being capable of replacing many of our organs.

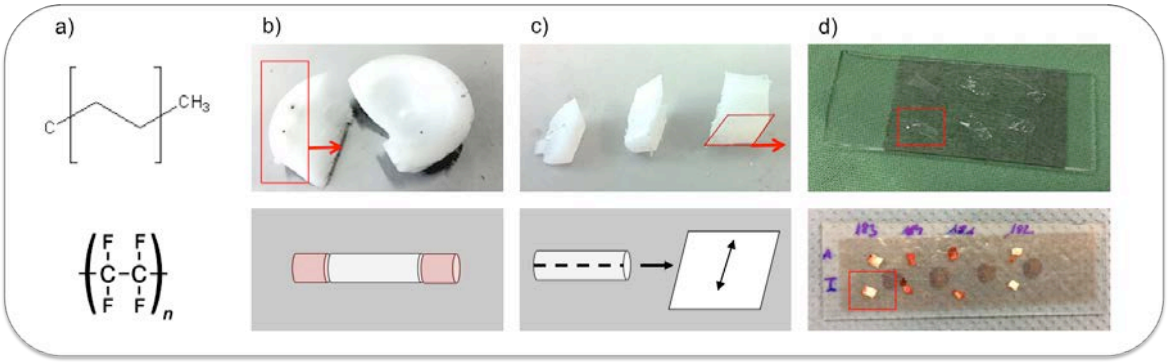

Figure 6: Biomaterial made from ultra high molecular weight polyethylene (1st row) and polytetrafluorethylene (2nd row): (a) Molecular structure; (b) Application as acetabular cup or blood vessel; (c) Sample preparation; (d) Thin slices for MSI application.

i. Non-degradable polymers used in artificial joint replacement surgery – PE-UHMW

Ultra high molecular weight polyethylene (PE-UHMW) is a commonly used and highly stable material resisting mechanical forces well. For total joint replacements it has been used as a bearing surface since 1962 because of its high biocompatibility and high wear resistance. The polymer is frequently used for application due to its easy adaptability and usability. Its biocompatibility and high chemical inertness prove it favorable for implantation [12, 13].

However, UHWMPE has also been reported to produce reasonable amounts of wear particles of sub-micron size and was claimed to enhance inflammation and apoptosis processes *in vivo* [14, 15].

UHWMPE is used for acetabular cup replacement, the sliding surface in the articulating hip joint. The polymer is in direct contact with the lubricating fluid, synovial fluid (SF), and its counterpart the femoral head, usually made of titanium or Al_2O_3. The mechanical forces are extremely high, not seldomly exceeding 110 Newton. Especially exposed areas can be found in the center regions of the acetabular cup, where the lubrication film is at its thinnest and mechanical load at its highest [16, 17].

PE-UHMW is a linear homopolymer, with a molecular mass of 3-8 x 10^6 g/mol of high homogeneity, yet contains crystalline and amorphous regions. It's very apolar surface, supports the capabilities of articulating in heavily exposed joint systems [18].

To ensure biocompatibility and high immune acceptance, UHWMPE needs to be sterilized before implantation. Gamma and electron beam irradiation have been proven to increase the oxygen uptake, resulting in enhanced material aging, whereas ethylene oxide does not show comparable effects, but is less sufficient for sterilization. So far mainly Fourier transform infrared (FTIR) spectroscopy and light microscopy have been used for characterizing the oxidation behavior of UHWMPE [19-21]. It was shown that oxidative environments, e.g. hydroperoxide, induce further oxidation in all kinds of UHWMPE, sterilized or non-sterilized. In light microscopy images white lines mark regions highly affected by oxidation and brittling, found often near the surface in contact with the oxidative environment. The defective region is usually found down to 5 mm underneath the exposed surface. Areas highly affected by oxidative stress, also show severe increase of roughness and heterogeneity after treatment with oxidative species [22, 23]. Oxidative species are usually described as carbonyl species and hydroperoxides and both have been co-localized with macroscopic material damage and abrasion. It has been proven that pure polyethylene is not prone to oxidation *in vivo*. Slightly oxidized species, like sterilized material, which can also contain radicals, is highly affected by further *in vivo* oxidation and radical formation [24, 25]. So it is easily understood that biodegradation of the polymer is further enhanced, in case of dysfunctional mechanics or pathological predisposition.

Implant loosening or acute inflammation mainly causes UHWMPE implant failure. However, also small failures in abrasion resulting in small particles inducing inflammation, significantly influences the bio-compartment. To prevent biological adsorption within an oxidative environment, UHWMPE has been modified by additives or coatings. Vitamin E/tocopherol, providing fat-soluble and antioxidants properties, has been used as a doping substance, to reduce oxidation [26]. Coating the polymer surface with polyethylenglycol (PEG) has been reported to increase the mechanical load and decreased wear for hip liners [27]. Also high cross-linking of UHWMPE has been reported to improve resistance to protein adsorption and consequently eventual oxidation [28].

Recent studies [29] proved the adsorption of protein compounds on PE-UHMW. The polymer has been incubated in protein standard solutions of high concentration. Fluorescence imaging proved homogeneous protein patterns for single proteins on the whole surface. However, those studies lack the information about competitive protein adsorption.

For lipid species it was published that very small lipid associated compounds have been found to diffuse into the polymer material [30]. Cholesterol and its pre- or by-products, e.g. squalene, were identified approximately 5 mm underneath the contact side and on the surface using infrared spectroscopy. This diffusion leads to a decrease in the comprehensive modulus and strength.

Synovial fluid (SF) is the natural lubricant of UHWMPE liners, between the contact side of the polymer and the articulating titanium, CoCr or Al_2O_3 femoral head. The major components are hyaluronic acids, albumin, immunoglobulins and apolipoproteins. Considering the lipid composition, SF contains high proportions cholesterol, mono, di- and triacylglycerides, ceramides and phospholipids.

In healthy joints, the main function of SF is lubrication and metabolism. It can be assumed that SF has to some extent also oxidative properties. This property may change during disease, as it is known that the generally very viscous SF changes its fluidity during osteoarthritis, arteriosclerosis and chronic or acute inflammation.

Proteins essential for the lubrication process are often considered as glycosylated. Alpha-1-acid glycoprotein and alpha-1-antitrypsin have been shown to enhance lubrication between PE-UHMW and Al_2O_3. Carbohydrates are supposed to induce a shear-reducing layer by adjustment of their hydrophilic carbohydrate chains. Furthermore phospholipids, especially phosphatidylethanolamine and phosphatidylcholine are essential for the lubrication process. However, the layer formation on the PE-UHMW surface possibly induces the adsorption of a variety of oxidative species and might alter material properties.

The described rough area after oxidation is supposed to be highly affected by protein adsorption, according to theoretical simulation assumptions [31].

Within this thesis the main aim is to identify components adsorbed on and diffused into UHWMPE hip liners. Incubation experiments were established to study adsorption behavior and analyte diffusion after interaction with the polymer in a static system. The interaction between the polymer and its surrounding compartment has to be understood to gain basic insight into the oxidation process, which is critical for materials' long-term success. MSI combined with conventional analytical techniques, e.g. protein precipitation followed by gel electrophoresis, provides the possibility to obtain information about the localization and the identity of interacting biomolecules in a very comprehensive approach (see Chapter 6, 7 and 8).

ii. Biodegradable polymer materials used for vacular prosthesis

Biodegradable materials are used to induce tissue growth replacing the initial polymer implant. Especially for blood vessel replacement, the physical properties of pulsed pressure resistivity, elasticity and flexibility within short time intervals are essential for the biopolymers [32]. Polytetrafluoroethylene has been identified to show good properties for vessel replacement, since it is easily degraded due to its low molecular weight and good biological accessibility [33]. It was found that bio-molecular adsorption starts directly after implantation [34]. The diffusion of small molecules such as lipids is supposed to change the polymer structure starting the degradation process. The adsorption of proteins leads to surface changes attracting cells to attach and form layers. Under the confluent layer, the polymer degrades until the replacement process is finished. The challenges for graft materials lye in the compromise between hydrophilic and hydrophobic properties as well as dynamic mobility and electrical repulsion [35]. The conducted experiments aimed to understand the adsorption behavior of proteins and lipids on different graft material *in vivo* after defined time points (see Chapter 9.a).

References

1. Fu F, X.S.X., Chen W, *Temperature- and frequency-dependent dielectric properties of biological tissues within the temperature and frequency ranges typically used for magnetic resonance imaging-guided focused ultrasound surgery.* Int. J. Hyperthermia, 2014. **30**(1): p. 56-65.
2. Xu, B.J., et al., *Proteomic patterns and prediction of glomerulosclerosis and its mechanisms.* J Am Soc Nephrol, 2005. **16**(10): p. 2967-2975.
3. Grobe, N., et al., *Mass spectrometry for the molecular imaging of angiotensin metabolism in kidney.* Am J Physiol Endocrinol Metab, 2012. **302**(8): p. E1016-24.
4. Nilsson, A., et al., *In situ mass spectrometry imaging and ex vivo characterization of renal crystalline deposits induced in multiple preclinical drug toxicology studies.* PLoS One, 2012. **7**(10): p. e47353.
5. Mainini, V., et al., *MALDI imaging mass spectrometry in glomerulonephritis: feasibility study.* Histopathology, 2013.
6. Kaneko, Y., et al., *Imaging mass spectrometry analysis reveals an altered lipid distribution pattern in the tubular areas of hyper-IgA murine kidneys.* Exp Mol Pathol, 2011. **91**(2): p. 614-621.
7. Bertucci, F., D. Birnbaum, and A. Goncalves, *Proteomics of breast cancer: principles and potential clinical applications.* Mol Cell Proteomics, 2006. **5**(10): p. 1772-1786.
8. Traub, F., et al., *SELDI-MS-based expression profiling of ductal invasive and lobular invasive human breast carcinomas.* Pathol Res Pract, 2005. **201**(12): p. 763-770.
9. Schone, C., H. Hofler, and A. Walch, *MALDI imaging mass spectrometry in cancer research: combining proteomic profiling and histological evaluation.* Clin Biochem, 2013. **46**(6): p. 539-545.
10. Rauser, S., et al., *Classification of HER2 receptor status in breast cancer tissues by MALDI imaging mass spectrometry.* J Proteome Res, 2010. **9**(4): p. 1854-1863.
11. Kang, H.S., et al., *Protein and lipid MALDI profiles classify breast cancers according to the intrinsic subtype.* BMC Cancer, 2011. **11**: p. 465.
12. Digas, G., *New polymer materials in total hip arthroplasty. Evaluation with radiostereometry, bone densitometry, radiography and clinical parameters.* Acta Orthop Suppl, 2005. **76**(315): p. 3-82.
13. Atienza, C., Jr. and W.J. Maloney, *Highly cross-linked polyethylene bearing surfaces in total hip arthroplasty.* J Surg Orthop Adv, 2008. **17**(1): p. 27-33.
14. Ren W P, M.D.C., Zhang R, Peng X, Wu B, Monica H, Wooley P H, *Association between PE-UHMW particle-induced inflammatory osteoclastogenesis and expression of RANKL, VEGF, and Flt-1 in vivo.* Biomaterials, 2006. **27**: p. 5161-5169.
15. Reno F, S.M., Cannas M, *Surface oxidation of PE-UHMW for orthopedic use increases apoptosis and necrosis in human granulocytes.* Journal of Materials Science: Materials in Medicine, 2003. **14**: p. 241-245.
16. Ge S, W.S., Gitis N, Vinogradov M, Jiao J, *Wear behavior and wear debris distribution of PE-UHMW against Si3N4 ball in bi-directional sliding.* Wear, 2008. **264**: p. 571-578.
17. Korhonen R K, K.A., Konttinen Y T, Santavirta S S, Lappalainen R, *The effect of geometry and abduction angle on the stresses in cemented PE-UHMW acetabular cups--finite element simulations and experimental tests.* Biomed Eng Online, 2005. **4**(32).
18. Sobieraj, M.C. and C.M. Rimnac, *Ultra high molecular weight polyethylene: mechanics, morphology, and clinical behavior.* J Mech Behav Biomed Mater, 2009. **2**(5): p. 433-443.
19. Greenbaum, E.S., et al., *Effect of lipid absorption on wear and compressive properties of unirradiated and highly crosslinked PE-UHMW: an in vitro experimental model.* Biomaterials, 2004. **25**(18): p. 4479-4484.
20. Costa, L., et al., *Oxidation in orthopaedic PE-UHMW sterilized by gamma-radiation and ethylene oxide.* Biomaterials, 1998. **19**(7-9): p. 659-668.
21. Goldman, M., et al., *Oxidation of ultrahigh molecular weight polyethylene characterized by Fourier Transform Infrared Spectrometry.* J Biomed Mater Res, 1997. **37**(1): p. 43-50.

22. Scott M, M.M., Mishra S R, Jani S, *Particle analysis for the determination of PE-UHMW wear.* J Biomed Mater Res, 2005. **73**(2): p. 325-337.
23. Rocha M, M.A., Mansur H, *Characterization and Accelerated Ageing of PE-UHMW Used in Orthopedic Prosthesis by Peroxide.* Materials, 2009. **2**: p. 562-576.
24. Costa, L., et al., *In vivo PE-UHMW biodegradation of retrieved prosthesis.* Biomaterials, 1998. **19**(15): p. 1371-1385.
25. Hardaker, C.S., Fisher J, Issac G, Stone M, Older J, *Quantification of the Effect of Shelf and In Vivo Aging on the In Vivo and In Vivo Wear Rates of a Series of Retrieved Charnley Acetabular Cups.* European Society of Biomaterials, 2000.
26. Oral, E. and O.K. Muratoglu, *Vitamin E diffused, highly crosslinked PE-UHMW: a review.* Int Orthop, 2011. **35**(2): p. 215-223.
27. Kane, S.R., P.D. Ashby, and L.A. Pruitt, *Microscale wear behavior and crosslinking of PEG-like coatings for total hip replacements.* J Mater Sci Mater Med, 2010. **21**(4): p. 1037-1045.
28. McCalden, R.W., et al., *Wear rate of highly cross-linked polyethylene in total hip arthroplasty. A randomized controlled trial.* J Bone Joint Surg Am, 2009. **91**(4): p. 773-82.
29. Serro, A.P., et al., *Adsorption of albumin and sodium hyaluronate on PE-UHMW: a QCM-D and AFM study.* Colloids Surf B Biointerfaces, 2010. **78**(1): p. 1-7.
30. Costa L, B.P., del Prever E B, Luda M P, Trossarelli L, *Analysis of products diffused into PE-UHMW prosthetic components in vivo.* Biomaterials, 2001. **22**(4): p. 307-315.
31. Kanaga Karuppiah K S, S.S., Xu Z H, Li X, *The effect of protein adsorption on the friction behaviour of ultra-high molecular weight polyethylene.* Tribology Letters, 2006. **22**(2): p. 181-188.
32. Gui, L., et al., *Development of novel biodegradable polymer scaffolds for vascular tissue engineering.* Tissue Eng Part A, 2011. **17**(9-10): p. 1191-1200.
33. Soldani G, B.M., Losi P, Crucean A, Chiappino D, Burchielli S, Bernini F, *In vitro experiments and in vivo implants to evaluate a new silicone-based polyurethane material for replacement of small vessel.* Cardiology Young, 2004. **14**.
34. van Wachem, P.B., et al., *The influence of protein adsorption on interactions of cultured human endothelial cells with polymers.* J Biomed Mater Res, 1987. **21**(6): p. 701-718.
35. Choi J, L.B.S., Park K, Han D K, *Beneficial Effect of Sulfonated PEO-grafted Polyurethanes on Calcification and Lipid Adsorption of Vascular Implants.* Macromolecular Research, 2010. **18**(11): p. 1133-1136.

4. Analyte identification

a. Protein analysis by gel electrophoretic separation and MALDI-TOF analysis

MSI is capable of either localizing intact proteins or cleaved protein fragments, peptides respectively. However, molecular weight determination or sequence information can often hardly be determined due to the low concentration of analytes. Within the present thesis protein identification is based on molecular weight determination and sequencing of peptides.

The biological question of investigating proteins adsorbed on polymer surfaces can effectively be assisted by protein analysis techniques favoring mass and sequence determination such as gel electrophoretic separation followed peptide mass mapping and sequencing.

The focus of the present thesis lies on protein analysis approaches involving the precipitation of almost the complete proteome of a biological fluid, removal of interfering substances, separation of proteins and identification of each protein in a separate approach. Despite the existence of many different approaches this method was chosen to characterize the bio-fluids in a more comprehensive way.

Gel electrophoresis (GE) provides an easy and practical approach to separate complex protein samples according to their size or/and charge, when conducted at native state. GE methods have been developed for separation in solution or in stabilized matrices.

The basic principle of GE is rather simple. Molecules with a specific size and charge are accelerated by an electrical field force and decelerated by the friction force induced by the matrix particles diameter and cross-linking. The balance between those two influences determines the velocity and mobility of analytes (Equ. 13). Mobility is defined as the interaction between traveling velocity and field strength. The ideal mobility considers an ideally shaped spherical particle, which is retarded depending on the charge state *z*, the elemental charge *e*, solution's viscosity η and the Stoke's radius *r*, according to Stoke's law (Equ. 14). For the separation of non-globular analytes, e.g., mobility is also impacted by charge *q* and molecular mass *M*.

$$v = \frac{qE}{f_c} = uE \qquad (13)$$

$$u_{ideal} = \frac{ze}{6\pi\eta r} \qquad (14)$$

$$u = \frac{q}{\sqrt[3]{M^2}} \qquad (15)$$

Technically the separation of proteins in a gel can be realized in a vertical or horizontal set up. For this, the gel matrix is composed of cross-linked molecules retarding the analytes. Acrylamide is one of the most popular monomers, besides agarose. Polyacrylamide, acrylamide cross-linked by N,N-methylene-bis-acrylamide after free radical polymerization, is chemically inert and very stable.

For the sole determination of protein size sodium-dodecylsulfate polyacrylamide gel electrophoresis (SDS-PAGE) is most frequently used. The technique is capable of separating proteins from a low mass range of a few 1000 Da up to several 100 kDa [1].

SDS-PAGE was introduced by Weber and Osborn in the 60s, improved by Laemmli (Lämmli 1970) in the 70s and is still frequently used today [2]. Proteins are denatured by heating between 75 and 100 °C in a mixture with SDS, leading to the break of hydrogen bonds. Additional to the protein's loss of conformation, SDS is non-covalently bound to the proteins at a constant ratio of approximately 1.4 g SDS per g protein [3]. However, the hydrophobicity of the backbone is influencing this ratio. The SDS addition covers the net charge of the protein introducing a rather constant mass-to-charge ratio. Additionally SDS as a detergent increases protein solubility leading to decreased protein precipitation. The addition of dithiotreitol or β-mercaptoethanol reduces disulfide bonds present in proteins and leads to complete denaturation. Separation of proteins in the resolving gel matrix is consequently based only on the size of the SDS/protein complex. Comparison with the migration of standard protein markers of known molecular weight allows determination of the apparent molecular mass of analytes. The mass determination for denatured, reduced proteins was shown to be sufficient for most biochemical questions for a long time due to a linear correlation between electrophoretic mobility of the protein complex and the molecular weight of the protein itself [4]. Yet, proteins can show unexpected migration behavior. Glycosylation, sulfation or phosphorylation leads to deviated mass values. For glycosylated proteins it was observed that proteins migrate slower than their corresponding non-modified protein [5].

Various staining possibilities are available where the dye directly binds to the protein [6]. Due to its sensitivity and compatibility with MS analysis [7], the most frequently used is silver staining with a reported detection limit of 1 ng [8]. Coomassie Brilliant Blue R-250 and G-250, triphenylmethane dyes, are other possibilities [9], however are comparably less sensitive, with detection limits of approximately 5 ng protein analyte [10].

To further determine the molecular weight of proteins, SDS results are often combined with MALDI-TOF MS analysis. MALDI-TOF MS usually generates single or double charged ions ($[M+H]^+$, $[M+2H]^{2+}$) and has widely been reported for good mass accuracy identifying larger proteins. However, labile groups such as sialic acid or sulfate groups might get lost due to high energy transfer in the MALDI process, leading to underestimated molecular masses [11]. Besides the fact that MALDI-TOF covers a very broad mass range, sensitivity is far below the pM range depending on the analyte and instrument, allowing the detection of proteins not visible in gel electrophoresis.

Protein identification solely by molecular weight, either obtained by SDS-PAGE or MALDI-TOF analysis or both, is critical as the number of potential proteins rises exponentially with the molecular mass. However, both methods assist the molecular mass determination of the intact protein and can comprehensively be assisted by peptide mass mapping strategies.

Statistically reliable protein identification is possible by peptide mass fingerprint analysis. Peptide mass fingerprint is the statistical collection and rearrangement of protein fragments obtained after enzymatic cleavage [12]. Various groups have established the method during the early 90s [13]. Proteins are enzymatically degraded using an enzyme after disulfide bond stabilization. Derived peptides are detected using mass spectrometry and rearranged to the complete protein by statistical algorithms [14]. Mass accuracy and efficient protein cleavage increases the statistical chance to calculate the theoretically possible sequence for the associate protein [15]. Search algorithms and databases have been developed containing species and tissue specific proteomic data sets of large extent [16]. Of course identification is only possible if the digested protein is registered in the respective database. Otherwise comparison of the obtained fragment ions and their abundance

proportions can be performed, delivering theoretical sequence information. The less proteins are included in a peptide mass fingerprint (PMF), the higher is the statistical possibility of reliable identification. However, excising protein bands from one-dimensional gel electrophoresis includes the possibility of having more than one protein present in the gel band. This makes MALDI-TOF PMF analysis without prior additional LC-separation more complex. Modern algorithms are capable of dealing with up to 4 present proteins in one spectrum, while even more protein sequences are possible with significantly reduced identification scores.

For unknown proteins or uncertain identification scores, peptide sequencing by PSD or CID is an additional or supporting possibility for protein identification, referred to as peptide sequencing [17]. The fragmentation of peptide ions delivers information about the amino acid composition. Efficient fragmentation procedures enable the recalculation of the complete peptide sequence from both the N- and C-terminal end. Sequencing is based on fragmentation of peptides, which can be achieved by PSD, CID or electron transfer dissociation, charge remote fragmentation, electron capture dissociation, which will not be discussed in detail in the present thesis [18]. The weakest and most likely site of fragmentation is the peptide bond. Depending on the fragmentation technique applied, peptides fragment differently, producing characteristic ions. Fig. 6 shows most frequent fragmentation sites. a-, b- and c- ions originating from the N-terminus, whereas x-, y- and z- ions contain the C-terminal end. PSD majorly induces a-, b- and y-ions, whereas c-, y- and z-ions are associated with ETD fragmentation. During CID fragmentation mainly b- and y-ions are generated with the possibility of further fragmentation within the amino acid residues, providing more detailed information. x-ions are least likely to occur.

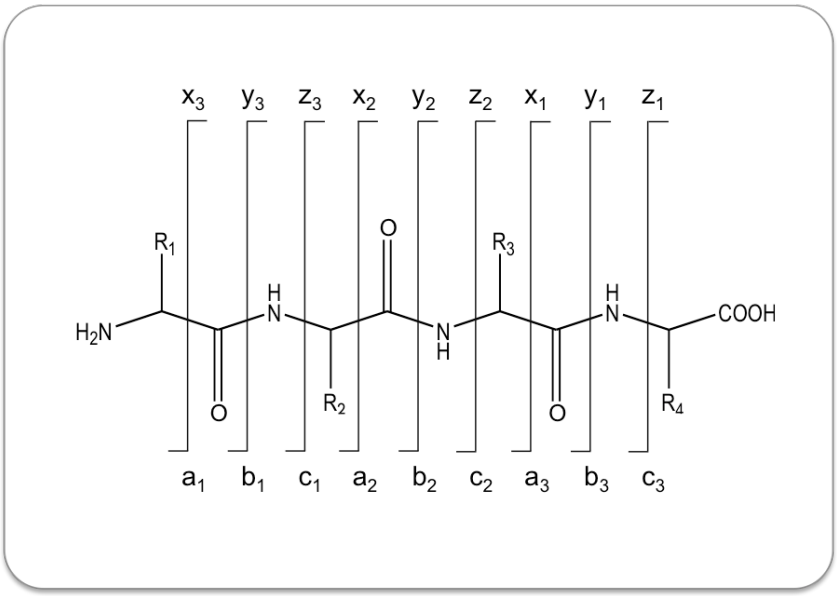

Figure 6: Fragmentation pattern for peptides. According to the conventional nomenclature peptide fragments are assigned according to their position related to the peptide bond and the N- or C-terminal end of the peptide.

b. Lipid analysis by thin layer chromatography separation and MS/MS analysis

Even though proteins and peptides have been of major attention as potential signal molecules and biomarkers, lipids have become increasingly relevant over the last decades. Lipids have been found

to play a major role in health and pathology, including preventive medicine and early stage diagnosis. The reason can be found in the very dominant presence of lipids in biological functions and systems. Lipids are relevant in bio-membranes, energy storage, signaling processes, vitamin cascades, metabolism and many more [19].

Lipids can be divided into 7 main groups: fetty acids, triacylglycerides, waxes, phospholipids, sphingolipids, lipopolysaccharides and isoprenoids. For animal cells and especially for the focus of this thesis, biomaterial investigations, the major relevant lipid classes are phospholipids, including phosphatidylcholine (PC), phosphatidylserine (PS), phosphatidylethanolamine (PE), phosphatidylinositol (PI), phosphatidic acid (PA) and phosphatidylglycerol (PG), but also sphingomyelin (SM, cholesterol, free fatty acids or di- and triglycerides [20]. Phospholipids and cholesterol derivates show very different core structures, latter however relevant for analytical techniques. Whereas PC and SM have positively charged head groups, PE and PI exist in neutral or negatively charge states. The core structure in many cases is a fatty acid linked to a glycerol backbone by an ester bond. However, also alkyl or alkenyl linkages, referred to as etherlipids or plasmalogens, can be found if the structure derives from a fatty aldehydes.

Lipids have had a long history of mass spectrometric analysis, with emphasis on ESI applications. In recent years MALDI analysis however, has found it's way to lipid investigations [21-23]. The critical point for both applications is the extraction process for the analyte. Due to their large variety of physicochemical properties, it is almost impossible to find an extraction procedure for the complete lipidome. Defined mixtures of chloroform, methanol and water have been described already in the late 50s by Bligh and Dyer [24] and Folch [25]. Those two methods still remain the most frequently used and efficient ones for lipid analysis, though a lot of very specific methods for particular lipid classes were developed later on.

As described, SM and PC provide favorable qualities for MS analysis due to their already charged head groups. This leads to unfavorable ion suppression effects during MS analysis for other lipid classes if analyzed in parallel. For such lipids even identification by fragmentation is difficult due to signals of low intensity. For separation of lipids prior to MS analysis, chromatography, either liquid (LC) or thin layer (TLC), proved very capable. Whereas LC provides high resolving power and the advantage of on-line coupling to ESI-MS, TLC has been established for quick and easy separation of lipids [26]. TLC is not sensitive to contaminations and as every analysis uses a new TLC plate does not exhibit carry-over effects. The basic principle of chromatography remains the same for LC and TLC: analytes are applied in liquid solvent to a stationary phase and separation is based on their interaction with the stationary phase while the solvent moves along the separation distance, in case of TLC movement results from capillary action.

In TLC the stationary phase is composed of sorbent particles on a glass or aluminum supportive. Silica is the most commonly applied sorbent for the stationary phase, besides reversed phase hydrocarbon coatings or modified hydrophilic layers.

One of the most important parameters for separation quality is the particle size of the stationary phase. High performance TLC (HPTLC) usually facilitates particles with an average diameter of 5 µm compared to 12 µm for standard TLC applications. Solvent combinations for the mobile phase are characterized by different polarity and volatility to ensure analyte solubility but also sufficient separation for a variety of applied lipids. To further enhance lipid separation for HPTLC, a 2 dimensional separation system can be employed. The second dimension usually is a physicochemical

very different system, in order to differentiate analytes not sufficiently separated in the first dimension. Per definition the 2nd development step may also be taken literally in a geometrical set up by turning the plate by 90 ° before the 2nd solvent is applied. However, this technique limits TLC analysis to one sample per plate. More often the 2nd dimension is simply a second development in the same direction as the 1st dimension but using a completely different solvent system. Usually this is applied to obtain separation for polar and apolar lipids.

Fluorescence and Coomassie Brilliant Blue staining are the most frequently used techniques for native lipid visualization after HPTLC. If it is intended to analyze lipids after HPTLC separation, which is in fact possible, compatibility of the staining with MS is the most important parameter. Fluorescence stains are usually favored, due to their easy applicability by spraying and low detection limits. Primuline, a very lipophilic fluorescent reagent, revealed highest sensitivity rates and very high MS compatibility [27]. The molecule binds non-covalently to many lipid structures, which induces fluorescence detected at 366 nm [28].

After separation and visualization species are distinguished by characteristic retarding values (*R*), which are calculated from the migration distance of the front (Z_{front}-$Z_{application}$) and the analyte (Z_{sample}).

$$R = \frac{Z_{sample}}{Z_{front} - Z_{application}} \qquad (16)$$

The resolution is hereby directly proportional to the possible migration distance and inversely proportional to the particle size.

HPTLC is frequently directly coupled to MALDI-TOF MS analysis for profiling or MSI experiments. Schiller et al. besides a few other groups have successfully proven the possibility to analyze and identify lipid species directly from the HPTLC plate, despite its insulating properties and high noise background [29]. The direct analysis is difficult due to low concentrations of analytes on the silica material. Moreover, analyte accessibility and different positions of desorption/ionization may decrease mass accuracy but also sensitivity (details see Chapter 1.b and 2.b). Besides, not all ion source geometries are applicable for this approach as the plate height changes the electrical acceleration field, which results in decreased ion transmission. As a consequence, the majority of HPTLC separations are followed by liquid extraction of the lipid from the silica plate. Extraction procedures are very similar to procedures developed for the initial lipid extraction.

The critical issue for MALDI-TOF analysis is to obtain charged particles from lipid extracts that are vacuum stable, yet volatile enough for the MALDI process and soluble in the solvent and matrix systems. Besides those issues, MALDI as a soft ionization technique is ideal for intact lipid analysis, especially without the need for solvent mixtures and no disadvantageous sensitivity to salt content.

A variety of MALDI matrices have been reported to show good results for lipid analysis. 2,5-dihydroxybenzoic acid (DHB) is one of the most commonly used matrices. Besides DHB, CHCA, SA and DAN performed successfully in lipid analysis. 2,6-dihydroxyacetophenone and 1,4,6-trihydroxacetophenone are not vacuum stable, but show very beneficial ionization and fragmentation qualities, especially for phospholipid analysis. The latter two favor the formation of potassium and lithium adducts, enhancing acyl chain fragmentation. Azathiothymin, a matrix producing exclusively hydrogen protonated ions, is of high interest for lipid analysis, where no fragmentation or structural elucidation is intended [30, 31].

Regarding phospholipids, sphingolipids and triglycerides, the fragmentation yield can significantly be improved by the addition of metal or salt ions, whereas protonated lipid ions show only head group loss during fragmentation. Adding for instance sodium and potassium chloride produce majorly singly or less frequently doubly charged protonated ions. The attachment of alkali ions induces moreover acyl side chain fragmentation, providing more information about the lipid structure. Sterol structures are not *per se* lipids but their amphiphilic nature classifies them as lipids and they show similar effects for MS analysis. Cholesterol is found in MALDI experiments majorly as singly charged protonated ion with the loss of the hydroxyl group. Fragmentation has been reported to be effective for the hydrolyzed protonated ion.

For some studies adduct ion formation is not favorable. For this, washing procedures with low amounts (0.1 %) of trifluoracetic acid have been established, including matrix recrystallization, which improves analyte incorporation and desorption efficiency for reproducible homogeneous matrix layers [32, 33].

Contrary to peptide fragmentation, no systematic nomenclature has become accepted to describe lipid fragments, despite a few attempts [33]. For phospholipids head groups, fragments are usually described by their chemical compositions or theirs names and the acyl chains by the number of carbon atoms. For all other lipids, no generally used nomenclature is established.

Figure 7 gives an overview to the major relevant lipid classes in biological systems and their core structure: phospholipids, sphingomyelin, cholesterol and triglycerides.

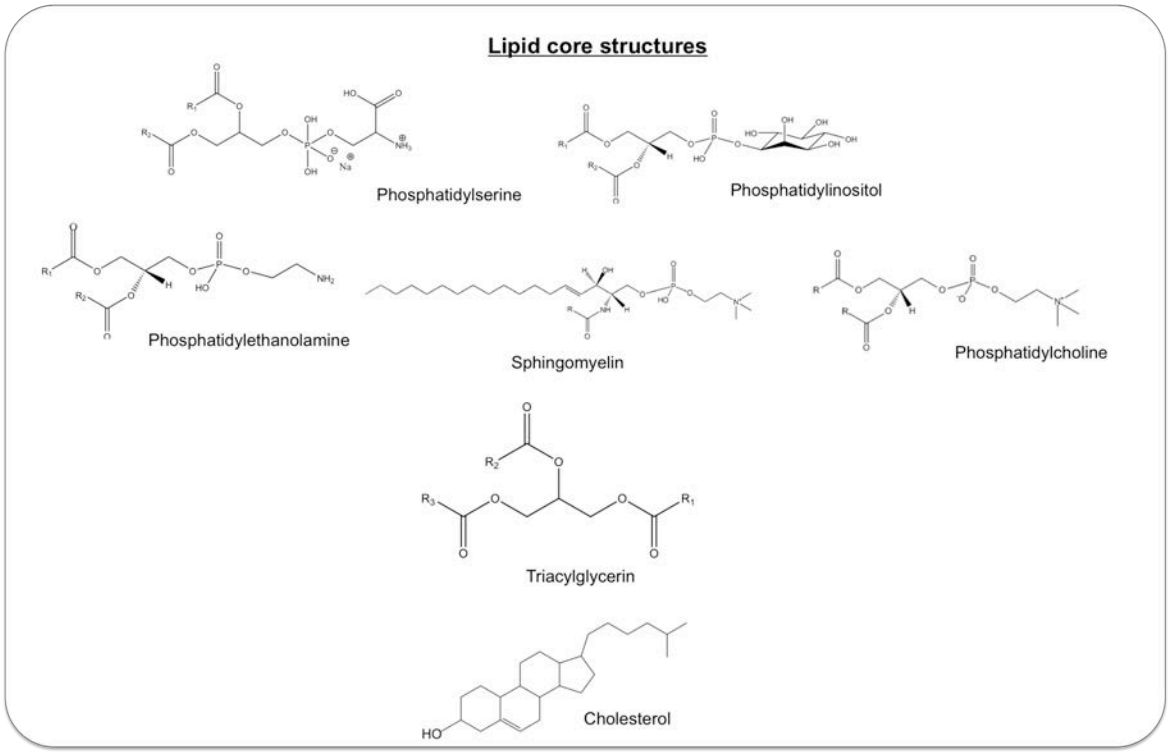

Figure 7: Lipid core structures of the biologically most relevant lipid species: phosphatidylcholine, phosphatidylserine, phosphatidylinositol, phosphatidylethanolamine, sphingomyelin, triglycerides and cholesterol.

Phospholipids are easy to identify by MS/MS analysis because of the characteristic daughter ions of their head groups. Glycerophosphatidylcholine (PC) shows characteristic $[M+H]^+$ fragment ions of the

head group: m/z 86.09 corresponding to dehydrocholine, m/z 125.00 to cyclophosphane in the protonated form and m/z 184.07, the protonated cholinephosphate. The fragmentation yield can be improved by using potassium and sodium salts, resulting in $[M+Na]^+$ and $[M+K]^+$ daughter ion at m/z 146.98 and m/z 162.26 for cyclophosphane. PCs can further be identified based on their characteristic neutral losses of trimethylamine (59 u), dehydrocholine (86 u), cholinephosphate (183 u) and sodiated cyclophosphane (147 u). Monoacylglycerophoasphatidylcholine (LPO) is structurally identical to PC, except the acyl chain composition resulting in a decreased molecular weight.

Sphingomyelin (SM) and PC show the same characteristic fragmentation products during MS/MS due to their phosphocholine head group, however SM is structurally a ceramide having the acyl chain attached by an amide bond. SM can be identified based on its molecular mass difference due to the incorporated nitrogen atom compared to PC.

Glycerophosphatidylethanolamine (PE) shows characteristic neutral losses of ethanolamine (43 u) or the head group ethanolaminephosphate (141 u). Signals of the sodiated polar head are detected at m/z 164.01 and m/z 120.97 without ethanolamine or m/z 179.99 for the potassium adducts.

For Glycerophosphatidylinositol (PI) the characteristic losses of neutral inositol (161 u), inositol phosphate (260 u) and the corresponding potassium adduct (299 u) are applicable for identification. The only characteristic fragment ion for PI is the potassium adduct ion of inositol phosphate $[M+K]^+$ at m/z 298.99.

Glycerophosphatidylserine (PS) can be identified by the neutral loss of the serine head group (87 u). Triacylglycerides (TG) and diacylglycerides (DG) are usually detected as potassium or sodium adduct ions, showing neutral losses of acyl chains during MS/MS analysis. Cholesterol is often identified with the dehydrated precursor ion of m/z 369 $[M+H-H_2O]^+$ using CHCA as matrix of choice. The main primary fragmentation product, the loss of the carbon backbone between C_{17} and C_{20} according to IUPAC nomenclature, with m/z 256.36 can be identified besides several secondary fragmentation products. The other fragmentation products are localized in the sterol ring system including m/z 81.34 and m/z 172.27 between C_8/C_{14} and C_{12}/C_{13}, m/z 95.36 and m/z 161.38 between C_8/C_{14} and C_{11}/C_{12}, between C_{11}/C_{12} and C_8/C_{12} and m/z 147.37 between C_9/C_{11} and C_8/C_{14}.

Several data base projects have been established for lipid analysis, however, the demand is not very high to automize data analysis. Lipid Maps [34] is the largest data base, including structural and functional informations about lipid species. Mmass libraries have been established based on those data sets.

c. Histology

Despite originating from the combination of the Greek words *histos* referring to tissue and *logos* to science, histological techniques are relevant for any type of analyte investigated using MSI applications. The methods mainly involve cell and tissue analysis by means of microscopy, staining procedures and allied sample preparation procedures. Recent developments include the automated surface, mostly tissue, analysis by mathematical algorithms.

Biomaterials, such as UHWMPE, benefit from staining procedures to improve the visualization of their lamellar structure. Due to their very homogeneous surface in the virgin native state, structural differentiation and information can hardly be obtained by low-resolution microscopic techniques. Scanning electron microscopy and atomic force microscopy was successfully applied for the

structural investigation of native and aged PE-UHMW surfaces [35-37]. However, to obtain more insight to the lamellar structure of differently cross-linked PE-UHMW, staining methods were combined with transmission electron microscopy [38]. Selective staining of polymer particles was conducted to identify wear particles in tissue and revealed comparable results to conventional polarized light microscopy [39]. Moreover, for polymer surfaces, mechanical surface analysis data can be applied, resulting from tribology experiments. However, those informations hardly deliver molecular or structural insight, needed for the correlation with MSI experiments.

The main drawback with staining procedures in tissue analysis is data interpretation by experienced users, which is not objectifiable. Immunological staining based on specific antibody/antigen interaction, on the other side lacks flexibility. Each antibody has to be designed for the particular antigen, still including the possibility of non-specific or prevented binding due to crosslinking or conformational changes within samples.

In addition MSI as a comprehensive visualization technique delivers informations, especially regarding tissue and cell analysis, which can only be verified by histological methods.

The process of histological examination is preferably conducted before MS analysis to avoid morphological stability without laser irradiation. The common principal is selective staining followed by microscopic tissue analysis. Staining provides the possibility to differentiate tissue structures, cell types and verify the presence of specific analytes on the macromolecular level. The principal is simple and based on acid/base chemistry or oxidation/reduction reactions.

To obtain information about tissue structures within a general approach, unspecific staining methods are used. Haematoxylin and Eosin (H/E) is the most frequently used approach, first described in 1876 by Wissowzky [40]. During the staining procedure haematoxylin is oxidized to hematein, which again forms a complex with aluminum resulting in hemalum, responsible for coloring cell nuclei dark blue. The second dye, eosin, functions as a counterstain preferentially dying eosinophilic, basic structures in red (pink). Differentiating protein from DNA, is possible by this procedure but also a good overview to any kind of tissue is given [41].

Another very commonly used staining technique is toluidine blue, staining nucleic acids and polysaccharides. The basic thiazine metachromatic dye provides a very high affinity for acidic tissue components and has already been discovered for histological applications in 1856 [42]. It has mainly been used for tumor tissue differentiation and was assumed to selectively stain tumor tissue in the 1960s [43]. However, later it was discovered that it the dye preferentially attaches to DNA, which is quantitatively more present in malignant tissue parts. Moreover, it was demonstrated that cancerous epithelium contained intracellular canals with larger diameters, easing dye penetration [44]. Besides those general staining methods, also specific staining methods exist for connective, fibrous or fat tissues as well as calcified tissue.

The big advantage of optical (microscopic) imaging approaches compared to MSI is the very high lateral resolution. Even though it is difficult for the observer to detect little variations or abnormalities within a small area, software algorithms have been developed to automate image analysis. Digital slide scanners today frequently replace high resolving light microscopes. The scanners obtain high-resolution images at high quality providing also data analysis features. Though the main parameter of instrument development focuses on resolution increase and image quality, software solutions provide an important tool for data analysis and correlation [45]. The main goal of

software developments is to implement automatic evaluation of large-scale data sets, which is time consuming and error-prone if done manually. The latest developments of computer-assisted diagnostics (CAD), is also of potentially high impact for MSI experiments.

One of the first software tools, applicable also to surface analysis in general, was ImageJ. The software is based on pattern recognition and delivers optical information as grey scale values for each pixel. Conventional picture document files as well as DICOM information can be processed. ImageJ is capable of cell counting, regional differentiation and surface analysis based on optical density parameters. Later developments also included gel analysis, magnet resonance imaging or computer tomography, radiology, live cell observation and even the combination of multiple approaches.

The easy implementation of image analysis into Matlab or Mathematica lead to an increasing number of in-house, stand alone software solutions implementing statistics. One of the latest publications in this respect presents image deconvolution combined with nuclei counting as a support vector machine melanoma classification model. The algorithm is capable of successfully differentiating melanoma and non-melanoma cells [46]. Other approaches use tissue heterogeneity indices to differentiate cancerous tissue regions and stroma rich areas with high chromatin content. This technique is mainly used as an assistive tool for breast cancer identification for further tissue treatment approaches [46, 47]. However, automated and subjective image analysis and comparison provides an incredible tool for any tissue type and analytical question [48].

References

1. Schagger, H. and G. von Jagow, *Tricine-sodium dodecyl sulfate-polyacrylamide gel electrophoresis for the separation of proteins in the range from 1 to 100 kDa.* Anal Biochem, 1987. **166**(2): p. 368-79.
2. Weber, K. and M. Osborn, *The reliability of molecular weight determinations by dodecyl sulfate-polyacrylamide gel electrophoresis.* J Biol Chem, 1969. **244**(16): p. 4406-12.
3. Reynolds J A, T.C., *Binding of dodecyl sulfate to proteins at high binding ratios. Possible implications for the state of proteins in biological membranes.* Proc Natl Acad Sci USA, 1970. **66**(3): p. 1002-1007.
4. P, L., *Reliability of molecular weight determination of proteins by polyacrylamide gradient gel electrophoresis in the presence of SDS.* Analytical Biochemistry, 1978. **85**: p. 114-125.
5. Müller R, M.-D.M., Elgass H, Breiteneder H, Kratzmeier M, Allmaier G, *Molecular weight determination of high molecular mass (glyco)proteins using CGE-on-a-chip, planar SDS-PAGE and MALDI-TOF-MS.* Electrophoresis, 2010. **31**: p. 3850-3862.
6. F, P.W., *Detection technologies in proteome analysis.* Journal of Chromatography B, 2002. **771**: p. 3-31.
7. Oakley, B.R., D.R. Kirsch, and N.R. Morris, *A simplified ultrasensitive silver stain for detecting proteins in polyacrylamide gels.* Anal Biochem, 1980. **105**(2): p. 361-3.
8. Winkler, C., et al., *Silver- and Coomassie-staining protocols: detection limits and compatibility with ESI MS.* Electrophoresis, 2007. **28**(12): p. 2095-9.
9. Fazekas De St Groth S, W.R., Datyner A, *Two new staining procedures for quantitative estimation of proteins on electrophoresis strips.* Biochimica and Biophysica Acta, 1963. **71**: p. 377-391.
10. Kang D, G.Y.S., Suh M, Kang C, *Highly Sensitive and Fast Protein Detection with Coomassie Brilliant Blue in Sodium Dodecyl Sulfate-Polyacrylamide Gel Electrophoresis.* Bulletins of the Korean Chemical Society, 2002. **23**(11): p. 1511-1512.
11. Wheeler, S.F., P. Domann, and D.J. Harvey, *Derivatization of sialic acids for stabilization in matrix-assisted laser desorption/ionization mass spectrometry and concomitant differentiation of alpha(2 --> 3)- and alpha(2 --> 6)-isomers.* Rapid Commun Mass Spectrom, 2009. **23**(2): p. 303-12.
12. Scheler, C., et al., *Peptide mass fingerprint sequence coverage from differently stained proteins on two-dimensional electrophoresis patterns by matrix assisted laser desorption/ionization-mass spectrometry (MALDI-MS).* Electrophoresis, 1998. **19**(6): p. 918-27.
13. Gevaert, K. and J. Vandekerckhove, *Protein identification methods in proteomics.* Electrophoresis, 2000. **21**(6): p. 1145-54.
14. Pappin, D.J., P. Hojrup, and A.J. Bleasby, *Rapid identification of proteins by peptide-mass fingerprinting.* Curr Biol, 1993. **3**(6): p. 327-32.
15. Dodds, E.D., et al., *Systematic characterization of high mass accuracy influence on false discovery and probability scoring in peptide mass fingerprinting.* Anal Biochem, 2008. **372**(2): p. 156-66.
16. Kapp, E. and F. Schutz, *Overview of tandem mass spectrometry (MS/MS) database search algorithms.* Curr Protoc Protein Sci, 2007. **Chapter 25**: p. Unit25 2.
17. Hettick, J.M., et al., *Optimization of sample preparation for peptide sequencing by MALDI-TOF photofragment mass spectrometry.* Anal Chem, 2001. **73**(22): p. 5378-86.
18. Yergey A L, C.J.R., Backlung Jr P S, Blank P S, Humphrey G A, Zimmerberg J, Campbell J M, Vestal M L, *De novo sequencing of peptides using MALDI/TOF-TOF.* J Am Soc Mass Spectrom, 2002. **13**(7): p. 784-791.
19. D, P.A., *Phospholipid lipidomics in health and disease.* Eur. J. Lipid Sci. Technol, 2009. **111**: p. 2-13.
20. Ivanova, P.T., et al., *Lipidomics: a mass spectrometry based systems level analysis of cellular lipids.* Curr Opin Chem Biol, 2009. **13**(5-6): p. 526-31.

21. Schiller, J., et al., *MALDI-TOF MS in lipidomics.* Front Biosci, 2007. **12**: p. 2568-79.
22. Fuchs, B., et al., *Capabilities and drawbacks of phospholipid analysis by MALDI-TOF mass spectrometry.* Methods Mol Biol, 2009. **579**: p. 103-25.
23. Murphy, R.C. and A.H. Merrill, Jr., *Lipidomics and imaging mass spectrometry.* Biochim Biophys Acta, 2011. **1811**(11): p. 635-6.
24. Bligh, E.G. and W.J. Dyer, *A rapid method of total lipid extraction and purification.* Can J Biochem Physiol, 1959. **37**(8): p. 911-7.
25. Folch, J., M. Lees, and G.H. Sloane Stanley, *A simple method for the isolation and purification of total lipides from animal tissues.* J Biol Chem, 1957. **226**(1): p. 497-509.
26. Cheng, S.C., M.Z. Huang, and J. Shiea, *Thin layer chromatography/mass spectrometry.* J Chromatogr A, 2011. **1218**(19): p. 2700-11.
27. White, T., et al., *High-resolution separation and quantification of neutral lipid and phospholipid species in mammalian cells and sera by multi-one-dimensional thin-layer chromatography.* Anal Biochem, 1998. **258**(1): p. 109-17.
28. Ibrahim, H., et al., *Interest of fluorescence derivatization and fluorescence probe assisted post-column detection of phospholipids: a short review.* Molecules, 2010. **15**(1): p. 352-73.
29. Fuchs, B., et al., *A direct and simple method of coupling matrix-assisted laser desorption and ionization time-of-flight mass spectrometry (MALDI-TOF MS) to thin-layer chromatography (TLC) for the analysis of phospholipids from egg yolk.* Anal Bioanal Chem, 2007. **389**(3): p. 827-34.
30. Zhou, P., et al., *Study of matrix additives for sensitive analysis of lipid A by matrix-assisted laser desorption ionization mass spectrometry.* Appl Environ Microbiol, 2010. **76**(11): p. 3437-43.
31. Fuchs, B., R. Suss, and J. Schiller, *An update of MALDI-TOF mass spectrometry in lipid research.* Prog Lipid Res, 2011. **50**(1): p. 132.
32. Pittenauer, E. and G. Allmaier, *The renaissance of high-energy CID for structural elucidation of complex lipids: MALDI-TOF/RTOF-MS of alkali cationized triacylglycerols.* J Am Soc Mass Spectrom, 2009. **20**(6): p. 1037-47.
33. Pittenauer E, A.G., *A universal product ion nomenclature for [M−H]−, [M+H]+ and [M+nNa−(n − 1)H]+ (n = 1–3) glycerophospholipid precursor ions based on high-energy CID by MALDI-TOF/RTOF mass spectrometry.* International Journal of Mass Spectrometry, 2011. **301**(1-3): p. 90-101.
34. Fahy, E., et al., *LIPID MAPS online tools for lipid research.* Nucleic Acids Res, 2007. **35**(Web Server issue): p. W606-12.
35. Rocha M, M.A., Mansur H, *Characterization and Accelerated Ageing of PE-UHMW Used in Orthopedic Prosthesis by Peroxide.* Materials, 2009. **2**: p. 562-576.
36. Shi W, D.H., Bell T, *Tribological behaviour and microscopic wear mechanisms of PE-UHMW sliding against thermal oxidation-treated Ti6Al4V.* Materials Science and Engineering, 2000. **A291**: p. 27-36.
37. Scott, M., et al., *Particle analysis for the determination of PE-UHMW wear.* J Biomed Mater Res B Appl Biomater, 2005. **73**(2): p. 325-37.
38. Stara H, S.M., Lednicky F, Pavlova E, Baldrian J, Stary Z, *New and Simple Staining Method for Visualizing UHWMPE Lamellar Structure in TEM.* Journal of Macromolecular Science, 2008. **47**: p. 1148-1160.
39. Schmalzried, T.P., et al., *Histologic identification of polyethylene wear debris using Oil Red O stain.* J Appl Biomater, 1993. **4**(2): p. 119-25.
40. A, W., *Ueber das eosin als reagenz auf hämoglobin und die Bildung von Blutgefässen und Blutkörperchen bei säugetier und hühnerembryonen.* Archiv für mikroskopische Anatomie, 1876. **13**: p. 479-496.
41. Fischer, A.H., et al., *Hematoxylin and eosin staining of tissue and cell sections.* CSH Protoc, 2008. **2008**: p. pdb prot4986.
42. H, P.W., *Aniline purple*. 1856: UK.
43. Sridharan, G. and A.A. Shankar, *Toluidine blue: A review of its chemistry and clinical utility.* J Oral Maxillofac Pathol, 2012. **16**(2): p. 251-5.

44. Epstein JB, S.C., Spinelli J, *Toluidine blue and Lugol's iodine application in the assessment of oral malignant disease and lesions at risk of malignancy.* J. Oral Pathol Med., 1992. **83**: p. 537-47.
45. Mulrane, L., et al., *Automated image analysis in histopathology: a valuable tool in medical diagnostics.* Expert Rev Mol Diagn, 2008. **8**(6): p. 707-25.
46. Rexhepaj, E., et al., *A texture based pattern recognition approach to distinguish melanoma from non-melanoma cells in histopathological tissue microarray sections.* PLoS One, 2013. **8**(5): p. e62070.
47. Wang, C.W., et al., *Robust automated tumour segmentation on histological and immunohistochemical tissue images.* PLoS One, 2011. **6**(2): p. e15818.
48. Foran, D.J., W. Chen, and L. Yang, *Automated image interpretation and computer-assisted diagnostics.* Stud Health Technol Inform, 2013. **185**: p. 77-108.

5. Renopathological Microstructure Visualization from Formalin Fixed Kidney Tissue by Matrix-Assisted Laser Desorption/Ionization-Time-of-Flight Mass Spectrometry Imaging

Proceedings of the MACPROGEN Final Conference held
at Ohrid, Republic of Macedonia, March 29-April 1 2012

RENOPATHOLOGICAL MICROSTRUCTURE VISUALIZATION FROM FORMALIN FIXED KIDNEY TISSUE BY MATRIX-ASSISTED LASER/DESORPTION IONIZATION-TIME-OF-FLIGHT MASS SPECTROMETRY IMAGING

Fröhlich S[1], Putz B[1], Schachner H[2], Kerjaschki D[2], Allmaier G[1], Marchetti-Deschmann M[1,*]

***Corresponding Author:** Dr. Martina Marchetti-Deschmann, Vienna University of Technology, Institute of Chemical Technologies and Analytics, Getreidemarkt 9/164-IAC, 1060 Vienna, Austria; Tel.: +43-1-58801-15152; Mobile: +43+664-605887663; Fax: +43-1-58801-915162; E-mail: martina.marchetti-deschmann@tuwien.ac.at

ABSTRACT

Understanding early stage renal malfunctions with regard to the glomerular filtration processes is essential for nephropathological prescreening strategies and intervention at an early stage. Mass spectrometry imaging (MSI) in combination with histopathology can provide an universal analytical approach. Proteomic and lipidomic aspects of glomerular biocompositions were applied for microstructural differentiation in healthy rat kidney samples. Usability of commonly used tissue embedding media and the compatibility of histological staining and fixation methods were of interest. It was demonstrated that ultra-thin tissue samples (500 nm, 1 and 10 µm) can be used for lipid and peptide-based differentiation at the glomerular resolution level in formalin-fixed tissue samples in combination with preceding histological staining for correlating optical and molecular mass images.

Keywords: Glomerular microstructures, Lipids, Matrix-assisted laser desorption/ionization-time of flight (MALDI-TOF) mass spectrometry (MS) imaging, Nephropathy, Proteins

[1] Vienna University of Technology, Institute of Chemical Technologies and Analytics, Vienna, Austria

[2] Medical University of Vienna, Department of Clinical Pathology, Vienna, Austria

INTRODUCTION

A combination of histopathology and mass spectrometry imaging (MSI) offers comprehensive information regarding structure, molecular composition and pathological information in tissue samples. Mass spectrometry imaging is a rapidly developing technique using spatially resolved mass spectrometry (MS) techniques to simultaneously trace distributions of hundreds of biomolecules directly from tissue samples using essentially the same technology. Peptides, proteins, pharmaceuticals and metabolites can also be analyzed but without a label and without prior knowledge. With MSI, molecular peak information is correlated to the underlying tissue architecture and a virtual image is rebuilt with respect to the intensity of each molecular species to understand the distribution of differential signals.

Renal dysfunction has a high demand for early stage identification to initiate healing processes. Recent investigations proved nephropathy is associated with insulin resistance leading to malfunctions of the glomerular filtration [1], manifested in potential glomerular basement membrane modifications [2]. Lipid phosphatase levels, promoting podocyte apoptosis leading to diabetic nephropathy, are upregulated before histological changes are observed [1]; moreover, the membrane contains protein complexes associated with cholesterol binding which alters the lipid environment [2]. Lipid accumulations

have been reported for diabetic kidney diseases [3] and oxidized phosphatidylcholine species seem to be associated with renal dysfunction [4]. Recently tubuli-related phosphatidylcholine classes identified by MSI were correlated to immunoglobulin A nephropathy [5].

Thus, for visualizing renopathological microstructures, MSI is a promising tool, allowing further discoveries of yet unknown disease-related analytes. Special challenges regarding ion suppression effects during the matrix-assisted laser desorption/ionization (MALDI) process were observed whilst obtaining lipidomic information using MSI. Consequently, special attention had to be paid to sample preparation methods, regarding washing procedures, matrix application and protein denaturation, making adaptation to the particular analytical question mandatory [6].

MATERIALS AND METHODS

Chemicals were of analytical grade (Sigma-Aldrich, St. Louis, MO, USA). Water (ddH_2O) was purified in a Simplicity system (Millipore, Billerica, MA, USA). Frozen rat kidney tissue (formalin-fixed, unfixed) embedded in paraffin (FFPE), optimal cutting temperature (OCT) compound (Sakura Finetek, Tokyo, Japan) or sucrose was sliced to 10, 5 and 0.5 µm using a cryo-microtome (Leica, Wetzlar, Germany) and mounted on indium-tin oxide coated glass slides (Sigma-Aldrich). The OCT compound and sucrose were removed by washing the samples five times (4°C) for 45 seconds with 200 µL ddH_2O/cm^2. A xylene bath followed by a descending ethanol gradient (100.0, 96.0, 70.0, 50.0, 0.0% in ddH_2O) removed the paraffin. All samples were washed three times with 200 µL 70.0% ethanol/cm^2 for 45 seconds (4°C) and vacuum dried for 15 min. before the MALDI matrix application. Samples were hematoxylin/eosin (H/E) stained before MSI treatment.

The MALDI matrices [α-cyano-4-hydroxycinnamic acid (HCCA), sinapinic acid, 2,5-dihydroxybenzoic acid] were dissolved in solvents containing 50.0 or 70.0% acetonitrile or ethanol in 0.1% aqueous trifluoroacetic acid. Matrix deposition was performed using a ChIP-1000 (Shimadzu Biotech Kratos Analytical). For protein identification, tissue was trypsinized before matrix deposition by depositing enzyme directly on pre defined tissue spots [1 ng/µL in 50 mM ammonium bicarbonate, 0.1% Rapigest (Waters, Manchester, Greater Manchester, UK)]. Samples were incubated in a humidified atmosphere overnight at 37°C before desiccation in vacuum and heat treatment (85°C).

Mass spectrometry imaging experiments were performed using a MALDI-TOF (time of flight) instrument (AXIMA TOF^2; Shimadzu Biotech Kratos Analytical, Manchester, Greater Manchester, UK; 337nm nitrogen laser, 20Hz) and a MALDI-QqTOF instrument (Synapt HDMS, Waters; 355nm Nd-YAG laser, 200Hz). The optical diameter of 60 µm was reduced to an operational resolution of 35 µm by over sampling.

Peptide and lipid identification was based on post source decay (PSD) and collision induced dissociation (CID) fragmentation in combination with database search [proteins: SwissProt (http://www.uniprot.org/help/ uniprotkb); lipids: Lipid Maps (http://www.lipidmaps.org/ data/structure/)]. Selected ion images were generated using BioMAP (Novartis, Basel, Switzerland).

RESULTS AND DISCUSSION

Histology and Mass Spectrometry Imaging. Integrating MSI in histopathology necessitates the combination of different requirements from pathology and MS. The primary demands for histology are the preservation of high spatial resolution for tissue structures, long lasting analyte preservation and low sample consumption. For MS, spatial resolution can usually be disregarded and analytes have to be mobilized instead of preserved. For MSI, additionally, histological information has to be retained and tissue disintegration has to be limited to a minimum. We present an approach arranging histological staining prior to MSI using ultra-thin tissue sections showing good molecular results comparable to microscopic images.

It was found that MALDI-TOF MSI analysis of H/E-stained tissue showed no limiting aspects concerning proteomic approaches. Protein digestion directly from the tissue and measuring peptides by MS could be achieved. Stain-related signals, however, were observed below m/z signals of 500, eventually leading to ion suppression effects for neutral lipids. Phospholipid classes were obtained unaffected from

ultra-thin sucrose samples. Histological images of OCT embedded samples were often difficult to correlate to MSI results because of structural changes after thawing. Sucrose embedding in combination with cutting thickness of 1 µm was sufficient for IMS analysis, even reducing signal background and enhancing signal quality. The selected ultra-thin samples considerably improved signal quality whilst preserving spatial resolution.

Lipid Differentiation. Lipid-based histological differentiation was performed using unfixed rat kidney samples embedded in sucrose and formalin-fixed tissue embedded in OCT Low embedding medium related signals and intensive species-related signals were obtained from both OCT and sucrose embedded samples. Several lipid classes could be localized, identified and characterized by fragmentation experiments. Unfixed tissue species revealed different distribution pattern phosphoatidylcholine species with varying alkyl chain lengths. The 1-tetradecanoyl-2-sn-glycero-3-phosphocholine, 1-hexadecanolyl-2-sn-glycero-3-phosphocholine and 1-octadecanoyl-2-sn-glycero-3-phosphocholine showed specifiable areas related to kidney structures, *i.e.,* cortex, medulla and pelvis (Figure 1). The 1-hexadecyl-2-acetyl-sn-glycero-3-phosphocholine and 1-hexadecanoyl-sn-glycero-3-phosphocholine exhibited different localization as well as 1-O-(1Z-tetradecenyl)-2-(9Z-octadecenoyl)-sn-glycerol and its oxidized co-species. Besides 16 different phospholipids, diacylglycerophosphoethanolamine, N-(tetracosanoyl)-sphing-4-enine-1-phospho-choline and two glomeruli specific metabolites, cholesterol and squalene, were also discovered. Histological correlation revealed the potential to identify pathologically modified membrane structures in glomerular associated diseases.

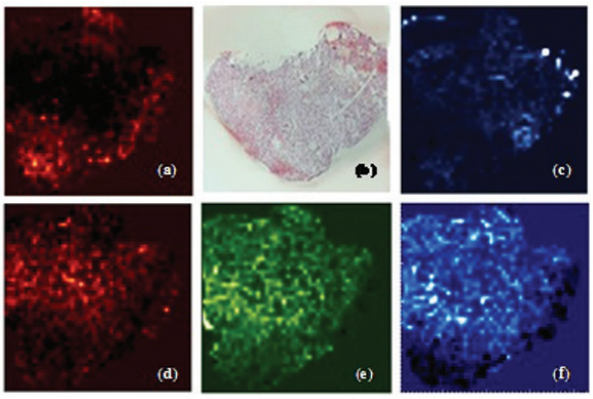

Figure 1. Tissue differentiation according to identified lipid species. Distribution of **(a)** diacylglycerol on **(b)** 5 µm OCT embedded unfixed kidney tissue; **(c)** oxidized diacylglycerol; **(d)** 1-tetradecanoyl-2-sn-glycero-3-phos-phocholine; **(e)** 1-hexadecanolyl-2-sn-glycero-3-phosphocholine; **(f)** 1-octadecanoyl-2-sn-glycero-3-phosphocholine.

Protein Identification. To detect most of the proteins available in an ultra-thin sample, several washing steps were required for complete removal of analyte species which are much easier to ionize than proteins, *e.g.,* lipids [7]. Our study showed that mass spectra quality for tissue analysis was enhanced by heat treatment before MSI experiments. Several tissue-related peptides could be identified by PSD and CID, revealing the possibility to distinguish pelvis and cortex, both tissue macrostructures. For all investigated embedding materials as well as fixation methods, it was possible to obtain sufficient signals up to m/z values of 10000 (Figure 2). The application of danaturation agents and heat treatment supports subsequent on-tissue enzymatic

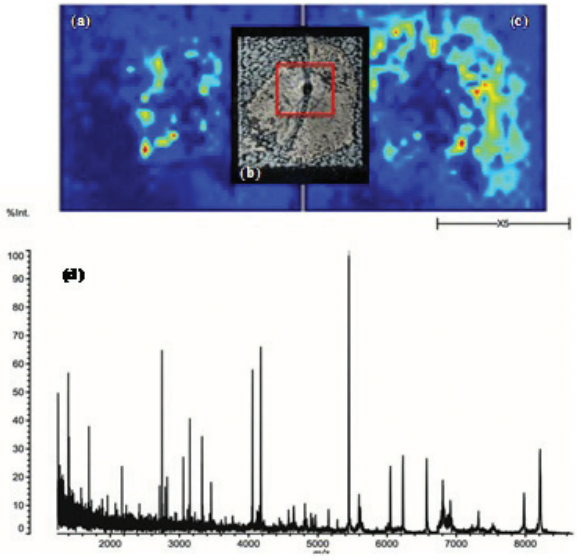

Figure 2. Protein based differentiation of **(a)** medulla and **(c)** cortex in; **(b)** FFPE rat kidney tissue (10 µm) after HCCA application; **(d)** MALDI-TOF-MS profile of the marked sample area (red).

treatment for protein identification on fixed and embedded rat kidney. Highly cross-linked proteins (formalin) showed improved signal intensities for tryptic peptides after denaturation, which significantly supported protein identification based on peptide fragmentation. For protein identification in MSI approaches, peptide sequencing was indispensable because of protein co-localization and the non

applicable approach of peptide mass fingerprinting. The presented protocol on ultra-thin tissue sections allowed the identification of Tubulin and Claudin-4, besides seven other peptide fragments on differentiated, but so far unspecific, tissue regions.

Perspectives. Combining histopathology and MSI for investigating structural membrane modifications associated with glomerular related nephropathology looks promising. Structural modifications and molecular changes can be detected and investigated very early in progression.

REFERENCES

1. Hyvönen ME, Saurus P, Wasik A, *et al.* Lipid phosphotase SHIP2 downregulates insulin signalling in podocytes. Mol Cell Endocrinol. 2010; 328(1-2): 70-79.
2. Kibel G, Heilhecker A, Von Bruchhausen F. Lipids associated with bovine kidney glomerular basement membranes. Biochem J. 1976; 155(3): 535-541.
3. Wang Z, Jiang T, Li J, *et al.* Regulation of renal lipid metabolism, lipid accumulation, and glomerulosclerosis in FVBdb/db mice with type 2 diabetes. Diabetes. 2005; 54(8): 2328-2335.
4. Jimi S, Uesugi N, Saku K, *et al.* Possible induction of renal dysfunction in patients with lecithin:cholesterol acyltransferase deficiency by oxidized phosphatidylcholine in glomeruli. Arterioscler Thromb Vasc Biol. 1999; 19(3): 794-801.
5. Kaneko Y, Obata Y, Nishino T, *et al.* Imaging mass spectrometry analysis reveals an altered lipid distribution pattern in the tubular areas of hyper-IgA murine kidneys. Exp Mol Pathol. 2011; 91(2): 614-621.
6. Kaletaş BK, van der Wiel IM, Stauber J, *et al.* Sample preparation issues for tissue imaging by imaging MS. Proteomics. 2009; 9(10): 2622-2633.
7. van Hove ER, Smith DF, Fornai L, *et al.* An alternative paper based tissue washing method for mass spectrometry imaging: localized washing and fragile tissue analysis. J Am Soc Mass Spectrom. 2011; 22(10): 1885-1890.

6. The influence of sample type and preparation on MALDI-TOF mass spectrometry imaging

To be submitted to Journal of the American Society of Mass Spectrometry (2014)

Address reprint requests to Assoc.-Prof. Dr. Martina Marchetti-Deschmann, Austria – 1060 Vienna, Getreidemarkt 9/164-IAC, T: +43 – 158851 – 15162, F: +41 (1) 58801 - 915162, E: martina.marchetti-deschmann@tuwien.ac.at

The influence of sample type and preparation on MALDI-TOF mass spectrometry imaging

Sophie Fröhlich[1,2], Paul Rigger[1] , Michael Vellekoop[3], Dontscho Kerjaschki[2], Vasiliki-Maria Archodoulaki[4], Günter Allmaier[1], Martina Marchetti-Deschmann[1]

1) *Institute of Chemical Technologies and Analytics, Vienna University of Technology, Vienna, Austria*
2) *Clinical Institute of Pathology, Medical University of Vienna, Vienna, Austria*
3) *Institute of Sensor and Actuator Systems, Vienna University of Technology, Vienna, Austria*
4) *Institute of Materials Science and - Technology, Vienna University of Technology, Vienna, Austria*

Running Title: Tissue surface influence on MSI

Keywords: MALDI, mass spectrometry imaging, sample preparation, sample surface parameters, mass accuracy

ABSTRACT

The use of mass spectrometry for localizing analytes on surfaces, also referred to as mass spectrometry imaging (MSI), lead to new horizons for analytical investigations. However, investigated samples are rarely characterized for their physical properties and the respective impact on results. A closer look on matrix application was taken. Operating conditions were optimized for MALDI matrix application by a chemical inkjet printer, revealing the ideal set up for homogeneous layer generation. It was observed, that accurate MALDI matrix application with favorable small crystals were created under pre-cooled printing environment using very volatile solvent systems. In addition the present study looks at the influence of physical sample properties on the concept of MALDI-TOF MSI by comparing theoretical calculations to practical measurements. Mass deviation was evaluated for two different axial MALDI-TOF/RTOF and an orthogonal MALDI-TOF/RTOF instrument. Besides this formalin fixed paraffin embedded (FFPE) tissue, ultra-high molecular weight polyethylene (UHMWPE) and a standardized silicium wafer, three samples of significantly different permittivity, were evaluated and showed significant m/z deviations for investigated peptides. This study presents the importance of homogeneous sample surface and sample permittivity to enhance mass accuracy in MSI experiments.

1. INTRODUCTION

Drawing a two-dimensional map of analyte distributions based on their mass-to-charge (m/z) ratio is the core aim of mass spectrometry imaging (MSI), an analytical technique which has been in use for over 14 years by now [1]. MSI is able to detect and localize multiple unlabeled molecules directly and in parallel in any tissue section [2]. The possibility of parallel distribution visualization and identification of analytes in a mass spectrometric approach allowed the application in new areas [3-4]. Besides consistent utilization in forensic medicine [5-7], plant analysis [8-9] and microbiology [10-11], the number and variety of applications has grown rapidly, especially for the fields of proteomics, lipidomics and metabolomics [12] using matrix assisted laser desorption (MALDI) time of flight (TOF) approaches. Besides visualization of the spatial distribution, the key to answering scientific questions lies in the identification of analytes. High mass accuracy for a broad mass range is therefore mandatory and can be achieved by reproducible conditions in sample preparation, desorption, ionization and detection [13-15]. Especially within MALDI-TOF MSI experiments homogeneous analyte incorporation supports the energy transfer efficiency but does not compensate sample surface inherent properties such as height and relative permittivity (ε_r). Furthermore, commercially available MALDI-TOF devices contain instrument inherent characteristics for their mechanics (i.e. accuracy) and ion optics, however both significantly influence MSI experiment accuracy and comparability. Besides those constraints, matrix application is one of the most crucial steps for a successful MALDI-MSI experiment [16-17]. The ChIP-1000 [18], a microscale piezo printer, has proven to provide one of the most accurate methods to homogeneously deposit MALDI matrix to any kind of sample surface due to its adaptability. However, drawbacks in its usability (print head clogging, long operating time, difficult optimization

of settings) made matrix deposition susceptible for deviance in the past and difficult to reproduce in high throughput approaches [19].

The influence of topography for imaging experiments using SIMS has already been studied [20], pointing out the importance of even surfaces. In this study the possibility to use height differences to ascertain, whether local intensity maxima correlate to topological features or represent genuine features of interest, was suggested. What has not been considered in detail in this study is the fact, that m/z deviations are also generated in tissue samples of significant thickness and that this is of importance especially for the mass range usually addressed in an MALDI time-of-flight (TOF) based MSI experiment

Besides the sample height, also the sample's ε_r has to be considered as an important impact factor, which will be evaluated in the present study. Both factors are relevant for the desorption/ionization process. As an important parameter for mass resolution the influence of delayed extraction time, will further be evaluated. In the presented study we investigate the potential of delayed extraction values to correct for tissue inhomogeneities. To our knowledge the influence of sample surfaces on mass deviation has not been presented yet, although mass accuracy has a major influence in many fields, e.g. on the false positive discovery rate of protein identification [21-22]. Highest mass accuracy for MSI experiments has been achieved on Orbitrap and FT-ICR systems [22]. So far the highest reported experimental accuracy for TOF systems used in MSI experiment was 30 ppm on a orthogonal acceleration (oa) TOF [23] and only 200 ppm for axial TOF mass analyzers [24]. Therefore, oa systems are usually recommended for MSI [12]. But they usually have limited accessible mass ranges and higher molecular weight compounds (> 20 kDa) are difficult to detect. Moreover, it has to be considered that these systems are sometimes lacking absolute sensitivity compared to axial systems [25] as they usually work

under intermediate or even atmospheric pressure in comparison to the high-vacuum ion sources of axial TOF systems.

This study focuses on estimating and circumventing the impact of height differences and sample material characteristics on mass deviation for the, in our opinion, favorable axial TOF system for MSI experiments. Highly reproducible matrix application using an automated micro-spotting device, as well as sample thickness and roughness were investigated in respect to ion intensities and mass deviations, and theoretical considerations for the correlation of mass accuracy to material characteristics are shown. Finally, the effect of sample surface parameters is evaluated with standardized samples on instruments with different ion source geometry.

2. EXPERIMENTAL SECTION

Sample preparation

Chemicals and peptide standard mixture

All chemicals were of analytical grade if not otherwise stated. Peptide standards used for external calibration and examination of height differences were purchased from Sigma-Aldrich (Steinheim, Germany). Solutions were prepared using acetonitrile (ACN, purity ≥ 99.5 %; Merck, Darmstadt, Germany). Ultra high quality water was obtained from a Simplicity water purification system (specific conductivity Ωm ≤ 18 S/cm; Millipore Billerica, MA, USA). Trifluoracetic acid (TFA, purity ≥ 99 %) was obtained from Pierce (Rockford, IL, USA). A peptide mixture containing 1 pmol per peptide was prepared by mixing Angiotensin I, Angiotensin II, Glu1-Fibrinopeptide B, $ACTH_{1-17}$, $ACTH_{18-39}$ and $ACTH_{7-38}$ each prepared in 70/30 (v/v) ACN / 0.1 % TFA. 0.5 µL was applied directly on investigated surfaces or pre-mixed with matrix for mass spectrometric calibration (see later section). α-cyano-4-hydroxycinnamic acid (CHCA), sinapinic acid (SA) or 2,5-dihydroxybenzoic acid (DHB) (for all purity > 99%) were all purchased from Sigma Aldrich.

Sample preparation

All tissue samples were mounted on indium tin oxide (ITO) coated glass slides (Sigma Aldrich, Steinheim, Germany), which were applied on the target holder using double sided tape in case of the AXIMA TOF^2 and the Synapt HDMS mass spectrometer (details see later). Tissue sections of 5 µm were obtained from frozen rat kidney embedded in paraffin using a rotation microtome (Leica, Nussloch, Germany). Paraffin was removed from kidney tissue by washing samples with xylene (Sigma Aldrich) followed by a descending ethanol (Sigma Aldrich) gradient – 100 %, 96 % 70 %, 50 % and 0 %. Tissue samples

were washed three times with 200 µL 70 % ethanol per cm^2 at 4 °C for 45 s and vacuum dried in a vacuum desiccator for 15 min before matrix application.

Ultra high molecular weight polyethylene (UHMWPE) samples were stabilized with O.C.T. (optimum cutting temperature) compound (Tissue Tek, Sakura Finetek, USA) and sliced using a Leica cryostat (Leica, Nussloch, Germany). Slices of 5 to 10 and of 12, 14, 16, 18, 20, 25, 30 and 35 µm were mounted on ITO glass slides by carefully flattening them with a silicon brush on double-sided conductive tape (Shimadzu Kratos Analytical, Kyoto, Japan). Microtome specificity was evaluated applying a dial gauge (Käfer, Villingen-Schwenningen, Germany) on UHMWPE slices.

O.C.T. compound was removed from UHMWPE samples by washing samples five times with 200 µL ddH_2O per cm^2 at 4 °C for 45 s.

Height profile standards

m/z deviation according to sample surface and thickness specificities was investigated using standardized surfaces regarding ε_r and height. Fig. 1 shows a scheme for the overall experimental setup.

Investigations for samples of very low ε_r, almost insulators, were conducted on UHMWPE sliced into samples of 5 to 35 µm thickness (see sample acquisition) and mounted on a conductive tape (Shimadzu Kratos Analytical) with a thickness of 80 µm (Fig. 1a). A phosphor-doped silicium-wafer with a total height of 548 µm, mounted on a stainless steel target with double-sided adhesive tape of 109 µm thickness was used as a model for conductive surfaces. Three different height steps were evaluated: 28.34, 70.21 and 162.87 µm below total sample height (Fig. 1b).

0.5 µL standard peptide mixture was applied directly to the investigated sample areas (25 mm^2) before matrix application.

Sample planarity effects were investigated using unevenly mounted (folded) UHMWPE and kidney tissue, representing samples with very high and very low ε_r. UHMWPE had a nominal thickness of 20 µm compared to 40 to 60 µm within the folded area and kidney tissue with a nominal thickness of 4 µm after paraffin removal showed 7 µm within the folded area (Fig. 1c).

All sample heights were verified with a dial gauge (Käfer, Villingen-Schwenningen, Germany) specified to 1 µm. Operative reproducibility and accuracy were evaluated on UHMWPE samples ranging from 5 µm to 35 µm and proved constant quality with acceptable deviation within the dial gauges specification (± 1 µm).

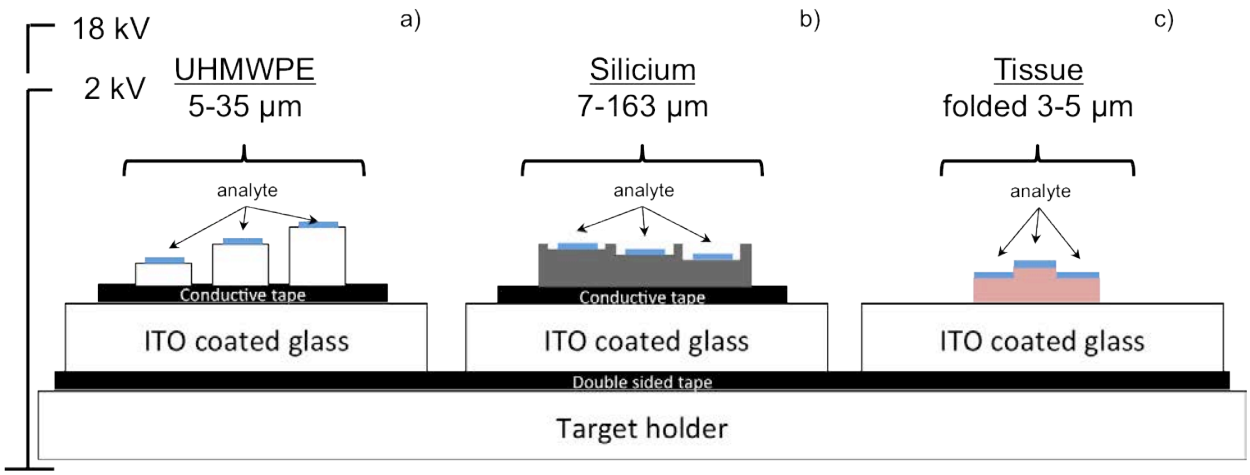

Figure 1: Scheme of experimental set up for evaluating height differences under the same technical conditions using an axial MALDI-TOF/RTOF mass spectrometer (AXIMA TOF², Shimadzu). 2 kV acceleration voltage for the first and 18 kV for the second region were applied; all samples are covered with a defined peptide standard and mounted on ITO coated glass slides using conductive tape for the polymer and metal samples; (a) UHMWPE cut to defined heights (b) Silicium wafer edged to defined step sizes (c) Folded formalin fixed and paraffin embedded tissue, 3 µm height with 7 µm within the folded region.

Matrix application

Automatic matrix deposition was performed using a chemical inkjet printer, the ChIP-1000 (Shimadzu, Kyoto, Japan). 8, 15 and 25 ng matrix per spot were applied by area or spatially resolved print settings. CHCA, SA or DHB were prepared using ACN or ethanol

(EtOH), 50 or 70 % in 0.1 % aqueous TFA (v/v). Samples were ultra-sonicated for 5 min before centrifugation at 3000 rpm for 15 min. Printing quality was evaluated considering operating temperatures (T, 15 – 25 °C), vapor pressure and surface tension of the matrix solvents with respect to the obtained printing accuracy. Matrix crystallization was evaluated using a scanning electron microscope (SEM, XL 30, FEI Philips, Eindhoven, The Netherlands) after sputtering samples with a thin gold layer for 30 s. SEM analysis was conducted at an acceleration voltage between 10 and 20 kV and a magnification between 1000 and 4000. Sample surface visualization was conducted using ImageJ 1.47 (National Institutes of Health, Bethesda, USA).

MALDI-TOF-MS

The m/z shift of peptides applied to materials with different ε_r was examined with a high-vacuum axial MALDI-TOF instrument, the AXIMA TOF^2 (Shimadzu Biotech Kratos Analytical, Kyoto, Japan). The instrument operated in reflectron or linear positive ion mode. Pulsed extraction was evaluated for optimized results of m/z 1000, 1500 and 2000. For the 337.1 nm nitrogen laser with a pulse duration of 3 ns, the maximum energy is restricted to approximately 160 µJ per shot and an average output of 6 mW. MSI experiments on standardized samples were performed by applying 20 shots per position, 60 arbitrary units at a repetition rate of 20 Hz and a lateral resolution of 60 µm.

Orthogonal acceleration TOF experiments were carried out on an intermediate pressure MALDI qTOF instrument, the Synapt HDMS (Waters Cooperation, Manchester, UK), using a 1000 Hz Nd-YAG laser in positive ion mode. Additional experiments for an axial MALDI-TOF device were performed on the UltrafleXtreme (Bruker Daltonics, Bremen, Germany) equipped with a 2000 Hz Smartbeam™ laser [26].

Theoretical simulations of all sample surface parameters were based on the ion optics and source geometry of the Shimadzu instrument. Practical evaluation for all samples was

performed on the MALDI-TOF AXIMA TOF[2], proof of principal for theoretical considerations were additionally carried out on the Synapt HDMS and the UltrafleXtreme.

TOF calculations

To estimate mass accuracy influenced by sample surface parameters, the time of flight (TOF) was calculated using Mathematica 9.0.1.0 [27] and is based on the following ion source scheme.

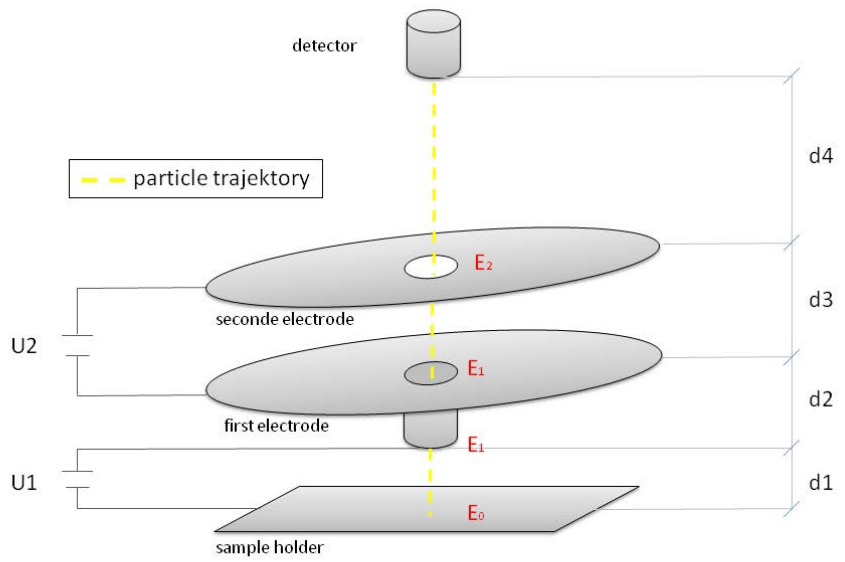

Figure 2: Simplified scheme of the considered MALDI ion source for basic TOF calculations including two acceleration regions (d_1,d_3) with their corresponding acceleration voltages (U_1, U_2) and two field free drift regions (d_2,d_4)

3. RESULTS and DISCUSSION

MSI is a technique, which can be assigned as a surface analysis method and yet surface properties are critical aspects for MSI. Sample roughness can lead to unequal desorption and ionization of analytes, whereas ε_r of the uppermost surface layer and charging effects within a sample are known to have influence on ion velocities during the extraction process. This results in unfavorable signal broadening especially for TOF instruments, which are most frequently used for MSI due to the overall mass range covered for singly charged ion species [12]. We discuss influences for various steps within a typical MALDI based MSI approach with a special focus on sample surface properties. For MSI experiments one has to be aware that some sample parameters highly influence mass accuracy but cannot be affected by the researcher e.g. target holder planarity, target carrier mechanics and target as well as sample's ε_r.

However, height differences due to sample geometry and good energy transfer from the laser to the analytes resulting from homogeneous MALDI matrix application are in fact parameters easily controlled by the user requiring high reproducibility and proper performance rating. To enhance mass accuracy, reproducibility and validity of MSI results, this study presents possibilities to evaluate the critical parameters: sample height, sample ε_r and planarity. Additionally, matrix application and instrument mechanics can be standardized.

Sample height and ε_r – theoretical considerations

The TOF analyzer is based on the principle of accelerating ions towards the detector with an applied electrical field to determine their masses based on their times of flight according to William Stephens [28]. The impact of height and ε_r differences can be calculated based on the geometry of the ion source of an instrument as shown later. In the AXIMA TOF^2 (Fig. 2) ions pass two extraction electrodes with two acceleration regions and two

field free drift regions in defined periods of time (t_1, t_3, t_2, t_4) making up a total TOF t, including the delayed extraction time t_{de}. Differences in sample height as well as ε_r only affect the first acceleration region and therefore t_1. The ion's flight distance, and consequently time, is influenced by various factors affecting the accurate value for one single mass: it's molecular weight, the distance from sample surface to the first acceleration electrode and the acceleration voltage applied between the electrode and the sample holder. Whereas the distance is determined by the sample height (actual distance from sample surface to extraction electrode), the acceleration voltage is directly correlated to the electrical properties of the sample surface. Insulating material causes a potential drop for the applied acceleration voltage and the kinetic energy E_1 is lower after the first acceleration region. As a consequence ions have a longer flight time and based on external calibration, the obtained m/z value are calculated to be higher than they actually are. If ions are accelerated from higher z-axis positions corresponding to sample height, those effects are leveled out by the reduced flight distance d_1 leading to a shorter TOF. However, those artifacts interact on a very complex level, as will be demonstrated.

The concept of focusing the energy distribution of an ion by introducing a delayed extraction time [29] to increase mass resolution furthermore enhances the complexity of mathematical calculations to get a value for a proper correction for varying sample heights. Delayed extraction compensates energy distributions by pulsing the acceleration field and as a side effect sharpens the energy profile of the ions. Consequently it can be considered that t_{de} is capable of compensating a diffuse z-axis profile, e.g. due to different sample heights, to a certain extent, which will be evaluated. The present study focuses on the understanding of those dynamics, relevant for almost all MSI applications, and finding ways to estimate them correctly.

Equations 1 describes the specific TOF t in the total region, from sample surface to detector, depending on the analyte's mass m, the applied acceleration voltages U_1 and U_2, the first distance between sample and acceleration electrode d_1, the three constant flight distances d_2, d_3, d_4, the initial kinetic energy E_0, the kinetic energy after the first acceleration region E_1, and the final kinetic energy E_2 (Equ. 2 and 3).

$$t = \frac{d_1 * m}{e * U_1 * (\frac{d_1 * m}{2 * d_1 * E_0 + 2 * e * U_1 * d_1})^{\frac{1}{2}}} + (\frac{m}{2 * E_1})^{\frac{1}{2}} * d_2 + \frac{d_3 * m}{e * U_2 * (\frac{d_3 * m}{2 * d_3 * E_1 + 2 * e * U_2 * d_3})^{\frac{1}{2}}} - \frac{d_3 * m}{e * U_2 * (\frac{d_3 * m}{2 * d_3 * E_1})^{\frac{1}{2}}} + (\frac{m}{2 * E_2} * d_4)^{\frac{1}{2}} + t_{de} \quad \text{[Equ 1]}$$

$$E_1 = E_0 + \frac{U * e}{d_1} * (d_1 - (\frac{2 * E_0}{m})^{\frac{1}{2}} * t_{de}) \quad \text{[Equ 2]}$$

$$E_2 = E_1 + U_2 * e \quad \text{[Equ 3]}$$

The usually negative potential difference, ΔU, caused by the varying sample to electrode distance d_1 (basically the sample height), the sample's $\varepsilon_{rmaterial}$ and its impact on the electrical acceleration field is described in equation 2, 3 and 4. The two variable parameters directly influence $U_{1material}$ in the acceleration field of the first acceleration region.

$$U_{1material} = U_1 - \frac{\frac{U_1}{(\frac{d_{vacuum}}{\varepsilon_{vacuum}} + \frac{d_{material}}{\varepsilon_{rmaterial}})}}{\varepsilon_{rmaterial}} * d_{material} \quad \text{[Equ 4]}$$

To evaluate the singular influence and dynamic interactions of the factors height, ε_r and delayed extraction time, those parameters were varied as independent as possible to estimate the degree of impact on the TOF of an ion.

For our estimations we examined in a first approach the relation between E, t and t_{de}. To study the influence of ε_r we considered stainless steel as the golden standard for MALDI

target material and compared it to an ITO surface, a glass surface and UHWMPE. The decrease of E_0, as a consequence of the material's ε_r, leads to an increased t at low t_{de} settings. A longer delay for the time of extraction leads in a first instance to a longer t. Yet for higher E_0 values (*i.e.* higher laser energies), the t decreases.

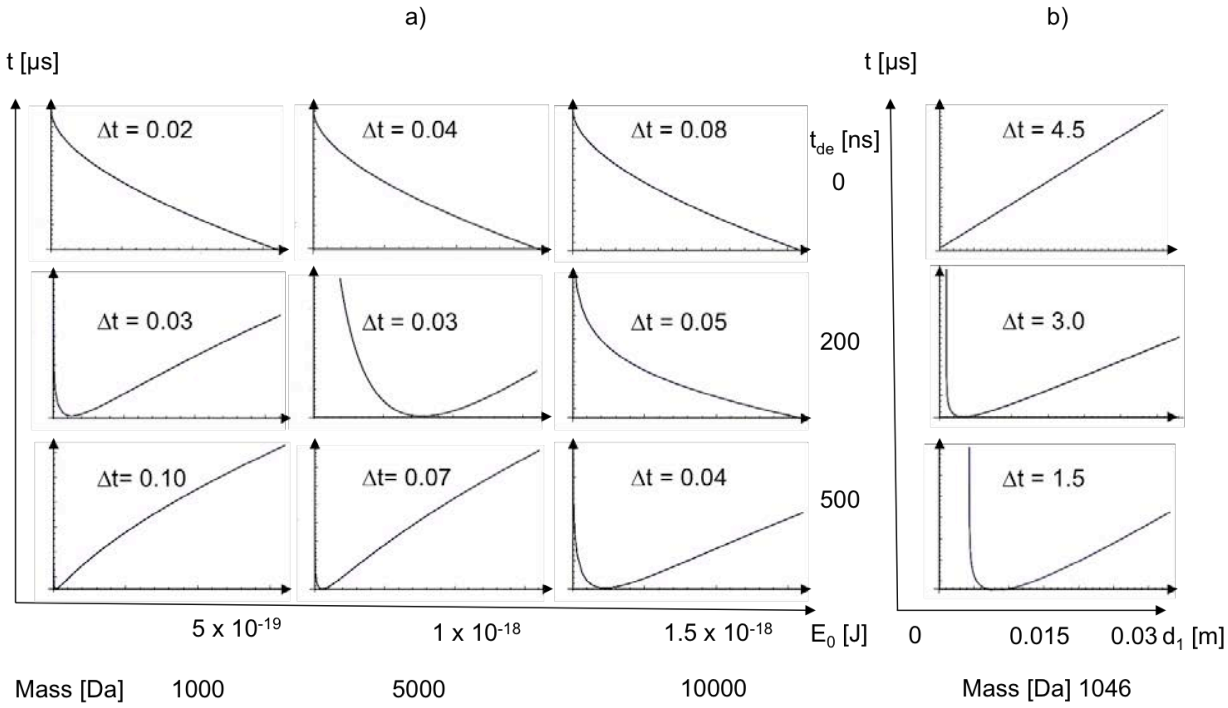

Figure 3: (a) TOF plotted against the initial kinetic energy E_0 for different m/z values (1000, 5000 and 10000) in correlation to varying t_{de} (0, 200 and 500 ns) in consideration of stainless steel as MALDI target and constant d_1; The maximal time divergence is expressed as Δt (b) TOF plotted against the acceleration region length d_1 calculated for m/z 1046 considering UHMWPE as sample surface (ε_r 20) for three t_{de}. All calculations are based on Equ. 1.

Fig. 3a shows exemplary curves for t plotted against the kinetic energies of ions with three different masses (column in Fig. 3a) and varying delayed extraction time settings (rows in Fig. 3a and b). The value for the initial kinetic energy is based on the average energy transferred in the MALDI process [30]. The variable kinetic energy in our calculations represents possible surface ε_r variation leading consequently to ΔU, which further affects acceleration voltage. Without setting a delayed extraction time a negative correlation between t and the kinetic energy can be observed (first row in Fig 3a). This

observation confirms the basic concept of TOF mass analysis, high E_0 lead to high ion velocities and short flight times. Introducing a time span between the laser pulse and acceleration voltage application (Fig. 3a row 2 and 3) leads to polynomial *t* curve characteristics. *t* increases and decreases can be observed, leading consequently to a considerable difference in m/z value: based on a TOF tube of 1.2531 m for the field free drift region and 0.0133 m for the acceleration region, the calculated TOF differences result in a mass deviation between 0.7 and 36.4 Da (all 3 calculated mass values, Fig. 3). This result highly emphasizes the importance of a homogeneous energy transfer during the desorption/ionization process and consequently consistent ion acceleration in axial TOF instruments. Homogeneous matrix layers can contribute to this aspired effect and can today easily be achieved over a larger sample surface (also see 3.3.). Another important point is the fact that biological tissue has diverse ε_r distributions, even within one rather "small" section. The application of surgical lasers to diverse kinds of tissue has already shown, that tissue and even substructures within tissues have significantly differing properties of energy uptake [31]. This of course influences the final mass resolution. However a factor that can hardly be influenced is the different accessibility of analytes. Protein cross-linking or histological environment hamper the desorption/ionization process and therefore may still vary the initially introduced kinetic energy significantly.

Besides this, height differences within samples can theoretically be well evaluated. Fig. 3b shows the correlation of *t* and the flight distance, respectively the sample height, for UHMWPE. Without any delayed extraction time, a positive linear correlation between the sample height and *t* can be observed. The introduction of a delayed extraction time, between 0 and 500 ns shows a polynomial *t* characteristics, with almost infinite *t* for very thick samples located already very closely to the first field free drift region. An increasing

t for reduced sample height is observed corresponding to the maximal d_1 in the first acceleration process. For m/z 1046.54, a t difference between 3 to 4 µs was calculated, initiating a theoretical mass deviation of up to 200 Da for variable d_1 on UHMWPE. These theoretical calculations also emphasize the findings discussed before consideration of sample properties like ε_r and height. Mass deviation in reality is lower which can be explained by the fact that we have taken a very simple model for our first calculations and that a lot of physical parameters not yet known were not taken into account. Furthermore dielectric properties over a certain (tissue) area cannot be calculated in detail, but impact the electrical field transmission and geometry in an unknown way.

Sample planarity after sample preparation

Tissue thickness accuracy, which was shown to highly influence mass accuracy in the latter paragraph, and reproducibility in sample sectioning, is related to microtome accuracy provided by the instrument and the thermal properties of the material. Especially within cryo-sectioning the contact time between sample and cooled knife can lead to material shrinking. The thermal expansion coefficient of biological samples/tissue highly affects the thickness if consecutive slices are cut at low cutting frequencies (2-3 slides/minute).

UHMWPE samples showed shrinking in the µm range at operating intervals of above 15 s when cut at -20 °C. Considering the linear temperature expansion coefficient of 108 x 10^{-6} m/m K for UHMWPE an expansion of the material was expected, however the shrinking is theoretically below the detection range for a sample thickness of 20 µm.

In contrast paraffin embedded tissue samples, stored at 4 °C but best sliced at room temperature, expand during the slicing process and require interim cooling after several (up to 10) consecutive slices due to smearing and tissue softness. The estimated change in thickness occurs in the nm to µm range. This is maybe not ultimately critical for MS

imaging experiments using tissue sections of 10 to 12 µm thickness. Yet some studies use thinner sections and for this signal intensity changes have to be considered to be caused not only by the varying analyte presence but also by varying sample thickness within one tissue slice used for MS imaging. For samples cut in 5 µm slices a tissue expansion of approx. 1-2 µm is observed already during the slicing process. This leads to an expansion of 0.1 µm per slice assuming a linear process for thermal density changes. In practice paraffin embedded tissue samples must be cooled during the slicing process to avoid smearing of paraffin, consequently harming the tissue morphology. This leads inevitably to thermal shrinking. An estimated height and material compacting of almost 20 % can be observed compared to the last cut slice as a consequence. For MSI experiments, this means a quantitative and qualitative change of analytes, which must be considered when consecutive slices are used for 3-dimensional reconstruction.

Histology is working not only with tissue sections of µm thickness but with samples cut in the nm range. And as MSI is very often correlated with histological methods, it is not surprising that thinner tissue sections are of interest for MSI experiments. Thin tissue sections have thicknesses of approx. 150 nm. Therefore a thickness change of 20 % caused by thawing during the cutting process has an enormous impact on analyte concentration and subsequently on detectability – a perspective of MSI addressed already in various studies [32-33]. But also for thicker tissue sections (1 to 15 µm) changes for the analytical sensitivity, impacting also quantification ambitions, have of course to be expected. For this it has to be pointed out that slicing frequency, sample and microtome operating temperature have a tremendous impact on comparability between consecutive slices or even more for independent tissue sections.

Attaching histological tissue samples to glass targets has to be done carefully and as planar as possible, using conventional histological handling procedures [34]. However, MSI

can be useful for any kind of material and sample. UHMWPE for example is a non-conductive and hydrophobic material without adhesive qualities for glass. So for MSI experiments the thin UHMWPE slices were fixed on ITO targets using conductive tape, which is intended to improve the transmission of the applied electrical acceleration field from the metallic target holder to the sample surface. This fixes the sample tightly on the sample carrier and insulating material properties are suppressed. However, new sources of height deviation are introduced. The conductive tape itself was evaluated on 32 different localized points after fixing it on a MALDI target and showed an average height of 80 ± 4 µm. As a consequence it can be stated that the major variability in sample height for a UHMWPE slice fixed with conductive tape is resulting from the tape itself. It is believed that this finding can be generalized – samples attached with conductive tape will show significant height deviation and for this rather bad mass resolution and even wrong m/z assignment can be expected for such samples.

Dial gauge analysis was also performed on paraffin embedded tissue samples and revealed unexpected shrinking of the tissue after removal of paraffin. Samples cut at 7 µm were measured to in fact only 4 µm ± 1 µm. Even though the dial gauge accuracy is eventually not accurate enough, the tendency of samples to shrink after removing embedding medium is nevertheless evident.

Other embedding media than paraffin, are usually of high viscosity and harden at low temperatures, whereas they melt and expand at higher temperatures. Tissue embedded in this kind of material is usually cut at -20 °C or even below and undergoes a temperature gradient of more than Δ 40 °C from slicing to analysis. Morphology is changing, sample density changes and to-date accompanying molecular changes are not known. It has to be stated that samples below 5 µm thickness or embedded in other media (e.g. O.C.T., sucrose) were not analyzed due to fragile morphology. It can, however, be assumed, that

the thermal expansion coefficient impacts these samples even more. FFPE samples are cut at room temperature showing a less steep temperature gradient and the described effects are not expected to have a severe impact on analysis.

Presented results prove the reproducibility of the slicing operation solely based on height evaluation but clearly shows that the sample's thermal expansion coefficient is critical. Furthermore, removal of embedding medium can lead to decreasing sample heights.

Homogeneous matrix distribution – enabling homogeneous energy transfer

Though providing one of the most accurate matrix deposition systems, the ChIP-1000 performance proved to be determined by printing time and volume [35]. The reported limits for the piezo-driven droplet delivering process (printing process) were matrix concentrations of 5 mg/ml CHCA dissolved in 50 / 5–10 / 40–45 ACN/isopropanol/0.1 % TFA (v/v/v) and printing durations of 2 h with a pitch size (distance from one spot center to the next) of 400 µm. Print head clogging remains the limiting factor for successful micro spotting and is induced by matrix particle crystallization on the print head edges. Clogging possibility is clearly determined by the choice of matrix, its solvent system and the operating temperature. Temperature directly affects solvent viscosity, matrix solubility and vapor pressure. So, all parameters highly impact droplet formation. To systematically evaluate matrix application performance the matrices, solvent systems and operating temperature were varied. As the ChIP-1000 does not have a built-in temperature control, the operating temperature was reduced by placing pre-cooled cool bags (-20 °C) near the piezo-head, while recording the temperature over the printing time. The application of four cool bags (-20 °C) reduced the operating temperature by 2-3 °C for two h. Pre-cooling the system in this way for two h and frequent exchange of the cool bags allowed a temperature decrease of 4-5 °C. Frequent exchanges also during the printing operation proved useful despite the required process interruption. A temperature

decrease of 7-8 °C was achieved utilizing a pre-cooled target holder, which directly affected the sample surface and the piezo print head's immediate thermal environment.

For all tested matrix/solvent systems (ethanol, ACN, ethanol/ddH_2O and ACN/ddH_2O both 50/50, v/v) vapor pressure and viscosity were measured showing increasing values for the first and decreasing for the latter (temperature range: 15 - 25 °C). As a consequence also the surface tension is negatively correlated to the temperature (Clausius-Clapeyron relation [36]). Low temperatures favor high surface tensions giving good printing properties for solvent systems initially not used for piezo printing (i.e. ethanol without water addition). In addition samples are permanently cooled reducing possible enzymatic tissue degradation.

We also observed that pre-cooling of the steel target holder for the ChIP-1000 and the glass slides (no tissue) for 30 to 45 min at 4° C strongly influences matrix crystallization and printing results. Although it was not possible to permanently control the target holder and glass slide temperature, a temperature increase from 4 °C to 8 °C was observed after 10 min of printing in a pre-cooled environment caused by the movement of mechanical parts. Matrix application with matrix deposition of 1.5 ng CHCA dissolved in ACN/ddH_2O or ethanol/ddH_2O (both 50/50, v/v) was investigated after that time and showed a very inhomogeneous crystallization process on the glass surface, especially for ACN containing solutions. From this result we concluded that temperature differences between the solvent system and the sample surface can lead to random matrix crystallization dynamics giving matrix layers with unfavorable MALDI performance (low ion intensities).

High throughput experiments using high printing volumes (7500 pL per spot applied by applying 80 pL per round, 47 rounds in total) of 7.5 ng CHCA dissolved in ACN/ddH_2O or ethanol/ddH_2O (50/50, v/v) and long printing durations (8 h) over larger areas (75 x 25

mm) showed very good stability at 15 °C. Stacked spots were accurately applied on the same position, no satellite droplets deposited away from the target spot were observed, except for a few rows at the edges, and no print head clogging was experienced. It can be said that low matrix concentrations, ultra sonication and centrifugation of the matrix/solvent system before use reduces the possibility of matrix particles remaining in the print head which leads to matrix micro-crystallization and subsequently to clogging.

For ACN containing solutions, most frequently used in MSI experiments addressing proteomic or peptidomic questions, temperature-controlled conditions showed significant printing improvement. Operating times of up to 5 h and 10 cm^2 with very good printability and accuracy in terms of spatial deviation for 8 layers of droplets without satellite formation could be achieved.

Matrix crystal formation is also a determining parameter for spatial resolution and analyte incorporation. The lowest spatial resolution is found in the size of a matrix particle, which depends not only on optimal temperature/matrix/solvent conditions but also on sample surface properties. Surface hydrophobicity highly impacts the spatial resolution in the printing process. Fig. 4a shows a spatially resolved matrix application and in Fig 4b a matrix application totally covering UHMWPE. The high flexibility for printing parameter adjustment allows full covering of the sample despite its very hydrophobic surface characteristics. However, spatially unresolved matrix application provides high risk of analyte diffusion. As a consequence covering the total area demands careful adjustment of drying times between single droplet applications and this varies for each specific material (*e.g.* tissue, polymer, glass). Although UHMWPE requires long droplet intervals for optimal drying between printing cycles, it nevertheless supports homogeneous crystallization. SEM experiments showed that the matrix crystals using the ChIP-1000 are very small (Fig 4c) and provide constant desorption qualities over a large

area. For the spatially resolved print, the accuracy of 6 droplet layers could be determined in the nanometer range (Fig. 4d). Considering a laser ablation area of 10 nm in the smallest case (*i.e.* Smartbeam™ laser), the area affected by crystallization inhomogeneities will totally be smaller than the ablated area and is therefore not of significant influence for intensity distributions.

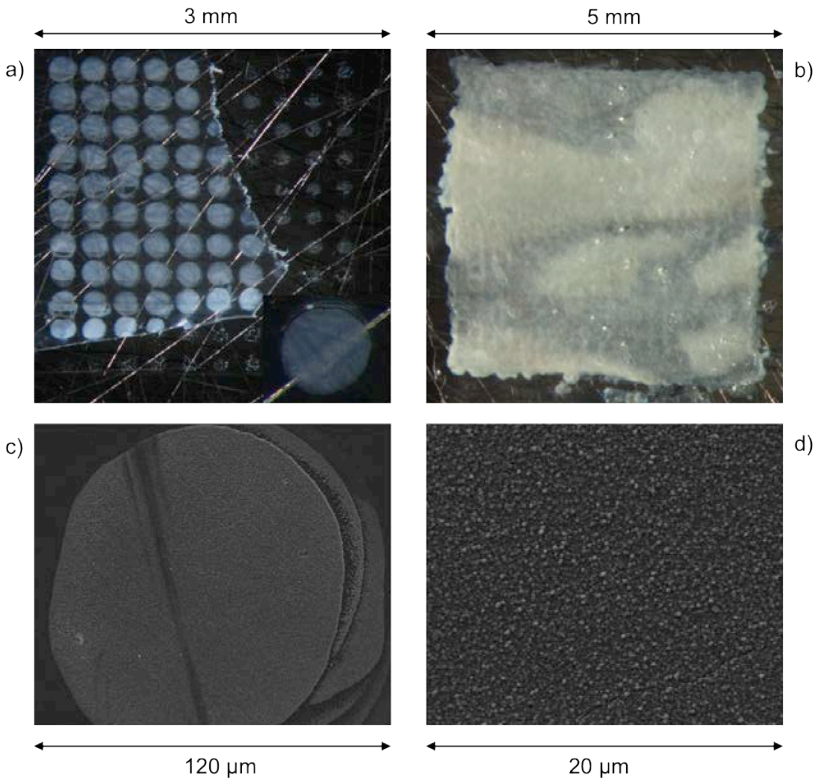

Figure 4: Light microscope (a, b) and SEM (c, d) images of CHCA printed on UHMWPE using the ChIP-1000; (a) spatially resolved printing with 200 µm pitch size after 6 printing cycles (equaling 6 stacked CHCA spots); (b) area print mode using a pitch size of 80 µm; (c) 6 stacked CHCA spots confirming the high print accuracy and reproducibility of the printing process; (d) fine and homogeneous microcrystal structures are observable for CHCA dissolved in ACN solution applied onto UHMWPE.

Target holder and mechanics – setup reducing mass accuracy

Target material and surface as possible source for mass deviation

MSI experiments are not only affected by different tissue samples (sample material), also the choice of the proper sample holder is essential. We studied the influence of sample

size, sample holder surface (glass, ITO covered glass and stainless steel) and MALDI target holder construction (connecting pin to the glass slide, connection by conductive tape).

For MSI experiments glass targets with standard dimensions of 75 x 25 mm are commonly used tissue sample holders. They are usually Indium Tin Oxide (ITO) coated on one side and native (mainly silicon dioxide, lime and sodium oxide) on the other side. Since most MALDI-TOF manufacturers provide their target holder with a little connecting metal pin, the applied electric field is assumed to be transmitted efficiently and equally onto the sample surface. For conductive sample surfaces, as biological tissue are, we hypothesized that this assumption is correct. For insulating material (*i.e.* UHMWPE) or larger areas under investigation we called this assumption into question.

The efficiency of energy transmission depending on the target holder geometry was evaluated for the pin solution compared to conductive tape. Furthermore, the non-conductive glass side, representing materials commonly used in histology, was compared to the ITO side. The expected mass deviation was analyzed in reflectron mode in order to enhance results by monoisotopic peak selection. To estimate the sample holder surface parameters, also its planarity had to be evaluated. Mass deviation over the whole sample holder was investigated for (i) the non-conductive glass side, (ii) the conductive ITO-covered glass side connected to steel by the conventional metal bind and (iii) the conductive ITO-covered side connected to steel by conductive tape over a mass range from 700 to 3500 Da representing the conventional mass range for peptide mass fingerprint approaches or lipid analysis.

For the whole the ITO-covered glass slide with an area of 1875 mm^2 connected to the stainless steel target holder by conductive tape, a mass deviation of $\Delta m/z$ -0.6 to 0.4 for Angiotensin I and Glu1-Fibrinopeptide B was observed with increased m/z deviation at the edges independent from the position of calibration. In the center region, an area of

1000 mm², Δm/z deviation was observed between 0.0 and 0.2. An equivalent deviation pattern was observed for the glass side and the ITO-covered side connected with the metal pin.

To examine the efficiency of electrical acceleration field transmission on sample carriers with different ε_r, calibration was performed on the stainless steel target holder directly next to the glass target to evaluate m/z deviation (Fig. 5). The glass slide surface and the stainless steel surface were leveled out to reduce height differences to the µm range.

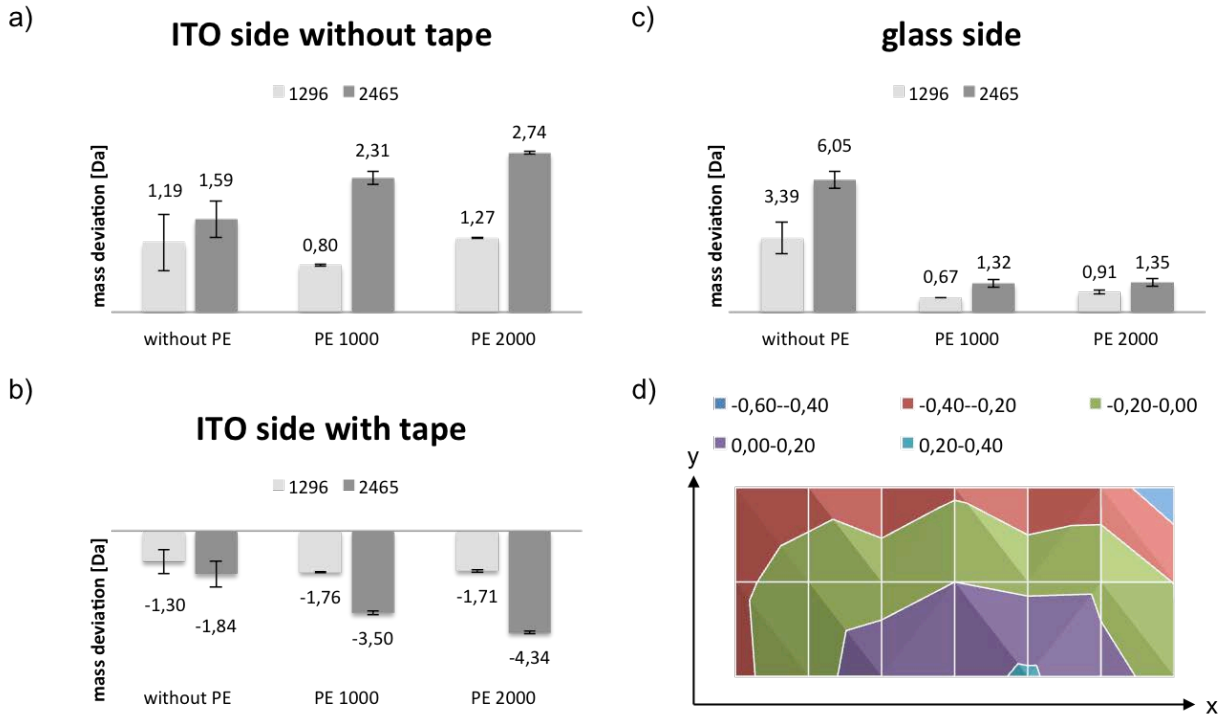

Figure 5: Average m/z deviation of 10 experiments observed on different surfaces for Angiotensin I and ACTH$_{18-39}$ (a) applied on a ITO coated glass slide, with a high ε_r but not connected to the conductive target holder (b) applied to the ITO coated side of the glass target with an additional connection (conductive tape) to the conductive target holder (c) applied to the non-conductive glass side; (d) Typical m/z deviation pattern independent from conductivity for a 75 x 25 mm target slide.

Fig. 5 shows the obtained m/z deviation for one particular point on the glass slides with different ε_r in relation to calibration on stainless steel. Both the conductive ITO side connected to stainless steel by pin geometry (Fig 5a) and the glass side (Fig 5b) show positive m/z deviations. Results for the ITO side supported by conductive tape show a

negative m/z deviation (Fig. 5c). This can be explained by the enhanced acceleration due to the ITO coated surface and efficient field transmission. Without delayed extraction time the height difference of a few µm between the slide and the target holder is of high influence leading to a negative Δm/z due to reduced d_1 at an effectively transmitted acceleration field.

The introduction of a delayed extraction time positively affects the degree of Δm/z for insulating material (conventional glass slide). The time span relevant for an increased expansion of the matrix plume might improve d_1, reducing the effect of poor field transmission. Conductive materials, such as the ITO slide either with good or bad field transmission reveal higher Δm/z by introducing t_{de}. Bad field transmission combined with t_{de}, may lead to a retarded acceleration process, whereas d_1 is even more reduced for good field transmission leading to an increased negative Δm/z.

Fig. 5d shows the pattern of m/z deviation over the whole target area of 1.875 cm^2. It can be concluded, based on the assumption, that the deviation pattern is a result of sample holder planarity issues, that the center region is favorable for sample application. Reasons can be found in eventual target planarity issues, variations in the ITO coating or unknown factors impacting electrical field transmission.

Nevertheless, the basic experiments concerning the impact of target holder geometry, sample holder planarity and material emphasize the importance of considering the MSI set up in every detail. In summary it can be said that small differences in planarity have a huge impact on mass accuracy. Besides this, the material is of high importance influencing desorption qualities. Materials leading to decreased potentials for the electrical acceleration field (i.e. insulators) negatively influence the desorption process. Additionally the influence of ε_r changes was studied only considering the sample carrier properties. From this experimental set up for different planarity and ε_r it can be deduced,

that the delayed extraction time is capable of compensating material properties. However, it has been shown, that the effect of the delayed extraction time is very sensitive to the ε_r. Those findings, regarding electrical field transmission and the dynamics of the delayed extraction time are further evaluated in the next section with different materials providing varying ε_r values and sample heights. These obtained results point out the inevitability of calibrant application near the sample and on reference material with identical height and ε_r characteristics.

Sample height within MSI experiments – the crucial parameter evaluated on standardized surfaces (silicium, UHMWPE)

Defined height standards were used for further studies of sample height on m/z deviation. By using different sample surfaces, sample ε_r can also be considered. Silicium with a ε_r of 11.2 and UHMWPE with a ε_r of 2 were used for practical evaluation. m/z deviation was investigated in the reflectron mode on an axial MALDI-TOF device using different delayed extraction time settings. A peptide standard mixture (Bradykinin$_{1-5}$, Bradykinin$_{1-7}$, Angiotensin II, Angiotensin I, Glu1-Fibrinopeptide B, N-Acetyl Renin, ACTH$_{1-17}$, ACTH$_{18-39}$, ACTH$_{7-38}$) was deposited on top of each defined surface for calculating the m/z deviation relative to the expected m/z value. Calibration was performed directly next to the measured area of interest.

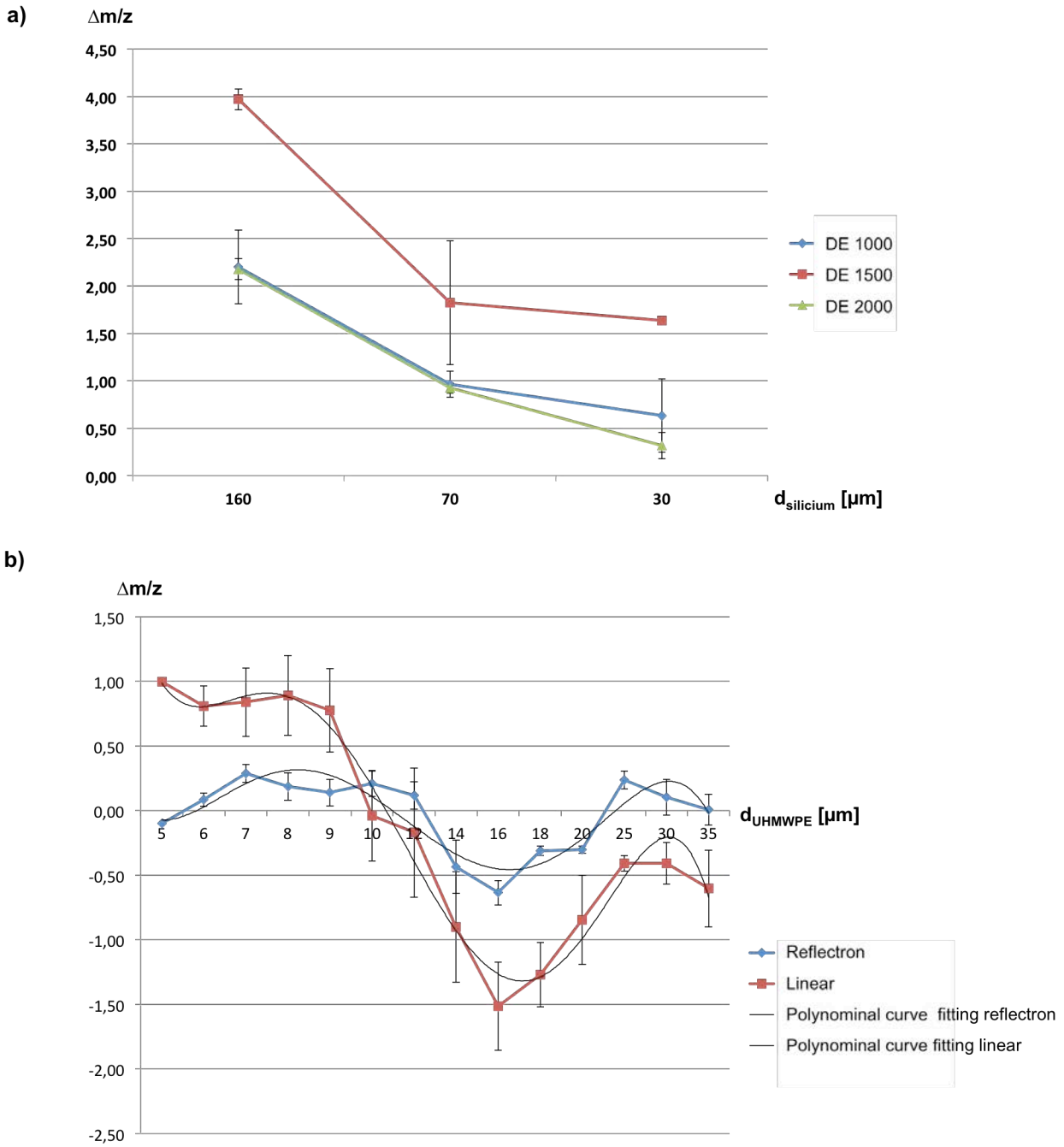

Figure 6: (a) m/z deviation for Glu1-Fibrinopeptide B $[M+H]^+$ (m/z 1570,68) applied on a silicium surface with edged steps (160, 70 and 30 µm); Three different pulsed extraction settings (m/z 1000, 1500 and 2000) were evaluated indicating a significant m/z increase (b) m/z deviation for Angiotensin II ($[M+H]^+$, m/z 1046.54) applied on UHMWPE samples with a thickness of 5 to 35 µm. Both curves show a comparable m/z deviation over the different samples

Silicium samples were calibrated on the wafer directly next to the edged recess. Three given incremental distances, 30, 70 and 160 µm, were measured and showed Δ m/z values of + 0.6 and + 2.2 for Glu1-Fibrinopeptide B ($[M+H]^+$, m/z 1570.68) if t_{de} was set to m/z 1000 (Fig. 6a). Varying the delayed extraction time between m/z 1000 and 2000 revealed a significant Δ m/z between 0.6 and 4.0 for the same peptide ion. t_{de} settings of 0 revealed m/z deviation between +2.38 and +2.78. The analysis of further analytes (between $[M+H]^+$ m/z 757 and 2495, detailed data not shown) showed the limited mass range of a few 100 Da of ideal set up conditions of the delayed extraction time. For silicium it was found that with increasing distance between electrode and sample surface, the obtained m/z deviation increased.

UHMPWE samples showed a higher complexity regarding the interaction of height, ε_r and the applied electrical field. Samples were mounted on conductive tape as described and analyzed for a sample height variation from 5 to 35 µm (without the conductive tape; 80 µm), which correlates in total to a reduced acceleration region of 3.3 to 3.2 mm. Calibration for the presented results was performed on the ITO slide itself to enhance the m/z shift and therefore to more accurately calculate m/z differences coming from height variations. We considered in that study not only the reflectron but also the linear mode of detection. Mass deviations were examined for a peptide mixture containing $Bradykinin_{1-5}$, $Bradykinin_{1-7}$, Angiotensin II, Angiotensin I, Glu1-Fibrinopeptide B, N-Acetyl Renin, $ACTH_{1-17}$, $ACTH_{18-39}$ and $ACTH_{7-38}$. Data are shown for Angiotensin II only ($[M+H]^+$, m/z 1046.54). As it is shown in Fig. 6b, an incremental m/z deviation was monitored in reflectron mode for the peptide ions applied to 5-12 µm and 20-55 µm. However, for slices between 12 and 20 µm a negative m/z deviation was obtained with a maximum of Δm/z −0.6. A similar distribution of the m/z deviation was observed for the linear ion detection mode.

Overall m/z deviation ranged from Δm/z -0.6 to 0.4 for the reflector mode and Δm/z -1.5 to 1 in linear mode. High standard deviations were calculated for the majority of samples, though microtome operating accuracy was validated to be ± 1 µm using a dial gauge.

Due to the previous results, showing linear correlations between height, ε_r and Δm/z the curve slope reveals more complex conditions. Ion source and electric field geometry and the transmission of the applied acceleration field through the material are unknown parameters. The increased height results in a negative mass deviation, which is valid for a small height range (shorter distance to detector gives shorter flight time and lower detected m/z values). The fact that similar patterns for linear and reflectron mode measurements were observed (Fig. 6) for both silicium and UHWM-PE, emphasized the hypothesis of considering height difference not as the only reason for deviation. ε_r as a sole parameter, however leads within the particular distance range to a linear decrease of TOF almost independent from t_{de}.

However, the most crucial parameter, which cannot be calculated in detail, is the electrical acceleration field transmission. Within the applied field the conductive tape and the attached sample form a very complex insulating system, where the field dynamics and field shape are not known and therefore also energy transmission is difficult to estimate. The thickness of insulating material very likely changes the field transmission properties. Additionally the conductive tape contains short, singular steel fibers inducing an interfering electric flux. Even though those facts clearly emphasize the difficulty of calculating mass deviations, the importance of its estimation can clearly be demonstrated. Such samples need either internal recalibration or require a decoupling of the MALDI source from the TOF tube. The latter setup is given in orthogonal mass analyzer designs.

Alternative geometries: Orthogonal Q-TOF (Synapt HDMS) and MALDI-TOF/RTOF (UltrafleXtreme)

As was hypothesized before mass accuracy is affected by sample height and ε_r for instruments with axial ion transfer into the TOF mass analyzer. Orthogonal ion injection was therefore used to proof this hypothesis. The decoupling of the desorption/ionization process from m/z analysis is expected to sufficiently eliminate any differences in energy distribution and TOF for effects occurring in the acceleration region. Again a peptide mix containing six peptides (Bradykinin$_{1-7}$, Angiotensin II, Glu1-Fibrinopeptide B, N-acetyl renin, ACTH$_{1-17}$ and ACTH$_{18-39}$) in a mass range from m/z 756.4 to 2465.2 for the $[M+H]^+$ ions was spotted on top of UHMWPE slices of various thickness mounted on stainless steel targets using conductive tape and measured on a Synapt HDMS with instrument parameters optimized for peptide ions in the mass range between m/z 300-5000. Mass deviations for applied peptide standard mixtures on the described steps between 5 and 35 µm were below $\Delta m/z \pm 0.0001$ for all peptides. Similar results were obtained for the silicium wafer. As a consequence differences in tissue substructures and disparities in the height profile do not affect precision and lead to no change in mass accuracy. Decoupling ion generation from TOF separation is certainly advantageous for imaging experiments, if no internal recalibration system is considered.

Verifying the impact of height and ε_r differences on the UltrafleXtreme revealed critical issues. Built as an axial MALDI-TOF/RTOF system, we were interested in comparing axial instruments, with differently constructed ion sources. For the standardized silicium wafer, prepared as described, no data acquisition was possible due to signals far below the detection limit. It can be assumed that ion source geometry prevents successful analyte detection for non-conductive samples thicker than 0.1 mm.

In contrary data acquisition war possible for the standardized UHMWPE samples. The total height of maximal 115 µm above the ITO glass slide surface was sufficient for signal generation. The UHMWPE region between 14 and 20 µm sample height was investigated with a similar trend in Δm/z. The average deviation of 10 measurements was found between Δm/z -0.15 and -0.44, which is below the results obtained for the Shimadzu instrument. However, ion signals always revealed double peaks and a very broad peak shape. Even though the accuracy for the UltrafleXtreme seems to be less affected by insulating material, data interpretation and recalibration is even more complicated because of peak shape variations.

Δm/z as a consequence of height differences in MSI experiments

Within MSI experiments, the transfer to the glass target, including sample mounting, fixation and preparation steps, is one of the most critical steps. Especially for tissue samples showing less than 1 µm thickness and mechanically fragile materials folding of the tissue is a considerable problem. Folds are inducing height differences and as a consequence impact mass accuracy. Moreover, for embedded tissues embedding media are trapped in the folds and usually hard to remove.

To examine the extent of sample inherent artifacts regarding height and ε_r, FFPE rat kidney tissue and UHMWPE were attached to the glass target, both exhibiting sample folding (Fig. 7). m/z deviation, was investigated within the folded region for homogeneously distributed Angiotensin II (calibration was performed next to the sample). When paraffin has been removed and samples were treated with ethanol for washing procedures before analysis, it can be assumed, that an eventual signal background based on residues is neglectable. It has to be considered, that over a large area, each analyte of interest has an average mass deviation distribution, which is not exactly known and has to be determined individually.

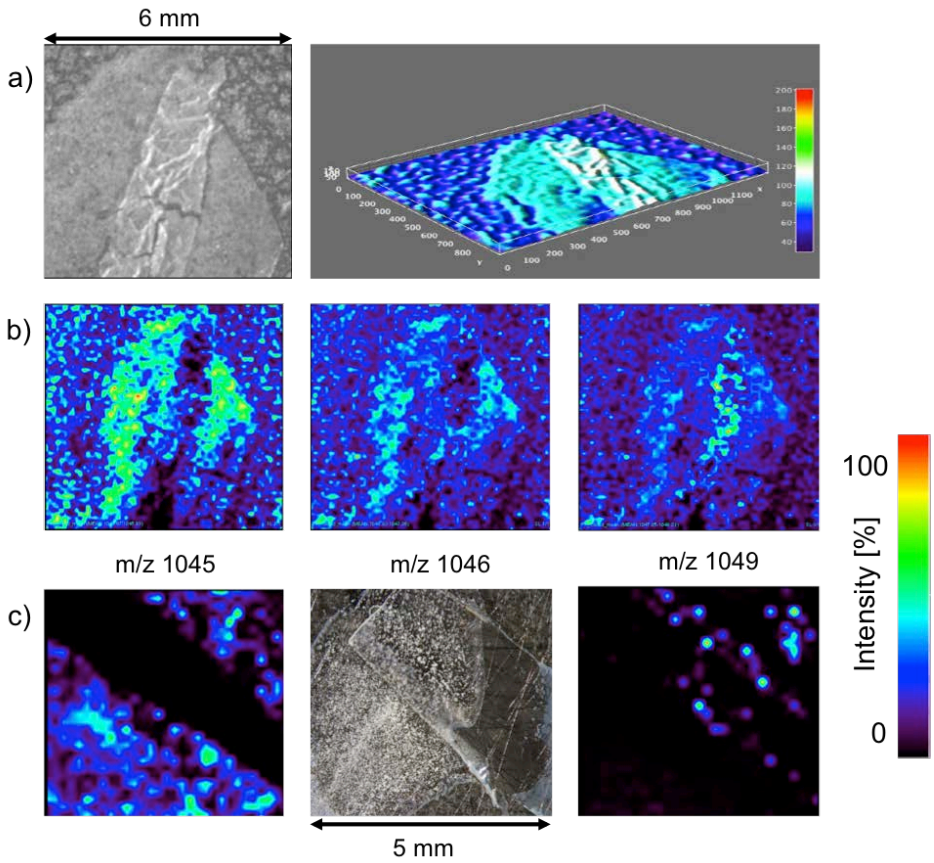

Figure 7: m/z deviation on MSI samples; (a) Light microscopy and surface visualization (ImageJ) of FFPE tissue sample sliced to 3 µm with a 7 µm folded region; (b) Visualization of the intensity distribution of found m/z values all corresponding to the monoisotopic Angiotensin II (m/z 1046.54) signal deviating due to the folded region (c) Light microscopy and intensity distribution of identified m/z values of the applied peptide on UHMPWE samples sliced to 20 µm with a folded region of 60 µm.

On the investigated FFPE sample (except the folded region), m/z deviations between -0.88 and +0.32 were observed. Given a sample thickness of 3-4 µm, this is an expectable variation as a result of different height and ε_r in comparison to the standard applied on flat surface of the stainless steel/glass sample holder. For the folded region deviations up to Δm/z +2.93 were measured (Fig. 7b). This is in contrast to our previous assumptions where a negative m/z deviation was expected for tissue samples with high ε_r. The investigated FFPE sample had an average thickness of 3-4 µm over the whole region and 7-8 µm within the folded region. According to our calculations, 3 to 4 µm height increase leads to a mass deviation below Δm/z 1 for material having the same ε_r. However, a tissue

height of 7-8 µm combined with a significant change in ε_r from theoretically infinite for native tissue to 2.1-2.5 for embedded tissue, leads to an increase in TOF of approximately 0.05 µs. Yet we observed even larger m/z differences. This can at the moment only explained by unpredictable tissue morphology changes, inhomogeneous electrical transmission and incomplete paraffin removal. Due to the folding, paraffin is not removed completely, inducing a ε_r change with a higher impact than height differences.

For UHMWPE the same observation was made for the folded region. For the evenly mounted UHMWPE only a slight m/z deviation of + 0.21 was detected. Yet within the folded sample area with a height of 60 µm a m/z deviation of up to + 2.9 was observed (Fig. 7c). This can be explained by a reduced field transmission assumed for the folded region. Additionally the geometry of sharp edges, resulting from microtomic processing, again leads to non-uniform electric flux lines, distorting the electric field and negatively influencing desorption the ion acceleration step.

The results confirm the assumption that samples with low ε_r lead to a potential drop causing reduced acceleration. Samples with an increase in height, or inhomogeneous height profiles, suffer from different starting points for acceleration. Both factors result in m/z deviations for axial MALDI-TOF geometries. However, those sample properties change the acceleration properties of analytes. An eventually reduced acceleration field combined with a curtated region leads to reduced signal quality, impeding results quality especially for low abundant analytes.

Conclusion

Manipulable and non-manipulable parameters impact mass accuracy of axial MSI MALDI-TOF experiments to critical extent. It could be demonstrated, that even very small changes like residual embedding media within a complex sample surface lead to tremendous m/z

deviation. Of course, internal mass calibration is able to compensate those parameters. However internal calibration is not always applicable, ionization of low abundant analytes of interest may be suppressed or the area of investigation is so small that it a simple question of available space on the sample. Moreover, double peak formation complicates the correct recalibration over a broad mass range. The alternative of a decoupled ion source is often not applicable due to limiting instrument requirements regarding sensitivity or mass range of interest for intermediate or atmospheric pressure instrument configurations. It is of course possible to enhance mass accuracy by using equivalent surfaces to apply the calibrating on, but then again height and ε_r have to be identical, which is difficult to achieve for biological samples. Certainly even for identical surfaces it was demonstrated that considerable m/z deviations still remain.

From our point of view the first step to improve mass accuracy for MSI experiments is to investigate physical characteristics of sample materials. Small differences within the sample surface can lead to stress peaks or potential differences, which can completely change the ion acceleration process from one point of acquisition to the other. Yet, a low acceleration voltage for the first acceleration region can reduce these artifacts. So the most crucial effect is the homogeneity of the electrical field lines within the ion source, which are affected by the sample. Sample preparation, from sample sectioning to matrix application is the most crucial step to generate homogeneous surfaces and homogeneous matrix layers for desorption/ionization. Especially for large and complex samples the TOF is influenced by the described artifacts, seriously impacting obtained m/z values. The focus for further investigation will be on the detailed surface examination of MSI samples prior to analysis in order to enhance measurement optimization.

Acknowledgements

We thank the Federal Ministry for Transport, Innovation and Technology and FEMtech for financial support (FFG project 826132/GENIE) and G. Skrbensky (Clinical Institute for Orthopedics, Medical University of Vienna) for providing UHMWPE explants. We thank Emanuelle Claude (Waters Corporation) and Omar Belgacem (Shimadzu Kratos Analytical) for technical support. The Synapt HDMS was made available by UniInfra IV (Federal Ministry for Transport, Innovation and Technology) and the UltrafleXtreme and the ChIP-1000 printer by two innovative projects of the Vienna University of Technology. Furthermore we acknowledge COST BM1104 (Mass Spectrometry Imaging: New Tools for Healthcare Research) for valuable discussions and know-how transfer.

Figure legends

Figure 1: Scheme of experimental set up for evaluating height differences under the same technical conditions using an axial MALDI-TOF/RTOF mass spectrometer (AXIMA TOF^2, Shimadzu). 2 kV acceleration voltage for the first and 18 kV for the second region were applied; all samples are covered with a defined peptide standard and mounted on ITO coated glass slides using conductive tape for the polymer and metal samples; (a) UHMWPE cut to defined heights (b) Silicium wafer edged to defined step sizes (c) Folded formalin fixed and paraffin embedded tissue, 3 µm height with 7 µm within the folded region.

Figure 2: Simplified scheme of the considered MALDI ion source for basic TOF calculations including two acceleration regions (d_1,d_3) with their corresponding acceleration voltages (U_1, U_2) and two field free drift regions (d_2,d_4)

Figure 3: (a) TOF plotted against the initial kinetic energy E_0 for different m/z values (1000, 5000 and 10000) in correlation to varying t_{de} (0, 200 and 500 ns) in consideration of stainless steel as MALDI target and constant d_1; The maximal time divergence is expressed as Δt (b) TOF plotted against the acceleration region length d_1 calculated for m/z 1046 considering UHMWPE as sample surface (ε_r 20) for three t_{de}. All calculations are based on Equ. 1.

Figure 4: Light microscope (a, b) and SEM (c, d) images of CHCA printed on UHMWPE using the ChIP-1000; (a) spatially resolved printing with 200 µm pitch size after 6 printing cycles (equaling 6 stacked CHCA spots); (b) area print mode using a pitch size of 80 µm; (c) 6 stacked CHCA spots confirming the high print accuracy and reproducibility of the printing process; (d) fine and homogeneous microcrystal structures are observable for CHCA dissolved in ACN solution applied onto UHMWPE.

Figure 5: m/z deviation observed on different surfaces for Angiotensin I and $ACTH_{18-39}$ (a) applied on a ITO coated glass slide, with a high ε_r but not connected to the conductive target holder (b) applied to the ITO coated side of the glass target with an additional connection (conductive tape) to the conductive target holder (c) applied to the non-conductive glass side; (d) Typical m/z deviation pattern independent from conductivity for a 75 x 25 mm target slide.

Figure 6: (a) m/z deviation for Glu1-Fibrinopeptide B $[M+H]^+$ (m/z 1570,68) applied on a silicium surface with edged steps (160, 70 and 30 µm); Three different pulsed extraction settings (m/z 1000, 1500 and 2000) were evaluated indicating a significant m/z increase (b) m/z deviation for Angiotensin II ($[M+H]^+$, m/z 1046.54) applied on UHMWPE samples with a thickness of 5 to 35 µm. Both curves show a comparable m/z deviation over the different samples.

Figure 7: m/z deviation on MSI samples; (a) Light microscopy and surface visualization (ImageJ) of FFPE tissue sample sliced to 3 µm with a 7 µm folded region; (b) Visualization of the intensity distribution of found m/z values all corresponding to the monoisotopic Angiotensin II (m/z 1046.54) signal deviating due to the folded region (c) Light

microscopy and intensity distribution of identified m/z values of the applied peptide on UHMPWE samples sliced to 20 μm with a folded region of 60 μm.

References

1. Caprioli, R. M.; Farmer, T. B.; Gile, J., Molecular imaging of biological samples: localization of peptides and proteins using MALDI-TOF MS. *Anal Chem* **1997,** *69* (23), 4751-60.

2. Chaurand, P.; Schwartz, S. A.; Reyzer, M. L.; Caprioli, R. M., Imaging mass spectrometry: principles and potentials. *Toxicol Pathol* **2005,** *33* (1), 92-101.

3. Stoeckli, M.; Chaurand, P.; Hallahan, D. E.; Caprioli, R. M., Imaging mass spectrometry: a new technology for the analysis of protein expression in mammalian tissues. *Nat Med* **2001,** *7* (4), 493-6.

4. Todd, P. J.; Schaaff, T. G.; Chaurand, P.; Caprioli, R. M., Organic ion imaging of biological tissue with secondary ion mass spectrometry and matrix-assisted laser desorption/ionization. *J Mass Spectrom* **2001,** *36* (4), 355-69.

5. Sparvero, L. J.; Amoscato, A. A.; Kochanek, P. M.; Pitt, B. R.; Kagan, V. E.; Bayir, H., Mass-spectrometry based oxidative lipidomics and lipid imaging: applications in traumatic brain injury. *J Neurochem* **2010,** *115* (6), 1322-36.

6. Waki, M. L.; Onoue, K.; Takahashi, T.; Goto, K.; Saito, Y.; Inami, K.; Makita, I.; Angata, Y.; Suzuki, T.; Yamashita, M.; Sato, N.; Nakamura, S.; Yuki, D.; Sugiura, Y.; Zaima, N.; Goto-Inoue, N.; Hayasaka, T.; Shimomura, Y.; Setou, M., Investigation by imaging mass spectrometry of biomarker candidates for aging in the hair cortex. *PLoS One* **2011,** *6* (10), e26721.

7. Ifa, D. R.; Manicke, N. E.; Dill, A. L.; Cooks, R. G., Latent fingerprint chemical imaging by mass spectrometry. *Science* **2008,** *321* (5890), 805.

8. Grassl, J.; Taylor, N. L.; Millar, A. H., Matrix-assisted laser desorption/ionisation mass spectrometry imaging and its development for plant protein imaging. *Plant Methods* **2011,** *7* (1), 21.

9. Yoshimura, Y.; Zaima, N.; Moriyama, T.; Kawamura, Y., Different localization patterns of anthocyanin species in the pericarp of black rice revealed by imaging mass spectrometry. *PLoS One* **2012,** *7* (2), e31285.

10. Gonzalez, D. J.; Haste, N. M.; Hollands, A.; Fleming, T. C.; Hamby, M.; Pogliano, K.; Nizet, V.; Dorrestein, P. C., Microbial competition between Bacillus subtilis and Staphylococcus aureus monitored by imaging mass spectrometry. *Microbiology* **2011,** *157* (Pt 9), 2485-92.

11. Moree, W. J.; Phelan, V. V.; Wu, C. H.; Bandeira, N.; Cornett, D. S.; Duggan, B. M.; Dorrestein, P. C., Interkingdom metabolic transformations captured by microbial imaging mass spectrometry. *Proc Natl Acad Sci U S A* **2012,** *109* (34), 13811-6.

12. Chughtai, K.; Heeren, R. M., Mass spectrometric imaging for biomedical tissue analysis. *Chem Rev* **2010,** *110* (5), 3237-77.

13. Casadonte, R.; Caprioli, R. M., Proteomic analysis of formalin-fixed paraffin-embedded tissue by MALDI imaging mass spectrometry. *Nat Protoc* **2011,** *6* (11), 1695-709.

14. Jungmann, J. H.; Heeren, R. M., Emerging technologies in mass spectrometry imaging. *J Proteomics* **2012,** *75* (16), 5077-92.

15. Gustafsson, J. O.; Eddes, J. S.; Meding, S.; Koudelka, T.; Oehler, M. K.; McColl, S. R.; Hoffmann, P., Internal calibrants allow high accuracy peptide matching between MALDI imaging MS and LC-MS/MS. *J Proteomics* **2012,** *75* (16), 5093-105.

16. Aerni, H. R.; Cornett, D. S.; Caprioli, R. M., Automated acoustic matrix deposition for MALDI sample preparation. *Anal Chem* **2006,** *78* (3), 827-34.

17. Goodwin, R. J., Sample preparation for mass spectrometry imaging: small mistakes can lead to big consequences. *J Proteomics* **2012,** *75* (16), 4893-911.

18. Sloane, A. J.; Duff, J. L.; Wilson, N. L.; Gandhi, P. S.; Hill, C. J.; Hopwood, F. G.; Smith, P. E.; Thomas, M. L.; Cole, R. A.; Packer, N. H.; Breen, E. J.; Cooley, P. W.; Wallace, D. B.; Williams, K. L.; Gooley, A. A., High throughput peptide mass fingerprinting and protein macroarray analysis using chemical printing strategies. *Mol Cell Proteomics* **2002,** *1* (7), 490-9.

19. Franck, J.; Arafah, K.; Barnes, A.; Wisztorski, M.; Salzet, M.; Fournier, I., Improving tissue preparation for matrix-assisted laser desorption ionization mass spectrometry imaging. Part 1: using microspotting. *Anal Chem* **2009,** *81* (19), 8193-202.

20. McDonnell, L. A.; Mize, T. H.; Luxembourg, S. L.; Koster, S.; Eijkel, G. B.; Verpoorte, E.; de Rooij, N. F.; Heeren, R. M., Using matrix peaks to map topography: increased mass resolution and enhanced sensitivity in chemical imaging. *Anal Chem* **2003,** *75* (17), 4373-81.

21. Clauser, K. R.; Baker, P.; Burlingame, A. L., Role of accurate mass measurement (+/- 10 ppm) in protein identification strategies employing MS or MS/MS and database searching. *Anal Chem* **1999,** *71* (14), 2871-82.

22. Schober, Y.; Schramm, T.; Spengler, B.; Rompp, A., Protein identification by accurate mass matrix-assisted laser desorption/ionization imaging of tryptic peptides. *Rapid Commun Mass Spectrom* **2011,** *25* (17), 2475-83.

23. Djidja, M. C.; Claude, E.; Snel, M. F.; Francese, S.; Scriven, P.; Carolan, V.; Clench, M. R., Novel molecular tumour classification using MALDI-mass spectrometry imaging of tissue micro-array. *Anal Bioanal Chem* **2010,** *397* (2), 587-601.

24. Maddalo, G.; Petrucci, F.; Iezzi, M.; Pannellini, T.; Del Boccio, P.; Ciavardelli, D.; Biroccio, A.; Forli, F.; Di Ilio, C.; Ballone, E.; Urbani, A.; Federici, G., Analytical assessment of MALDI-TOF Imaging Mass Spectrometry on thin histological samples. An insight in proteome investigation. *Clin Chim Acta* **2005,** *357* (2), 210-8.

25. Laiko, V. V.; Baldwin, M. A.; Burlingame, A. L., Atmospheric pressure matrix-assisted laser desorption/ionization mass spectrometry. *Anal Chem* **2000,** *72* (4), 652-7.

26. Holle, A.; Haase, A.; Kayser, M.; Hohndorf, J., Optimizing UV laser focus profiles for improved MALDI performance. *J Mass Spectrom* **2006,** *41* (6), 705-16.

27. Wolfram Research, I., Mathematica Edition: Version 9.0.1.0. Wolfram Research, Inc.: Champaign, Illinois, USA, 2013.

28. Stephens, W. Mass Spectrometer. 1952-09-30
, 1952.

29. Brown, R. S.; Lennon, J. J., Mass resolution improvement by incorporation of pulsed ion extraction in a matrix-assisted laser desorption/ionization linear time-of-flight mass spectrometer. *Anal Chem* **1995,** *67* (13), 1998-2003.

30. Knochenmuss, R., Ion formation mechanisms in UV-MALDI. *Analyst* **2006,** *131* (9), 966-86.

31. Stelzle, F.; Terwey, I.; Knipfer, C.; Adler, W.; Tangermann-Gerk, K.; Nkenke, E.; Schmidt, M., The impact of laser ablation on optical soft tissue differentiation for tissue specific laser surgery-an experimental ex vivo study. *J Transl Med* **2012,** *10*, 123.

32. Landgraf, R. R.; Garrett, T. J.; Conaway, M. C.; Calcutt, N. A.; Stacpoole, P. W.; Yost, R. A., Considerations for quantification of lipids in nerve tissue using matrix-assisted laser desorption/ionization mass spectrometric imaging. *Rapid Commun Mass Spectrom* **2011,** *25* (20), 3178-84.

33. Albalat, A.; Stalmach, A.; Bitsika, V.; Siwy, J.; Schanstra, J. P.; Petropoulos, A. D.; Vlahou, A.; Jankowski, J.; Persson, F.; Rossing, P.; Jaskolla, T. W.; Mischak, H.; Husi, H., Improving peptide relative quantification in MALDI-TOF MS for biomarker assessment. *Proteomics* **2013**.

34. Ellis, I. O.; Humphreys, S.; Michell, M.; Pinder, S. E.; Wells, C. A.; Zakhour, H. D., Best Practice No 179. Guidelines for breast needle core biopsy handling and reporting in breast screening assessment. *J Clin Pathol* **2004,** *57* (9), 897-902.

35. Jurchen, J. C.; Rubakhin, S. S.; Sweedler, J. V., MALDI-MS imaging of features smaller than the size of the laser beam. *J Am Soc Mass Spectrom* **2005,** *16* (10), 1654-9.

36. Clausius, R., Ueber die bewegende Kraft der Wärme und die Gesetze, welche sich daraus für die Wärmelehre selbst ableiten lassen. *Annalen der Physik* **1850,** *155* (4), 500-524.

7. Synovial Fluid Protein Adsorption on Artificial, Polymer-based Hip Joint Material Investigated by MALDI-TOF Mass Spectrometry Imaging

EuPA Open Proteomics (12. 2013) – revised manuscript

Synovial Fluid Protein Adsorption on Polymer-based Artificial Hip Joint Material Investigated by MALDI-TOF Mass Spectrometry Imaging

Sophie M. Fröhlich[1], Victoria Dorrer[1], Vasiliki-Maria Archodoulaki[2], Günter Allmaier[1], Martina Marchetti-Deschmann[1]

1) *Institute of Chemical Technologies and Analytics, Vienna University of Technology*
2) *Institute of Materials Science and Technology, Vienna University of Technology*

Abstract

PE-UHMW (ultra-high molecular weight polyethylene), the most frequently used material in acetabular cup replacement for artificial joint systems, is highly affected by the interaction with its surrounding biological compartment, the synovial fluid. It is assumed that protein layer formation is of high importance for lubrication, however can also alter polymer characteristics. Up to now no study is available investigating protein adsorption on polymer material from synovial fluids. The present study investigates protein adsorption on gamma-irradiated and Vitamin E doped PE-UHMW material using synovia as modeling system for static adsorption simulation. SDS PAGE and MALDI-TOF mass spectrometry imaging showed the adsorption of high abundance proteins in a molecular mass range between 2 and 200 kDa. Homogeneous protein layer formation was observed on planar PE-UHMW material, whereas morphologically modified PE-UHMW regions were highly affected by protein aggregation.

Keywords

PE-UHMW, protein adsorption, intact proteins, mass spectrometry imaging, synovial fluid, MALDI-TOF

Introduction

Ultra high molecular weight polyethylene (PE-UHMW) is a very frequently used material in artificial joint replacement systems. It provides easy usability, extreme high mechanical wear resistance, high biocompatibility and is to a certain extent self-lubricating [1]. However, the number of revision surgeries is still high, sometimes necessary because of the rapid shelf life aging process and *in vivo* degradation due to mechanical wear, oxidation and material modification [2-4]. Synovial fluid (SF), the major lubricating system in the joint compartment, directly interacts with the material surface, leading to biomolecule adsorption and diffusion [1, 5] possibly altering the polymer characteristics and stability. The major components have already been investigated, however it has not been determined yet, whether modified PE-UHMW surface areas lead to enhanced biomolecule adsorption and diffusion or *vice versa*. Furthermore, protein layer formation on PE-UHMW has so far not been investigated except for a few selected protein and carbohydrate species, e.g. albumin and hyaluronic acid [6]. It is known that the major abundant components of synovial fluid, e.g. hyaluronic acid, albumin or immunoglobulin, interact with PE-UHMW and tend to adsorb on the surface in model fluid systems. However, the interaction of the whole synovial proteome in the presence of lipids etc. with PE-UHMW has never been investigated. Because the synovial fluid composition is very similar to blood plasma (except for the high hyaluronic acid content) it is also highly affected by the patient's age, sex, life style and pathological status [7, 8]. Therefore it is of high interest, which proteins except albumin and immunoglobulin in fact adsorb on PE-UHMW before a deeper understanding of the pathological process can be obtained and/or material related selective adsorption effects can be gathered.

Different compositions of PE-UHMW, Vitamin E doped material, highly cross-linked PE-UHMW and materials undergoing different kinds of sterilization strategies have already been tested in clinical studies for improving the materials' properties and reducing protein adsorption. Highly abundant glycoproteins have been shown to adsorb on PE-UHMW in simulating models and adsorption has been investigated to occur unspecific and concentration independent [1]. In the same study model fluids containing only one glycoprotein of interest revealed that the formed protein layer enhances the lubrication and friction behavior of PE-UHMW. However, besides the selected glycoproteins also other high abundance and acute phase proteins occurring during inflammation and oxidative stress, e.g. during rheumatic diseases, are relevant for adsorption, friction behavior and consequently material modification.

The presented study focuses on the unbiased identification and localization of proteins present in synovial fluid adsorbing on different varieties of PE-UHMW material. To answer both questions, protein identity and spatial distribution, mass spectrometry imaging (MSI) by means of matrix assisted laser desorption/ionization time-of-flight (MALDI-TOF) examination was correlated to SDS PAGE analysis of adsorbed proteins. MSI is a well-established method for the localization and identification of analytes of interest within an untargeted approach [9]. To date MSI has been applied to a huge variety of biological samples [10-12] and it has to be mentioned that surface analysis of biomaterials is an exponentially growing field gaining more importance for the analysis of lubrication interaction and material modifications [13, 14].

One limiting fact of MSI is that protein identification in the high molecular mass range is only possible based on the tentative assignment of proteins to measured m/z values, respectively the molecular weight of detected molecules [15]. To corroborate protein assignment after MSI analysis, SDS PAGE analysis was chosen, providing the possibility to compare synovial protein patterns to patterns of protein compounds adsorbed on PE-UHMW of different compositions with respect to overall detected proteins. In parallel MS-based protein identification after *in-gel* digestion is feasible. Protein identification for adsorbed molecules was furthermore verified by *on-tissue* ("on polymer") digestion [16, 17]. The hydrophobic surface of PE-UHMW supports the preservation of protein localization during trypsin application in aqueous buffer systems, however, diffusion is a critical point for both enzyme and matrix application. To obtain reliable results homogeneous layers of trypsin and MALDI matrix solution were applied using a piezo printer (Chemical Inkjet Printer, ChIP-1000) to the protein-carrying PE-UHMW material.

Experimental

Materials

The Institute of Materials Science and Technology, Vienna University of Technology, provided gamma-irradiated PE-UHMW (GUR-1050 PE-UHMW) and PE-UHMW samples doped with Vitamin E. All chemicals and reagents, unless indicated specifically, were from Sigma-Aldrich (USA) with a purity of at least 99 % if not stated otherwise. Ultrapure water (uH_2O) was obtained from a Simplicity system (Millipore, USA) with a specific conductivity of $\Omega_m \leq 18$ S/cm. Human synovial fluid (SF), sampled after joint revision, was provided by the Institute of Materials Science and Technology.

Sample preparation

Virgin gamma irradiated GUR-1050 PE-UHMW and Vitamin E doped PE-UHMW samples were used. PE-UHMW was cut into small blocks (m = 85 ± 2 mg, V ≈ 125 mm^3), which were either used for incubation experiments or sliced to 15 µm using cryostat (CM1950, Leica, Germany) and mounted on indium-tin oxide (ITO) coated glass slides (Sigma Aldrich) using conductive tape (Shimadzu, Japan). The final polymer slice can exhibit folded regions after attachment. However, those regions were used to simulate uneven and rough regions and edges, as they actually occur *in vivo*, caused by mechanical wear and abrasion processes in the acetabular cup. All PE-UHMW samples were incubated in SF at 37 °C for 24 h. After incubation, samples were rinsed with uH_2O and vacuum dried.

For MS and MSI experiments standard MALDI matrices, α-cyano-4-hydroxycinnamic acid (HCCA) and sinapinic acid (SA) were dissolved in 70 % acetonitrile (ACN), 30 % uH_2O (v/v) containing 0.1 % trifluoroacetic acid (TFA) at a concentration of 13 (HCCA) and 25 (SA) mg/mL. Automatic matrix deposition was performed using a chemical inkjet printer ChIP-1000 (Shimadzu) or a commonly used airbrush device (Conrad, Germany). For the airbrush application of MALDI matrix a working distance of 10 to 12 cm was chosen with an approximate angle of 50 to 60 ° covering the sample in several iterative steps.

MS and MSI analysis

MSI experiments were performed on a MALDI-TOF/RTOF instrument (UltrafleXtreme, Bruker Daltonics, Germany) in positive linear or reflectron mode, equipped with a 355 nm SmartBeam laser pulsed at 2000 Hz [18] and on a MALDI-TOF/RTOF instrument (AXIMA TOF^2, Shimadzu Kratos Analytical, UK) equipped with a 20 Hz nitrogen (337 nm) laser. At a spatial resolution of 100 to 150 µm, mass spectra based on 1000 (AXIMA TOF^2) or 2000 (UltrafleXtreme) single laser shots were acquired per position over an average sample size of 8000 single imaging positions for polymer samples (approx. 8 × 8 mm) if not otherwise stated. For image reconstruction FlexImaging v. 3.0 software (Bruker Daltonics) and Biomap 38.04 (Novartis, Switzerland) was used.

Gel Electrophoresis

For protein extraction 200 µL SF, PE-UHMW blocks after incubation in synovia and blank material was deposited in 1200 µL uH_2O before 100 µL trichloroacetic acid (TCA; 20 %) were added 5 times and vortexed thoroughly between each single addition. Samples were incubated for 30 min at 4 °C and centrifuged at 14000 rpm and 4 °C for another 30 min. The supernatant and polymer blocks were removed and the protein pellet re-dissolved in 10 µL

lysis buffer (50 mM Tris/HCl pH 8.0, 2 mM dithiothreitol, 10 % v/v glycerol, 0.5 % v/v Tween 20, 10 % toluol). For protein precipitation with ethanol, 50 µL SF or the PE-UHMW blocks were mixed with 450 µL precooled ethanol (4 °C) and incubated at -70 °C for 2 h before centrifugation at 14000 rpm and room temperature for 30 min. The polymer blocks and the supernatant were removed and ethanol residues were evaporated in the vacuum centrifuge. After drying the pellet was re-dissolved in lysis buffer. Protein concentration was determined according to Bradford [19].

For SDS PAGE analysis protein pellets were dissolved in lithium dodecyl sulfate sample buffer (26.5 mM Tris HCl, 35.25 mM Tris Base, 0.5 % lithium dodecyl sulfate, 2.5 % glycerol, 0.1275 mM EDTA, 0.055 mM SERVA Blue G250, 0.044 mM Phenol Red, pH 8.5, 50 mM dithiothreitol) at 95 °C for 5 min and applied to a precast NuPAGE 4-12 % Bis-Tris polyacrylamide gel (Invitrogen, USA). Electrophoresis was conducted at 125 V (60 mA max., 12.5 W) in a XcellSurelock Mini Cell electrophoresis system (Invitrogen, USA). Gels were silver stained [20] for protein detection.

Protein identification

Proteins were either identified after SDS PAGE by *in-gel* or by *on-tissue* ("on polymer") digestion. For the first, gel bands were excised with a clean scalpel and destained using 100 mM $Na_2S_2O_3$ and 30 mM $K_4Fe(CN)_6$* $3H_2O$ (1:1, v/v). Gel pieces were treated with ACN and rehydrated with 100 mM NH_4HCO_3. After reduction (10 mM DTT in 100 mM NH_4HCO_3) and alkylation (50 mM iodoacetamide in 100 mM NH_4HCO_3) the gel pieces were dried in a vacuum centrifuge and rehydrated in approx. 10 µL 50 mM NH_4HCO_3 (pH 8.5) containing 5 % ACN and 125 ng trypsin (porcine, proteomics grade, Roche, Switzerland). Digestion was carried out for 24 h at 37 °C. Peptides were extracted with 50 mM NH_4HCO_3/ACN (1/1, v/v) and two times with uH_2O/ACN containing 0.1 % TFA (1/1, v/v), for 15 min each. All extracts of one respective spot were pooled and dried in a vacuum centrifuge. After reconstitution in 0.1 % TFA peptides were desalted using C_{18} ZipTips (Millipore, USA) and eluted with 5 mg/mL HCCA prepared in ACN/0.1 %TFA (50/50, v/v) in the final step. Peptide mass fingerprinting (PMF) and sequence tag analysis were carried out on a MALDI-TOF/RTOF instrument (UltrafleXtreme).

For "on polymer" enzymatic treatment, the ChIP-1000 was used for precise trypsin deposition at a standard concentration of 3 ng/µm^2 containing 1 % Rapigest (Waters, USA) dissolved in 50 mM NH_4HCO_3 (pH 7.5) containing 5% ACN. Trypsin solution was applied at a lateral resolution of 100 µm covering the complete sample area. For digestion samples were

stored at 37 ° C for 24 h in saturated atmosphere (ethanol/water, 50/50, v/v, 80 % relative humidity). After incubation samples were carefully washed with uH_2O to remove salts, delocalized peptides not adsorbed to the polymer and autolytic fragments from trypsin. Samples were vacuum dried for 15 min and HCCA was applied afterwards as described.

For all enzymatic digestion data, autolytic tryptic products, keratin and blank artifacts were assigned and removed before database search (SWISSPROT, Dec. 2013) using Mascot [21] with the following parameters: taxonomy *Homo sapiens*, monoisotopic mass values, peptide mass tolerance of ±0.3 Da (for PMF and PSD experiments), 2 missed cleavages, a fixed modification carboxyamidomethylation and methionine oxidations set as variable modification.

Results

Protein identification on PE-UHMW

Two different PE-UHMW materials were investigated concerning protein adsorption: conventionally used GUR-1050 PE-UHMW and Vitamin E doped PE-UHMW, which is claimed to be more resistant to oxidative degradation [5]. After incubating the two different materials in the same synovia at 37 °C for 24 h, adsorbed proteins were extracted. Similar to plasma, 85 % of synovia consists of the same well-described high abundance proteins. However, to identify proteins actually adsorbing in a concerted manner from synovia on PE-UHMW in the bio-compartment, we decided against special synovia treatment (e.g. depletion) well aware of the possibility to identify exactly those high abundance proteins.

For this approach, two different extraction methods were evaluated: an ethanol and a TCA based extraction methods (details see Materials and Methods). Protein concentrations were determined to compare the efficiency of both approaches. The protein concentration obtained according to Bradford differed significantly yielding 14.68 ± 4.24 µg/µL for the ethanol (n = 15) based method and 7.74 ± 1.89 µg/µL for the same polymer type extracted with TCA (n = 15). However, no qualitative differences were observed for the SDS PAGE protein pattern and the number of protein lanes was comparable in the apparent molecular mass range between 3 and 200 kDa. For proceeding experiments TCA precipitation was applied, in order to avoid eventual lipid or glycan contamination (easily extracted with ethanol) and based on the higher reproducibility.

Protein analysis from the two different PE-UHMW species revealed an average protein concentration of 9.46 µg/µL for GUR-1050 PE-UHMW after extraction with TCA and 13.08 µg/µL for Vitamin E doped samples. Applying concentration-matched samples to SDS PAGE

revealed lighter stained protein bands for the Vitamin E doped samples. More than 10 high abundance proteins could be identified after *in-gel* digestion (Fig. 1).

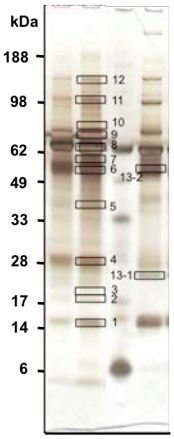

Protein ID (Gel band number)	molecular weight				
	Literature [kDa]	SDS-PAGE [kDa]	MALDI profiling [m/z]	Peptides associated	Carbohydrate [%]
Fibrinogen	340	n.d.	n.d.	n.d.	3
IgG (13-1, 13-2)	150	28(13-1) / 50(13-2)	147421	8	3
Ceruloplasmin (12)	135	140	133255	25	7
Haptoglobin (11)	104	103	100399	4	16
Plasminogen	81 / 90.1 (MADLI)	n.d.	88940	20	3
Transferrin (10)	79.1	77	78052	23	6
Comp C3-b (9)	75	75	73956	9	**
Albumin (8)	66.4	68	66615	18	x
Vitronectin	65-75 / 59.8 (MALDI)	n.d.	58595	9	30
α1-Antichymotrypsin (7)	52.3	55	53942	9	27
Apo A-4 (6)	43.4	n.d.	44501	21	x
α1 Acid glycoprotein	40 / 33-36 (MALDI)	40	n.d.	8	45
Apo E (5)	34.2	35	33302	18	x
Apo A-I (4)	28.1	29	29528	19	x
Apo D (3)	22.5	23	22301	2	x
Apo H-III (HDL) (2)	17	18	16656	n.d.	x
Transthyretin (1)	13.8	15	13659	1	x
Apo C-II	8.9	n.d.	8894	1	x
Apo C-III	8.8	n.d.	8740	n.d.	0-15
Apo A-II	8.7	n.d.	8592	3	x
Apo C-I	6.6	n.d.	6343	1	x*

n.d.: not detected, x* no glycosylation, **no available information

Figure 1: Summary of SDS PAGE analysis and protein identification of high abundance proteins in synovia and proteins recovered from PE-UHMW surfaces after incubation in synovia for 24 h. SDS PAGE: Proteins recovered from Vitamin E doped PE-UHMW (lane A), GUR-1050 PE-UHMW (lane B), Seeblue Prestained Marker (lane C) and Synovial fluid extracts (lane D). Table: proteins identified after *in-gel* digestion in comparison to m/z values detected on PE-UHMW (GUR-1050 and Vitamin E doped) by MALDI profiling. Number of peptides derived by "*on-polymer*" digestion associated to respective proteins and degree of glycosylation listed in the database.

Compared to protein extracts from SF, it can be seen that all high abundance proteins adsorb on both PE-UHMW types. Relative protein intensities within the protein extracts are comparable except for the light chain of IgG, which seems to be less abundant on the polymers compared to plain synovia.

Aside from gel electrophoretic analysis, adsorbed proteins were also detected as intact molecules on the polymer surfaces using MALDI-TOF MS (MALDI profiling) after washing the polymer with uH_2O. Synovia contains a very high amount of salts, therefore the washing procedure had to be repeated if salt residues were still visible as small crystals under the light microscope. HCCA and SA were deposited directly on the washed polymer using the airbrush instrument. At this point the maintenance of localization of the proteins was not of importance. Thin MALDI matrix layers were obtained on the very hydrophobic surface using both matrices with ACN/0.1 % TFA at a ratio of 70:30 (v/v) as solvent. For MS profiling experiments the whole polymer area, approx. 25 mm^2, was measured with a laser spot diameter of 50 µm and a broad energy profile to avoid polymer degradation (all experiments performed on the UltrafleXtreme). Fig. 2 shows the protein pattern from GUR-1050 PE-UHMW surface for two different mass ranges accumulating 5000 shots for each spectrum.

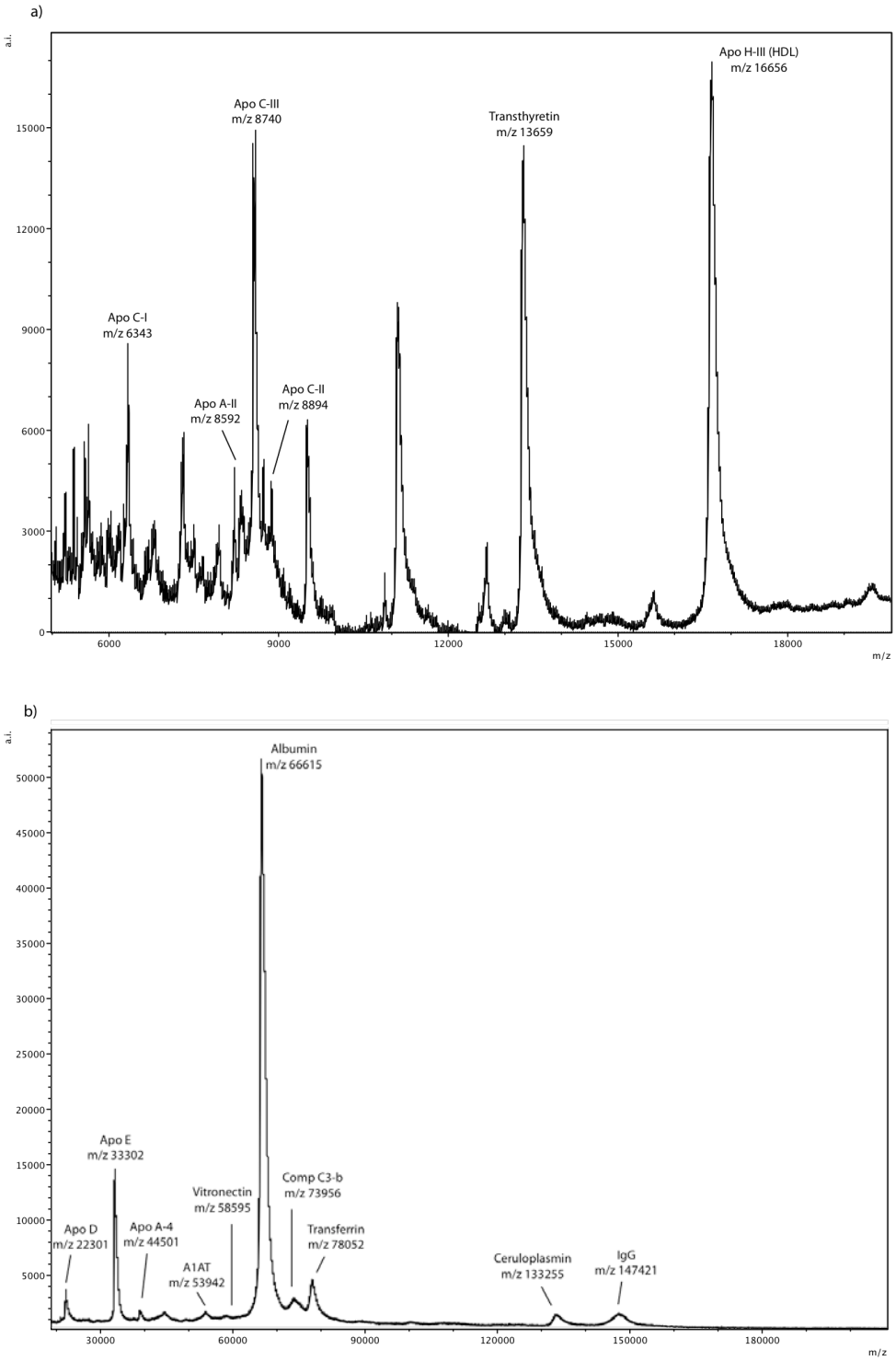

Figure 2: Positive ion MALDI mass spectra obtained by MS profiling of GUR-1050 PE-UHMW incubated in synovia for 24 h at 37 °C. a) HCCA was used as matrix for the molecular mass range between 2 and 20 kDa and b) SA was used as matrix for the molecular mass range between 20 and 200 kDa.

HCCA proved successful for the molecular mass range between 2 and 20 kDa and as expected SA performed best for the higher range, 20 to 200 kDa. In both cases $[M+H]^+$ ions were generated. Even though PE-UHMW is a highly insulating material, interfering therefore with the MALDI process itself, mass resolution (FWHM) was kept between 5000 and 10000 for the linear ion mode and 300 to 4000 for reflectron mode. Ion intensities and mass resolution were sufficient for unambiguous peak assignment. The table in Fig. 1 illustrates that after incubation with SF the determined m/z values most likely correspond to apolipoproteins of different classes (Apo C-I, Apo A-II, Apo C-III, Apo C-II, Apo D, Apo A-I, Apo E, Apo A-4), transthyretin, α1-antichymotrypsin, albumin, complement C3-b, transferrin, haptoglobin, ceruloplasmin and the light as well as heavy chain of IgG. They were all detected on both, GUR-1050 PE-UHMW and Vitamin E doped PE-UHMW material.

SDS PAGE and MALDI profiling showed that all identified proteins and detected signals are belonging to high abundance proteins present in SF. However, it is observed that many of the tentatively assigned apolipoprotein subunits are present in MALDI profiling analysis alone. This can either be explained by the fact that this lower molecular weight protein fraction is not accessed in conventional SDS PAGE, or that these subunits are specifically attaching to the polymer surfaces and cannot be removed by protein precipitation using TCA. It has to be mentioned that only a small percentage of the proteins identified after *in-gel* digestion represent glycoproteins (see table in Fig. 1) and that from this no clear conclusion can be drawn whether glycoproteins or otherwise post-translationally modified proteins are preferentially adsorbed to the PE-UHMW material. The same conclusion can be drawn for the feature protein hydrophobicity. It was also observed that SDS PAGE band intensities gave no unambiguously hint to the assumption that the size of a protein has a significant effect on adsorption.

MALDI matrix application on hydrophobic surfaces for MSI experiments

Investigating protein adsorption on polymer surfaces by MALDI-TOF MS requires thorough optimization of sample preparation particularly due the low analyte concentrations. The most critical step is the generation of a homogenous MALDI matrix layer on a large sample surface. The hydrophobic surface of the PE-UHMW samples favored the formation of a liquid film if the matrix was not carefully applied droplet by droplet. Especially folded regions, which can occur after applying the thin polymer samples to the ITO slides after cryo-microtomy, provide problems regarding matrix crystallization. MALDI matrix solution application with slowly evaporating solvents leads to a matrix flow leaving no matrix on

folded areas but large crystals on planar regions. This can of course favor disadvantageous analyte diffusion. Additionally it is known that protein desorption/ionization during the MALDI process is more effective after incorporating analytes in solvent systems containing acidic components, as a consequence of efficient protonation. On the polymer surfaces, however, organic solvent systems were shown in preliminary results to have better crystallization properties, most likely due to their much higher volatility [22]. Further studies showed now that organic solvent systems revealed very small crystal sizes and homogenous covering of the polymeric material, while aqueous solvent systems resulted in improved signal quality but less favorable sweet spot formation in combination with sometimes very small areas covered with high concentrations of matrix. The matrix/solvent system turned out to be performing best with respect to signal quality (signal-to-noise, intensity and mass resolution), surface coverage and applicability was a solution of ACN / aqueous 0.1 % TFA at a ratio of 70 / 30 for both HCCA and SA.

For matrix application the piezo printer (Chip 1000) and the airbrush instrument were compared with special respect to analyte diffusion. To prevent the formation of a thin solvent layer on top of the polymer due to droplets trickling away, the distance between single matrix droplets (approx. 80 pL) applied with the piezo printer was set to 100 µm. To cover the total area of 25 mm^2 long printing operation times were necessary (up to 5 h). For this, analyte diffusion was investigated when using an airbrush system instead of the piezo printer for MALDI matrix deposition to reduce overall operating times. A peptide standard, 500 fM leucine-enkephalin, was deposited on an ITO target with the piezo printer using the area print mode of the instrument, which leads to a complete covering of a pre-defined area. This area was then covered with HCCA as MALDI matrix using the airbrush. We observed a recognizable liquid layer of solvent on the ITO target, which evaporated more slowly than the MALDI matrix/solvent systems applied by the piezo printer. Thus after drying, light microscopy revealed a thin matrix layer with homogeneous crystal distribution. Moreover MSI experiments demonstrated (Fig. 3) that the airbrush represents a matrix application device sufficient for matrix application without significant analyte dislocation at a lateral resolution of 100 µm. The very sharp edged area visualized for the peptide ion emphasizes the accuracy of peptide application by the piezo printer. The applied peptide was perfectly preserved and detected after MALDI matrix application.

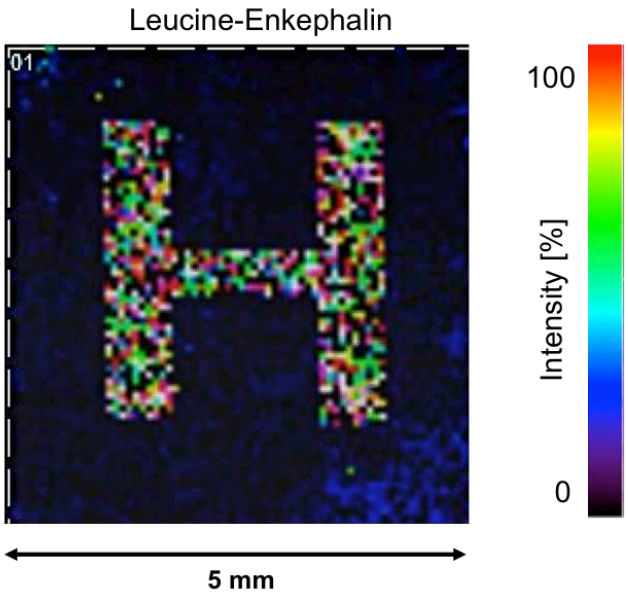

Figure 3: Non-normalized intensity distribution of Leucine-Enkephalin (transparent peptide solution) printed with the piezo printer in an "H"-shaped area on transparent ITO glass before HCCA (ACN/aqueous TFA (50/0.1, v/v)) application with an airbrush. Visualization: FlexImaging. Lateral resolution of the MSI experiment: 100 µm.

Visualizing intact protein distribution on PE-UHMW up to 204 kDa

Besides the finding that proteins adsorb on PE-UHMW aside from their post-translational modifications or hydrophobic quality, it is necessary to localize proteins adsorbing on PE-UHMW in order to correlate them to polymer qualities such as surface roughness or oxidation.

For this the 15 µm PE-UHMW slices, incubated in SF for 24 h, were investigated concerning the adsorbed protein layer and the localization of certain proteins in a MSI approach. HCCA for the low or SA for the high molecular mass range were applied using the piezo printer at a lateral resolution of 100 µm covering the whole PE-UHMW sample homogeneously. Fig. 4a shows an exemplary covered PE-UHMW sample after applying HCCA with the piezo printer. A rather thick matrix layer with fine crystal formation is observed. Similar results were obtained for SA. The same proteins as in profiling experiments were detected, i.e. all highly abundant species such as albumin, IgG and the apolipoprotein subclasses.

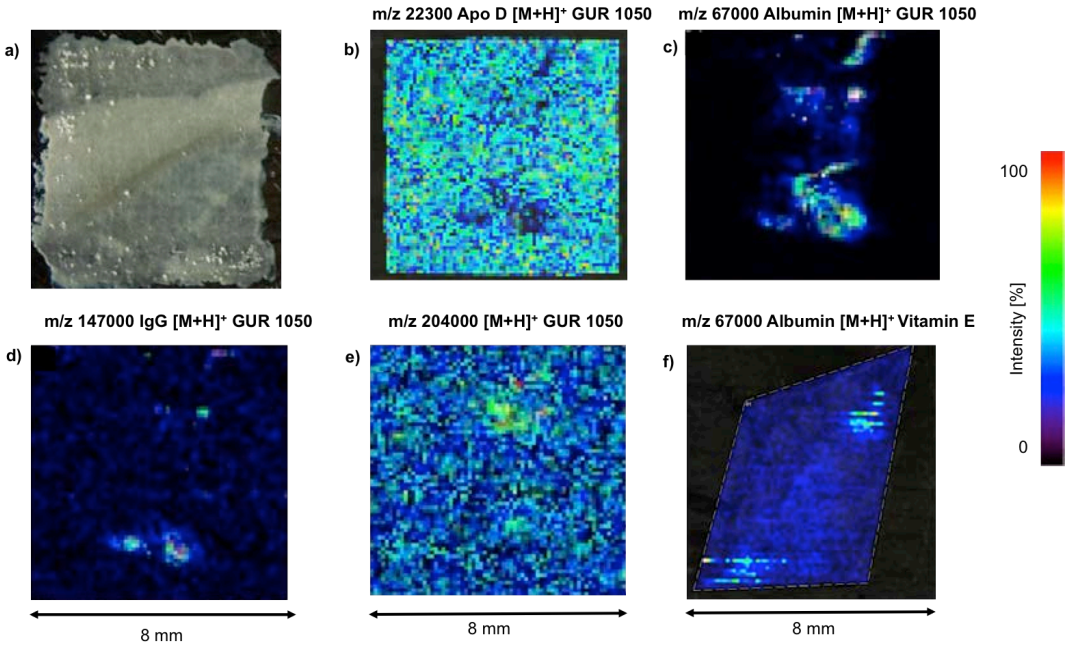

Figure 4: MSI experiments of GUR-1050 and Vitamin E doped PE-UHMW incubated in synovia for 24 h at 37 °C. a) Matrix crystallization on PE-UHMW using HCCA in ACN/0.1 % TFA (70/30, v/v). MSI experiments to localize b) Apo D ($[M+H]^+$, m/z 22301), c) Albumin ($[M+H]^+$, m/z 66615) d) IgG ($[M+H]^+$, m/z 147000) and e) m/z 204000 ($[M+H]^+$) on GUR-1050 PE-UHMW (transparent) and f) Albumin $[M+H]^+$ on Vitamin E doped PE-UHMW (transparent) were performed at a lateral resolution of 100 µm.

Profile mass spectra were already presented in Fig 2a and 2b showing protein adsorption up to 204 kDa. Yet some proteins exhibited characteristic localization on the polymer material. Fig. 4b shows the intensity distribution of apolipoprotein D $[M+H]^+$ (m/z 22301) and Fig. 4e the distribution of the unknown protein at 204 kDa on GUR-1050 PE-UHMW after total ion current (TIC) normalization. Molecules were almost homogeneously distributed on the polymer. The analyzed PE-UHMW sample showed a small folded area in the center, whereas the majority area was mounted completely planar to the conductive tape. On perfectly prepared samples all proteins were detected with a similar homogeneous lateral distributions. Interestingly that in the few areas not covered with Apo D especially albumin was found (Fig. 4c). On both polymer variants, GUR-1050 and Vitamin E doped, m/z values correlating to $[M+H]^+$ ions of human serum albumin (m/z 66615) were detected in the center region of the polymer slice, with especially high intensities in folded area (Fig 4c,f). The area of high intensity on top of the sample results from protein adsorption on the conductive tape on which the polymer is mounted. Compared to the conventionally used GUR-1050 PE-UHMW, Vitamin E doped material (Fig 4f) showed less signal intensities for all detected proteins. However, adsorbed proteins, IgG and an unidentified compound with m/z 204000 (Fig. 4d, e), revealed similar preferences for folded regions and sharp edges. To

investigate the influence of protein degradation due to protease activity, MSI experiments were performed on samples removed from SF incubation after 15, 30, 60 min and 3 h. It was found that homogeneous protein layers are formed already after 30 min of incubation and no loss of signal intensity or increased signal-to-noise ratio excelling biological variation was observed (data not shown).

Identification of high molecular weight proteins by "on polymer" digestion

To verify tentative protein identifications on PE-UHMW material, adsorbed proteins have to be enzymatically digested and the generated peptides have to be sequenced by mass spectrometry. To perform enzymatic treatment comparable to "*on-tissue*" digestion described in literature, the possibility of analyte delocalization after trypsin application was investigated. Using the piezo printer a 20 pM albumin solution was applied at a resolution of 100 µm covering 25 mm^2 homogeneously on an ITO surface and dried at room temperature. Trypsin was applied in a small rectangular shape (2 x 5 mm, 100 µm resolution) in the central area of the albumin square with the piezo printer before the sample was incubated overnight at 37 °C in an atmosphere saturated with ethanol/water (1:1, v/v). Solvents were removed on the next day by vacuum drying and MALDI matrix was applied as described again with the piezo printer. In MSI analysis the localization of albumin related peptides was investigated (Fig. 5). Albumin was identified by peptide mass fingerprinting and selected peptides further identified by PSD fragmentation. It could be demonstrated that albumin fragments were primary located in the area of previous trypsin application at a lateral resolution of 80 µm. The intensity distribution of the non-normalized data set shown in Fig. 5 reveals several signals outside the defined area, which can be related to artifacts or slight peptide diffusion. Data normalization based on the TIC levels those signals out and reveals them as noise.

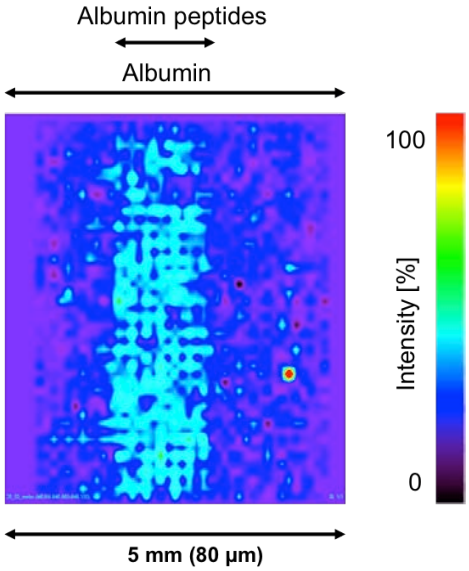

Figure 5: Non-normalized intensity distribution of a tryptic peptide (m/z 1424, [25-36] r.DAHKSEVAHRFK.d) of albumin after enzymatic digestion of an "I"-shaped area visualized with Biomap at a lateral resolution of 60 µm. The intact bovine serum albumin solution (transparent) was printed with the piezo printer in area mode on transparent ITO glass, trypsin was applied also with the piezo printer at a lateral resolution of 80 µm and the matrix (HCCA) was applied with the airbrush.

After proofing the peptide localization and protein identification process of the MSI approach with albumin, proteins adsorbed to PE-UHMW were investigated. For enzymatic treatment of PE-UHMW after synovia incubation, trypsin was applied on the total polymer surface. For this, buffer adjustment turned out to be very critical as PE-UHMW is sensitive to basic pH and thus polymer hydrolysis can occur already at pH 8.5 (a pH usually adjusted for efficient tryptic digestion). The addition of Rapigest solution to enhance proteolytic degradation by denaturing proteins allowed a pH adjustment to 7.5. At this pH value sufficient enzymatic cleavage of protein was observed while polymer hydrolysis was prevented.

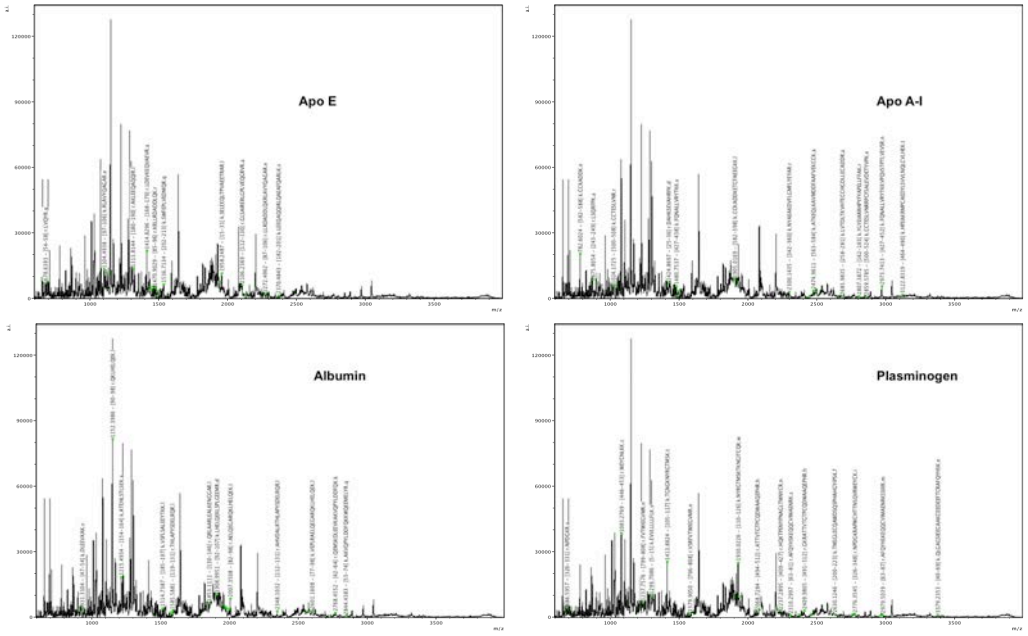

Figure 6: Profile mass spectrum of an "on polymer" digestion. Peptides are separately assigned to proteins according to theoretical cleavages exemplarily for apolipoprotein E, apolipoprotein A-I, human serum albumin and plasminogen.

During the MALDI process PE-UHMW acts as an insulating material. This effect usually results in peak broadening due to increased energy transfer for ion desorption/ionization and therefore increased energy distributions as well as decreased ion extraction efficiencies. While this disadvantageous behavior is not critical for intact protein analysis as pointed out before, it clearly limits the possibilities of unambiguous protein identification because of low absolute signal intensities and partial loss of mass resolution for the generated protonated peptides. On average 120 m/z signals were obtained within each mass spectrum generated for each position of the MSI experiment. Mass spectra were compared to m/z lists derived from *in silico* digests of already identified proteins. It was possible to correlate m/z values with peptides belonging to proteins present in synovia. Fig. 6 shows an exemplary profile spectrum of an "*on-polymer*" digest and the annotation of tryptic peptides for each identified protein.

For unambiguous identification peptides were fragmented by PSD experiments, however, signal intensities were only sufficient to generate neutral losses from the precursor ion and fragments related to the first few amino acids from the termini, which was not sufficient for automated database identification but confirmed protein identity when PSD spectra were interpreted manually.

Detected peptide signals were again analyzed for their distribution on the polymer samples. Similar localization preferences were found as for the respective proteins. Peptide

distribution was particularly correlated with folded PE-UHMW regions, rough areas and sharp edges. Fig. 7 shows the distribution of selected peptide signals associated with albumin (m/z 1024, [500-508] k.CCTESLVNR.r) and apolipoprotein E (m/z 1104, [97-106] k.RLAVYQAGAR.e). The list of associated peptide fragments (Fig. 1) includes all high abundance proteins and the majority of low abundance proteins were also found in SDS PAGE analysis.

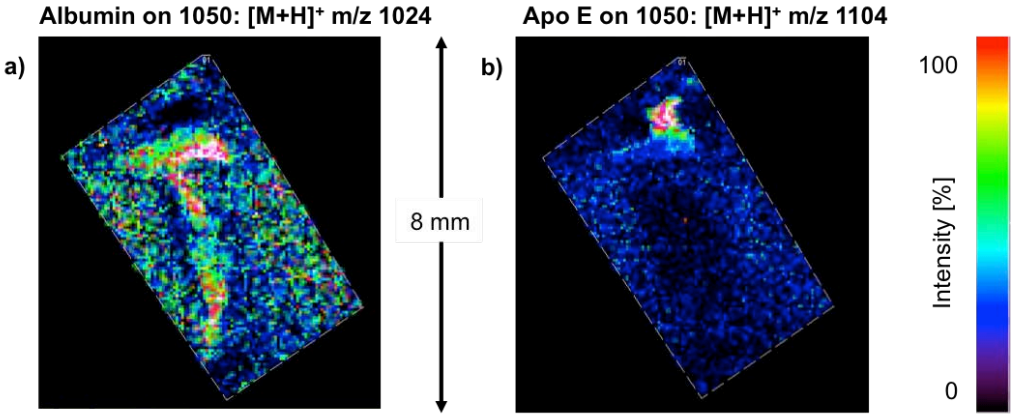

Figure 7: Peptide distribution after enzymatic treatment of GUR-1050 PE-UHMW (transparent) with trypsin: a) Peptide m/z 1024 ([500-508] k.CCTESLVNR.r) associated with albumin b) m/z 1104 ([97-106] k.RLAVYQAGAR.e) associated with Apo E. Lateral resolution: 50 µm, TIC normalized data.

Discussion

Protein adsorption on PE-UHMW

Protein patterns found in SDS PAGE and MALDI-TOF analysis clearly demonstrated that synovial proteins adsorb on the polymer surface after a short time of incubation. Previous studies have been conducted only for the major synovia components in separated experiments using single molecular species like only albumin or only hyaluronic acid. Within the present study for the first time a global view on adsorbed proteins out of the complex SF was approached. Protein adsorption from synovia on differently polymer material was compared to proteins directly extracted from the very same synovia.

Protein concentrations obtained for samples containing proteins desorbed from PE-UHMW material after incubation in synovia differed significantly if two different extraction methods (ethanol and TCA precipitation) were applied. However, so far no differences for the extracted protein species were observed. The obviously low amount of detected proteins can be ascribed to the fact that SF shows very low cell count rates (< a few 1000 cells/mm^3) and consists predominantly of water. Similar to blood plasma over 85 % are high abundant

proteins, very good characterized regarding functionality and relevant pathways. Only major protein components of synovia were identified in this study observing the adsorption behavior on PE-UHMW in the native SF composition. The increased protein concentration observed for the extraction methods using ethanol might be related to enhanced carbohydrate and lipid extraction. These analytes are of course not detectable by SDS PAGE but may falsify protein concentration results if photometric assay are applied.

Interestingly it was observed that Vitamin E doped PE-UHMW revealed significantly higher protein concentrations according to Bradford although supposed to be less affected by protein adsorption. Vitamin E has a lipophilic structure and is therefore very likely coming off the polymer surface during extraction altering protein concentration results. SDS PAGE of proteins resulting from synovia and PE-UHMW extraction showed a very broad distribution covering a molecular mass range from 6 kDa to 204 kDa. The dominant proteins forming a layer on GUR-1050 PE-UHMW and Vitamin E doped PE-UHMW were identified to be the high abundance proteins from synovia. Intensity of protein bands shows less intense bands for Vitamin E doped material, which can be interpreted as confirmation of the fact that this material adsorbs less proteins from the biological surrounding liquid. SDS PAGE also revealed that protein size did not have an effect on adsorption as no significant intensity difference was observed for high and low molecular weight proteins. Also the degree of glycosylation of proteins seems to have no influence on preferences for PE-UHMW adsorption. Most proteins, identified on the polymer have function in signal cascades, transportation pathways or can be associated with acute phase inflammation. Latter can be explained by the fact that the SF was taken after joint revision, where inflammation is evident. However, a large number of detected proteins are associated with lipid transportation and apolipoprotein subunits were detected on all samples. Lipids are an essential part of the lubrication process and have been reported to participate in the layer formation [23]. The functionally similar apolipoproteins found on the polymer may enhance or at least support lipid layer formation.

Protein layer formation and localization on PE-UHMW

PE-UHMW has a very hydrophobic surface and sample preparation for MALDI profiling and MSI experiments are critical because of polymer hydrolysis. The balance between quickly evaporating solvents, neutral pH, good analyte incorporation into the matrix and sufficient protein desorption/ionization for MS analysis is important to be kept. Especially large proteins at very low concentrations are difficult to be finally detected. The chosen

compromise for MALDI matrix concentration, solvent type and application method produced rather thick matrix layers, but ensured efficient extraction and analyte incorporation. The time span of matrix application was observed to be the most critical point during the application process. Enough time for matrix crystallization between droplet depositions of each matrix layer is mandatory to ensure fine matrix crystallization also on folded or rough surface regions.

In MSI homogeneous protein patterns were observed for evenly mounted PE-UHMW samples. The fact that glycoproteins and post-translationally unmodified proteins adsorb without specific cluster formation ensures equal lubrication properties for the whole cup. For the acetabular cup *in vivo*, this means that on a new, unused acetabular PE-UHMW cup, shortly after contact with the SF, a homogeneous protein layer is formed with equal adsorption of all proteins. However, it has to be considered that the theoretical assumptions consider the interaction between SF and PE-UHMW without taking into account additional mechanical forces. In the performed *in vitro* experiments, applying SF to unused polymer samples, protein adsorption is a matter of compound concentration. And so it was of special interest that apolipoproteins, associated with a relevant function for the articulating process but not high abundant, are homogeneously distributed over the whole PE-UHMW samples already after a very short time of interaction. Vitamin E doped PE-UHMW, which is expected to be less affected by protein adsorption, showed reduced signal intensities. However, protein adsorption behavior was observed to be similar.

On both polymer materials it was interesting to see that unevenly mounted polymer slices exhibiting folded regions, rough edges or slight cuts showed preferential protein adsorption on exactly those positions. *In vivo* PE-UHMW aging goes along with polymer oxidation, which has been reported to result in very brittle surfaces [4], similar to cup irritation resulting from mechanical stress. In our experiments, morphologically altered regions were highly affected by protein adsorption According to the presented results, this means that *in vivo* stressed and damaged regions are more prone to protein adsorption. Theoretically this can imply a compensation effect due to better lubrication by the protein layer but also further damage to the material because of oxidative interaction of the protein with the polymer.

PMF identification of proteins on PE-UHMW

PMF and peptide sequencing after "*on-polymer*" digestion revealed two major problems: PMF identification based on theoretical peptide assignment is critical and sufficient

abundant peptide PSD or CID spectra are - due to the insulating properties of PE-UHMW - difficult to obtain.

However, very complex mass spectra including the potential peptides of all enzymatically cleaved proteins from synovia were acquired. After comparing theoretical protein digests to measured m/z values, tentatively protein names, assigned after intact protein MSI experiments, were confirmed. Manual data interpretation of fragmented peptides confirmed those results. Again all detected peptides were found preferentially on sharp edges and folded areas.

However, PMF experiments on the polymer were also conducted to investigate the protein adsorption behavior. Peptides conserved in space after tryptic digestion and washing of the sample are considered to be strongly adsorbed on the polymer and this fact points to the possibility that these peptides are in fact those supporting the protein to stick to the material. So, investigating the adsorption behavior of single peptides can provide new insights into binding behavior and probably also diffusion behavior of proteins to modified PE-UHMW . This of course needs further investigation.

Conclusions

The present study shows that PE-UHMW is highly affected by protein adsorption after interaction with SF. The presented incubation experiments allowed studying whether protein adsorption is competitive if PE-UHMW materials of different types are exposed to complete SF proteomes and lipids as well as other SF components. It was observed in MSI and by gel electrophoretic experiments that all high abundance proteins in fact adsorb to PE-UHMW. The observation of homogeneous protein layers allows the conclusion that virgin PE-UHMW is completely covered with a protein layer supporting lubrication shortly after contact with SF. However, morphologically modified or rough PE-UHMW surface regions are highly affected by protein adsorption. Proteins obviously tend to adsorb on uneven surfaces. *In vivo* this behavior might induce enhanced lubrication on damaged polymer material surfaces and can result in a compensation mechanism to ensure the articulating process. Despite the expectation that Vitamin E doped UHWM-PE would be less affected, we found higher protein concentrations and comparable adsorption. Vitamin E might change the surface properties especially for preferred adsorption of either lipid or glycan species, which have not been investigated in the present study. Homogeneous layer formation has been found for both materials, which is absolutely favorable for lubrication and reduced shear stress. Nevertheless it has to be mentioned that the presented model is only a static *in vitro* model and that temperature, mechanical forces and cell stress affect protein conformation

and might change *in vivo* adsorption behavior. Further investigation is necessary to evaluate protein adsorption behavior under mechanical stress to understand the interaction between PE-UHMW and SF compounds in more detail.

Acknowledgements

This project was supported by the Vienna University of Technology (Innovative Projects 2009/Chip-1000 and 2011/UltrafleXtreme) and the Austrian Federal Ministry for Transport, Innovation and Technology (FFG project 826132/GENIE). Furthermore we acknowledge COST BM1104 (Mass Spectrometry Imaging: New Tools for Healthcare Research) for valuable discussions and know-how transfer.

Figure Legends

Figure 1: Summary of SDS PAGE analysis and protein identification of high abundance proteins in synovia and proteins recovered from PE-UHMW surfaces after incubation in synovia for 24 h. SDS PAGE: Proteins recovered from Vitamin E doped PE-UHMW (lane A), GUR-1050 PE-UHMW (lane B), Seeblue Prestained Marker (lane C) and Synovial fluid extracts (lane D). Table: proteins identified after *in-gel* digestion in comparison to m/z values detected on PE-UHMW (GUR-1050 and Vitamin E doped) by MALDI profiling. Number of peptides derived by "*on-polymer*" digestion associated to respective proteins and degree of glycosylation listed in the database.

Figure 2: Positive ion MALDI mass spectra obtained by MS profiling of GUR-1050 PE-UHMW incubated in synovia for 24 h at 37 °C. a) HCCA was used as matrix for the molecular mass range between 2 and 20 kDa and b) SA was used as matrix for the molecular mass range between 20 and 200 kDa.

Figure 3: Non-normalized intensity distribution of Leucine-Enkephalin (transparent peptide solution) printed with the piezo printer in an "H"-shaped area on transparent ITO glass before HCCA (ACN/aqueous TFA (50/0.1, v/v)) application with an airbrush. Visualization: FlexImaging. Lateral resolution of the MSI experiment: 100 µm.

Figure 4: MSI experiments of GUR-1050 and Vitamin E doped PE-UHMW incubated in synovia for 24 h at 37 °C. a) Matrix crystallization on PE-UHMW using HCCA in ACN/0.1 % TFA (70/30, v/v). MSI experiments to localize b) Apo D ($[M+H]^+$, m/z 22301), c) Albumin ($[M+H]^+$, m/z 66615) d) IgG ($[M+H]^+$, m/z 147000) and e) m/z 204000 ($[M+H]^+$) on GUR-1050 PE-UHMW (transparent) and f) Albumin $[M+H]^+$ on Vitamin E doped PE-UHMW (transparent) were performed at a lateral resolution of 100 µm.

Figure 5: Non-normalized intensity distribution of a tryptic peptide (m/z 1424, [25-36] r.DAHKSEVAHRFK.d) of albumin after enzymatic digestion of an "I"-shaped area visualized with Biomap at a lateral resolution of 60 µm. The intact bovine serum albumin solution (transparent) was printed with the piezo printer in area mode on transparent ITO glass, trypsin was applied also with the piezo printer at a lateral resolution of 80 µm and the matrix (HCCA) was applied with the airbrush.

Figure 6: Profile mass spectrum of an “on polymer” digestion. Peptides are separately assigned to proteins according to theoretical cleavages exemplarily for apolipoprotein E, apolipoprotein A-I, human serum albumin and plasminogen.

Figure 7: Peptide distribution after enzymatic treatment of GUR-1050 PE-UHMW (transparent) with trypsin: a) Peptide m/z 1024 ([500-508] k.CCTESLVNR.r) associated with albumin b) m/z 1104 ([97-106] k.RLAVYQAGAR.e) associated with Apo E. Lateral resolution: 50 µm, TIC normalized data.

References

1. Roba, M., et al., *The adsorption and lubrication behavior of synovial fluid proteins and glycoproteins on the bearing-surface materials of hip replacements.* Biomaterials, 2009. **30**(11): p. 2072-8.
2. Brach Del Prever, E.M., et al., *UHMWPE for arthroplasty: past or future?* J Orthop Traumatol, 2009. **10**(1): p. 1-8.
3. Fiorito, S., et al., *Increase in free radicals on UHMWPE hip prostheses components due to inflamed synovial cell products.* J Biomed Mater Res, 2001. **57**(1): p. 35-40.
4. Besong, A.A., et al., *A study of the combined effects of shelf ageing following irradiation in air and counterface roughness on the wear of UHMWPE.* Biomed Mater Eng, 1997. **7**(1): p. 59-65.
5. Bracco, P. and E. Oral, *Vitamin E-stabilized UHMWPE for total joint implants: a review.* Clin Orthop Relat Res, 2011. **469**(8): p. 2286-93.
6. Serro, A.P., et al., *Adsorption of albumin and sodium hyaluronate on UHMWPE: a QCM-D and AFM study.* Colloids Surf B Biointerfaces, 2010. **78**(1): p. 1-7.
7. Hamada, Y., et al., *Severity of arthroscopically observed pathology and levels of inflammatory cytokines in the synovial fluid before and after visually guided temporomandibular joint irrigation correlated with the clinical outcome in patients with chronic closed lock.* Oral Surg Oral Med Oral Pathol Oral Radiol Endod, 2008. **106**(3): p. 343-9.
8. Teloh, H.A., *Clinical pathology of synovial fluid.* Ann Clin Lab Sci, 1975. **5**(4): p. 282-7.
9. Amstalden van Hove, E.R., D.F. Smith, and R.M. Heeren, *A concise review of mass spectrometry imaging.* J Chromatogr A, 2010. **1217**(25): p. 3946-54.
10. MacAleese, L., J. Stauber, and R.M. Heeren, *Perspectives for imaging mass spectrometry in the proteomics landscape.* Proteomics, 2009. **9**(4): p. 819-34.
11. Murphy, R.C. and A.H. Merrill, Jr., *Lipidomics and imaging mass spectrometry.* Biochim Biophys Acta, 2011. **1811**(11): p. 635-6.
12. Miura, D., Y. Fujimura, and H. Wariishi, *In situ metabolomic mass spectrometry imaging: recent advances and difficulties.* J Proteomics, 2012. **75**(16): p. 5052-60.
13. Jin, Z.M., D. Dowson, and J. Fisher, *Analysis of fluid film lubrication in artificial hip joint replacements with surfaces of high elastic modulus.* Proc Inst Mech Eng H, 1997. **211**(3): p. 247-56.
14. Kingshott, P., et al., *Surface modification and chemical surface analysis of biomaterials.* Curr Opin Chem Biol, 2011. **15**(5): p. 667-76.
15. Meetani, M.A. and K.J. Voorhees, *MALDI mass spectrometry analysis of high molecular weight proteins from whole bacterial cells: pretreatment of samples with surfactants.* J Am Soc Mass Spectrom, 2005. **16**(9): p. 1422-6.
16. Stauber, J., et al., *On-tissue protein identification and imaging by MALDI-ion mobility mass spectrometry.* J Am Soc Mass Spectrom, 2010. **21**(3): p. 338-47.

17. Jiao, J., et al., *Realization of on-tissue protein identification by highly efficient in situ digestion with graphene-immobilized trypsin for MALDI imaging analysis.* Analyst, 2013. **138**(6): p. 1645-8.
18. Holle, A., et al., *Optimizing UV laser focus profiles for improved MALDI performance.* J Mass Spectrom, 2006. **41**(6): p. 705-16.
19. Bradford, M.M., *A rapid and sensitive method for the quantitation of microgram quantities of protein utilizing the principle of protein-dye binding.* Anal Biochem, 1976. **72**: p. 248-54.
20. Shevchenko, A., et al., *Mass spectrometric sequencing of proteins silver-stained polyacrylamide gels.* Anal Chem, 1996. **68**(5): p. 850-8.
21. Perkins, D.N., et al., *Probability-based protein identification by searching sequence databases using mass spectrometry data.* Electrophoresis, 1999. **20**(18): p. 3551-67.
22. Marchetti-Deschmann, M., Gahler, J., Archodoulaki, V., Allmaier, G. *"Ultra-high Molecular Weight Polyethylene (PE-UHMW) Joint Implants - Choosing the Most Valuable Desorption Process (i/vMALDI and DESI) for Imaging MS";* . in *58th ASMS Conference on Mass Spectrometry and Allied Topics*. Paper-Nr. TP23 534 (1482), 1 S, 2010. Salt Lake City, UT, USA: American Society of Mass Spectrometry.
23. Greenbaum, E.S., et al., *Effect of lipid absorption on wear and compressive properties of unirradiated and highly crosslinked UHMWPE: an in vitro experimental model.* Biomaterials, 2004. **25**(18): p. 4479-84.

8. MALDI-TOF mass spectrometry imaging reveals changes on molecular level for ultra-high molecular weight polyethylene joint implants in correlation with lipid adsorption

To be submitted Analytical Chemistry (2014)

MALDI-TOF mass spectrometry imaging reveals changes on molecular level for ultra-high molecular weight polyethylene joint implants in correlation with lipid adsorption

*Sophie M. Fröhlich[1], Vasiliki-Maria Archodoulaki[2], Günter Allmaier[1], Martina Marchetti-Deschmann[1]**

1) Institute of Chemical Technologies and Analytics, Vienna University of Technology, Getreidemarkt 9, 1090 Vienna, Austria

2) Institute of Materials Science and Technology, Vienna University of Technology, Favoritenstrasse 9-11, 1040 Vienna, Austria

KEYWORDS: PE-UHMW, material characterization, MS imaging, polymer modification, lipid adsorption, MS/MS imaging

ABSTRACT: PE-UHMW (ultra-high molecular weight polyethylene), a material with high biocompatibility and excellent mechanical properties, is amongst the most commonly used materials for acetabular cup replacement in artificial joint systems. It is assumed that the interaction with synovial fluid, the bio-compartment, leads to significant changes relevant for material failure. Besides hyaluronic acid, especially lipids are relevant for the lubrication process in an articulating process. This study investigates synovial lipid adsorption on two different PE-UHMW materials (GUR-1050 and Vitamin E doped) in an *in vitro* model system by MALDI-TOF mass spectrometry imaging (MSI). Lipids were identified by high performance thin layer chromatography and MS/MS analysis with the analytical focus on phospholipids and cholesterol, both being species of high importance for lubrication. Scanning Electron Microscopy analysis was introduced to the study to correlate molecular information with PE-UHMW material qualities. It could be demonstrated that lipid adsorption preferentially occurs in rough or oxidized polymer regions. Polymer modifications were co-localized with adsorbed lipids and found with high density at regions identified by SEM. Explanted, *in-vivo* polymer material showed comparable and even more obvious polymer damage and lipid adsorption when compared to the static *in vitro* model. A 3-dimensional reconstruction of MSI results from consecutive PE-UHMW slices reveals detailed information about the diffusion process of lipids in the acetabular cup and provides for the first time a promising starting point for future studies correlating molecular information with commonly used techniques for material analysis (i.e. Fourier-Transform Infrared spectroscopy, nano-indenter).

INTRODUCTION

Ultra high molecular weight polyethylene (PE-UHMW) has been widely accepted as a commonly used material in replacing the acetabular cup in hip joints and cartilage in the knee joint. Several material benefits such as easiness in surgical handling, high biocompatibility, high resistance to abrasion, very low coefficient of friction and its self-lubricating properties are reason for its widespread application. However, the number of joint revisions cannot be ignored: the average *in vivo* time is only 2 to 5 years[1-3]. PE-UHMW's major drawback lies in shelf life aging, leading to oxidation and consequently *in vivo* aging[4]. Even though surface coating with Vitamin E and polyethylene glycol (PEG) protects the material from oxidation and enhances material hardness[5-7], none of them proved long term success. Apart from the patient's compliance and pathological predisposition harming the implant, PE-UHMW is in permanent contact with synovial fluid (SF) while being affected from very high mechanical forces.

To some extent protein interaction from SF with PE-UHMW was already studied by others[8-11] but also from our group (EOP, accepted for publication[12]). Furthermore it has been shown that small cholesterol-related lipid components tend to diffuse from SF into the material[13]. To date it is known that the polymer material interacts with its bio-compartment, by inducing inflammation related cell signals, through abraded polymer particles[14-15]. However, neither the PE-UHMW surface has ever been analyzed regarding the distribution of adsorbed and diffused lipid compounds, nor has the interaction with the synovial lipidome been studied. SF contains besides high abundant glycosaminoglycans and proteins also a high concentration of lipids. Lipids are known to quickly respond to pathological changes, leading to concentration or side chain conformation changes[16-17]. Di- and triglycerides, cholesterol, cholesterol esters, phospholipids, sphingomyelins and free fatty acids are the relevant, rather high abundant lipid species available in SF for interaction[18]. Especially phospholipids have been reported to be essential for the

lubrication process in the native joint as well as in the artificial replacement system[19-21]. The formation of lipid layers on the PE-UHMW acetabular cup combined with the constant mechanical load and shear forces from the metal based femoral head lead to enhanced interaction. It is essential for material improvement to understand the regulating system of material oxidation, mechanical loading and the interaction with the bio-compartment. The present study identifies and localizes for the first time high abundance synovial lipid components in three dimensions after interaction with PE-UHMW.

Mass spectrometry imaging (MSI) by matrix assisted laser desorption/ionization (MALDI) mass spectrometry (MS) coupled to a time of flight (TOF) mass analyzer provides the possibility to gather information concerning the localization and identity of an analyte of interest within one experiment without prior knowledge of the biomolecule[22]. With this unbiased method it is possible to characterize adsorbed synovial compounds and PE-UHMW modifications on a molecular level. MSI has been used for a huge variety of biological[23-25] applications ranging from microbiology to polymer based membrane analysis and pathology[26-29] but has never been used for characterizing material at biological interfaces before.

To visualize correct analyte distributions, MSI experiments require very homogeneous MALDI matrix application to circumvent artifacts resulting from ion suppression and uncontrolled matrix cluster formation[30]. Therefore the very hydrophobic sample surface of PE-UHMW is an exceptional challenge, when simultaneously high desorption/ionization efficiencies for lipid analysis are intended. A chemical inkjet printer was used in this study providing the possibility to form homogeneous and fine crystallized matrix layers by depositing aqueous solutions on hydrophobic surfaces[31] while retaining the analytes' positions. Using this technique it is possible to determine lipid adsorption on and diffusion patterns into PE-UHMW implant

material. To corroborate the obtained results, the synovial lipidome is investigated using high performance thin layer chromatography (HP-TLC) in combination with MS. The method has been proofed to give a quick, reproducible and comprehensive way for lipid analysis and further identification[32-33].

EXPERIMENTAL SECTION

Materials. The Institute of Materials Science and Technology, Vienna University of Technology, provided virgin γ-irradiated PE-UHMW (GUR-1050), Vitamin E doped and explanted γ-irradiated GUR-1050 (ultrasonicated after revision) samples.

All chemicals and reagents, unless indicated specifically, were purchased from Sigma-Aldrich (St. Louis, USA) with a purity of at least 99 % if not stated otherwise. Double distilled water (ddH_2O) was obtained from a Simplicity system (Millipore, Billerica, USA) with a specific conductivity of $\Omega_m \leq 18$ S/cm.

PE-UHMW preparation. PE-UHMW was cut into small blocks of similar geometry (avg m = 65 ± 2 mg, V ≈ 120 mm^3) and either incubated in SF or sliced to 15 µm using cryo-microtomy (Leica Biosystems, Nussloch, Germany). Slices were mounted onto indium-tin oxide (ITO) coated glass slides (Sigma-Aldrich) with adhesive-conductive tape (Shimadzu Kratos Analytical, Manchester, United Kingdom) (Fig.1a-c). Curling of the sample at the edge was most critical and prevented by stamping the samples with wetted KimWipes™ (Kimberley-Clark, Dallas, USA) covering a clean glass.

All PE-UHMW samples were incubated in bovine SF at 37 °C for 1 h and 24 h in a heating cabinet. After incubation, samples were rinsed twice with ddH_2O and vacuum dried. To simulate

surface changes, PE-UHMW blocks of constant mass and dimension were roughened with a milled-tooth file to increase the effective area or tightly smoothed with a scalpel.

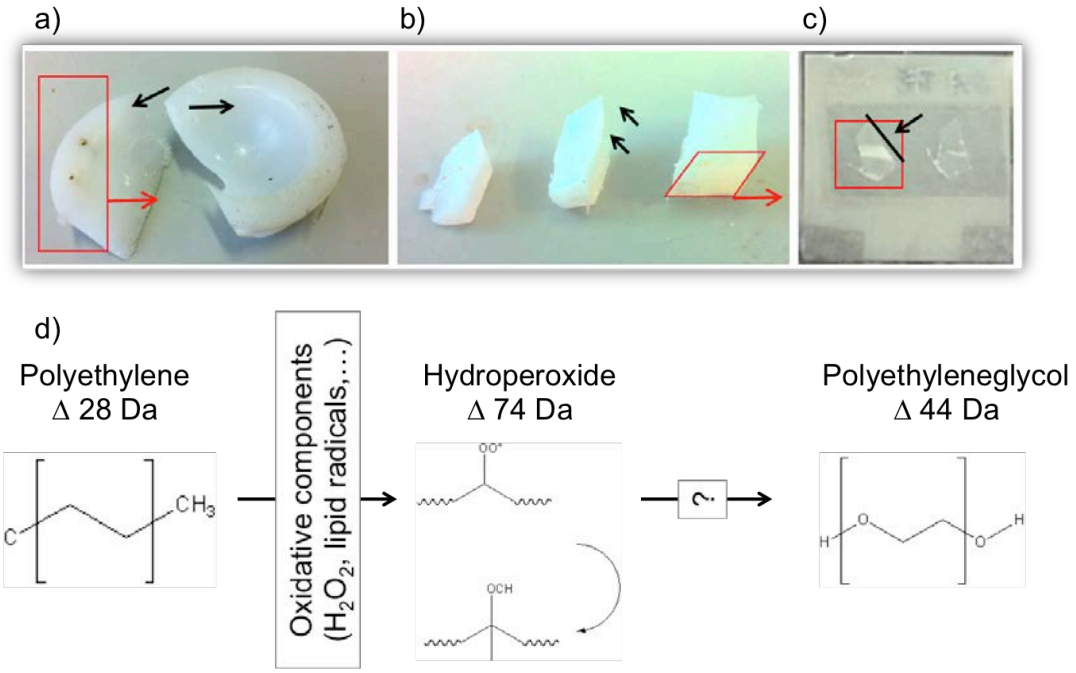

Figure 1: (a) PE-UHMW cups were cut into (b) smaller blocks and used for incubation. Blocks were also cut into (c) slices of 15 µm thickness and mounted on ITO slides using adhesive-conductive tape; (d) Proposed chemical change of PE-UHMW under the influence of oxidative species.

Lipid extraction. For lipid extraction PE-UHMW blocks incubated in SF as described were kept in 900 µL chloroform/methanol (2:1, v/v) for 1 hour at room temperature. 900 µL chloroform/ddH_2O (1:1, v/v) were added before centrifuging the samples at 3000 rpm at room temperature for 15 min. The organic phase was collected and evaporated under vacuum. SF was examined from two different species (human (HSF) and bovine (BSF)). HSF was collected from 12 different patients with varying biological background (sex, pathology, age). BSF was provided by local butchery services (Amstetten, Austria) directly after slaughter from 15

different cows, HSF samples were provided by the University Hospital of Orthopedics (Medical University of Vienna, Vienna, Austria). Lipids from synovia were extracted by mixing 20 µL synovia with 900 µL extraction solvent chloroform/methanol (2:1, v/v) and processed as described above or hexane/methanol (2:1, v/v) was used instead of ddH_2O (final mixture: chloroform/hexane/methanol 1/3.3/1.7, v/v/v). For further analysis lipid extracts were re-dissolved in 15 µL chloroform. 8 µL were applied to Silica gel 60 HP-TLC aluminum plates (Merck, Schwalbach am Taunus, Germany) using a syringe (see HP-TLC analysis). 7 µL were used for further MS analysis (see MS analysis).

HP-TLC analysis. Lipid separation on high performance thin layer chromatography (HP-TLC) plates (10 x 10 cm, layer thickness 0.2 mm, particle size 5-6 mm) was performed using a two-phase solvent system. The plate was developed in solvent system 1 (methyl acetate/1-propanol/chloroform/methanol/saturated aqueous potassium chloride, 25/25/25/10/0.25, v/v/v/v/v) until 66 % of the full length of the HP-TLC plate was reached to separate glycolipids from phospholipids. The plates were dried using warm air (heat gun, approx. 40-45 °C) to remove the mobile phase before further development in solvent system 2 (toluene/diethyl ether/ethanol/acetic acid, 60/40/1/0.05, v/v/v/v) for neutral lipid separation. Plates were developed not further than 95 % of the total plate length. Plates were stained with 0.05 % primuline in acetone/water (8/2, v/v) and lipid spots were detected at 337 nm. For further identification lipids were subsequently extracted from the plate using the same procedure as described above (chloroform/methanol followed by chloroform/ddH_2O solution). Extracts were analyzed on the MALDI-TOF/RTOF instrument (see MS analysis).

Matrix and matrix deposition. Standard MALDI matrices, α-cyano-4-hydroxycinnamic acid (CHCA), 2,5-dihydroxybenzoic acid (DHB) or 1,4,6-trihydroxyacetophenone monohydrate

(THAP) (Sigma-Aldrich) were dissolved either in 70 % acetonitrile, 30 % ddH_2O (v/v) containing 0.1 % trifluoroacetic acid (TFA) or potassium chloride saturated methanol. Samples were sonicated for 5 minutes before centrifugation at 3000 rpm for 15 minutes. For MSI experiments automatic matrix deposition was performed using a chemical inkjet printer, ChIP-1000 (Shimadzu Kratos Analytical) with a pitch size of 80 µm (distance between deposited spots) was used to apply 0.8 ng/spot. Alternatively matrix was applied with a commonly used airbrush device (Conrad Electronic International GmbH & Co, Hirschau, Germany) in 4 iterations, operated in a working distance of 10 to 12 cm at an angle of approx. 50° towards the sample. Matrix recrystallization was performed in a climate box at 80 % air humidity generated by ethanol/water solution (1/1, v/v) at 37 °C for 5 minutes.

For lipid analysis after extraction from PE-UHMW or HP-TLC plates, 20 mg/mL THAP were dissolved in 1 mL potassium chloride saturated methanol. Lipid extracts and matrix solution were mixed in a ratio of 1:1 and 1 µL was deposited on a polished stainless steel microtiter plate target (Bruker Daltonik, Bremen, Germany).

MS analysis. For HP-TLC/MALDI MS analysis the developed HP-TLC plate was mounted on a TLC adapter (Bruker Daltonik). THAP (20 mg/mL) in acetone was deposited manually on the identified areas (UV 337 nm) using a pipette. MALDI MS spectra for direct analysis of HP-TLC plates were acquired on a MALDI-TOF/RTOF instrument (UltrafleXtreme, Bruker Daltonik), equipped with a 2000 Hz Smartbeam™ laser (355 nm). Analyte identification was conducted by inducing post source decay (PSD) fragmentation.

MSI spectra were acquired with lateral resolutions between 10 and 150 µm depending on the experiment performed. Selected ion images from intact lipid species but also from characteristic

lipid fragments were generated using FlexImaging v. 3.0 (Bruker Daltonics), applying median data normalization algorithms. Polyethylene glycol (PEG) formation was tested additionally on another MALDI-TOF/RTOF instrument equipped with a 337 nm nitrogen laser (AXIMA TOF^2, Shimadzu Kratos Analytical). The same instrument was used for lipid identification by collision induced dissociation at high energy (HE-CID, 20 keV).

Scanning electron microscopy (SEM) analysis. PE-UHMW samples (GUR-1050 and Vitamin E doped), incubated in SF and further handled as described above. After washing with ddH_2O PE-UHMW samples were pre-sputtered for 1 min with a thin gold film to enhance conductivity. SEM images were acquired from exemplary PE-UHMW positions affected by lipid adsorption at an acceleration voltage between 10 and 20 kV and a magnification between 1000 and 4000 on a XL 30 scanning electron microscope (FEI Philips, Hillsboro, USA).

RESULTS & DISCUSSION

To better understand the process dynamics between PE-UHMW implants and SF, we first need to understand the interaction between the polymer and its biological environment without any additional mechanical forces. Furthermore it is necessary to know which potentially interacting lipids are present in SF and compare them to lipid species adsorbed on the polymer. To gain first ideas for diffusion behavior of lipids interacting with porous polymer, lipid localization on PE-UHMW is necessary. To have a controlled experimental situation, virgin polymer material was incubated with SF and lipid analysis was performed (*in vitro*). Lipid pattern detected on the polymer surfaces were compared to lipids extracted from the very same SF. Finally the results obtained in this simulation were compared to lipid pattern detected in actually explanted PE-UHMW material (*in vivo*).

SF lipid components. Regarding it's lipidomic composition SF consists majorly of cholesterol and cholesterol esters, besides triglycerides, ceramides and phospholipids[34].

To compare the composition of lipids adsorbed on PE-UHMW, the composition of the actual SF has to be studied. For this, lipids were extracted and separated by HP-TLC. In Fig. 2 one can see that the major components described for SF are present in both, human and bovine SF samples.

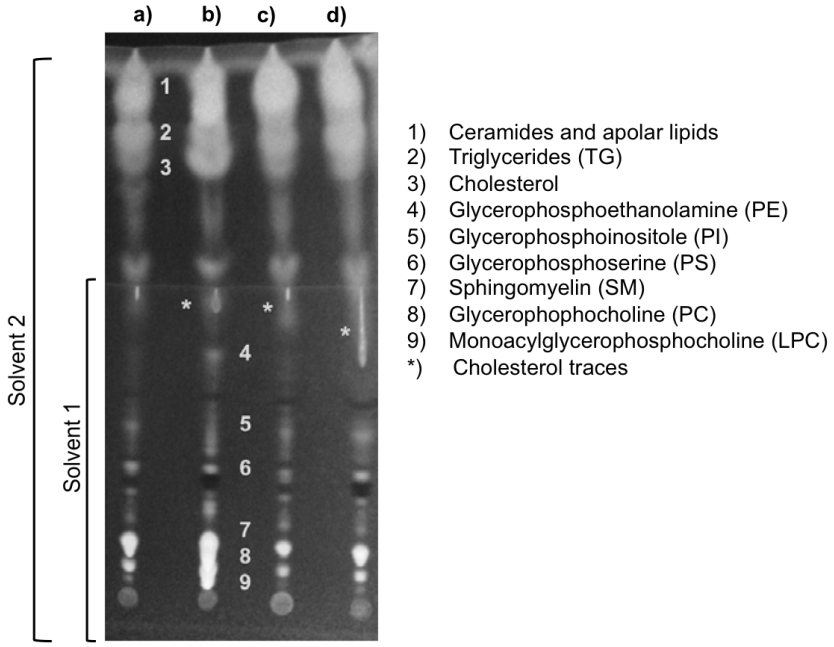

Figure 2: HP-TLC separation of lipids extracted from (a) bovine synovial fluid (BSF), (b) human synovial fluid (HSF) with a medical record of acute inflammation from osteoporotic dissection surgery, (c) GUR-1050 PE-UHMW incubated in BSF for 24 h and (d) Vitamin E doped PE-UHMW incubated in BSF for 24 h.

Up to 11 characteristic bands were observed. Lipids were identified based on their R_f values and extracted for identification by HE-CID tandem mass spectrometry (MS/MS). Besides the characteristic lipid head groups, lipids could further be characterized regarding their fatty acid

composition using MS/MS. Details on lipid fragmentation and identification after HP-TLC see supplemental data. Several unidentified non-polar lipids were found in all samples. As shown in Fig. 2 the highly concentrated polar lipids, as well as the non-polar lipids in the second separation step are nicely resolved. Spots not assigned in Fig. 2 belong to variations of the main phospholipid classes (see supplement for details).

Based on the HP-TLC separation and lipid identification, BSF can be considered as a comparable model fluid for HSF for investigating the adsorption of high abundance lipids on PE-UHMW. Comparing 12 HSF samples from patients suffering different stages of inflammation, quantitative differences in the lipid composition are evident (data not shown) as described in literature [35]. Especially PE, PS and cholesterol differ from sample to sample. For further *in vitro* experiments, those differences can be neglected due to ion suppression effects occurring during MSI where LPC, PC and SM signals are favoured. Furthermore LPCs, PCs and SMs have been reported to show constant proportions [34] (ratios do not change with biological variation) and are of particular interest for PE-UHMW analysis, since they represent the components of the synovial lipidome relevant for lubrication.

The comparability of BSF as a model fluid for HSF proved sufficient, as all major lipid components were detected and no significant pattern variation was observed for all BSFs under investigation. Lipid extracts from conventional GUR-1050 PE-UHMW and its Vitamin E doped form reveal similar pattern for extracted lipids (Fig 2). However, Vitamin E doped samples seemed to be more affected by cholesterol uptake, visible in an even more present smearing of cholesterol traces in the lower region of HP-TLC separation (Fig. 2 asterisk, data of experiments with high loads of cholesterol standard exhibiting similar pattern not shown). Such effect might occur as a consequence of the increased hydrophobicity resulting from Vitamin E doping.

Synovia residues and PE-UHMW surface modifications after incubation. For examining the interaction of SF lipids with PE-UHMW, *in vitro* experiments were conducted considering the time span and the material composition and predisposition as major factors of interest for adsorption.

The interaction between SF and PE-UHMW was first investigated by SEM (Fig. 3).

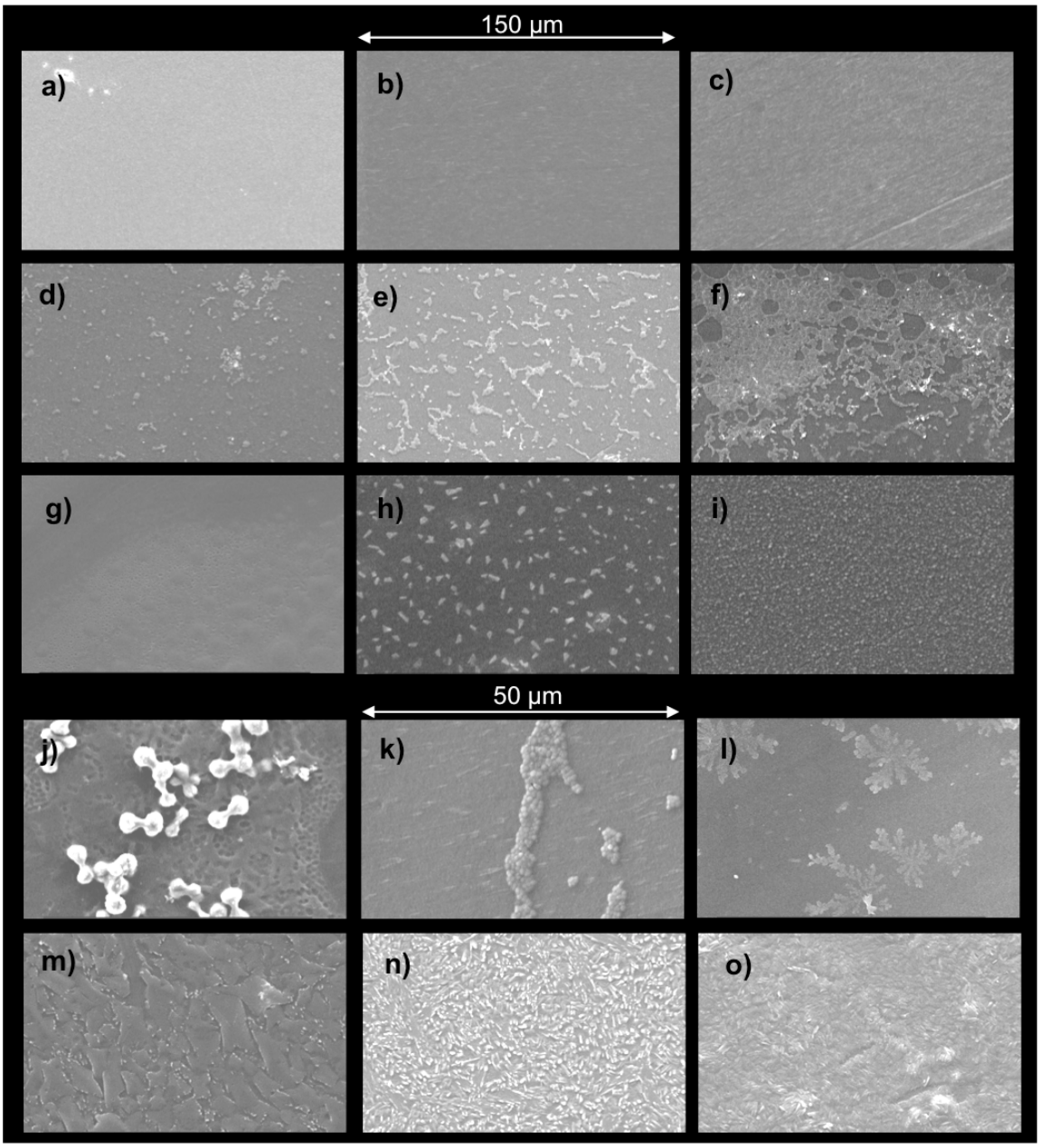

Figure 3: SEM analysis of different types of PE-UHMW after being in contact with SF for defined time spans: (a) native PE-UHMW GUR-1050 (b) incubated for 1 d and (c) 3 d; Biological residues on PE-UHMW incubated for 24 h: (d) GUR-1050 (e) Vitamin E doped (f) explanted GUR-1050; (g) GUR-1050 explanted after 5 y *in vivo* showing (h) cholesterol crystals and (i) mechanically stressed areas; Modifications on explanted GUR-1050 PE-UHMW after 14

d SF incubation: (j) $CaCO_3$ crystals, (k) biological residues (l) salt crystals and (m-o) oxidized areas.

Virgin 1050 samples incubated in SF for a time span between 15 min and 14 days were examined concerning biological residues and polymer related surface modification. SEM analysis showed biological traces not being removed by washing procedures but also revealed PE-UHMW morphology changes when comparing the surface before (Fig. 3a) and after incubation (Fig. 3b,c). It is shown that even short incubation times of 1 to 3 days roughened the surface when compared to the smooth structure of untreated samples.

To investigate the influence of doping in PE-UHMW samples, Vitamin E doped virgin material, with improved resistance to adsorption, was compared to conventionally used GUR-1050 samples. Unexpectedly GUR-1050 samples were much less affected by biological adsorption (Fig. 3d) than Vitamin E doped samples (Fig. 3e).

Explanted PE-UHMW material was studied before and after incubation in SF under the same conditions to examine absorption effects induced by previous exposure to mechanical stress. As expected the surface before incubation showed increased roughness compared to virgin material (Fig 3g,i). After incubation almost convolute layers of biological residues were observed (Fig 3f). In areas of obviously severely stressed PE-UHMW even cholesterol crystals were detected (3h)[36]. After 14 days of SF incubation adsorbed residues were dominant. $CaCO_3$ crystals (Fig 3j), salt associated traces (Fig 3l) and unidentified biological residues (Fig 3k) could be visualized. Additionally the PE-UHMW surface was severely changed similar to previously described observations[37]. Lamellate formations with sharp edges, very rough areas and grained structures were detected, all co-localized with biological residues (Fig 3m-o).

According to SEM results, SF interacts with UHMPWE surfaces and leads to adsorption of biological residues. Also the correlation of surface changes and biological debris is evident. The results obtained for the incubated explant material indicate that previously damaged or modified material is even more prone to biological interaction with SF. Cholesterol crystals found only on explant PE-UHMW samples indicate the initial presence of cholesterol residues. Cholersterol may function as crystallisation nuclei, very likely explaining the high density and large size of the found crystals.

SF associated lipid adsorption on PE-UHMW. To investigate the adsorption of lipids on PE-UHMW, material blocks were incubated in SF before high abundance lipids were extracted and separated by HP-TLC. As demonstrated in Fig. 2, the lipid pattern extracted from PE-UHMW samples is comparable to the SF lipid extracts. All previously mentioned lipid species are present, but show higher signals for the very non-polar lipids such as cholesterol and TGs. Especially Vitamin E doped PE-UHMW effectively adsorbed cholesterol leading to smearing on the HP-TLC (Fig. 2d). By the use of mass- and dimension-matched PE-UHMW blocks with intentionally changed surfaces properties (roughened with a milled-tooth file or smoothed with scalpel) it was observed that the intensity of all lipid bands increased significantly for extracts from roughed surfaces. This indicates that lipid adsorption is more likely to occur on areas with rough surfaces. This is in fact the case for all areas of the acetabular cup that are exposed to mechanical stress or oxidation. Adsorbed lipids as a consequence can increase the possibility of further material oxidation and modification.

Lipid extract patterns from GUR-1050 PE-UHMW explants showed in comparison low signal intensities. The explants were stored at -70 °C for 2 years, yet the conditions of revision and

exact time span of sample storage are not known. So it was assumed that lipids were already leached out or degraded. However, it became evident that PE was dominantly detected compared to all other lipid classes. This might be explained by the high concentration of PEs in membranes increasing fluidity, which is necessary in lubricant systems. The lack of cholesterol and TGs can be explained by the reported tendency of very non-polar and small lipids to diffuse into the material, resulting in difficult accessibility for the extraction process. However, it has to be considered that the limited amount of explant samples allows no biological conclusion since biological variations cannot be statistically covered in this study.

PE-UHMW sample preparation for MSI. To examine and correlate adsorbed lipid species and polymer surface modifications on a molecular level, MSI analysis was conducted on PE-UHMW slices. The most critical step for a reliable MSI experiment with minimized occurrence of artifacts is sample preparation. In contrast to tissue sections PE-UHMW is an insulator and a rigid material tending to distort at very thin sample thickness. Thin samples are yet required in MSI experiments to reduce the possibility of mass deviation due to insulating material and height differences. For PE-UHMW the optimal cutting thicknesses was above 7 µm. Thinner samples showed severe cases of mechanical damage and were not reproducible in thickness and shape as a consequence of thermal expansion and shrinking during cryo-microtomy. Thin sections however have the drawback of low analyte concentrations. Although the optimal thickness was 20 µm with respect to sufficient analyte detection and 7 µm for an efficient MALDI process itself (minimum insulation), a comprehensive analysis demanded a compromise between analyte concentration, insulating properties of the material and microtome operation capabilities. For PE-UHMW the optimal cutting thickness was evaluated to lie between 14 and 16 µm.

The second critical step in sample preparation of PE-UHMW for MSI is MALDI matrix application. The very hydrophobic surface of PE-UHMW impedes matrix application in aqueous solvents. Highly volatile solvents with an organic solvent content of at least 70 % showed best results with respect to printing properties of the ChIP-1000, printing reproducibility, droplet accuracy. Homogeneous matrix layers were obtained by applying a total of 6-8 ng/µg CHCA and DHB (1:2, m/m) per lateral spot on the PE-UHMW surface providing sufficient desorption/ionization efficiency for lipids and polymers. This matrix combination resulted in very small crystals forming a homogeneous matrix layer. The use of methanol improved printing stability and crystallization on the polymer surface due to its high volatility. High volatile solvents also prevent analyte diffusion due to a fast incorporation and evaporation process before accelerated matrix crystallization. Complete matrix coating of the sample surface without analyte diffusion is possible and spatial resolution for the MSI experiments is limited solely by the laser spot diameter and its energy profile. Although rough surface areas inhibited fine crystallization, matrix recrystallization at 80 % air humidity (ethanol/water mixture) efficiently reduced crystal size to keep the lateral resolution of the MSI experiment low.

Identification of adsorbed lipids on PE-UHMW. Based on literature, describing PCs as the major lipids relevant for the lubrication process[38], MSI experiments focused on the distribution of PCs, SMs and cholesterol. Lipid extraction already showed that all lipid classes found in SF adsorb on PE-UHMW surfaces, with a tendency to better adsorb in rough areas. However, from these experiments it is not known, where exactly lipids adsorb and what kind of lipids are involved.

MSI experiments were carried out under the same conditions as previously described for SEM experiments, using conventional GUR-1050, Vitamin E doped PE-UHMW and explants for incubation and PE-UHMW explants without incubation. As a consequence of the highly insulating properties of PE-UHMW the MALDI process is negatively influenced. Lower signal intensities were observed for lipids in the generally preferred negative ion mode for lipid analysis. Consequently the more sensitive positive ion mode was chosen for analysis, favoring therefore PC, LPO, SM and cholesterol analysis. The presence of all other identified lipid species was proven by MS profiling and imaging experiments in positive and negative detection mode (details see supplemental data). Lipid identification is again based on characteristic fragment ions and neutral losses. Fig. 4 shows the distribution of characteristic fragment ions on PE-UHMW explants incubated for 24 h in SF corresponding to PC/SM, PE, PI and Cholesterol.

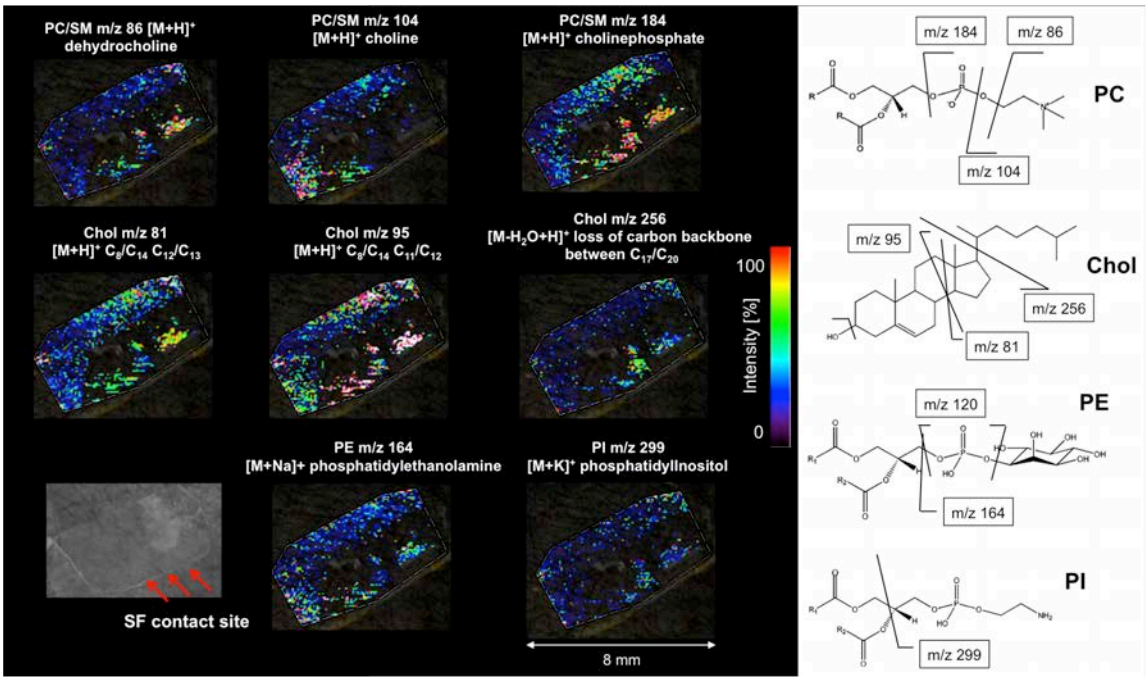

Figure 4: MS/MS imaging to visualize lipid distribution on GUR-1050 PE-UHMW after 24 hours of incubation in SF; major fragments relevant for lipid classification are marked in the

lipid core structure; The contact site of incubated PE-UHMW samples with SF is indicated by arrows.

In the center or the investigated area almost no fragment ions were detected, whereas high signal intensities were observed on the edges. However, the pattern for lipid related signals at edges follows engraved lines caused by possible *in vivo* mechanical stress. This can be explained by the assumption that mechanically stressed regions show less compact PE-UHMW, leading to an increase in surface area, favoring lipid adsorption as previously described. Those findings confirm results from SEM analysis of the same regions, revealing modified rough and possibly oxidized areas (Fig. 3). For explanted PE-UHMW samples especially cholesterol was found in centroid regions and at the direct contact side with SF in the joint compartment. Overall it can be said that all 4 lipid classes could be detected on all investigated sample categories. PC and SM were distributed homogeneously on samples providing very smooth surfaces (supplemental data).

Time-course of lipid adsorption studied by MSI. MSI experiments studying time related lipid uptake over 24 hours showed no significant time dependency or differences in localization for phospholipid classes. However, cholesterol related signals were not detected in the initial phase shortly after incubation, but were dominant after 1 hour on a well-defined area. After longer incubation times, no cholesterol related ions were observed. Those findings may indicate the dominant presence of cholesterol adsorbing in the initial lubrication phase, which further diffuses into the material. This possibility has in fact been reported before[13]. However, according to SEM analysis, cholesterol forms larger crystals after a while. Larger crystals can lead to decreased MALDI efficiencies caused by reduced incorporation into matrix crystals.

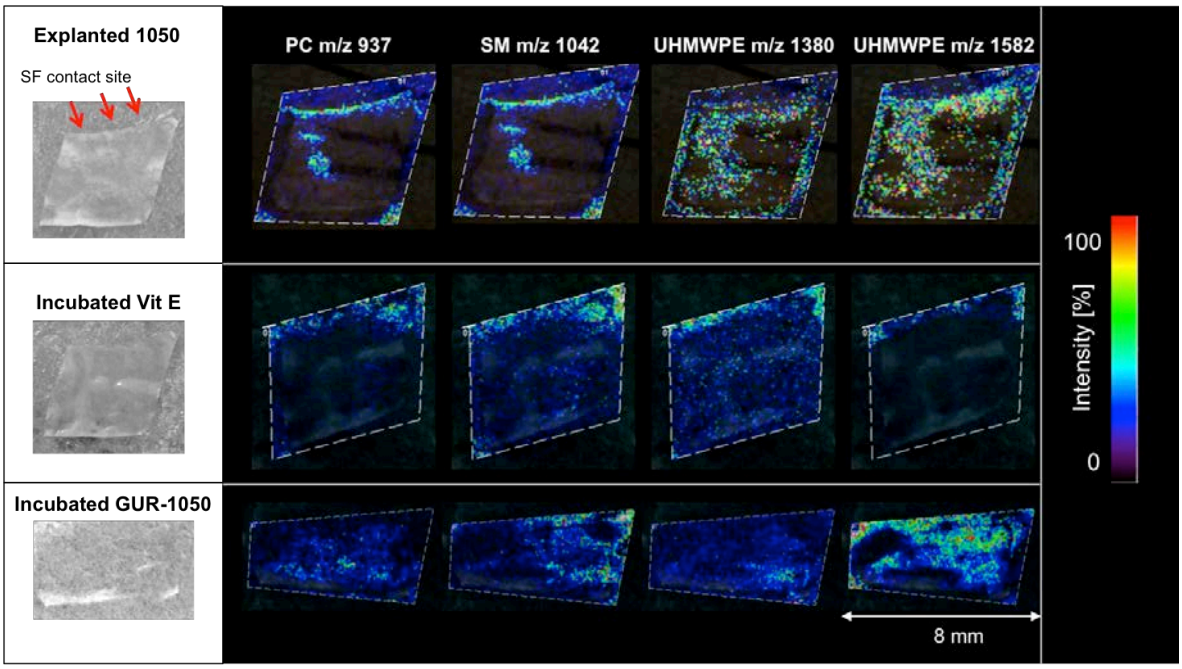

Figure 5: Visualization of lipid and polymer related signals on PE-UHMW (explant untreated, Vit. E doped, GUR-1050) incubated in SF for 24 h; m/z 937 PC (44:2), m/z 1042 SM (51:2) associated, m/z 1380 PE-UHMW hydroperoxide associated and m/z 1582 PE-UHMW PEG associated; Arrows mark the contact region of the polymer with SF on light microscope image of matrix-covered PE-UHMW samples.

Fig. 5 shows the distribution of two different lipid species on explanted PE-UHMW, one Vitamin E doped sample and a GUR-1050 PE-UHMW. It is evident that in the explant, lipids are present especially on the contact side with SF in the acetabular cup. Even diffusion into the material in possibly mechanically stressed regions, recognized in preceding SEM analysis, can be observed. The distinct pattern of lipid adsorption and diffusion can be co-localized with dominant but more diffuse PE-UHMW modifications like PE-UHMW hydroxides.

Vitamin E doped and GUR-1050 PE-UHMW samples incubated in SF (SF completely covered the sample) showed different lipid patterns. Lipids were identified on one particular edge possibly initiating the adsorption process there. On conventional GUR-1050 material, lipids were adsorbed in the center regions of the sample. Congruent signals were observed for polymer related signals belonging to PE-UHMW hydroperoxide and PEG. Correlating the experimental findings with previously performed SEM analysis, it can again be concluded that lipids preferentially adsorb on rough and brittle PE-UHMW areas as well as on sharp edges.

The diffusion of lipids into PE-UHMW has in general been described before[39], which proved to be correct in our studies for certain species. Nevertheless, to obtain more information about the diffusion behavior of high abundance lipids into PE-UHMW, consecutive slices of PE-UHMW explants were examined and 3-dimensionally reconstructed (Fig. 6). Cholesterol (m/z 369, $[M-H_2O+H]^+$) has been investigated on 4 consecutive slices from a potential mechanically stresses area in the acetabular cup. According to the detected intensity distribution, cholesterol diffused into the material after entering the SF contact site. The investigated consecutive slices represent a depth profile of almost 0.1 mm. Over the total PE-UHMW ”block” regions with distinct Cholesterol location are observed beside more diffuse regions, correlated with material modifications observed in SEM analysis. These results give first insights into significant changes of Cholesterol presence in three dimensions, but also allow conclusions for material failure.

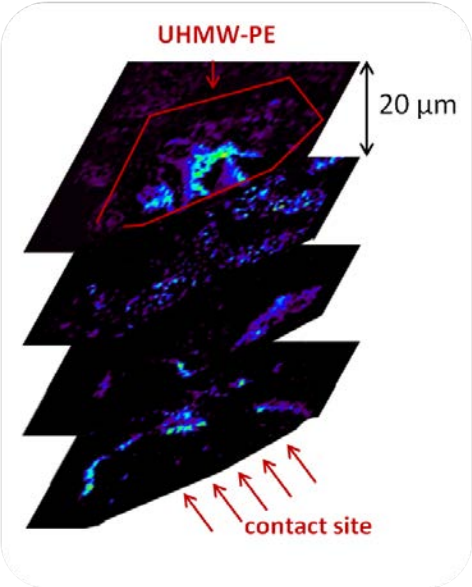

Figure 6: 3-dimensional reconstruction of cholesterol ($[M-H_2O+H]^+$ intensities at m/z 369) on consecutive PE-UHMW samples.

PE-UHMW modifications. As described, SEM observations did not only reveal biological residues but also showed severe polymer surface modifications. Using MSI, polymer related modifications were studied on the molecular level by analyzing the affected regions identified by SEM analysis. Polymer distributions with mass differences of Δ m/z 44 indicated the presence of PEG (details discussed later) and Δ m/z 74 indicated PE-UHMW hydroperoxide. Latter is a radical described to be involved in the oxidation process of shelf life aging of PE-UHMW[4, 40]. Hydroperoxide was found on all different PE-UHMW types, even after short contact (1 h) with SF. Short incubation times induced radical occurrence only at the SF contact sites, whereas after 24 h or more, hydroperoxide radicals were also found in more centroid regions, correlating nicely with signals of diffused cholesterol. Another polymer distribution with mass differences of Δ m/z 138 is not clearly identified yet. All modifications were found for GUR-1050 and Vitamin E doped PE-UHMW samples but also for PE-UHMW explants. Interestingly polymer

signals were found in areas showing the formation of unspecific carbon clusters (Δ m/z 12 and 24) during the MALDI process. These clusters were especially observed in rough and brittle areas of explant material.

All polymer modifications were found co-localized with extensive lipid adsorption. Considering the fact that SF contains a noticeable amount of reactive oxygen species (ROCs), the occurrence of polymer radicals can be explained, and radicals are the initiator for material oxidation, which is then observed *e.g.* in SEM analysis. Furthermore lipids can form radicals during their own oxidation process, which then also have oxidizing effects on PE-UHMW.

Besides the prior analyzed regions of interest, showing material oxidation identified by SEM, polymer modifications (*i.e.* hydroperoxide) were also found in apparently non-affected areas. This observation indicates a molecular change in the material, detectable prior to visually observable effects.

PEG formation. Within areas of high lipid adsorption also PEG modifications (Δ m/z 44 Da) were found (Fig. 5) on all PE-UHMW samples. The polymer distribution maxima were observed between m/z 1300 and 1500. GUR-1050 PE-UHMW incubated for 24 h in SF or BSF and explanted samples show large areas of PEG signals without distinct localization, whereas on Vitamin E doped samples PEG was only observed at regions correlating with lipid signals. Fragmentation analysis of the observed ions clearly identified the signal as PEG. PE-UHMW material was declared to be only PEG covered (vendor). Hence, PEG presence in deeper areas is difficult to explain. Based on the co-localization with lipids, it can be assumed that PEG is generated by the presence of oxidative species and PE-UHMW radicals in the aqueous environment (Fig. 1). As *in vivo* as well as shelf life oxidation have been reported for PE-

UHMW[41] it cannot be excluded that the laser energy works as a catalyst for PEG formation on exactly those previously modified PE-UHMW regions.

CONCLUSION

In the present study we demonstrate the possible application of MSI for material characterization of polymer based hip joint explants. The assumption that an interaction of the bio-compartment and PE-UHMW exists has been proven for GUR-1050, Vitamin E doped and explanted PE-UHMW samples by the presence of lipid residues. In the course of the study a sample preparation for MSI analysis of hydrophobic polymer surfaces was developed and analytes were identified by MS/MS analysis. All lipid classes relevant for the lubrication process were found and respective distributions were visualized by using characteristic fragment ions.

The combination of MSI and SEM analysis allowed for the first time the correlation of significantly modified PE-UHMW areas with lipid adsorption. Polymer modifications were identified to be PE-UHMW hydroperoxides and PEG.

3-dimensional reconstruction of acetabular cup areas investigated by MSI showed the relevance of MSI for even more profound material characterization and the possibility to combine it with state-of-the-art techniques like SEM, to obtain detailed information about the material failure process.

ASSOCIATED CONTENT

Supporting Information. Lipid identification; Time dependent cholesterol localization; This material is available free of charge via the Internet at http://pubs.acs.org.

Corresponding Author

*Martina Marchetti-Deschmann

Vienna University of Technology, Institute of Chemical Technologies and Analytics

Getreidemarkt 9/164AC, A-1060 Vienna, T: +43-1-58801-15162; F: +43-1-58801-915162

E: martina.marchetti-deschmann@tuwien.ac.at

Author Contributions

The manuscript was written through contributions of all authors. All authors have given approval to the final version of the manuscript.

Funding Sources

This project was supported by the Vienna University of Technology (Innovative Projects 2009/Chip-1000 and 2011/UltrafleXtreme) and the Austrian Federal Ministry for Transport, Innovation and Technology (FFG project 826132/GENIE).

ACKNOWLEDGMENT

We thank Dr. Sonia Walzer and Prof. Dr. Reinhard Windhager (Department of Orthopaedics, Medical University of Vienna) for providing HSF samples and helpful discussion and Dr. Thomas Koch (Institute of Materials Science and Technology, Vienna University of Technology) for kind assistance in SEM analysis. We further acknowledge the BMBS COST Action BM1104 (Mass Spectrometry Imaging: New Tools for Healthcare Research) for valuable discussions.

ABBREVIATIONS

BSF bovine synovial fluid, CHCA α-cyano-4-hdroxycinnamic acid, ddH_2O double distilled water, DHB 2,5-dihydroxybenzoic acid, HE-CID high energy collision induced dissociation, HP-TLC high performance thin layer chromatography, HSF human synovial fluid, ITO indium tin oxide, LPC Monoacylglycerophosphocholine, MALDI matrix assisted laser

desorption/ionization, MS mass spectrometry, MSI mass spectrometry imaging, PC Glycerophoshpatidylcholine, PE Glycerophosphatidylethanolamine, PEG polyethylene glycol, PI Glycerophosphatidylinositol, PS Glycerophosphatidylserine, PSD post source decay, RTOF reflector time of flight, SEM scanning electron microscopy, SF synovial fluid, SM Sphingomyelin, TG Triglyceride, THAP 1,4,6-trihydroxyacetophenone monohydrate, TOF time of flight, PE-UHMW ultra-high molecular weight polyethylene

REFERENCES

1. Eyerer, P.; Kurth, M.; McKellup, H. A.; Mittlmeier, T., Characterization of UHMWPE hip cups run on joint simulators. *J Biomed Mater Res* **1987,** *21* (3), 275-91.

2. Kurth, M.; Eyerer, P.; Ascherl, R.; Dittel, K.; Holz, U., An evaluation of retrieved UHMWPE hip joint cups. *J Biomater Appl* **1988,** *3* (1), 33-51.

3. Endo, M. M.; Barbour, P. S.; Barton, D. C.; Fisher, J.; Tipper, J. L.; Ingham, E.; Stone, M. H., Comparative wear and wear debris under three different counterface conditions of crosslinked and non-crosslinked ultra high molecular weight polyethylene. *Biomed Mater Eng* **2001,** *11* (1), 23-35.

4. Costa, L.; Luda, M. P.; Trossarelli, L.; Brach del Prever, E. M.; Crova, M.; Gallinaro, P., Oxidation in orthopaedic UHMWPE sterilized by gamma-radiation and ethylene oxide. *Biomaterials* **1998,** *19* (7-9), 659-68.

5. Kane, S. R.; Ashby, P. D.; Pruitt, L. A., Characterization and tribology of PEG-like coatings on UHMWPE for total hip replacements. *J Biomed Mater Res A* **2010,** *92* (4), 1500-9.

6. Del Prado, G.; Terriza, A.; Ortiz-Perez, A.; Molina-Manso, D.; Mahillo, I.; Yubero, F.; Puertolas, J. A.; Manrubia-Cobo, M.; Gomez Barrena, E.; Esteban, J., DLC coatings for UHMWPE: relationship between bacterial adherence and surface properties. *J Biomed Mater Res A* **2012,** *100* (10), 2813-20.

7. Esteban, J.; Molina-Manso, D.; Gomez-Barrena, E., Bacterial adherence to vitamin E UHMWPE. Considerations about in vitro studies. *J Orthop Res* **2012,** *30* (7), 1181: author reply 1181-2.

8. Roba, M.; Naka, M.; Gautier, E.; Spencer, N. D.; Crockett, R., The adsorption and lubrication behavior of synovial fluid proteins and glycoproteins on the bearing-surface materials of hip replacements. *Biomaterials* **2009,** *30* (11), 2072-8.

9. Serro, A. P.; Degiampietro, K.; Colaco, R.; Saramago, B., Adsorption of albumin and sodium hyaluronate on UHMWPE: a QCM-D and AFM study. *Colloids Surf B Biointerfaces* **2010,** *78* (1), 1-7.

10. Chen, C. P.; Hsu, C. C.; Yeh, W. L.; Lin, H. C.; Hsieh, S. Y.; Lin, S. C.; Chen, T. T.; Chen, M. J.; Tang, S. F., Optimizing human synovial fluid preparation for two-dimensional gel electrophoresis. *Proteome Sci* **2011,** *9*, 65.

11. Gobezie, R.; Kho, A.; Krastins, B.; Sarracino, D. A.; Thornhill, T. S.; Chase, M.; Millett, P. J.; Lee, D. M., High abundance synovial fluid proteome: distinct profiles in health and osteoarthritis. *Arthritis Res Ther* **2007,** *9* (2), R36.

12. Fröhlich S M, D. V., Archodoulaki V-M, Allmaier G, Marchetti-Deschmann M, Synovial Fluid Protein Adsorption on Artificial, Polymer-based Hip Joint Material Investigated by MALDI-TOF Mass Spectrometry Imaging. *EuPA Open Proteomics* **2014**.

13. Costa, L.; Bracco, P.; del Prever, E. B.; Luda, M. P.; Trossarelli, L., Analysis of products diffused into UHMWPE prosthetic components in vivo. *Biomaterials* **2001,** *22* (4), 307-15.

14. Bosetti, M.; Zanardi, L.; Bracco, P.; Costa, L.; Cannas, M., In vitro evaluation of the inflammatory activity of ultra-high molecular weight polyethylene. *Biomaterials* **2003,** *24* (8), 1419-26.

15. Reno, F.; Sabbatini, M.; Cannas, M., Surface oxidation of UHMWPE for orthopedic use increases apoptosis and necrosis in human granulocytes. *J Mater Sci Mater Med* **2003,** *14* (3), 241-5.

16. Rouser, G.; Yamamoto, A., Curvilinear regression course of human brain lipid composition changes with age. *Lipids* **1968,** *3* (3), 284-7.

17. Negre-Salvayre, A.; Auge, N.; Ayala, V.; Basaga, H.; Boada, J.; Brenke, R.; Chapple, S.; Cohen, G.; Feher, J.; Grune, T.; Lengyel, G.; Mann, G. E.; Pamplona, R.; Poli, G.; Portero-Otin, M.; Riahi, Y.; Salvayre, R.; Sasson, S.; Serrano, J.; Shamni, O.; Siems, W.; Siow, R. C.; Wiswedel, I.; Zarkovic, K.; Zarkovic, N., Pathological aspects of lipid peroxidation. *Free Radic Res* **2010,** *44* (10), 1125-71.

18. Hui, A. Y.; McCarty, W. J.; Masuda, K.; Firestein, G. S.; Sah, R. L., A systems biology approach to synovial joint lubrication in health, injury, and disease. *Wiley Interdiscip Rev Syst Biol Med* **2012,** *4* (1), 15-37.

19. Hills, B. A.; Crawford, R. W., Normal and prosthetic synovial joints are lubricated by surface-active phospholipid: a hypothesis. *J Arthroplasty* **2003,** *18* (4), 499-505.

20. Hills, B. A.; Butler, B. D., Surfactants identified in synovial fluid and their ability to act as boundary lubricants. *Ann Rheum Dis* **1984,** *43* (4), 641-8.

21. Nitzan, D. W., The process of lubrication impairment and its involvement in temporomandibular joint disc displacement: a theoretical concept. *J Oral Maxillofac Surg* **2001,** *59* (1), 36-45.

22. Amstalden van Hove, E. R.; Smith, D. F.; Heeren, R. M., A concise review of mass spectrometry imaging. *J Chromatogr A* **2010,** *1217* (25), 3946-54.

23. Neubert, P.; Walch, A., Current frontiers in clinical research application of MALDI imaging mass spectrometry. *Expert Rev Proteomics* **2013,** *10* (3), 259-73.

24. Murphy, R. C.; Merrill, A. H., Jr., Lipidomics and imaging mass spectrometry. *Biochim Biophys Acta* **2011,** *1811* (11), 635-6.

25. Spur, E. M.; Decelle, E. A.; Cheng, L. L., Metabolomic imaging of prostate cancer with magnetic resonance spectroscopy and mass spectrometry. *Eur J Nucl Med Mol Imaging* **2013,** *40 Suppl 1*, 60-71.

26. Krueger, K.; Terne, C.; Werner, C.; Freudenberg, U.; Jankowski, V.; Zidek, W.; Jankowski, J., Characterization of polymer membranes by MALDI mass-spectrometric imaging techniques. *Anal Chem* **2013,** *85* (10), 4998-5004.

27. Moree, W. J.; Yang, J. Y.; Zhao, X.; Liu, W. T.; Aparicio, M.; Atencio, L.; Ballesteros, J.; Sanchez, J.; Gavilan, R. G.; Gutierrez, M.; Dorrestein, P. C., Imaging Mass Spectrometry of a Coral Microbe Interaction with Fungi. *J Chem Ecol* **2013**.

28. Francese, S.; Bradshaw, R.; Ferguson, L. S.; Wolstenholme, R.; Clench, M. R.; Bleay, S., Beyond the ridge pattern: multi-informative analysis of latent fingermarks by MALDI mass spectrometry. *Analyst* **2013,** *138* (15), 4215-28.

29. Gabler, C.; Pittenauer, E.; Dorr, N.; Allmaier, G., Imaging of a tribolayer formed from ionic liquids by laser desorption/ionization-reflectron time-of-flight mass spectrometry. *Analytical chemistry* **2012,** *84* (24), 10708-14.

30. Goodwin, R. J., Sample preparation for mass spectrometry imaging: small mistakes can lead to big consequences. *J Proteomics* **2012,** *75* (16), 4893-911.

31. Sloane, A. J.; Duff, J. L.; Wilson, N. L.; Gandhi, P. S.; Hill, C. J.; Hopwood, F. G.; Smith, P. E.; Thomas, M. L.; Cole, R. A.; Packer, N. H.; Breen, E. J.; Cooley, P. W.; Wallace, D. B.; Williams, K. L.; Gooley, A. A., High throughput peptide mass fingerprinting and protein macroarray analysis using chemical printing strategies. *Mol Cell Proteomics* **2002,** *1* (7), 490-9.

32. Stubiger, G.; Pittenauer, E.; Belgacem, O.; Rehulka, P.; Widhalm, K.; Allmaier, G., Analysis of human plasma lipids and soybean lecithin by means of high-performance thin-layer chromatography and matrix-assisted laser desorption/ionization mass spectrometry. *Rapid Commun Mass Spectrom* **2009,** *23* (17), 2711-23.

33. Fuchs, B.; Schiller, J.; Suss, R.; Zscharnack, M.; Bader, A.; Muller, P.; Schurenberg, M.; Becker, M.; Suckau, D., Analysis of stem cell lipids by offline HPTLC-MALDI-TOF MS. *Anal Bioanal Chem* **2008,** *392* (5), 849-60.

34. Bole, G. G., Synovial fluid lipids in normal individuals and patients with rheumatoid arthritis. *Arthritis Rheum* **1962,** *5*, 589-601.

35. Kosinska, M. K.; Liebisch, G.; Lochnit, G.; Wilhelm, J.; Klein, H.; Kaesser, U.; Lasczkowski, G.; Rickert, M.; Schmitz, G.; Steinmeyer, J., A Lipidomic study of phospholipid classes and species in human synovial fluid. *Arthritis Rheum* **2013**.

36. Kellner-Weibel, G.; Yancey, P. G.; Jerome, W. G.; Walser, T.; Mason, R. P.; Phillips, M. C.; Rothblat, G. H., Crystallization of free cholesterol in model macrophage foam cells. *Arteriosclerosis, thrombosis, and vascular biology* **1999,** *19* (8), 1891-8.

37. Rocha M, M. A., Mansur H, Characterization and Accelerated Ageing of UHMWPE Used in Orthopedic Prosthesis by Peroxide. *materials* **2009,** *2*, 562-576.

38. Bell, J.; Tipper, J. L.; Ingham, E.; Stone, M. H.; Fisher, J., The influence of phospholipid concentration in protein-containing lubricants on the wear of ultra-high molecular weight polyethylene in artificial hip joints. *Proc Inst Mech Eng H* **2001,** *215* (2), 259-63.

39. O'Neill, P., Birkinshaw, C., Leahy, J.J., Buggy, M., Ashida, T., The distribution of oxidation products in irradiated ultra-high molecular weight polyethylene. *Polymer Degradation and Stability* **1995,** *49*, 239-244.

40. Costa, L.; Luda, M. P.; Trossarelli, L.; Brach del Prever, E. M.; Crova, M.; Gallinaro, P., In vivo UHMWPE biodegradation of retrieved prosthesis. *Biomaterials* **1998,** *19* (15), 1371-85.

41. Kurtz, S. M.; Siskey, R. L.; Dumbleton, J., Accelerated aqueous aging simulation of in vivo oxidation for gamma-sterilized UHMWPE. *J Biomed Mater Res B Appl Biomater* **2009,** *90* (1), 368-72.

TOC

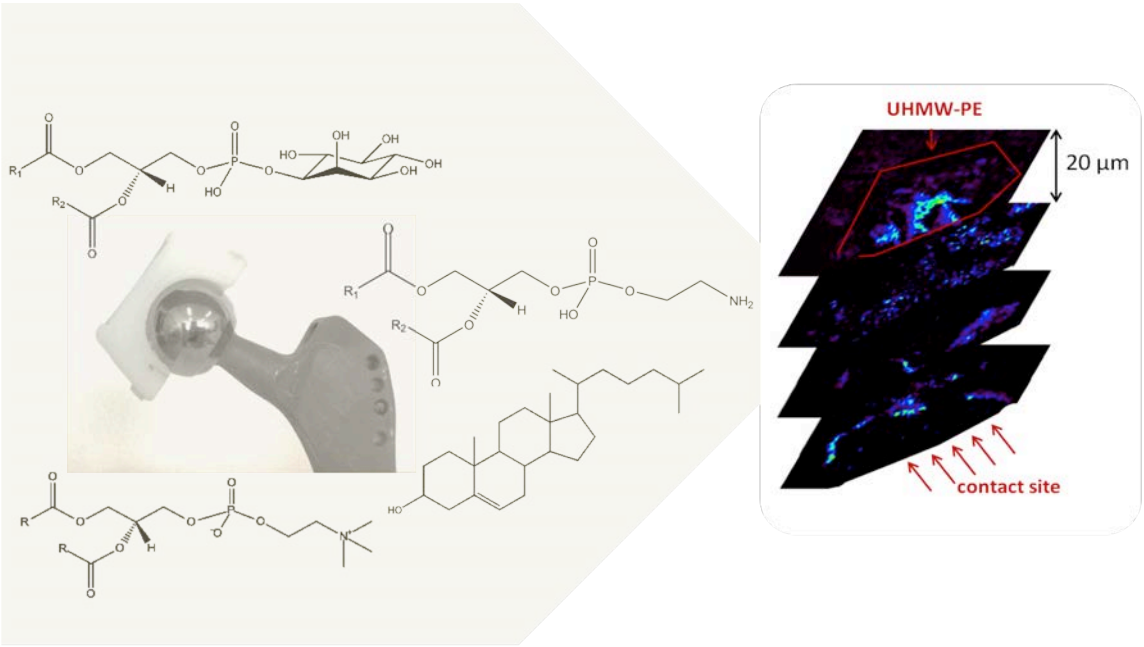

Supplemental Material

Figure 1: Cholesterol localization after incubation in SF (b) 15 min (c) 1 h (d) 24 h visualized by Biomap (Novartis, Zuerich, Switzerland); (e) Characteristic fragment ions for cholesterol $[M-H_2O+H]^+$, (f) minor fragmentation products; (g) MALDI-TOF-RTOF spectrum of cholesterol after PSD fragmentation

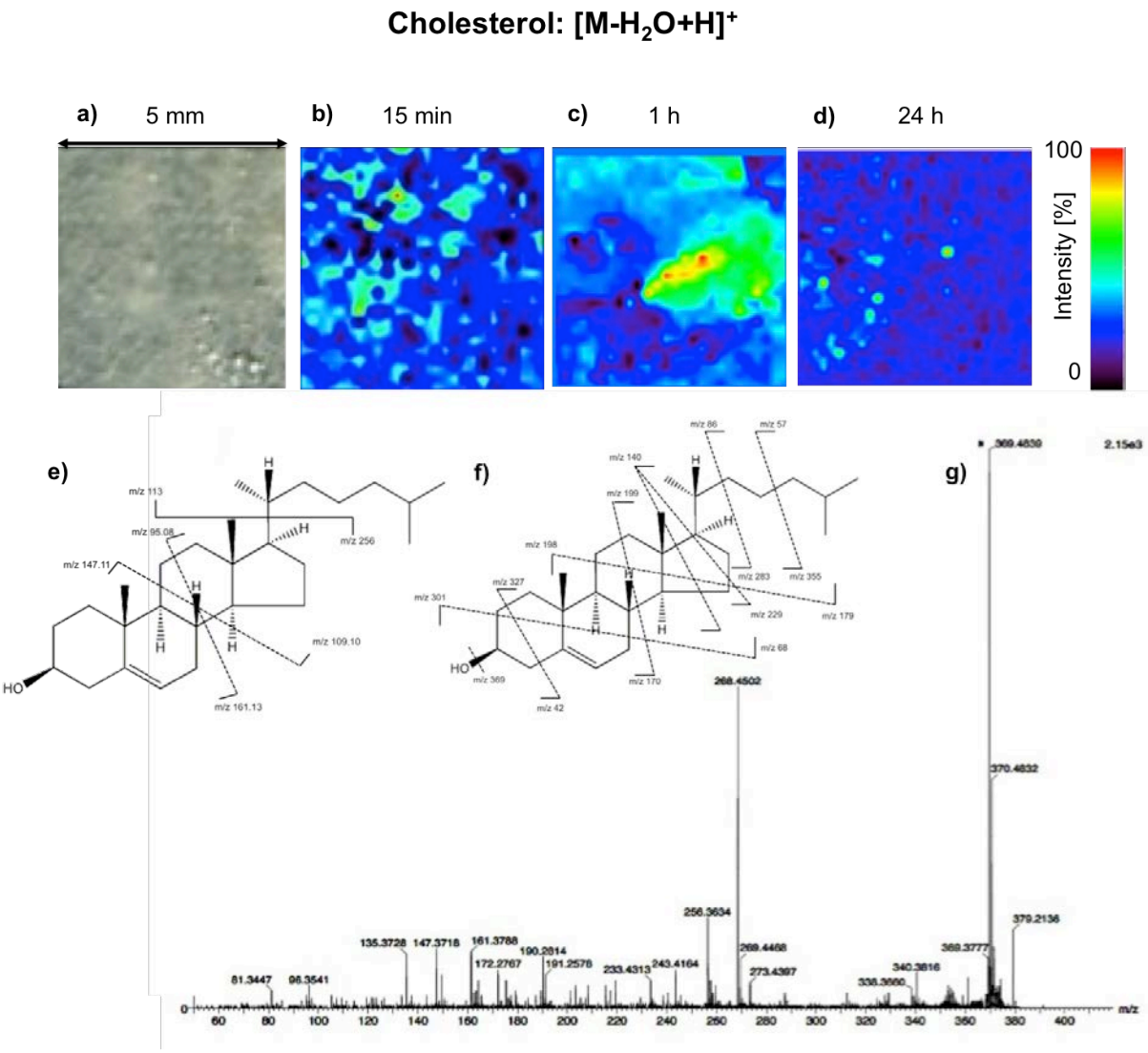

Identification of lipid species present on 1050, Vitamin E doped and explanted UHWM-PE samples, based on their characteristic fragment ions

Figure 2: Characteristic fragmentation ions and neutral losses for LPC, SM and PC; Identified lipid species are listed.

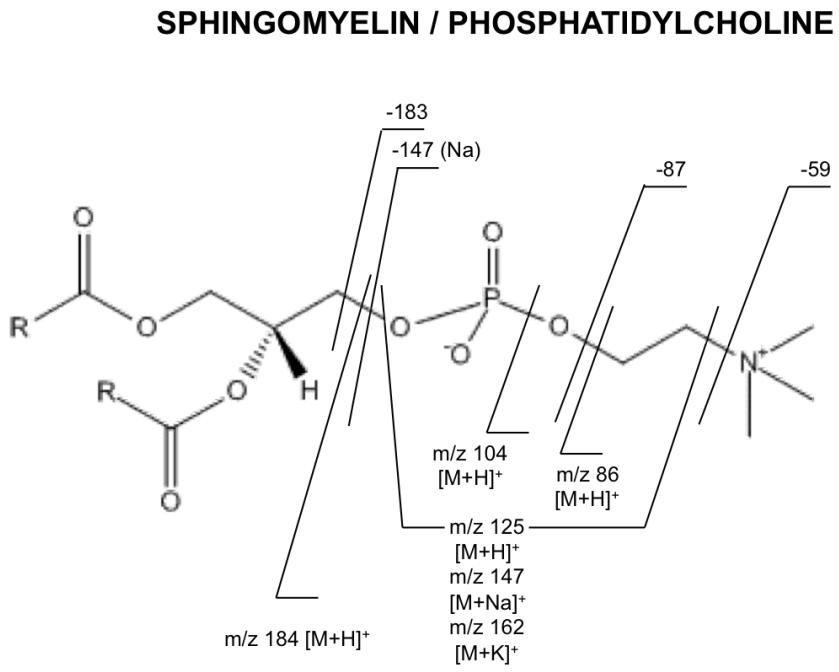

LPC	SM	PC
16:0	34:2	18:0/9:0
18:0	34:1	18:0/20:2
18:1	d18:0/13:0	15:1/20:4
18:2	d18:1/12:0	18:0/9:0
	36:1	20:4/15:1
	36:2	20:2/18:0
	38:1	32:0
	38:2	34:1
	40:1	34:2
	40:2	36:1
	42:1	36:2
	42:2	36:3
	42:3	36:4
	d18:1/16:0	38:3
	d18:1/15:0	38:4
	d18:1/18:1	38:5
	d18:1/18:0	38:6
	d18:1/20:1	40:6
	d18:1/20:0	18:0/18:2
	d18:0/20:0	16:0/16:0
	d18:1/22:1	16:0/18:2
	d18:1/22:0	16:0/18:1
	d18:2/24:1	18:2/18:2
	d18:1/24:1	18:1/18:2
		18:1/18:1
		18:1/18:0
		18:2/20:4
		18:1/20:4
		18:0/20:4

Figure 3: Characteristic fragmentation ions and neutral losses for PE; Identified lipid species are listed.

PHOSPHATIDYLETHANOLAMINE

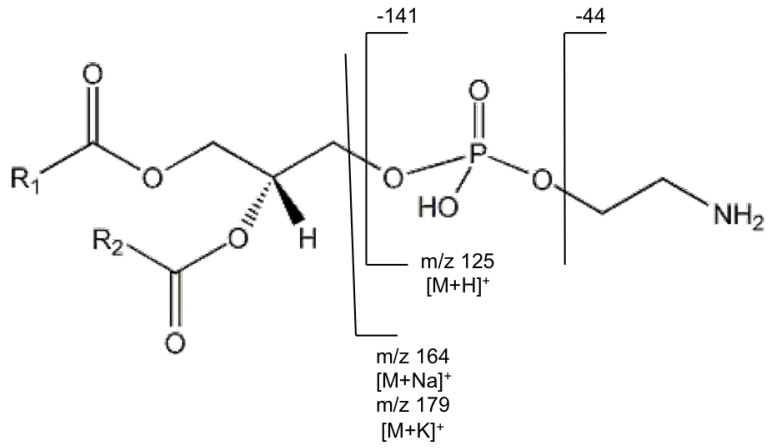

PE
18:2
16:0
20:2
14:0/23:1
18:2
23:1/14:0
16:0p/18:1
16:0p/20:4
18:0/18:0
18:0/18:1
18:0/20:4
18:0p/20:4
36:1p
36:2
36:2p
36:3p
38:5p
18:0/18:2
18:3/18:3
18:2/18:3
18:2/18:2
18:1/18:2
18:0/18:2
18:0/18:0
p18:0/20:4
18:2/20:4

Figure 4: Characteristic fragmentation ions and neutral losses for PI; Identified lipid species are listed.

PHOSPHATIDYLINOSITOL

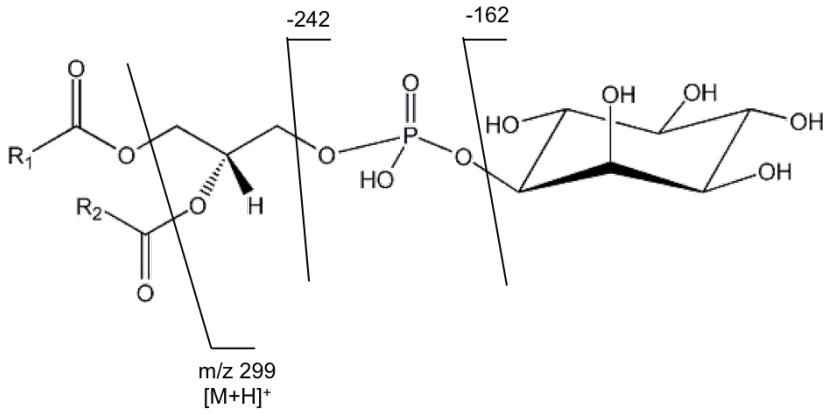

PI
34:1
18:1/18:1
18:0/20:4
18:0/18:1

Figure 5: Characteristic fragmentation ions and neutral losses for PS; Identified lipid species are listed.

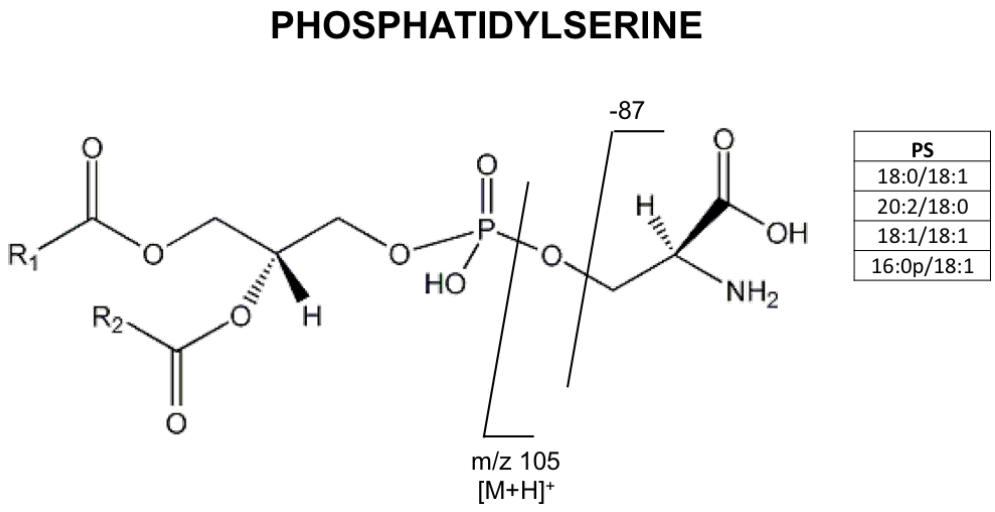

Figure 6: SM and PC distribution on smooth PE-UHMW surface after 24 h SF incubation visualized by Biomap (Novartis).

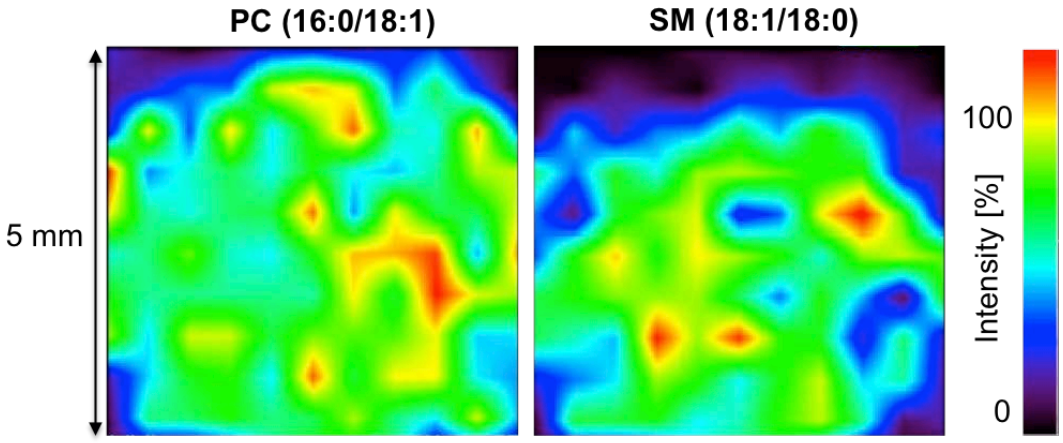

9. Additional Findings

a. Feasibility study to investigate biodegradable graft material used for artificial blood vessel replacement by mass spectrometry imaging

In contrary to polymer based hip joint replacement systems, artificial blood vessels are used to replace the native vessel in first instance, however to further induce cell growth and the formation of a new blood vessel along with replacement of the polymer. Biodegradable polymer grafts were analyzed by the developed approach for non-degradable UHMWPE analysis to obtain information about the protein and lipid adsorption/diffusion process, which can often be correlated with polymer modifications. Adapted approaches regarding sample preparation are required as a consequence of the different stability properties.

MATERIALS & METHODS

All chemicals and reagents, unless indicated specifically, were from Sigma-Aldrich (USA) with a purity of at least 99 % if not stated otherwise. Double distilled water (ddH_2O) was obtained from a Simplicity system (Millipore, USA) with a specific conductivity of $\Omega_m \leq 18$ S/cm. Grafts were synthesized at the Institute of Applied Synthesis (Vienna University of Technology, Austria) and along with native aorta and rat blood, provided by the Institute of Biomedical Research (Medical University Vienna, Austria). Blood samples and native aorta were taken from rats after explant surgery.

Graft samples were analyzed concerning their lipid and protein interaction after 10 minutes and 7 days *in vivo*, followed by mass spectrometry imaging (MSI) analysis. All samples were cut to 25 mm^2 and washed with double distilled water (ddH_2O) before analysis.

Graft material is further referred to as EG for hard-block biodegradable thermoplastic polyurethane material and ePTFE for expanded polytetrafluoroethylene.

For lipid extraction samples were incubated in 900 µL chloroform/methanol (2:1, v/v) at 22 °C for 1 hour. 900 µL chloroform/water (1:1, v/v) were added before centrifugation at 3000 rpm at 22 °C for 15 min. The organic phase was collected and dried under vacuum. The residues were re-dissolved in chloroform and applied to Silica gel 60 HP-TLC aluminum plates (10 x 10 cm, layer thickness 0.2 mm, particle size 3-4 µm, Merck) using a syringe. HP-TLC separation was performed as previously described [1] followed by identification on a MALDI-TOF/TOF instrument (UltrafleXtreme, Bruker) based on collision-induced dissociation. For protein extraction samples were incubated in ddH_2O/trichloracetic acid (12:1, v/w) at 4 °C for 30 min and centrifuged at 14000 rpm and 4 °C for another 30 min. The pellet was dissolved in 10 µL ddH_2O and incubated in SDS-PAGE sample buffer (106 mM Tris HCl, 141 mM Tris Base, 2 % lithium dodecyl sulfate, 10 % glycerol, 0.51 mM EDTA, 0.22 mM SERVA Blue G250, 0.175 mM Phenol Red, pH 8.5, 50mM dithiothreitol, Life Technology, Vienna, Austria) at 95 °C for 5 minutes. SDS-PAGE analysis was performed on a 10 cm ready-made 4-12 % separating polyacrylamide gel (Life Technology, Austria). Electrophoresis was carried out at max. 125 V, 60 mA and 12.5 W in a XCell Sure Lock System (Life Technology). Gels were silver stained [2] for protein detection. Proteins were identified after SDS-PAGE by *in-gel* digestion. Gel bands were excised with a clean scalpel and destained using 100 mM $Na_2S_2O_3$ and 30 mM $K_4Fe(CN)_6{}^{*}3H_2O$ (1:1, v/v). Gel pieces were treated with ACN and rehydrated with 100 mM NH_4HCO_3. After reduction (10 mM DTT in 100 mM NH_4HCO_3) and alkylation (50 mM iodoacetamide in 100 mM NH_4HCO_3) the gel pieces were dried in a vacuum centrifuge and rehydrated in approx. 10 µL 50 mM NH_4HCO_3 (pH 8.5)

containing 5 % ACN and 125 ng trypsin (porcine, proteomics grade, Roche, Switzerland). Digestion was carried out for 24 h at 37 °C. Peptides were extracted with 50 mM NH_4HCO_3/ACN (1/1, v/v) and two times with ddH_2O/ACN containing 0.1 % TFA (1/1, v/v), for 15 min each. All extracts of one respective spot were pooled and dried in a vacuum centrifuge. After reconstitution in 0.1 % TFA peptides were desalted using C_{18} ZipTips (Millipore, USA) and eluted with 5 mg/mL CHCA prepared in ACN/0.1 %TFA (50/50, v/v) in the final step. Peptide mass fingerprinting (PMF) and sequence tag analysis were carried out on a MALDI-TOF/RTOF instrument (UltrafleXtreme). For MSI, graft samples were mounted planar on indium tin oxide coated target slides (Bruker) using conductive tape (Shimadzu Kratos Analytical). α-cyano-4-hydroxycinnamic acid and sinapic acid mixtures (1:3 and 1:1) in acetone/ddH_2O/TFA (70/30/0.1, v/v/v) were applied using an airbrush device (Conrad Electronics, Germany). Samples were analyzed on the mass spectrometer described above at a lateral resolution of 15 and 60 µm. MSI analysis was visualized with FlexAnalysis (Bruker) applying median normalization.

RESULTS & DISCUSSION

Lipid analysis revealed that all relevant plasma lipid classes (lyso-phosphatidylcholine, sphingomyelin, phosphatidylcholine, phosphatidylserine, phosphatidylinositol, phosphatidylethanolamine, triglycerides, cholesterol and ceramides) present in blood did in fact adsorb on all types of polymer material. For EG enhanced cholesterol adsorption was observed and both polymer types showed extensive glycolipid adsorption. However, no significant time-related difference was detected (Fig. 1a).

SDS-PAGE revealed extensive protein adsorption after 10 minutes *in vivo*, which was not observed after 7 days (Fig. 1a). Both materials showed similar protein patterns in gel electrophoretic separation and major blood components were identified: hemoglobin subunits, immunglobuline classes, apo-lipoproteins classes, proteins related to muscle growth and endothelial formation, albumin, myosin and several other proteins (see Chapter 9.b).

Despite significantly different graft properties, a reproducible and identical sample preparation method could be developed for MSI. Spatially highly resolved analyte distributions were measured. Lipid detection was successful for the mass range covering cholesterol, major phospholipid classes (Fig. 1b) and glycolipids. Extensive lipid clusters could be detected on the inside of both graft materials, which were not detected on the outside. This might indicate enhanced interaction inside the vascular prosthesis and proves the capacity of MSI experiments to give information on degradation and layer formation processes. Besides lipids also proteins in the mass range from 2 to 70 kDa could be detected and localized. Areas of homogeneous layer formation were observed, where clustering groups, e.g. lipid species and protein groups, have to be further evaluated concerning their biological functionality.

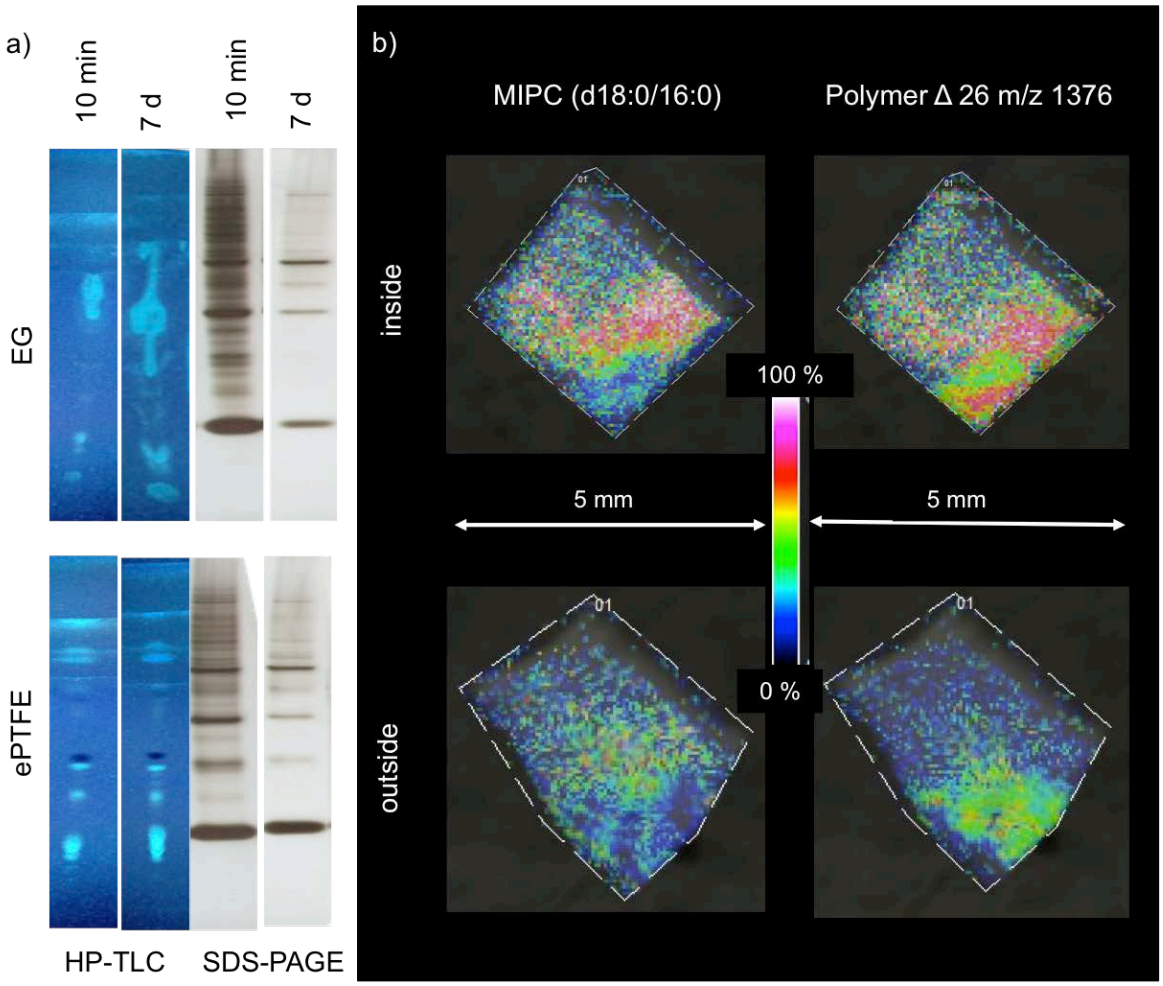

Figure 1: a) Comparison of two different graft materials (EG and ePTFE) regarding the lipidomic (HP-TLC) and proteomic pattern (1D gel electrophoresis, SDS-PAGE) after 10 minutes and 7 days *in vivo* b) MSI results of the inner and outer surface of a graft sample; the ceramide phospholipid MIPC(d18:0/16:0) (N-(hexadecanoyl)-sphinganine-1-O-[D-mannopyranosyl-α1-2-myo-inositol-1-phosphate]) and a polymer related signal were chosen for visualization of respective intensity distributions (intensity values correspond to the color bar)

1. Stubiger, G., E. Pittenauer, et al. (2009). "Analysis of human plasma lipids and soybean lecithin by means of high-performance thin-layer chromatography and matrix-assisted laser desorption/ionization mass spectrometry." Rapid communications in mass spectrometry : RCM **23**(17): 2711-2723.

2. Shevchenko, A., M. Wilm, et al. (1996). "Mass spectrometric sequencing of proteins silver-stained polyacrylamide gels." Analytical chemistry **68**(5): 850-858.

Some results are used in the manuscript (submitted to Acta Biomaterialia, 04. 2014): ***Biodegradable, Thermoplastic Polyurethane Grafts For Small Diameter Vascular Replacement*** (Helga Bergmeister, Nargiz Seyidova, Catharina Schreiber, Magdalena Strobl, Christian Grasl, Ingrid Walter, Barbara Messner, Stefan Baudis, Sophie Fröhlich, Martina Marchetti-Deschmann, Markus Griesser, Matt di Franco, Martin Krssak, Robert Liska, Heinrich Schima)

b. Analytical investigations for biodegradable graft material used for artificial blood vessel replacement

Based on initial experiments it is assumed that biological adsorption starts with small apolar lipids (cholesterol and other sterols), followed by subsequent adsorption and polar lipid layer formation exhibiting saturated and unsaturated acyl side chains (glycerophospholipids, sphingomyelins), leading consequently to enhanced adsorption of proteins and the formation of a glycan-layer.

MATERIALS & METHODS

Materials: All chemicals and reagents, unless indicated specifically, were from Sigma-Aldrich (USA) with a purity of at least 99 % if not stated otherwise. Double distilled water (ddH_2O) was obtained from a Simplicity system (Millipore, USA) with a specific conductivity of $\Omega_m \leq 18$ S/cm. Grafts were synthesized at the Institute of Applied Synthesis (Vienna University of Technology, Austria) and along with native aorta and rat blood, provided by the Institute of Biomedical Research (Medical University Vienna, Austria). Blood samples and native aorta were taken from rats after explant surgery.

MS profiling and MSI analysis: samples were attached on indium tin coated (ITO) glass slides using conductive tape (Fig. 2). The sized grafts were flattened using wetted lint free tissue and vacuum dried. For cross section analysis explanted graft materials were stabilized in optimal cutting temperature (O.C.T. TissueTek) embedding medium and sliced to 10 µm using a microtome (Reichert-Jung). All samples were further washed using 0.1 % TFA and again vacuum dried. For protein analysis sinapic acid and ferulic acid were mixed 1:1 to obtain a saturated matrix solution in acetonitril/methanol (7/3, v/v) containing 0.1 % TFA. For MS and MSI experiments investigating proteins, standard MALDI matrices, SA and FA were dissolved 1:1 in acetonitrile (ACN), ethanol (v/v) containing 0.1 % TFA (6/3/1, v/v/v) at a concentration of 25 (SA) and 20 (FA) mg/mL. Lipid analysis was performed using saturated 2,4,6-trihydroxacetophenone in potassium chloride saturated methanol. Matrix deposition was performed using an airbrush device (Conrad), at a working distance of 10 to 12 cm with an approximate angle of 50 to 60°, covering the sample in several iterative steps. MS profiling and MSI experiments were performed on a MALDI-TOF/RTOF instrument (UltrafleXtreme, Bruker) in positive linear or reflectron mode, equipped with a SmartBeam™ laser pulsed at 2000 Hz. At a spatial resolution of 7 to 130 µm, mass spectra based on 1000 (lipids) or 2000 (proteins) single laser shots were acquired per position over an average sample size of 25 mm^2 for all samples (approx. 15 × 8 mm) if not otherwise stated. For image reconstruction FlexImaging v. 3.0 software (Bruker Daltonics) was used. All MSI data sets are presented as Median normalized but were also verified for outliers and artifacts by Route Mean Square and Total Ion Current normalization.

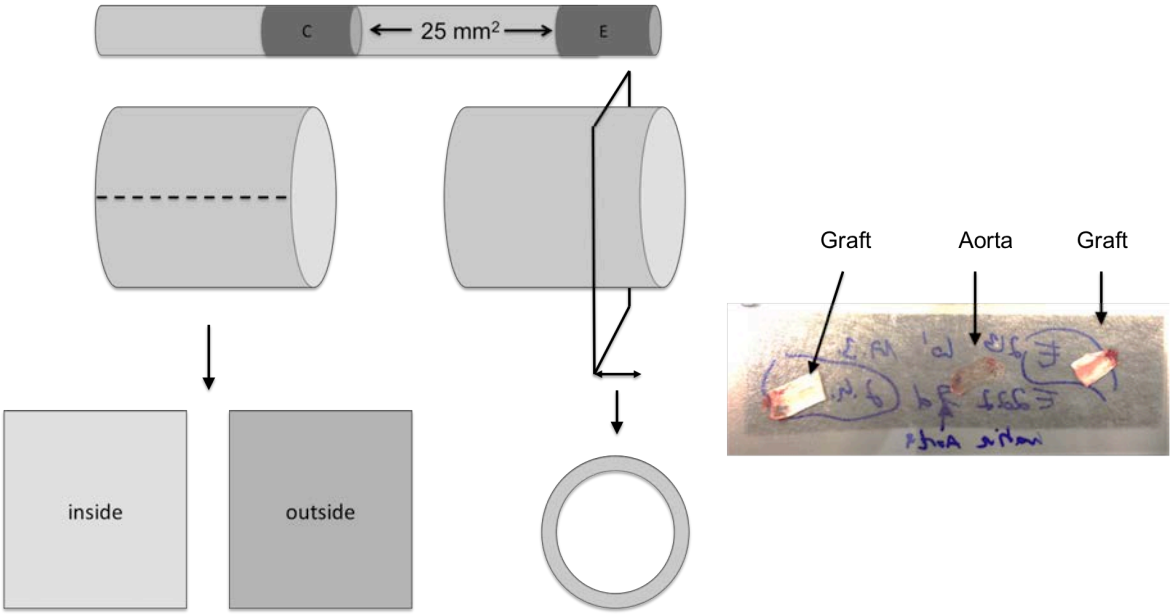

Figure 2: Protein and lipid adsorption for artificial blood vessels were investigated; Samples were cut and MSI analysis was approached either on the inner or outer surface of centroid (C) or edge (E) regions or at the cross-section; For MSI analysis grafts were mounted on ITO targets using double sided conductive tape.

Lipid analysis: For lipid extraction from explant material 4 mm graf material was incubated in 900 µL chloroform/methanol (2:1, v/v) for 1 hour at room temperature. 900 µL chloroform/water (1:1, v/v) were added before centrifugation at 3000 rpm and room temperature for 15 min. The organic phase (lower solvent layer) was collected and the solvent evaporated under vacuum. As reference, 20 µL blood from rat blood and rat aorta were treated as described above. For further analysis dried lipids were dissolved in 15 µL chloroform. Lipid separation was conducted by HP-TLC analysis. 8 µL chloroform extract were applied to the Silica gel 60 HP-TLC aluminum plates (10 x 10 cm, layer thickness 0.2 mm, particle size 3-4 µm, (Merck) using a syringe. HP-TLC separation was performed using two-different separations in the same dimension. First Separation: 65 % of the sample-loaded plate was developed with solvent system A (methyl acetate/1-propanol/chloroform/methanol/ aqueous saturated potassium chloride, 25/25/25/10/0.5, v/v/v/v/v) to separate glycolipids from phospholipids. The HP-TLC plates were dried using a heat gun to remove the mobile phase before further development. Second Separation: 95 % of the plate was developed in solvent system B (toluene/diethyl ether/ethanol/acetic acid, 60/40/1/0.05, v/v/v/v) for neutral lipid separation. For lipid visualization HP-TLC plates were stained with 0.05 % primuline in acetone/water (8/2, v/v) and lipid spots were detected at 337 nm. For matrix assisted laser desorption/ionization time-of-flight mass spectrometry (MALDI-TOF-MS) analysis 2,4,6-trihydroxyactophenone (THAP) dissolved in KCl saturated methanol. Lipid sample and matrix solution were mixed 1/1 and 1 µL was deposited on a polished 384-well stainless steel microtiter plate target (Bruker, Germany). MALDI MS spectra were acquired on an intermediate pressure MALDI-qTOF instrument (Synapt G2, Waters, UK), equipped with a 1000 Hz Nd:YAG laser (355 nm) and an ion mobility cell and on a high vacuum MALDI-TOF/TOF instrument (UltrafleXtreme, Bruker, Germany), equipped with a 2000 Hz Smartbeam laser (355 nm) in the positive linear and reflectron detection mode. For MALDI-TOF-MS analysis directly from HP-TLC plates, the developed plate was mounted on a TLC adapter (Bruker) and THAP (20 mg/ml) in acetone was deposited with a pipette on the identified areas of lipid spots. Spectra acquisition was again performed on the MALDI-TOF/TOF instrument.

Protein analysis: For protein extraction 4 mm graft material was deposited in 1200 µL ddH_2O before 100 µL trichloracetic acid (20% in ddH_2O) were added 5 times subsequently after vortexing thoroughly in-between. Samples were incubated for 30 min at 4 °C and centrifuged at 14000 rpm and 4 °C for another 30 min. The VP material was removed, the supernatant discarded and the pellet re-dissolved in 10 µL ddH_2O. Protein concentration was determined according to Bradford [1]. For SDS-PAGE analysis protein pellets were dissolved in lithium dodecyl sulfate sample buffer (26.5 mM Tris HCl, 35.25 mM Tris Base, 0.5 % lithium dodecyl sulfate, 2.5 % glycerol, 0.1275 mM EDTA, 0.055 mM SERVA Blue G250, 0.044 mM Phenol Red, pH 8.5, 50 mM dithiothreitol) at 95 °C for 5 minutes and applied to a precast NuPAGE 4-12 % Bis-Tris polyacrylamide gel (Life Technology, USA). Electrophoresis was conducted at 125 V (60 mA max., 12.5 W) in a XCell Surelock Mini Cell electrophoresis system (Life Technology, USA). Protein identification was performed as described in 9.a. For all enzymatic digestion data, autolytic tryptic products, keratin and blank artifacts were assigned and removed before database search (SWISSPROT, Jan. 2014) using Mascot [3] with the following parameters: taxonomy *Rattus norvegicus*, monoisotopic mass values, peptide mass tolerance of ±0.3 Da (for PMF and PSD experiments), 2 missed cleavages, a fixed modification carboxyamidomethylation and methionine oxidations set as variable modification.

RESULTS & DISCUSSION

Lipid analysis

HP-TLC separation to compare the biological system (aorta and blood) with lipids adsorbed on the implanted graft material depending on the *in vivo* time was studied. Lipids have not been quantified after extraction and before separation, however the comparable graft dimension was taken for extraction.

HP-TLC analysis (Fig. 3) revealed the presence of all biological relevant lipid classes: glycerophosphatidylcholine (PC), lyso-phosphatidylcholine (LPC), sphingomyelin (SM), glycerophosphatidylserine (PS), glycerophosphatidylinositol (PI), glycerophosphatidylethanolamine (PE), cholesterol, triglycerides, ceramides and several unspecified apolar glycolipids.

Compared to the native state, represented by blood and aorta tissue, ePTFE revealed a very similar lipid pattern after 10 minutes of incubation. By comparison EG already showed extensive cholesterol traces (marked with *) and substances, which were not dissolved in the solvent and remained at the application point. Those are assumed to be very polar lipid species, which are not transported by the apolar liquid phase. For EG the lipid pattern after 7 d *in situ*, no obvious pattern change could be estimated, which is however difficult to conduct due to the extensive overload with cholesterol. For ePTFE on the contrary an increased amount of cholesterol and also phospholipids, especially PE and PI was observed.

Concerning EG, the presence of high amounts of glycolipids is interesting. This finding correlates nicely with the assumed glycolayer formation on the material increasing hydrophilic properties and consequently protein adsorption [4]. It is also expected that this type of lipid is eventually relevant for the change of blood flow parameters and shear forces depending on to glycosylation. Cholesterol is very dominant in EG samples. In polymers, not supposed to degrade or be replaced over time, this is assumed to open the polymer matrix slightly, enhancing lipid diffusion and furthermore protein adsorption [5]. If this finding is hypothesized to be similar to the biological interaction of cholesterol

with the prosthesis it can be assumed that cholesterol is a starting point for the prosthesis replacement by blood vessels.

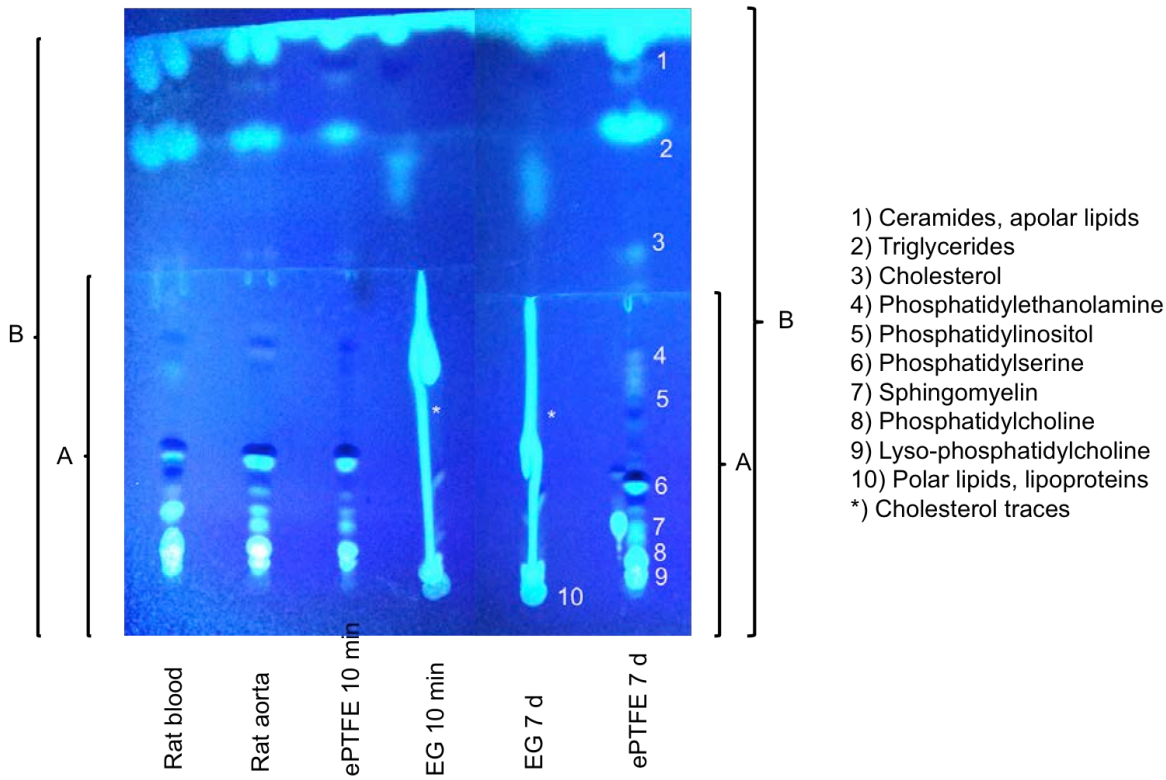

Figure 3: Lipid extracts from aorta, blood and graft material separated by HP-TLC separation developed with 2 solvent systems.

For all samples, enough material was available to analyze two different regions of the prosthesis with respect to the lipid profile: one sample was taken from the center region of the VP and one from the direct vessel contact side (edge region (Fig. 2)). Lipid pattern comparison revealed no significant differences (data not shown); however the cholesterol level was slightly higher in the center region. Further lipid quantification is necessary to address the significance of this finding.

For exemplary identification lipid extracts from the TLC plate were analyzed to determine the head group and reveal possible insight in acyl chain length distribution. Table 1 shows a list of lipids, which were chosen due to their dominant distribution pattern by MSI, identified from lipid extracts based on MALDI-TOF/RTOF analysis and PSD fragmentation.

Table 1: Exemplary identified lipid species from lipid extracts of graft material.

m/z	Species	Common name	Systematic name
641.4	**neutral glycosphingolipid**		N-(hexadecanoyl)-1-β-glucosyl-4E,6E-tetradecasphingadienine
679.4	**diacylglycerophosphoserine**	PS(14:0/14:0)	1,2-ditetradecanoyl-sn-glycero-3-phosphoserine
711.5	**glycerophosphocholine**		PC(13:0/18:4(6Z,9Z,12Z,15Z))
737.5	**glycerophosphocholine**	PC (18:4/P-16:0)	
759.5	**glycerophosphocholine**	PC (16:0/18:1)	PC (16:0/18:1)
787.6	**glycerophosphocholine**	PC (18:0/18:1)	PC (18:0/18:1)
771.5	**glycerophosphocholine**	PC (13:0/22:0(13Z,16Z)	1-tridecanoyl-2-(1Z,16Z-docosadienoyl)-glycero-3-phosphocholine
943.5	**ceramide phosphoinositol**	MIPC(d18:0/16:0)	N-(hexadecanoyl)-sphinganine-1-O-[D-mannopyranosyl-α1-2-myo-inositol-1-phosphate]
981.7	**ceramide phosphoinositol**	PI-Cer(t20:0/26:0(2OH))	N-(2-hydroxyhexacosanoyl)-4R-hydroxyeicosasphinganine-1-phospho-(1'-myo-
1493,9	**acidic glycosphingolipid**		GalNAcβ1-4(NeuAcα2-3)Galβ1-4Glcβ-Cer(d18:1/26:1(17Z))
1517.8	**acidic glycosphingolipid**	dCer(18:1/16:0)	

For polymer samples, ion mobility separation proved useful for identification of polymer degradation products, relevant in the materials failure process and was successfully applied to graft material (Fig. 4). However deeper and more detailed investigations are necessary to correctly interpret data.

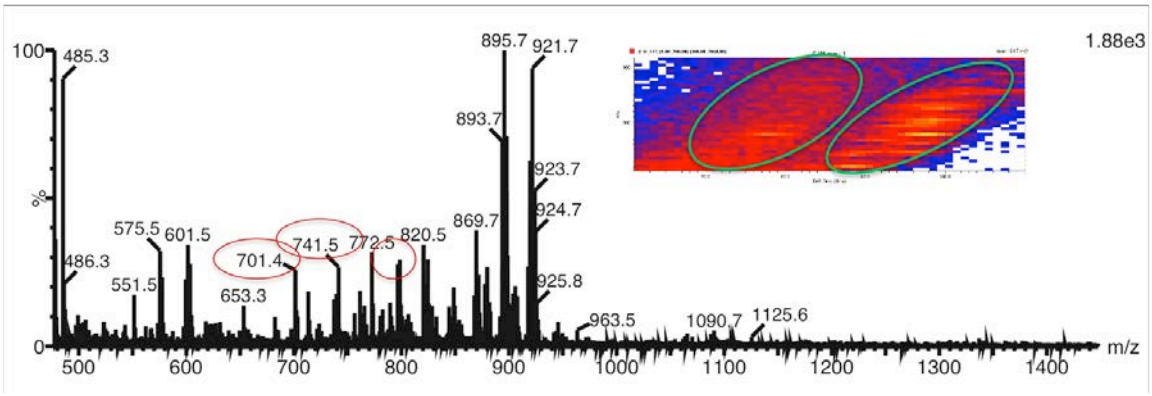

Figure 4: Feasibility study of ion mobility separation for lipid and polymer analysis of graft materials.

Results - protein analysis

SDS-PAGE analysis was chosen to obtain further insight into protein adsorption on different graft materials after 10 min and 7 d *in vivo*. As described for lipid analysis, exactly the same graft dimensions were chosen for protein extraction and compared to protein components present in rat blood. 8 replicates were analyzed for each time point and material, revealing significant variations regarding protein pattern and concentration (Fig. 5). However, it was observed that after 7 d *in situ*, protein concentration has decreased and high abundant proteins were dominant. For one ePTFE sample after 7 d *in vivo*, IgG components were detected with high abundance.

Major identified components are hemoglobin, albumin, fibrinogen, actin and myosin. It has been shown by SDS-PAGE that especially proteins with an apparent molecular weight below 100 kDa adsorb at higher quantities (more intensive staining) on the material. Further identified proteins are listed in Table 2. However, due to the high number of detected proteins, 2D gel electrophoresis is highly recommended for further identification and valid comparison of the polymers as well as the VP regions. An alternative approach is protein identification by LC-MS analysis after in gel digestion instead of MALDI-TOF/TOF, which usually increases the number of significant identifications.

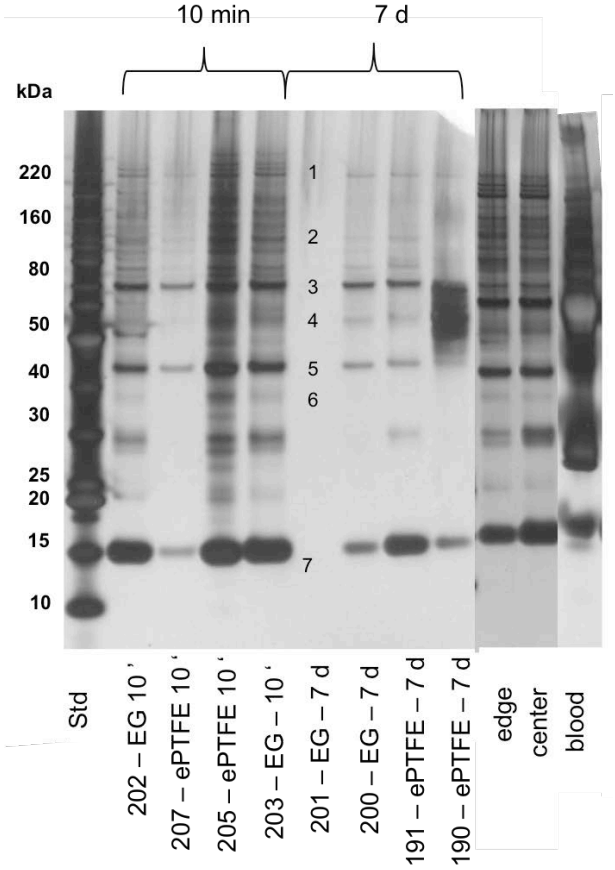

Figure 5: SDS-PAGE separation of protein extracts from different graft material and rat blood.

SDS-PAGE pattern comparison of the center and vessel contract region of the stent revealed extensive protein adsorption in the center of the VP, in all extracts (Fig. 5).

Table 2: Proteins identified from in-gel digestion after SDS-PAGE separation of protein extracts from graft material; Proteins were identified based on peptide mapping and peptide sequencing by MALDI-TOF/RTOF applying PSD fragmentation.

Protein	Abbreviation	Score	PMF sequence coverage [%] (number of identified peptieds)	Nominal mass [Da]
Up-regulated during skeletal muscle growth protein 5	USMG5_RAT	58	79 (3)	6460
Putative double homeobox protein	DUX2_RAT	66	96 (3)	9312
Hemoglobin subunit alpha-1/2 (7)	HBA_RAT	64	50 (4)	15490
Hemoglobin subunit b1 (7)	HBB1_RAT	86	68 (8)	16083
Hemoglobin subunit beta-2 (7)	HBB2_RAT	53	62 (6)	16086
Apolipoprotein A-I (6)	APOA1_RAT	92	61 (6)	30759
2-methoxy-6-polyprenyl-1,4-benzoquinol methylase	COQ5_RAT	60	45 (4)	37402
Actin (5)	ACTB_RAT	58	23 (3)	42052
Actin, cytoplasmic 2 (5)	ACTG_RAT	51	22 (2)	42108
Fibrinogen gamma chain (4)	FIBG_RAT	105	62 (7)	51228

Myocardial zonula adherens protein	MYZAP_RAT	46	12 (3)	54093
Fibrinogen beta chain (4)	FIBB_RAT	132	53 (9)	54828
Nuclear protein localization protein 4 homolog	NPL4_RAT	63	17 (5)	68982
Albumin (3)	ALBU_RAT	117	68 (15)	70682
Serotransferrin	TRFE_RAT	119	48 (3)	79294
Probable carboxypeptidase X1	CPXM1_RAT	56	9 (8)	82243
Dynamin 1 like protein	DNM1L	60	36 (5)	84369
IQ and AAA domain-containing protein 1-like	IQCAL_RAT	52	35 (6)	95964
DNA-binding protein SMUBP-2	SMBP2_RAT	62	21 (5)	109994
Myosin-7 (2)	MYH7_RAT	60	26 (9)	223,083
Adenomatous polyposis coli protein (1)	APC_RAT	60	18 (6)	310,533

Protein profiling analysis by directly analyzing the graft material using MALDI-LTOF revealed valuable analyte signals (Fig. 6). The protein pattern observed is similar to blood plasma and was detected from m/z 5000 to 80000, including proteins strongly correlating with gel findings.

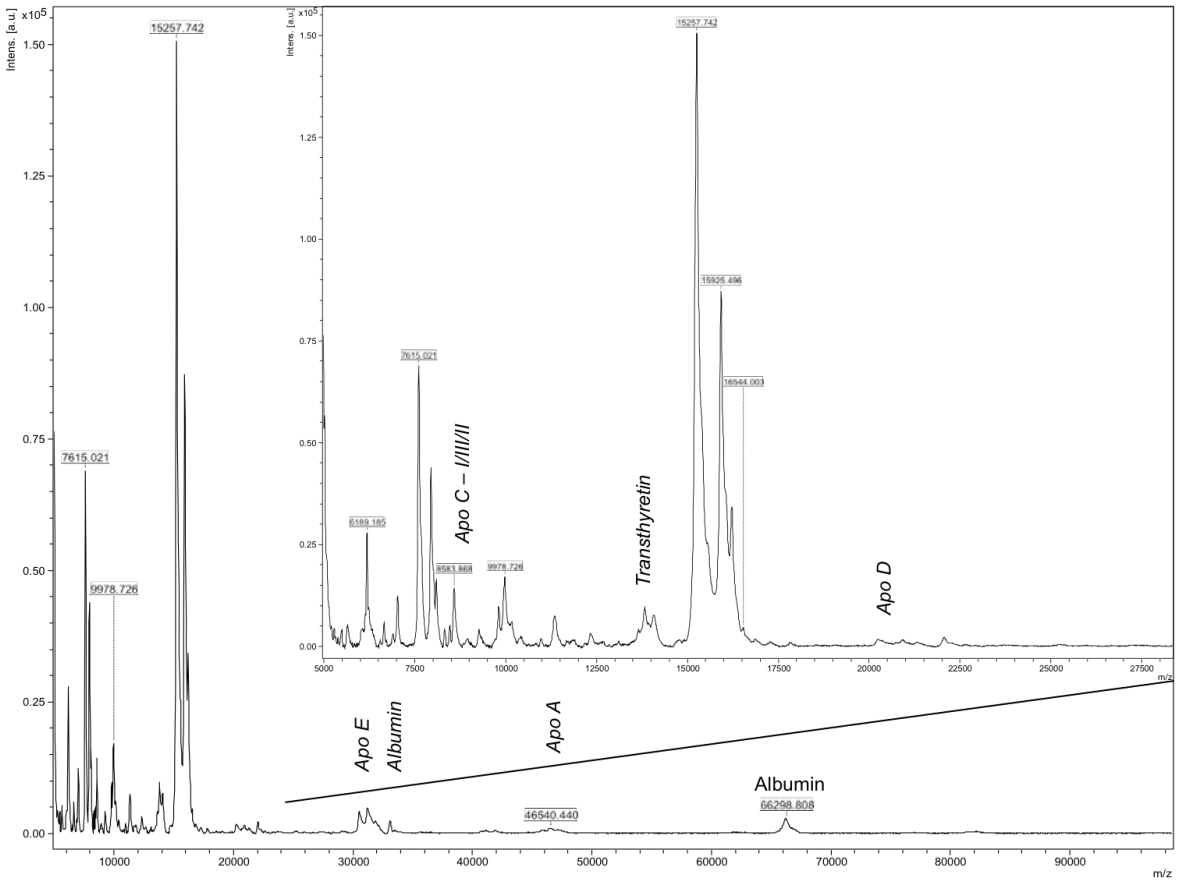

Figure 6: MALDI-LTOF protein pattern measured directly from graft material.

Results – MSI

For MSI experiments it has to be considered that due to the significant differences regarding hydrophobicity of the VPs, sample preparation parameters (matrix and/or solvent systems) were optimized for each polymer. Though this should be considered as technically not comparable, the possibility of "biological" comparison is considered valid, if spectra normalization is applied and similar analytes of interest are observed. Furthermore a lot of samples, revealed extensive salt content highly affecting signal quality and leading to no valid results.

Protein and lipid adsorption was investigated on comparable polymer segments, whereas polymer related signals were only observed in the lipid mass region (m/z 500-3500)

Fig. 7 shows detected phospholipid patterns and polymer cluster signals on the inner and outer side of ePTFE grafts. It can be observed that the polymer is co-localized with a detected sphingolipid on both sides. Similar observations were made for all described phospholipids. Additionally it can be said that EG exhibited the same behavior (data not shown).

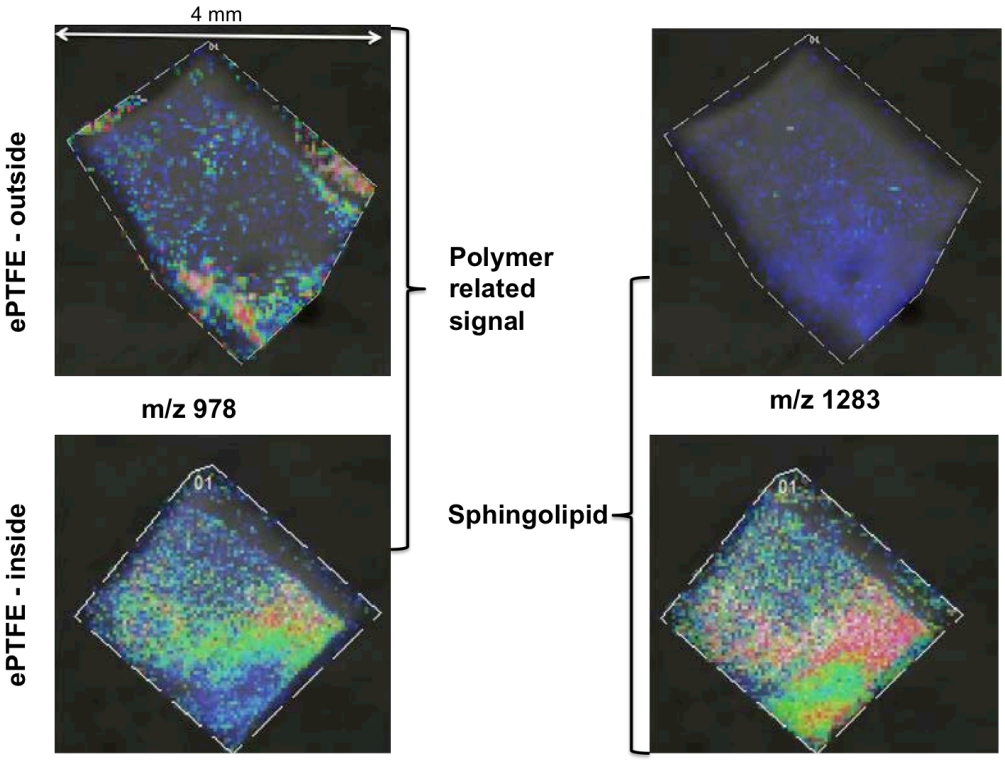

Figure 7: Comparison of the inner and outer surface of ePTFE graft material; Polymer related signal distribution was compared to sphingolipid localization by MALDI-TOF/RTOF analysis.

Peptide and protein localization was possible for all samples in a mass range between m/z 3000 and 20000. Proteins above m/z 30000 were only observable for samples without salt residues. In that case albumin and proteins between m/z 50000 and 80000 were observed with similar distribution. Fig. 8 shows spatial distributions of selected not identified peptides and proteins on the inner surface of an ePTFE graft (7 d *in situ*). The light microscope image reveals blood residues at the point of native blood vessel/graft connection. Interestingly, compared to lipid localization, different protein/peptide species show very diverse adsorption pattern with higher intensities a few mm behind the vessel/graft connection.

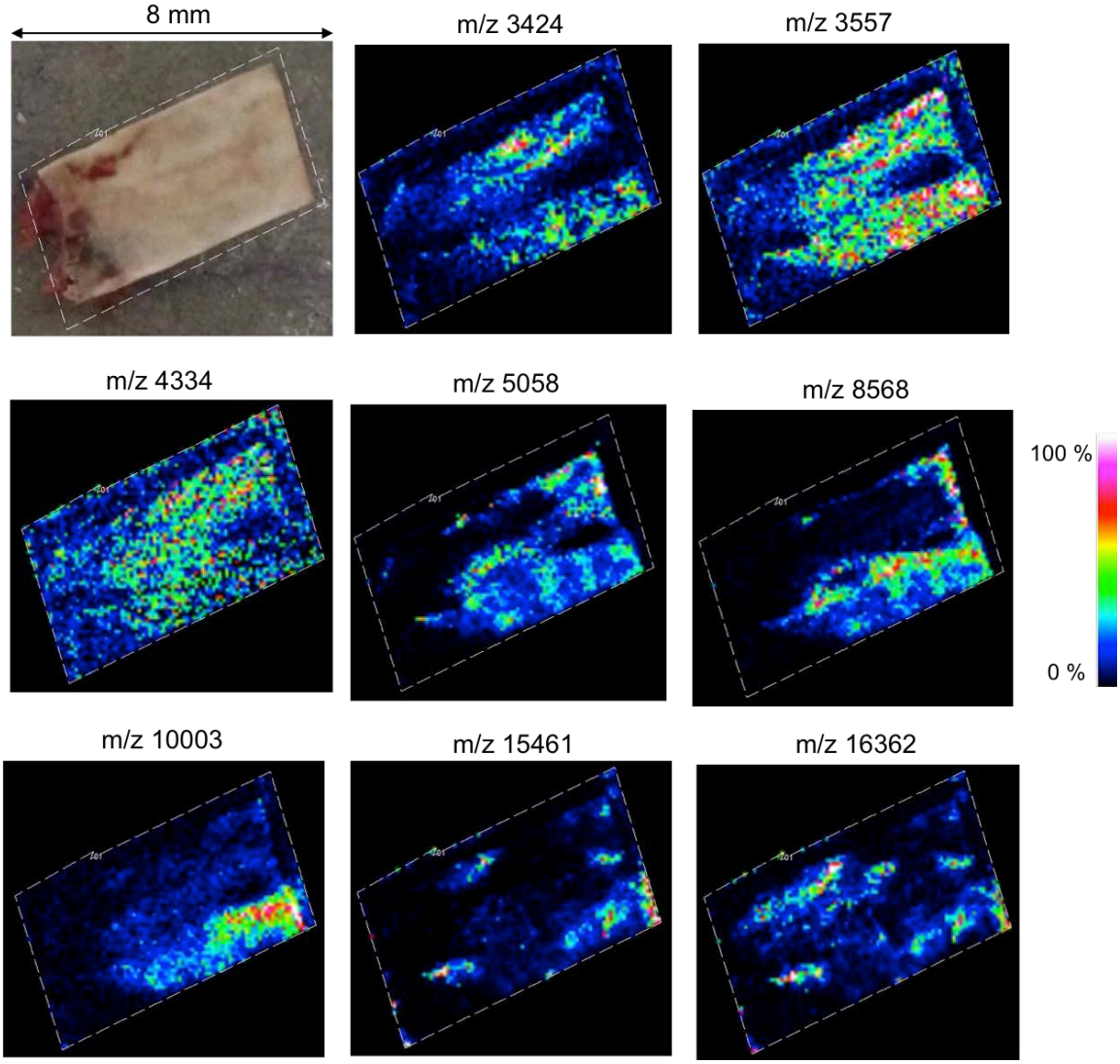

Figure 8: MSI MALDI-LTOF analysis in the peptide/protein mass range revealing very diverse signal localization for the inner surface of ePTFE graft material.

The same graft material was investigated regarding protein/peptide adsorption on the outer surface (Fig. 9). Homogeneous analyte distributions especially for small analytes were observed; yet several distinct regions revealed reduced analyte intensity. However, based on results for other analytes as shown in Fig. 9, it can be assumed that matrix application was sufficient. The signal pattern may be related for both samples, inner and outer graft sides, to beginning polymer degradation or functional protein aggregation. The latter may be emphasized by MSI analysis of aorta native material (Fig. 10), which revealed similar protein distributions.

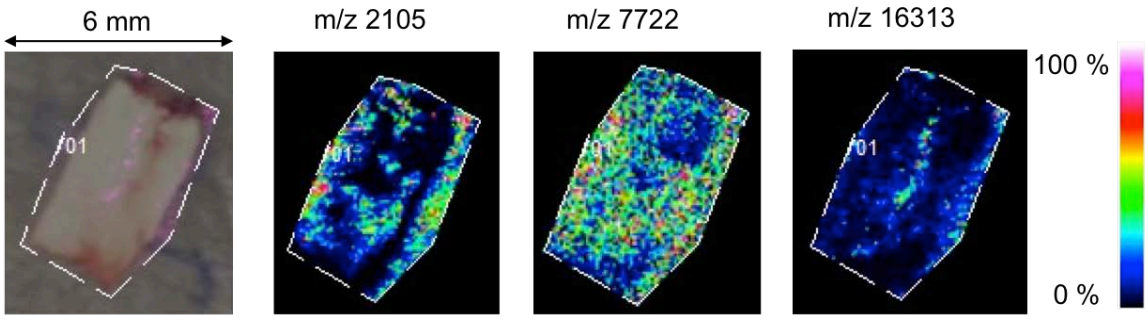

Figure 9: MSI MALDI-LTOF analysis in the peptide/protein mass range revealing also very diverse signal localization for the outer surface of ePTFE graft material.

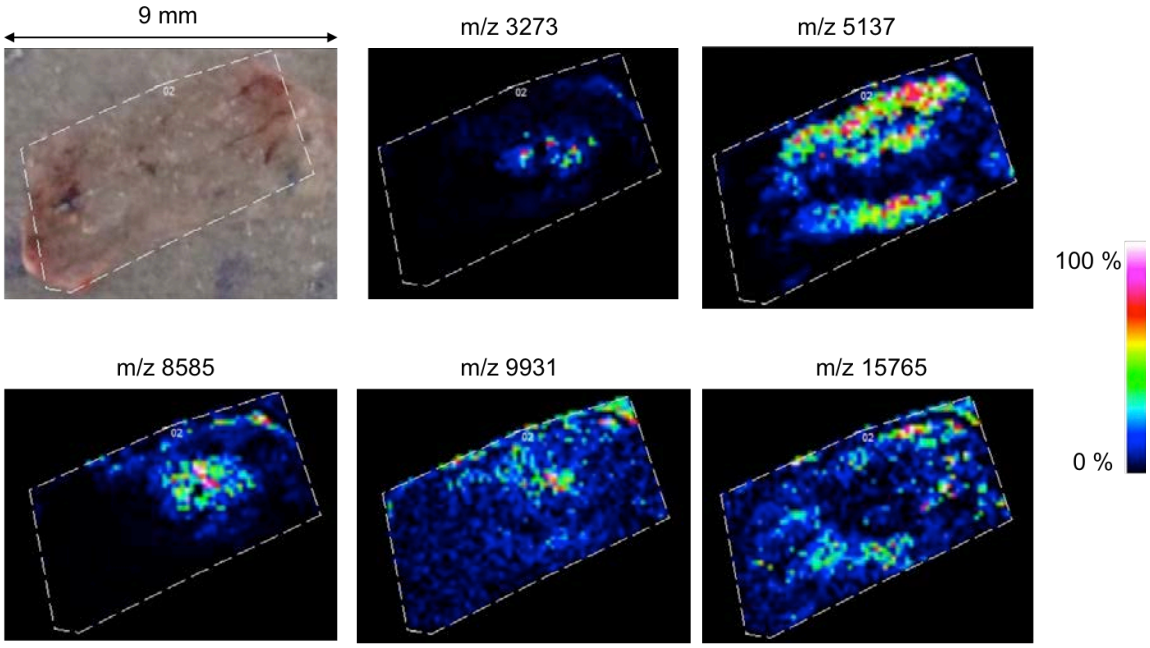

Figure 10: MSI MALDI-LTOF analysis in the peptide/protein mass range of native rat aorta tissue.

To obtain enhanced information about the degradation behavior and possible biological diffusion, cross sections from intact blood vessels were analyzed. Technically the cross-section could be analyzed efficiently at a lateral resolution of 15 µm. Polymer hydrolysis, with a not yet identified mass difference of 26 Da and lipid diffusion into the polymer were observed (Fig. 11). Cholesterol, the major component showing high prevalence and interactive behavior with polymer based implants [6], was visualized bedside several PCs.

Analyzing cross-sections provides the possibility of gaining very detailed insight into the polymer replacement and the formation process of the vessel material.

Figure 11: Cross-section analysis of ePTFE graft (7 d *in situ*) revealing Cholesterol diffusion and polymer modification.

The present study reveals the applicability of MSI to obtain profound information about the adsorption and diffusion behavior of proteins, peptides and lipids on different graft materials used for vascular prosthesis. Due to the very limited number of available vessels, statistical analysis cannot be conducted and data interpretation has to be considered carefully. Even though it could be demonstrated that protein and lipid adsorption patterns are distinctly different.

References

1. Bradford, M.M., *A rapid and sensitive method for the quantitation of microgram quantities of protein utilizing the principle of protein-dye binding.* Anal Biochem, 1976. **72**: p. 248-54.
2. Shevchenko, A., et al., *Mass spectrometric sequencing of proteins silver-stained polyacrylamide gels.* Anal Chem, 1996. **68**(5): p. 850-8.
3. Perkins, D.N., et al., *Probability-based protein identification by searching sequence databases using mass spectrometry data.* Electrophoresis, 1999. **20**(18): p. 3551-67.
4. M, A.T., *The use of glycolipids and hydrophilic polymers in avoiding rapid uptake of liposomes by the mononuclear phagocyte system.* Advanced Drug Delivery Reviews, 1994. **13**(3): p. 285-309.
5. Vermette, P., et al., *Lipid uptake in expanded polytetrafluoroethylene vascular grafts.* J Vasc Surg, 1998. **28**(3): p. 527-34.
6. Cho, E.J., et al., *Tailored delivery of active keratinocyte growth factor from biodegradable polymer formulations.* J Biomed Mater Res A, 2003. **66**(2): p. 417-24.

c. Feasibility study to use MSI for salamander secrete

MSI was used to visualize Salamander footprints after walking across a simple glass slide. The bioglue the salamander is excreting was the analyte of interest. However, to increase the amount of secreted substance, salamanders (*Plethodon shermani*) were shacken in a box to stressfully induce the secretion of glue of the foil Aclarfilm.

The covered glass slides were examined regarding ionization and desorption qualities for MSI experiments followed by eventual species identification.

For protein analysis the native glue was covered with commonly used MALDI matrices: either CHCA (7 mg/mL in 70 % methanol containing 0.2 % TFA or 50 % acetonitrile containing 0.1 % TFA) or sinapic acid (20 mg/mL in 50 % acetonitrile containing 0.1% TFA). For lipid analysis samples were either covered with 1,5-diaminonaphtalene (20 mg/mL in 50 % acetonitrile containing 0.1 % TFA), 2,5-dihydroxy benzoic acid (25 mg/mL in 50 % acetonitrile containing 0.1 % TFA) or CHCA (6 mg/mL in 2-propanol). MALDI matrix application was performed either with a pipette for profiling experiment or by chemical inkjet printing (ChIP-1000, Shimadzu Kratos Analytical). MS acquisition was performed on two different MALDI-TOF-RTOF instruments. Both Shimadzu instruments (AXIMA CFR^+ and AXIMA TOF^2, Kratos Analytical, Japan) are equipped with N_2 lasers of 10 and 20 Hz, whereas the AXIMA CFR^+ is additionally equipped with a high mass detector (CovalX, Switzerland). For MS and MSI analysis 1000 shots were accumulated for each single spectrum in reflectron, linear or linear high mass detection mode. MSI experiments were performed at a lateral resolution of 60 µm in both reflectron and linear ion detection mode. Lipid species were identified by high-energy (20 kV) collision induced dissociation fragmentation. Samples were also examined with the even more sensitive UltrafleXtreme (Bruker Daltonics), equipped with a modified Nd:YAG laser providing a laser repetition rate of 2000 Hz. Data visualization for MSI experiments was performed using Biomap (Novartis, Switzerland).

Sample preparation revealed very hydrophobic qualities for the glue. For high concentrations of glue material, e.g. thick areas, signal generation was difficult. Increasing the amount of matrix to enhance the proportion was not conducted successfully, indicating too high salt concentrations as possible inhibiting factors. The theory is supported by results from lipid analysis. Despite previous washing of samples using 0.1 % TFA, lipid signals were majorly detected as $[M+Na]^+$, $[M-H+2Na]^+$, $[M+K]^+$, or $[M-H+2K]^+$ adducts. Figure 12 and table 3 show the identified lipid species for salamander glue sample. Despite no previous extraction experiments were performed, numerous PS, PE and glycolipid species were identified. Due to ion suppression effects, normally favoring PC and SM in MALDI-TOF detection, this indicates the high abundance of those lipid species or even the low abundance of PC and SM. In general low glue concentrations were observed to be optimal for lipid detection. It was also obvious that a lot of species were detected as their oxidized form. Considering standard storing conditions at -80 °C, oxidation might be related to initial biological conditions.

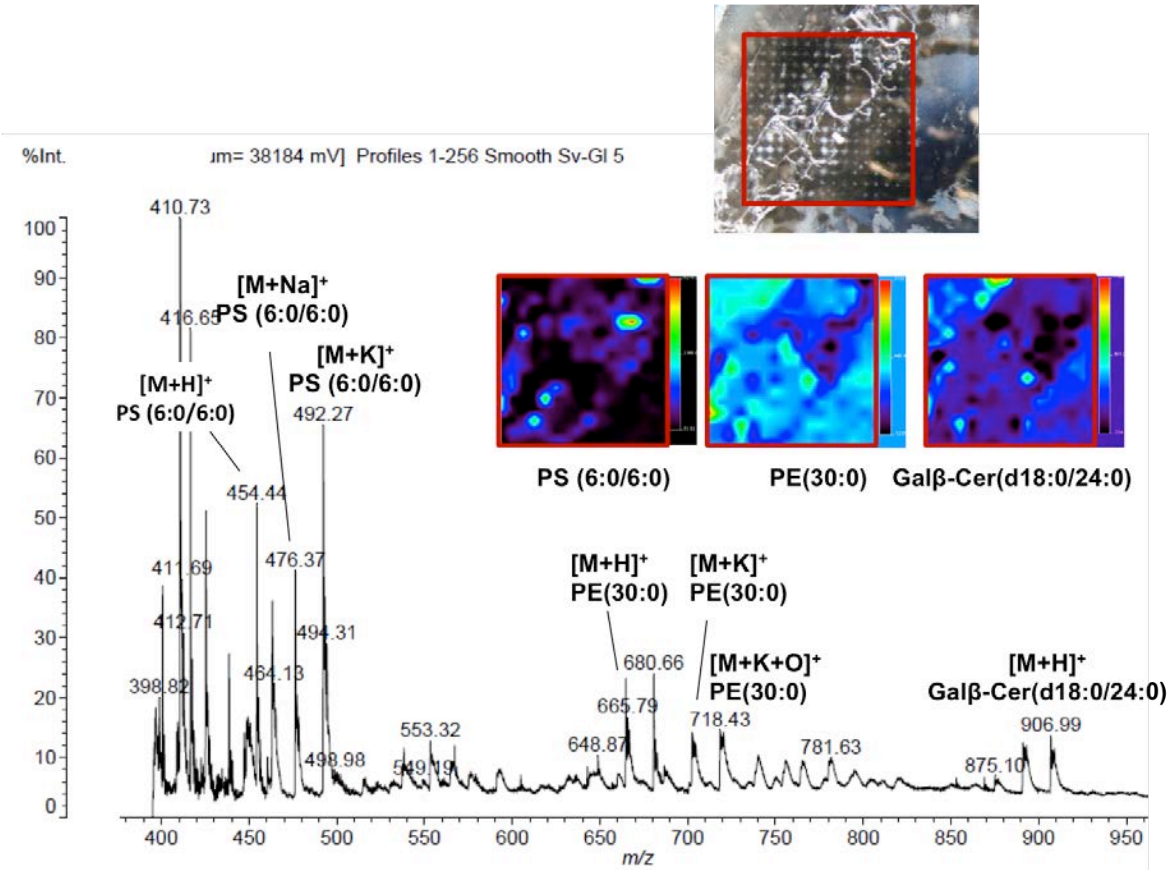

Figure 112: Lipid analysis by MALDI-TOF/RTOF MS followed by identification using HE-CID; High glue concentrations inhibit the MALDI process despite TFA washing. It is noticeable that despite expected ion suppression effects, majorly PS, PE and glycolipid species are detected in their cationized form.

Table 3: Exemplary identified lipids from salamander glue.

Species	Ion	m/z
PA (22:3)	$[M+K]^+$	681
PS (6:0/6:0)	$[M+K]^+$	492
PE (30:0), + O	$[M+H]^+$, $[M+H+O]^+$	664, 681
PC (30:2)	$[M+H]^+$	704
PC (42:2)	$[M+Na]^+$	892
Galβ-Cer(d18:0/24:0)	$[M+H]^+$	907

Protein analysis was even more affected by possible salt contaminations. Areas thickly covered with bioglue, revealed no MS signals. However, for areas with good matrix:analyte proportions (which could not clearly be evaluated in this feasibility study) showed sufficient protein signals for the mass range between 1 and 20 kDa (Fig. 13). MS spectra on both instruments revealed more than 25 signals with good intensities and S/N ratios for the linear ion detection mode. Similar observations were made for the peptide mass range below m/z 3000. Examination in the high mass range above 20 kDa was capable of detecting high very intensive signals, however with very broad peak shapes between 25 and 40 kDa. Even above 100 kDa signals, however with very low intensities were obtained. Localization conducted by MSI experiments correlated with light microscopic examinations indicate very good sensitivity of all examined instruments. Similar to lipid experiments, low amounts of glue showed best signal qualities.

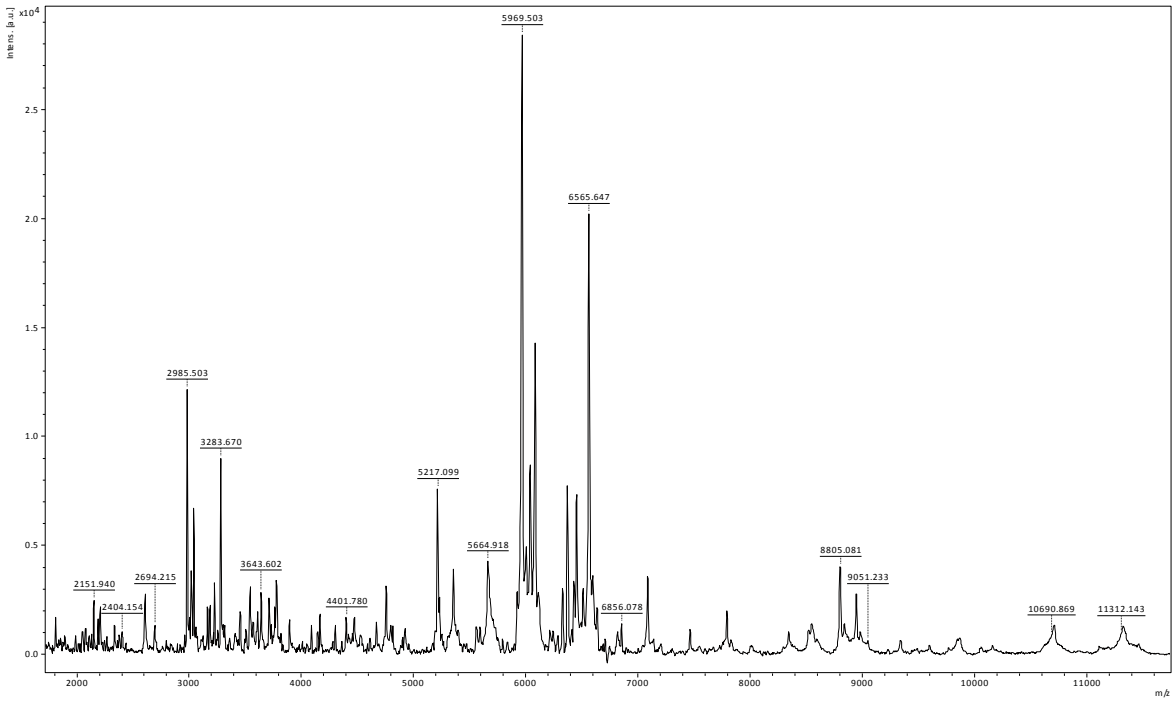

Figure 113: MALDI-LTOF analysis on UltrafleXtreme (Bruker Daltonics, Germany), Salamander glue was covered with HCCA (7 mg/mL in 70 % methanol containing 0.2 % TFA); Despite high salt concentrations good signal intensities and S/N ratios were obtained for the peptide and low molecular weight mass range between m/z 2000 and m/z 12000.

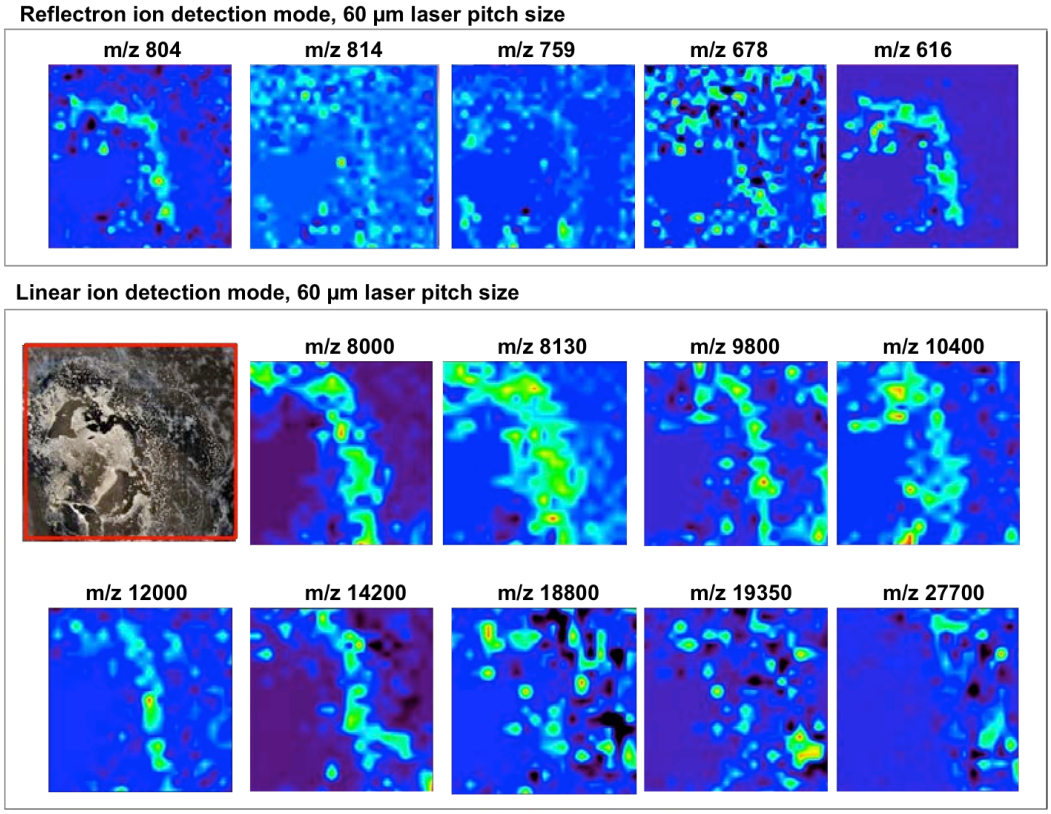

Figure 114: MSI analysis in reflectron and linear ion detection mode at a lateral resolution of 60 µm; signal qualities were observed to be significantly better in terms of intensity and S/N ratio in regions of low concentrated biofilm, however, could be correlated with presence of glue traces.

The feasibility experiments regarding the examination of salamander glue emphasize the capacity of the available instruments to detect, identify and localize analytes of interest with special focus on proteins and lipids. Both lipid and protein composition can be assumed to be very complex and biological species specific. Further investigations are summarized in the diploma thesis of Max Kosok.

d. Sample preparation strategies and differentiation of mamma carcinoma and associated lung metastasis by MSI and intact cell mass spectrometry

MSI methods, including sample preparation, matrix application and instrumental parameters, were developed based on samples with reliable complementary information, in this case histology. Well-established histological staining and evaluation tools have verified all methods.

Biologically and technically the main aim was, to increase the lateral resolution to distinguish substructures on cellular level. Methods developed for kidney tissue with well-defined distinct morphology, were further applied to mamma carcinoma tissue and associated lung metastasis. The differentiation based on the protein/peptide profile was the main target for those samples.

MATERIALS & METHODS

Samples: Mamma carcinoma (MC) samples were obtained from biopsies along with lung cancer metastasis biopsies. Samples were formalin fixed and either sucrose (FFSE) or paraffin (FFPE) embedded before microtome slicing to sections of 125 – 500 nm (FFSE) or 5 µm (FFPE). Providing the possibility of MSI and histological analysis, tissue sections were mounted on indium tin oxide (ITO) covered microscopic glass slides (Shimadzu Kratos Analytical, Kyoto, Japan). To obtain histological information by light microscopy samples were stained (toluidine blue, haematoxylin/eosine).

For further differentiation cell biopsies were cultivated to conduct intact cell mass spectrometry (ICMS) analysis. Cells were grown in fetal calf serum until a convolute cell layer ($4*10^6$ cells) was obtained. After short trypsinization (15 min) cells were centrifuged (1000 rpm) and washed twice with 0.01 M Phosphate Buffered Saline (PBS) buffer.

Antigen retrieval and sample washing: MSI analysis requires the removal of tissue stain, embedding media and if applicable the rescinding of cross-linking to improve S/N ratios and enhance spectral quality.

Table 4 shows the methods evaluated for efficient antigen retrieval.

Table 4: Evaluation of washing procedures applied to FFPE samples; -) no sufficient signal observable *) poor signal quality **) moderate signal quality *) good signal quality ****) excellent signal quality.**

	Procedure	MALDI-LTOF	MALDI-LTOF trypsin
Acetone	100 % acetone (4°C, 2h)	*	*
	100 % ethanol, 100 % acetone (4°C, 2h), 100 % acetone (4°C, 2h)	**	**
	90 % acetone (4°C, 4h)	*	*
TCA/acetone	60 % TCA (4°C, 3h), 90% acetone (4°C, 15 min)	**	**
$CHCl_3$/MeOH	7:3, v/v (4°C, 2.5h)	-	-
Citrate buffer	citrate buffer (90°C, 40 min), digestion buffer (10 min)	***	***
TRIS-HCl	digestion buffer (5 min), TRIS-HCl pH 9 (97°C, 30 min)	**	****

MALDI enzyme and matrix application: To ensure complete dry tissue, required for matrix application and further enhance protein denaturation tissue samples were incubated at 85 °C for 5 minutes.

Trypsin was dissolved in 100 mM NH_4HCO_3 digestion buffer containing 5 % Rapigest and 5 % acetonitrile. 1 ng/spot/µm was applied onto the tissue samples using the ChIP-1000. Samples were incubated at 37 °C in saturated atmosphere (ethanol/water, 1/1, v/v) for 18 h. Samples were shortly incubated at 50 °C to remove any residual liquid before matrix application.

Table 5 gives an overview to the examined MALDI matrices for MSI analysis of FFSE and FFPE samples.

Table 5: Evaluated MALDI matrices for MSI tissue applications, y – yes, n – no.

	Solvent system		**Application**		
	ACN/ddH$_2$O	**Methanol**	**ChIP-1000**	**Airbrush**	**Recrystallization****
2,4,6-trihydroxyacetophenone	y	y	y	y	n
1,4-dihydroxyacetophenone	y	y	y	n	n
2,5.dihydroxy benzoic acid	y	y	y	y	y
α-cyano-4-hydroxycinnamic acid	y	y	y	y	y
Sinapic acid	y	y	y	y	n
Ferulic acid	y	y	y	y	n
Diaminonaphtalene*	y	n	y	n	n
Coumaric acid	y	y	y	n	n
Azathiothymin	y	y	y	n	n

**) all available conformations*
***) lead to improvement*

MALDI matrix was applied using a Chemical inkjet printer (ChIP-1000, Shimadzu Kratos Analytical) covering the whole tissue sample homogeneously (1-10 ng/spot). For MSI protein analysis sinapic acid and ferulic acid were mixed 1:1 to obtain a saturated matrix solution in acetonitril/methanol (7/3, v/v) containing 0.1 % TFA. Matrix deposition was performed using an airbrush device (Conrad), at a working distance of 10 to 12 cm with an approximate angle of 50 to 60°, covering the sample in several iterative steps.

MALDI-MS analysis: The cell pellet was further centrifuged at 3000 rpm for 15 min before washing twice with double distilled water (ddH_2O) and centrifuging at 3000 rpm for 15 min. Afterwards the cell pellet was dissolved in saturated matrix (Sinapic acid, α-cyano-4-hydroxycinnamic acid, ferulic acid each dissolved in acetonitrile/methanol/0.1 % trifluoracetic acid, 50/25/25, v/v/v) and spotted to stainless steel MALDI target for ICMS analysis. ICMS analysis was conducted on the UltrafleXtreme in LTOF mode.

MSI experiments were conducted on three different instruments: high vacuum MALDI-TOF/RTOF (AXIMA TOF2, Shimadzu Kratos Analytical) equipped with a 20 Hz N_2-laser, high vacuum MALDI-TOF/RTOF (UltrafleXtreme, Bruker Corporation, Bremen, Germany) equipped with a 2 kHz SmartBeam™ laser and intermediate pressure MALDI-QRTOF system (Synapt G1 and HDMS, Waters Corporation, Manchester, UK) equipped either with a 200 Hz or 1 kHz Nd:YAG laser. Lateral resolution was set between 7 and 150 µm (stated for experiments in figure legends). For image reconstruction FlexImaging v. 3.0 software (Bruker Daltonics) was used. All MSI data sets are presented as Median normalized but were also verified for outliers and artifacts by Route Mean Square and Total Ion Current normalization.

RESULTS & DISCUSSION

Sample Washing & Antigen Retrieval

Histological evaluation is often based on tissue staining. Either H/E or toluidine blue are the most commonly used stains for sample examination regarding tumor or substructure differentiation. To verify the influence on MSI experiments, signal quality of H/E stained samples were compared to unstained tissue. Standard CHCA and SA matrix was applied to FFPE tissue (5 µm) to observe possible interfering signals in the peptide and protein mass range.

Fig. 15 shows exemplary spectra of the peptide/lipid mass range with identified interfering signals. The main found signals are found in the area of matrix cluster signals or possible residual lipid species. For peptide mapping experiments, however, those signals can be neglected. It was concluded that samples stained before MSI analysis, allow better correlation of experimental data and deliver no significantly interfering signals. However, if enzyme or antigen retrieval procedures are applied, stains are possibly removed due to the washing procedures at low or high pH range.

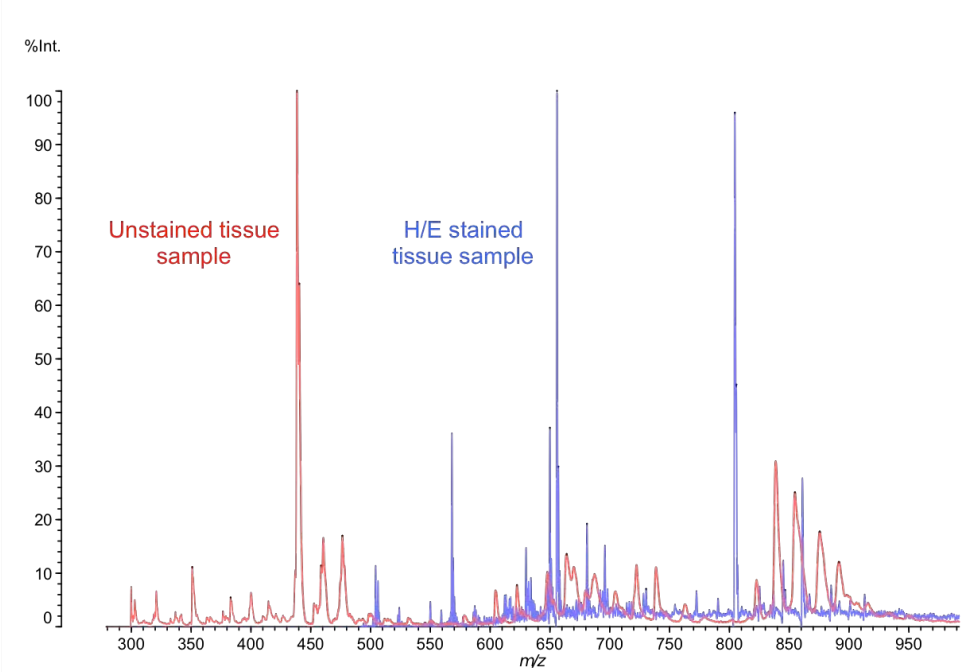

Figure 115: Evaluation of background signals related to H/E stain on FFPE tissue.

Despite the removal of eventual stains and residual embedding media, the extensive cross-linking of formalin fixed tissues has to be reversed and antigen retrieval is recommended for improved analyte accessibility.

Very good signal qualities for FFPE tissue above a cutting thickness of 3 µm were observed after application of a combined washing and antigen retrieval method. Samples were rehydrated in ethanol and incubated shortly in 5 % acetic acid before microwave treatment at 300 W in citrate buffer for 2 minutes. Tissue stain and signal background were removed and improved analysis significantly also for enzymatic treatment.

Based on conventional sample preparation for e.g. gel electrophoresis, protein denaturation can be achieved by temperature exposure between 75 and 95 °C. For MSI analysis, incubating samples at 85 °C for 5 minutes instead of vacuum. High temperature treatment conducted twice, e.g. during washing steps and before matrix application, was compatible with all tested tissue samples

Enzymatic treatment

For enzymatic treatment, either by trypsin or Lys C, enzymes are applied in a very thin buffer layer using the ChIP-1000. The thin liquid layer is capable of avoiding diffusion and enhancing the interaction between analyte and enzyme. Due to the small amount of liquid, samples can easily get too dry for an effective digestion process at 37 °C. A humidity box was constructed, filled with ethanol water (1/1, v/v) to create an 80 % humidified atmosphere. To avoid condensation at the top cover, tissue was stuck on top avoiding droplets leading to sample contamination.

The comparison of Lys C and trypsin, applied to FFPE mamma carcinoma tissue revealed the efficient applicability for a mass range between m/z 1500 and 20000 in MALDI-LTOF mode (Fig. 16). It is obvious that different protein fragments are generated, besides the fact that both enzymes work efficiently in the pH range between 7.5 and 9.5. The wide pH range can be explained due to buffer conditions on the tissue sample, which cannot exactly be determined.

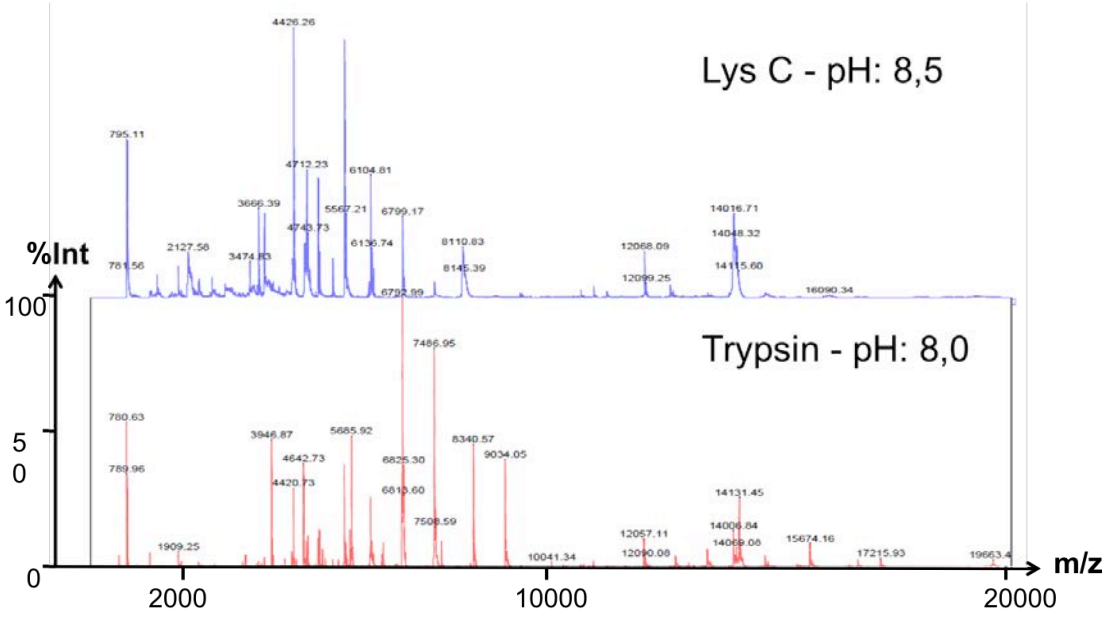

Figure 116: Comparison of trypsin and Lys C digestion of FFPE mamma carcinoma tissue evaluated by MALDI-LTOF (AXIMA TOF², Shimadzu Kratos Analytical).

The main challenge for the present tissue samples was to obtain signals in the peptide mass range with sufficient abundance and resolution for efficient fragmentation. Without valid information about the peptide sequence, identification in this case is not possible since it is not known, whether intact or cleaved proteins/peptides are detected.

The digestion procedure was enhanced by addition of MS compatible detergents. In the present case buffer solutions containing 1 to 5 % Rapigest, lead to improved signal quality in terms of S/N ratio, intensity and quantity of detected signals.

It was further observed that identical digestion (trypsin as described favorable) and matrix application procedures (CHCA favorable by ChIP-1000) for identical samples (FFPE mamma carcinoma) were not reproducible on two different instruments (UltrafleXtreme, AXIMA TOF^2). MALDI-LTOF spectra were not comparable for similar samples, revealing significant signal losses for data obtained using the UltrafleXtreme in LTOF mode. The RTOF mode however, showed comparable signals, with improved intensities. Considering the reproducible sample preparation strategy for a large number of samples (n > 10) with varying operators (n = 2), the technical differences are assumed to have high impact.

Matrix application

The evaluation of matrix systems suitable for MSI applications was based on the quality of the applied surface layer (homogeneity, printability, crystal size) and the spectral quality (S/N, intensity, number of obtained signals).

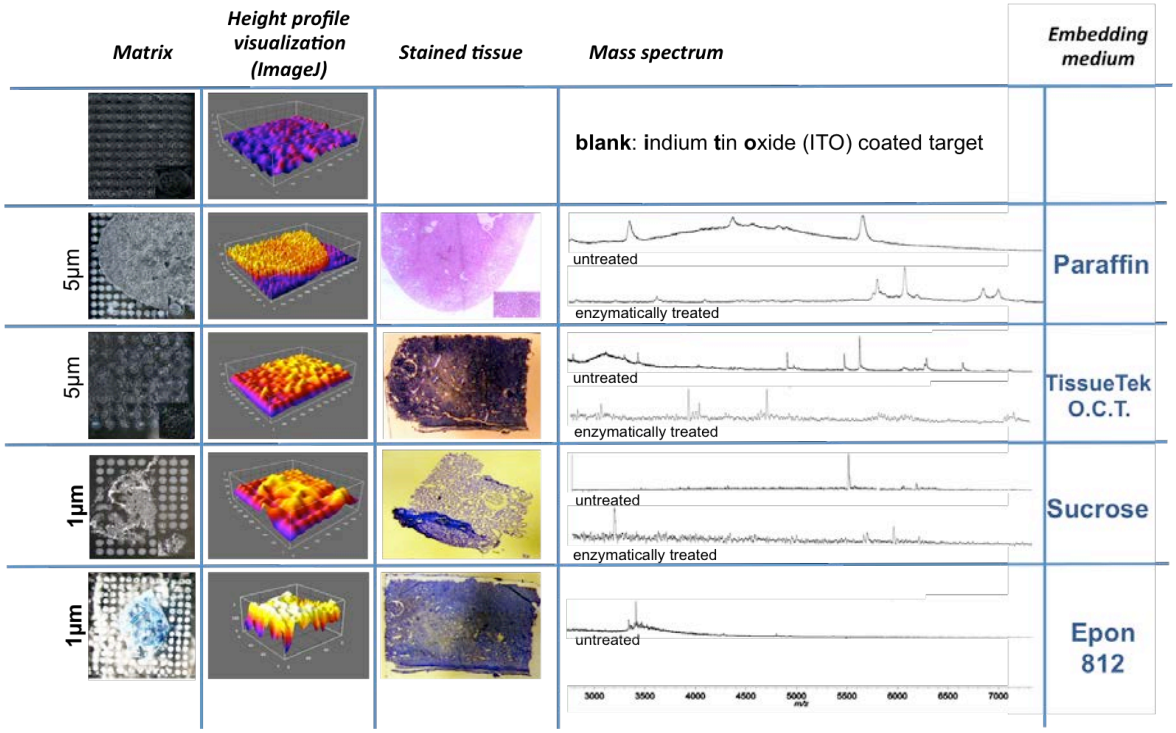

Figure 17: Evaluation of MALDI matrix application based on printing quality and signal generation on different embedding media.

Fig. 17 gives an overview to the first findings obtained in matrix application on different embedded tissue samples (kidney samples were first available and used in this study). CHCA in dissolved in ACN/0.1 % TFA (50/50, v/v) was applied (ChIP-1000) to the 4 most commonly used embedding media in histology.

The surface was examined by light microscopy before and after matrix application and visualized using ImageJ to obtain information about the homogeneity of the surface profile. Furthermore MALDI-LTOF signals (AXIMA TOF^2) were obtained from enzymatically untreated and trypsinized tissue samples in the peptide mass range. Matrix crystallization was found to vary depending on the hydrophobicity and sample morphology. Whereas paraffin and sucrose showed very defined and accurately deposited matrix spots, O.C.T. TissueTek, a polyglycol based embedding medium liquid at room temperature, and Epon 812, a very hydrophobic resin, both revealed blurred droplets with diffuse matrix crystal distribution. Sample morphology was preserved with high quality for paraffin and Epon 812 embedded tissue. Sucrose samples are very sensitive to tearing, due to ultra thin slices between 150 nm and 2 µm. O.C.T. samples are cut at -20°C at a thickness between 1 and 10 µm. The sample is unfixed in contrary to paraffin and sucrose, which both are formalin fixed, leading to loss of morphology. However, unfixed tissue is not affected by cross-linking, which leads to very good signal quantities and qualities for both untreated and trypsinized samples. Formalin fixed paraffin or sucrose embedded samples, revealed signal losses and decreased S/N ratio. However one has to be aware that especially for sucrose samples, this is also a consequence of reduced amount of analyte due to ultra thin slices.

For further analysis FFPE and FFSE samples were favored, however, O.C.T. samples showed good capacities for profiling and possible sequencing experiments.

Besides very effective MALDI matrix application with the ChIP-1000, sublimation was evaluated regarding its effect on analyte desorption from FFPE and O.C.T. tissue (both 5 µm). An in-house built sublimation construction (ERASMUS Center Rotterdam, Netherlands) was used in combination with 2,5-DHB and other commonly used matrices (CHCA, SA, FA), which were not sublimated efficiently and neglected for further evaluation. Tissue samples were tested untreated or trypsinized (standard trypsin procedure). For sublimation 5 ml matrix solution (10 mg/mL DHB in acetone) were applied to two glass slides with 2 slices each. Compared to the chemical inkjet printing, sublimation is capable of delivering very homogeneous, thin matrix layer (Fig. 18). Tissue microstructures, in that case glomeruli on a FFPE tissue sample, are still observable. Native samples did, however, not reveal any usable signals, whereas trypsinized tissue revealed a few low quality signals. To improve analyte protonation, samples were washed with trifluoracetic acid (TFA, 0.5 %, 200 $\mu L/cm^2$) for 2 minutes. TFA was removed using lint free tissue mounted on a glass stamp before vacuum desiccation for 10 minutes. Fig. 18 shows an exemplary spectrum for trypsinized FFPE tissue in the peptide mass range. Even though signal quality is still improvable, intensities and S/N ratios are improved.

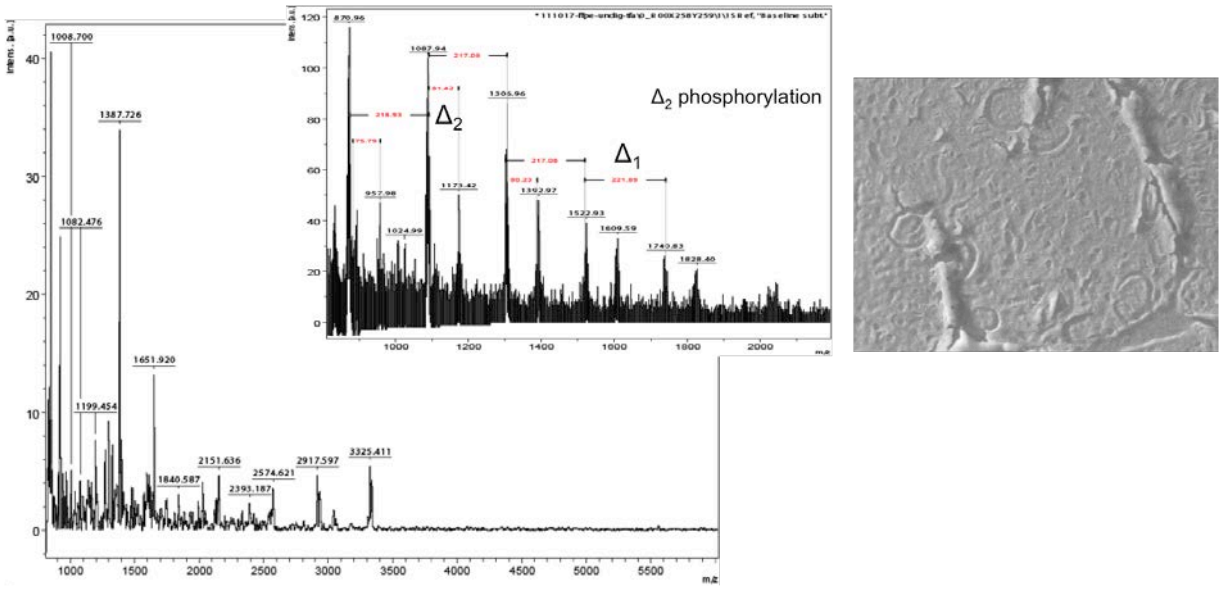

Figure 18: DHB sublimation on enzymatically treated FFPE tissue by MALDI-RTOF (Ultraflex II, Bruker); Light microscopy shows the very fine crystal size for an area of app. 3 mm.

It is assumed that DHB is not the best choice of matrix for peptide analysis. Due to the physical properties of CHCA, impeding sublimation, DHB sublimation was followed by applying 0.5 µL CHCA (7 mg/mL in acetone) using a pipette. The effect is similar to recrystallization, including the possibility of analyte delocalization however reducing crystal size and improving analyte incorporation. Fig. 19 shows the obtained mass spectrum and its associated light microscope picture. Crystal size is rather inhomogeneous but signal intensity and S/N ratio were improved. It can be concluded that sublimation provides very sufficient qualities regarding matrix application. The favorable small crystal size can be obtained homogeneously for very large areas within very short processing times.

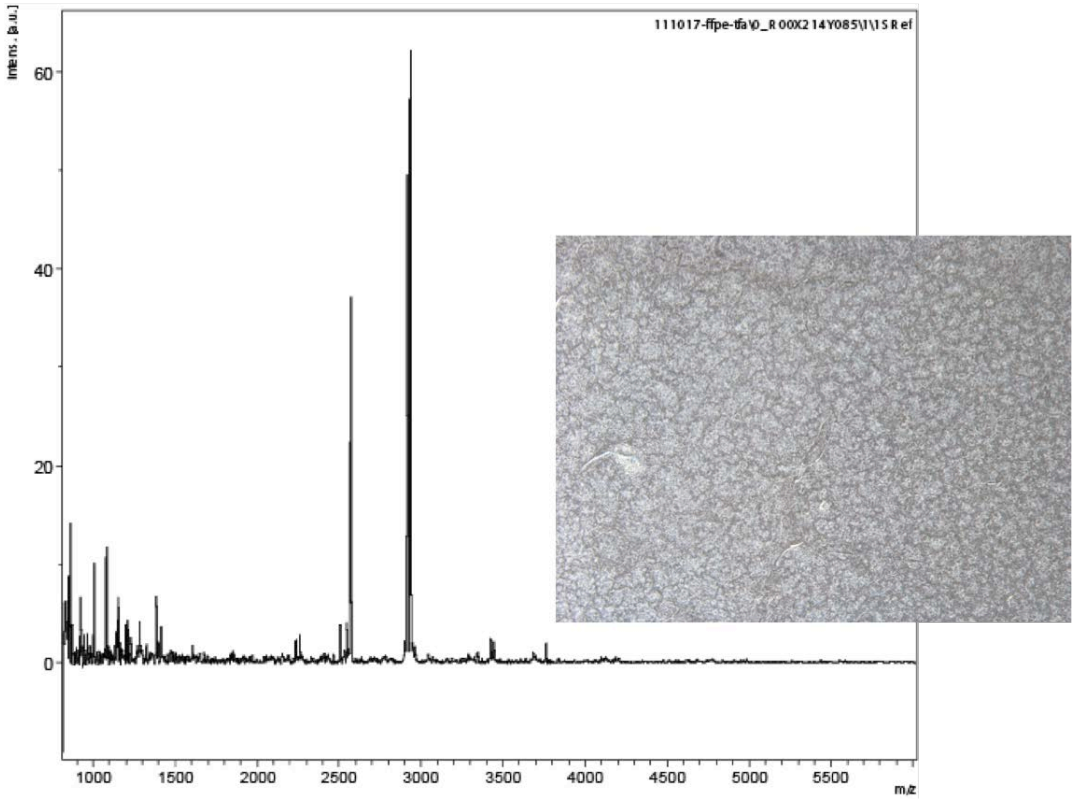

Figure 19: Signal after CHCA spotting after DHB sublimation on enzymatically treated FFPE tissue sample by MALDI-RTOF (Ultraflex II, Bruker).

Mamma carcinoma heterogeneity analysis by MSI analysis with emphasis on peptide signals

The primary observed limitation after good sample preparation is the laser diameter focus. The laser diameter and laser profile were adjusted to obtain signals with preferably high S/N ratio and signal intensity. Depending on the sample size and structure, laser diameters below the cellular resolution are required. Fig. 20 gives an overview to FFPE and FFSE samples with a constantly reduced laser diameter. Whereas very low lateral resolutions show recognizable pattern differences for large samples (5-8 mm) with defined morphology, this can hardly be obtained for small (1-2 mm) FFSE samples. Even for the large samples, 100 µm lateral resolution provides image information that shows a very defined pattern, which however, cannot be correlated directly with the histological alignment. For high-resolution images of FFSE samples, the laser diameter was set to 10 µm, still providing sufficient signal quality.

To further enhance the lateral resolution, and screen samples for particular ions of interest, the applicability of oversampling was evaluated. The technically minimal laser diameter was chosen at a lateral resolution below 10 µm (5-8 µm). For high abundant signals, the loss of analyte due to complete sample ablation is acceptable, however low abundant signals are considered to show too low signal intensities. Despite high quality images at 7 µm, the software is not capable of visualizing pixel information below that resolution. Moreover it has to be considered, despite a laser frequency of 2 kHz, operating times above 30 hours are necessary to obtain all data points for a very small sample below 2-4 mm^2 possibly harming analyte and matrix stability. As a consequence small areas of interest were chosen for analysis at very high resolution.

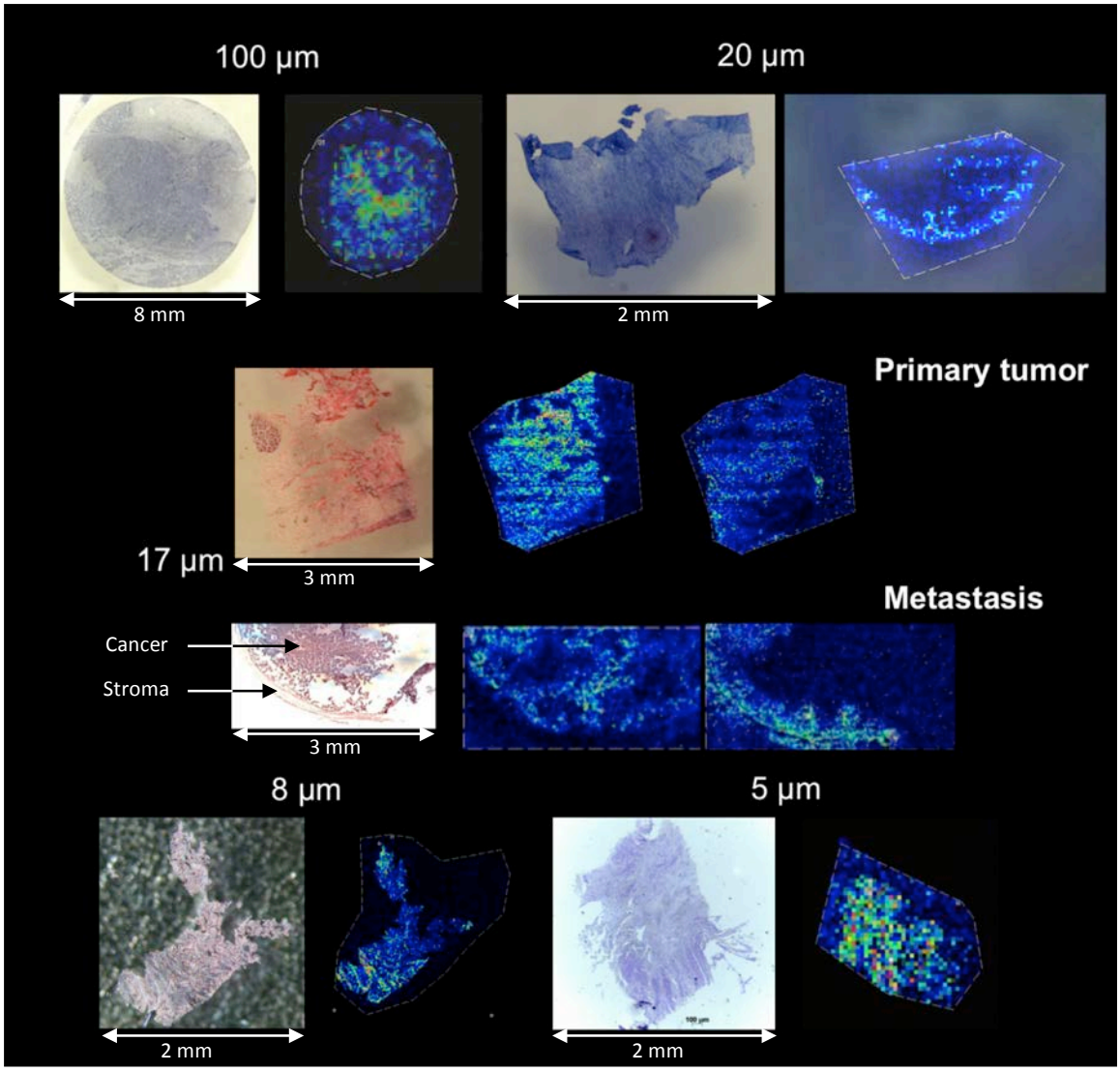

Figure 20: Varying lateral resolution from 100 µm (FFPE) to 5 µm (all FFSE).

For heterogeneity differentiation without aiming high resolution towards particular regions of interest, 17 µm was chosen as standard lateral resolution, providing sufficient information about low and high abundant analytes, without loosing lateral resolution. The areas observed reveal very distinct peptide patterns, which can be correlated with histologically characteristic areas. Especially stroma and cancerous regions could be differentiated (Fig. 20) for both primary tumor and associated lung metastasis. Region specific signals were further observed in branching regions, histologically not recognizable. It is assumed that cells at boarder regions can be differentiated on a molecular level, which is not possible by histological staining and evaluation. Further emphasis will lie on the signal identification.

Identifying relevant peptide signals for the differentiation of mamma carcinoma and associated lung metastasis requires the analysis of large data sets for both sample groups. Technical (n=10) and biological (n=4) replicates were analyzed regarding their peptide profile after enzymatic digestion using trypsin. Profile spectra were obtained for all samples using a flat and broad laser profile, which favors analyte desorption, however lacks lateral resolution and is not applicable for MSI experiments. Data sets were analyzed using principal component analysis (PCA) and cluster analysis, both at cross-

validated significance level. 49 peptides were identified after eliminating trypsin and matrix cluster signals. The two defined groups could be differentiated based on PCA, however revealing moderate dispersion for both signal groups based on the first three principal components. Cluster analysis showed interesting sample pairings. Tumor and metastasis were not differentiated in the first but in the third node, indicating similarities between the tissue types. Here it has to be considered that biopsies were taken from two different tissues. Even though the tumor was trimmed and residual tissue was removed, peptides relevant for organ related differentiation might be included. Tumor tissue contains a lot of structure or metabolism relevant proteins, which induce similarities for any type of tumor tissue. The crucial point is to identify the proteins/peptides relevant for tumor and metastasis differentiation but not associated with the organ itself or stroma. Sequence determination is therefore mandatory for further data interpretation and conclusion. So far the results demonstrate the applicability of the developed method for detailed investigation and possible differentiation of cancerous tissue samples.

As a consequence of the difficult desorption/ionization and further fragmentation properties, 3 known proteins of interest for differentiation were chosen and investigated for possibly associated peptide fragments: Cytokeratin 5 (590 AA, 62 kDa), Cytokeratin 7 (469 AA, 52 kDa) and HER 2 MLN NEU NGL (1255 AA, 138 kDa).

Cytokeratin 5

MSRQSSVSFRSGGSRSFSTASAITPSVSRTSFTSVSRSGGGGGGGFGRVSLAGACGVGGYGSRSLYNLGGSKRISISTSGGSFRNRFGAGAGGG
YGFGGGAGSGFGFGGGAGGGFGLGGGAGFGGGFGGPGFPVCPPGGIQEVTVNQSLLTPLNLQIDPSIQRVRTEEREQIKTLNNKFASFIDKVR
FLEQQNKVLDTKWTLLQEQGTKTVRQNLEPLFEQYINNLRRQLDSIVGERGRLDSELRNMQDLVEDFKNKYEDEINKRTTAENEFVMLKKDVD
AAYMNKVELEAKVDALMDEINFMKMFFDAELSQMQTHVSDTSVVLSMDNNRNLDLDSIIAEVKAQYEEIANRSRTEAESWYQTKYEELQQT
AGRHGDDLRNTKHEISEMNRMIQRLRAEIDNVKKQCANLQNAIADAEQRGELALKDARNKLAELEEALQKAKQDMARLLREYQELMNTKLA
LDVEIATYRKLLEGEECRLSGEGVGPVNISVVTSSVSSGYGSGSGYGGGLGGGLGGGLGGGLAGGSSGSYYSSSSGGVGLGGGLSVGGSGFSAS
SGRGLGVGFGSGGGSSSSVKFVSTTSSSRKSFKS

Cytokeratin 7

MSIHFSSPVFTSRSAAFSGRGAQVRLSSARPGGLGSSSLYGLGASRPRVAVRSAYGGPVGAGIREVTINQSLLAPLRLDADPSLQRVRQEESEQI
KTLNNKFASFIDKVRFLEQQNKLLETKWTLLQEQKSAKSSRLPDIFEAQIAGLRGQLEALQVDGGRLEAELRSMQDVVEDFKNKYEDEINHRTA
AENEFVVLKKDVDAAYMSKVELEAKVDALNDEINFLRTLNETELTELQSQISDTSVVLSMDNSRSLDLDGIIAEVKAQYEEMAKCSRAEAEAWY
QTKFETLQAQAGKHGDDLRNTRNEISEMNRAIQRLQAEIDNIKNQRAKLEAAIAEAEERGELALKDARAKQEELEAALQRGKQDMARQLREY
QELMSVKLALDIEIATYRKLLEGEESRLAGDGVGAVNISVMNSTGGSSSGGGIGLTLGGTMGSNALSFSSSAGPGLLKAYSIRTASASRRSARD

HER 2 NEU

MELAALCRWGLLLALLPPGAASTQVCTGTDMKLRLPASPETHLDMLRHLYQGCQVVQGNLELTYLPTNASLSFLQDIQEVQGYVLIAHNQVR
QVPLQRLRIVRGTQLFEDNYALAVLDNGDPLNNTTPVTGASPGGLRELQLRSLTEILKGGVLIQRNPQLCYQDTILWKDIFHKNNQLALTLIDTN
RSRACHPCSPMCKGSRCWGESSEDCQSLTRTVCAGGCARCKGPLPTDCCHEQCAAGCTGPKHSDCLACLHFNHSGICELHCPALVTYNTDTF
ESMPNPEGRYTFGASCVTACPYNYLSTDVGSCTLVCPLHNQEVTAEDGTQRCEKCSKPCARVCYGLGMEHLREVRAVTSANIQEFAGCKKIFG
SLAFLPESFDGDPASNTAPLQPEQLQVFETLEEITGYLYISAWPDSLPDLSVFQNLQVIRGRILHNGAYSLTLQGLGISWLGLRSLRELGSGLALIH
HNTHLCFVHTVPWDQLFRNPHQALLHTANRPEDECVGEGLACHQLCARGHCWGPGPTQCVNCSQFLRGQECVEECRVLQGLPREYVNAR
HCLPCHPECQPQNGSVTCFGPEADQCVACAHYKDPPFCVARCPSGVKPDLSYMPIWKFPDEEGACQPCPINCTHSCVDLDDKGCPAEQRAS
PLTSIISAVVGILLVVVLGVVFGILIKRRQQKIRKYTMRRLLQETELVEPLTPSGAMPNQAQMRILKETELRKVKVLGSGAFGTVYKGIWIPDGEN
VKIPVAIKVLRENTSPKANKEILDEAYVMAGVGSPYVSRLLGICLTSTVQLVTQLMPYGCLLDHVRENRGRLGSQDLLNWCMQIAKGMSYLED
VRLVHRDLAARNVLVKSPNHVKITDFGLARLLDIDETEYHADGGKVPIKWMALESILRRRFTHQSDVWSYGVTVWELMTFGAKPYDGIPAREI
PDLLEKGERLPQPPICTIDVYMIMVKCWMIDSECRPRFRELVSEFSRMARDPQRFVVIQNEDLGPASPLDSTFYRSLLEDDDMGDLVDAEEYLV
PQQGFFCPDPAPGAGGMVHHRHRSSSTRSGGGDLTLGLEPSEEEAPRSPLAPSEGAGSDVFDGDLGMGAAKGLQSLPTHDPSPLQRYSEDPT
VPLPSETDGYVAPLTCSPQPEYVNQPDVRPQPPSPREGPLPAARPAGATLERPKTLSPGKNGVVKDVFAFGGAVENPEYLTPQGGAAPQPHP
PPAFSPAFDNLYYWDQDPPERGAPPSTFKGTPTAENPEYLGLDVPV

5 signals were identified with excellent ROC (receiver operating characteristics) above 0.92, which can be considered as significant for sample differentiation: m/z 852, 1013, 1195 and 1289. No accurate mass is displayed, due to m/z deviation of Δm/z 0.05 for tissue analysis of FFSE samples. The above shown sequence was investigated for theoretical peptide fragments after trypsin cleavage. For Cytokeratin 5 m/z 1195 $[M+H]^+$ was found correlating with the peptide fragment 365-374: (K)YEELQQTAGR(H). Further investigations will focus on the identification of relevant signals, with adjusted ROC limits.

Sample differentiation ICMS analysis

As described, cell cultures were grown and harvested from biopsies of both tumor and metastatic tissue. The main intention by taking on the concept of ICMS analysis was to identify signals relevant for differentiation in an unfixed state without eventual analyte loss.

After dissolving the cells in SA, FA and CHCA solutions analyte incorporation, crystallization and signal quality (S/N, intensity, quantity of valid signals) were evaluated (Fig. 21). Preliminary experiments with human epithelial cell culture showed that both SA and CHCA deliver differentiation relevant information, whereas poor signal quality was observed for FA. Signals were observed in the positive LTOF mode for a mass range between m/z 5000 and 50000.

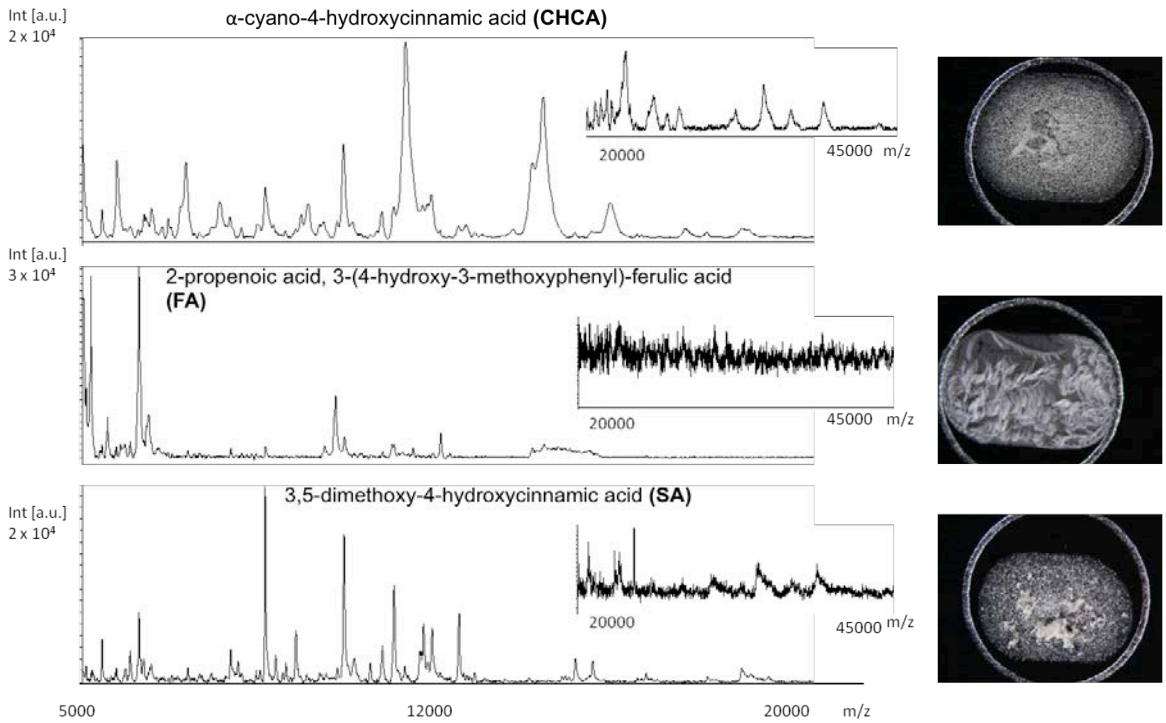

Figure 21: Evaluating commonly used MALDI matrices (CHCA, FA and SA) for their applicability to ICMS of tumor cell cultures by MALDI-LTOF.

PCA and cluster analysis models were evaluated for different MALDI matrices to verify the observations statistically. Matrix differentiation was based on 58 signals and exposed signal variations for SA and CHCA based on the first node of cluster analysis and showed distinct differentiation profiles for the three principal components.

Method reliability was evaluated by repeating the washing procedure after the sample was dissolved and removed for analysis. No cell pellet was visible, however, matrix solution was dissolved in the reaction vial and analyzed. Furthermore the cell medium was analyzed by the same MALDI-LTOF method to verify the cell related signal content (Fig. 22). Signals proved to originate from the cell pellet, whereas cell medium showed a completely different protein pattern containing mostly albumin and IgG species. The investigated supernatant exhibited proteins correlating with cell medium. As a consequence statistical analysis revealed very distinct differentiation for PCA and cluster analysis based on 64 signals.

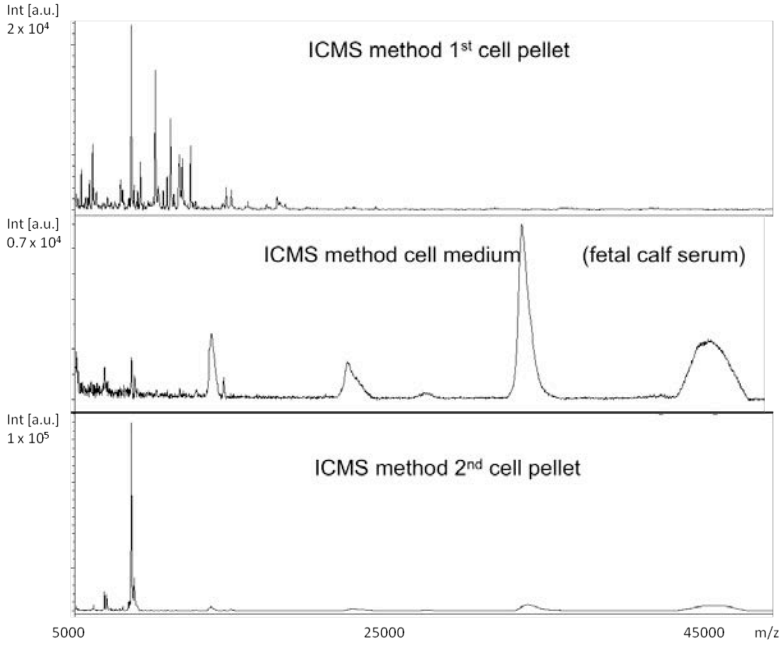

Figure 22: Evaluation of signals associated with cell culture and cell medium background.

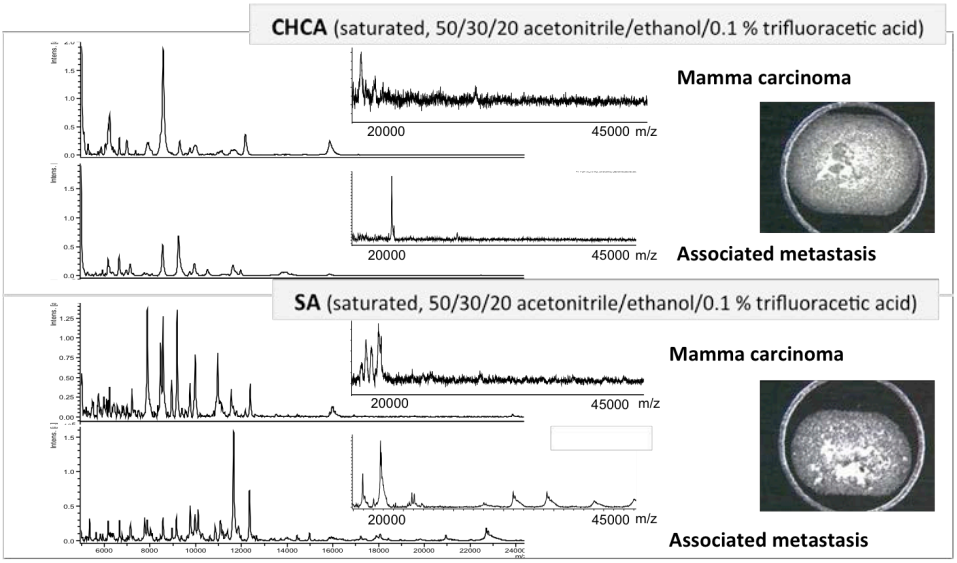

Figure 23: ICMS analysis of cell culture derived from mamma carcinoma or associated lung metastasis by SA and CHCA in MALDI-LTOF mode (UltrafleXtreme, Bruker).

Consequently the next step was to test the developed methods on cell cultures from healthy tissue and biopsies. Even though the observed protein pattern seemed resembling (Fig. 23), statistical analysis revealed significant differences. Cluster analysis differentiated the epithelial cell from both cancerous cells in the first node. Further primary tumor and metastasis were distinguished. Also PCA revealed sharp differentiation based on the first two principal components.

For each approach, using either CHCA or SA, 10 signals with ROC scores above 0.95 were identified. Signals were found between m/z 5000 and 14000.

The presented method is obviously capable of differentiating primary tumor cell culture and metastatic origins. For further evaluation eventually protein separation for detailed examination and identification is needed to verify the identified signals. The method is further expected to differentiate different tumor stages, which might give profound insight in the process of metastasis.

Sophie Fröhlich

Mühlgasse 30, Perchtoldsdorf, 2380
Phone: 0676 9289889 E-Mail: sofroehlich@gmx.net

Date of Birth: 28. 02. 1985

Experience

Project assistant, Vienna University of Technology, Institute of Chemical Technologies and Analytics, Division of Bio- and Polymer Analysis
Nov. 2010 – Feb. 2014

Project assistant, Medical University of Technology, Clinical Institute of Pathology
Nov. 2012 – Nov. 2013

Web administrator, European Proteomics Association and Research Group Bio- & Polymer Analysis at the Institute of Chemical Technologies and Analytics, VUT
Nov. 2012 – present

Short Term Scientific Mission, Erasmus Center Rotterdam, Rotterdam, Netherlands
Sept. 2011

Trainee, Master Thesis, Baxter AG, Vienna & Orth, Austria
Nov. 2009 - Aug. 2010

Summer Trainee, Baxter AG, Orth, Austria
Jun. 2009 - Aug. 2009

Technical Assistant, Bachelor Thesis, Center for Brain Research, Medical University of Vienna
Jan. 2008 - Mar. 2008

Summer Trainee, Center for Brain Research, Medical University of Vienna
Jun. 2007 - Aug. 2007

Education

Technical Chemistry (E 786 800), PhD
Nov. 2010 – April 2014
Thesis: The impact of bio-compartments on polymers used for artificial bio-replacement by mass spectrometry imaging and conventional bio-analytics.
Vienna University of Technology, 1040 Vienna

Masters Degree Program Biomedical Engineering Sciences – Cell & Tissue Engineering (0228), MSc (summa cum laude)
Sep. 2008 - Sep. 2010
Thesis: Characterization of peptide hormones in sealant matrix by liquid chromatography coupled to mass spectrometry
University of Applied Sciences, 1200 Vienna

Bachelors Degree Program Biomedical Engineering (0227), BSc (summa cum laude)
Sep. 2005 - Jun. 2008
Thesis: "Generierung und Charakterisierung zweier Antikörper gegen die α-Untereinheit des $GABA_A$ Rezeptors" & "Untersuchung der Protein-Protein Interaktion anhand der Yeast-Two-Hybrid- und FRET-Technik";
University of Applied Sciences, 1200 Vienna

AHS Matura 2003 (with distinction)
Bundesrealgymnasium Gröhrmühlgasse, 2700 Wr. Neustadt

Awards & Additional Education

Johanna Dohnal Förderpreis 2012
Leistungsstipendium Biomedical Engineering 2009, FH Technikum Wien

„Ausbildung zum Laserschutzbeauftragten“, Vienna University of Technology (2011)
„Ausbildung zum Strahlenschutzexperten“, Seibersdorf Laboratories (2008)

Oral & Poster Contributions

S. Fröhlich, H. Schachner, D. Kerjaschki, G. Allmaier, M. Marchetti-Deschmann: "*Differentiating primary mamma carcinoma tumors and metastasis by MALDI-TOF-MS imaging and intact cell mass spectrometry*"; 25th Mass Spectrometry Discussion Meeting, Vienna, Austria; 17.02.2014 - 19.02.2014.

S. Fröhlich, M. Marchetti-Deschmann: "*Correlating molecular changes of prostheses material to biomolecule adsorption by MALDI--TOF imaging mass spectrometry*"; Main lecture: 26th Tandem Mass Spectrometry Workshop, Fairmont Chateau Lake Louise, Alberta, Canada; 04.12.2013 - 07.12.2013.

S. Fröhlich, M. Kennedy, V. Archodoulaki, G. Allmaier, M. Marchetti-Deschmann: " *Lipid adsorption and diffusion correlated with UHMW-PE modifications investigated by MALDI mass spectrometry imaging, ion mobility separation and CID*"; Talk: 30th Informal Meeting on Mass Spectrometry, Palermo, Italy; 02.05.2013 - 06.05.2013.

S. Fröhlich, T. Luider, V. Archodoulaki, G. Allmaier, M. Marchetti-Deschmann: "*MALDI-TOF mass spectrometry imaging - A tool to investigate time-dependent biomolecule adsorption in correlation to induced polymer changes on UHMW-PE hip joints*"; Talk: 5th Vienna Biomaterials Symposium, Vienna; 19.11.2012 - 21.11.2012.

S. Fröhlich, L. Dekker, M.-V. Archodoulaki, T. Luider, G. Allmaier, M. Marchetti-Deschmann: “*Correlating surface changes of UHMW-PE hip joint explants to time-dependent biomolecule adsorption by MALDI-TOF imaging mass spectrometry*“; Talk: 60th ASMS Conference on Mass Spectrometry and Allied Topics, Vancouver, Can; 20.05.2012 - 24.05.2012; in: "*Proceedings of the 60th ASMS Conference on Mass Spectrometry and Allied Topics*", (2012)

S. Fröhlich, B. Putz, H. Schachner, D. Kerjaschki, G. Allmaier, M. Marchetti-Deschmann: "*Renopathological microstructure visualization from formalin fixed tissue by MALDI-RTOF-MSI*"; Main talk: MACPROGEN, Skopje (invited); 29.03.2012 - 01.04.2012.

S. Fröhlich: “*Determining the impact of sample (bio)surface properties on MALDI molecular imaging mass spectrometry*”; Talk: Progress in Bioscience Seminar, Vienna University of Technology, Vienna; 13.01.2012

S. Fröhlich: “*Imaging mass spectrometry of biological surfaces";* Talk: Protein Chemistry, University of Applied Sciences Technikum Wien, Vienna; 08.12.2011

S. Fröhlich, H. Schachner, D. Kerjaschki, G. Allmaier, M. Marchetti-Deschmann: "*MALDI imaging mass spectrometry of ultra thin kidney tissue samples*"; Talk: 7. ASAC JunganalytikerInnen Forum, Linz; 25.09.2011 - 26.09.2011; in: "*7. ASAC JunganalytikerInnen Forum Book of Abstracts*", (2011)

S. Fröhlich, R. Markut-Kohl, V. Archodoulaki, D. Kerjaschki, G. Allmaier, M. Marchetti-Deschmann: "*UHMWPE joint implants - investigating simulated synovial compound adsorption by MALDI imaging mass spectrometry*"; Talk: 9th Austrian Proteomics Research Symposium - Special focus on clinical proteomics, Vienna; 08.11.2011 - 09.11.2011.

M. Kosok, S. Fröhlich, G. Allmaier, J. van Byern, M. Marchetti-Deschmann: "*Analyses of adhesive biomolecules secreted by the salamander Plethodon shermani*"; Talk: The Topical Issues of Mineral Resources Management, National Mineral Resources University, St. Petersburg; 24.04.2013 - 26.04.2013.

M. Marchetti-Deschmann, S. Fröhlich, A. Lehner, V. Weiss, W. Szymanski, M. Kennedy, G. Allmaier: "*MALDI (matrix-assisted laser desorption ionization) and ES(I) (electrospray (ionization)) techniques for the characterization of natural (latex surfaces, gelatin nano particles and polysaccharides) and synthetic (UHMW-PE) polymers*"; Talk: Austrian - Slovenian Polymer Meeting - ASPM 2013, Bled (invited); 03.04.2013 - 05.04.2013; in: "The Proceedings of the Austrian - Slovenian Polymer Meeting 2013", (2013), ISBN: 978-961-269-992-5; S. 65 - 66.

M. Marchetti-Deschmann, S. Fröhlich, R. Heeren, D. Kerjaschki, G. Allmaier: “Tissue sections of 100 nm to 2 µm to increase the spatial resolution in mass spectrometry imaging”; Talk: 24th Mass Spectrometric Discussion-Meeting, Vienna: 19.02.-21.02.2013

M. Marchetti-Deschmann, S. Fröhlich, E. Pittenauer, C. Gabler, N. Koulakiotis, G. Allmaier: "*Molecular Imaging Mass Spectrometry: Concepts and Applications in Life and Organic Material Sciences*"; Talk: Imaging in Life Sciences, TU Wien, Vienna; 12.11.2012.

M. Marchetti-Deschmann, S. Fröhlich, G. Allmaier: "*Using MALDI mass spectrometry for localization and structure elucidation of surface/tissue associated peptides*"; Talk: 13th Naples Workshop on Bioactive Peptides, Naples, Italy (invited); 07.06.2012 - 10.06.2012; in: "*13th Naples Workshop on Bioactive Peptides - Book of Abstracts*", (2012), S. 30.

M. Bonta, S. Fröhlich, M. Hafner, E. Pittenauer, V.-M. Archodoulaki, G. Allmaier, M. Marchetti-Deschmann: “*MALDI-RTOF analysis of lipid compounds in synovial fluid separated by two dimensional thin layer chromatography”*; Talk: 23rd Mass Spectrometric Discussion-Meeting, Vienna; 21.02.-22.02.2012

M. Marchetti-Deschmann, S. Fröhlich, P. Rigger, H. Schachner, D. Kerjaschki, G. Allmaier: "*Seeing is believing: Imaging mass spectrometry of biological surfaces without labeling*"; Talk: 9th Austrian Proteomics Research Symposium - Special focus on clinical proteomics, Vienna; 08.11.2011 - 09.11.2011

S. Fröhlich, M. Kennedy, V. Archodoulaki, G. Allmaier, M. Marchetti-Deschmann: "*Correlating UHMW-PE degradation and modification with biomolecular adsorption by means of MALDI imaging mass spectrometry*"; Poster: 5th Vienna Biomaterials Symposium, Vienna; 19.11.2012 - 21.11.2012.

S. Fröhlich, S. Schrotshamer, E. Claude, M. Kennedy, V. Archodoulaki, G. Allmaier, M. Marchetti-Deschmann: "*Time dependent in vitro adsorption of synovial compounds on ultra-high molecular weight polyethylene investigated by MALDI imaging mass spectrometry*"; Poster: 10th Austrian Proteomic Research Symposium, Graz; 24.09.2012 - 26.09.2012.

S. Fröhlich, E. Claude, M. Kennedy, V. Archodoulaki, G. Allmaier, M. Marchetti-Deschmann: "*Correlating UHMW-PE cross-linking with biomolecular induced material modifications by means of MALDI-RTOF imaging mass spectrometry*"; Poster: Ourence Conference on Imaging Mass Spectrometry, Ourense, Spain; 03.09.2012 - 05.09.2012.

M. Marchetti-Deschmann, S. Fröhlich, H. Schachner, D. Kerjaschki, G. Allmaier: “*Obtaining lipidomic based distinction and localization of kidney microstructures by MALDI-RTOF imaging mass spectrometry”*; Poster: 1st Conference on Imaging Mass Spectrometry, OurCon 2012, Ourense, E; 02.09.2012-05.09.2012

S. Fröhlich, V.-M. Archodoulaki, G. Allmaier, M. Marchetti-Deschmann: “*Protein Adsorption On Ultra-high Molecular Weight Polyethylene Joints – Proteomics Correlated To MALDI Imaging Mass Spectrometry Data*”; Poster: Conference of the European Proteomics Association, Glasgow, UK; 10.07.2012 – 14.07.2012.

M. Marchetti-Deschmann, S. Fröhlich, B. Putz, O. Belgacem, A. Barnes, H. Schachner, D. Kerjaschki, G. Allmaier: "*Histodiagnostic differentiation of microstructures on formalin-fixed ultra-thin rat kidney tissue by MALDI-TOF imaging mass spectrometry*"; Poster: 60th ASMS conference, Vancouver, CAN; 20.05.2012 - 24.05.2012; in: "*Proceedings of the 60th American Society of Mass Spectrometry Conference*", American Society of Mass Spectrometry, (2012), Paper-Nr. TP23, 458

M. Bonta, S. Fröhlich, M. Hafner, E. Pittenauer, V.-M. Archodoulaki, G. Allmaier, M. Marchetti-Deschmann: “*MALDI-RTOF analysis of lipid compounds in synovial fluid separated by two dimensional thin layer chromatography”*; Poster: 2nd Graz Lipid Mass Spec Meeting, Graz; 06.03.-07.03.2012

M. Marchetti-Deschmann, S. Fröhlich, H. Schachner, O. Belgacem, A. Barnes, D. Kerjaschki, G. Allmaier: "*Developing a sample preparation technique for MALDI mass spectrometry imaging of ultra-thin kidney tissue samples*"; Poster: 59th ASMS Conference on Mass Spectrometry and Allied Topics, Denver, USA; 05.06.2011 - 09.06.2011; in: "*Proceedings of the 59th ASMS Conference on Mass Spectrometry and Allied Topics*", (2011), Paper-Nr. ThP24 435, 1 S.